ULPGC Universidad de Las Palmas de Gran Canaria | IOCAG Instituto Universitario de Oceanografía y Cambio Global

Doctorado en Oceanografía y Cambio Global

Universidad de Las Palmas de Gran Canaria

Tesis Doctotal

Seasonal variations in the structure and function of zooplankton and micronekton communities: implications for the carbon cycle in the context of climate change.

María Couret Huertas

Las Palmas de Gran Canaria, Abril 2025

A mi familia

Acknowledgements

Ahora que llega el momento de finalizar este camino tan complejo y lleno de dificultades es inevitable recordar la ayuda, la motivación y el apoyo de todas las personas que me han ayudado llegar hasta aquí.

En primer lugar, me gustaría agradecer a mis directores, Santiago Hernández León y José María Landeira, por la oportunidad que me brindaron de realizar mi tesis doctoral bajo su supervisión. Sin ellos no habría sido posible llegar hasta aquí.

Esta aventura comenzó gracias a la oportunidad que tuve de embarcarme en la campaña oceanográfica RAPROCAN1903. Por ello, quiero darle las gracias al Dr. Pedro Vélez Belchí por darme la motivación necesaria para comenzar mi carrera investigadora. Por supuesto, esta campaña no habría sido lo mismo sin Carmen Presas. Gracias Carmen por enseñarme a afrontar todos los problemas que pueden surgir en un barco con la mejor de las actitudes. Contigo aprendí que para ser buen profesional primero hay que ser buena persona. Tras otra campaña RAPROCAN pensaba que no podía ir a mejor hasta que Raúl Laiz y José María Quintanilla participaron en la campaña RAP2103. Con ellos aprendí que la investigación tiene que ir de la mano con el compañerismo y el buen rollo para que todo funcione. Gracias a los dos por los buenos momentos, los consejos, el apoyo, el conocimiento que me habéis proporcionado, y por los "refrescos" en cubierta sentados en una silla de playa oxidada después de un largo día de muestreo. Por supuesto, gracias a la tripulación del Ángeles Alvariño y a los compañeros con los que he podido compartir las distintas RAPROCANES en las que he participado.

En este largo camino, he podido participar en una campaña de mesocosmos dirigida por el Prof. Ulf Riesbesell. Quisiera agradecer a su grupo de investigación por su ayuda durante mi participación en el experimento. Al Prof. Arild Folkvord por su actitud carismática y apoyo incondicional durante los largos días de experimentos. Todavía sonrío cada

vez que recuerdo cuando en los -pocos- días soleados nos veía encerrados en el laboratorio y nos obligaba a salir a tomar el sol. Agradecer a Greg Börner y Daniel Brüggemann por los buenos momentos dentro de ese laboratorio rodeados de peces y experimentos sin fin. Y por supuesto, gracias a la Dra. Marta Moyano pues sin ti no habría tenido esta oportunidad. Marta, por supuesto tengo que agradecerte tu apoyo en el ámbito profesional, pues me has enseñado a realizar experimentos y trabajar con esos datos, pero lo que me aportaste en el ámbito personal está por encima de eso. Trabajar contigo ha sido una experiencia tan enriquecedora que no tengo palabras para agradecértelo. Conocer a alguien que vive la ciencia desde el compañerismo y la empatía, y no desde el ego y la posición profesional, me hizo cambiar mi perspectiva sobre la ciencia.

Agradecer a Dra. Mari Luz Fernández de Puelles por acogerme en su laboratorio y enseñarme la taxonomía de los copépodos. Todavía me surgen dudas sobre el número de artejos que hay que diferenciar de la rama exopodial, el tipo de morfología de las espinas externas de los exopoditos y cuántas ramas caudales estrechas y de longitud igual a la de los 3 últimos segmentos abdominales se deben de tener para diferenciar dos especies … Algún día todo tendrá sentido. También me gustaría agradecer al Dr. Antonio Bode y al Dr. Gerardo Aceves por recibirme con los brazos abiertos en sus laboratorios.

Terminando con las estancias, me gustaría agradecerle de todo corazón a la Dra. Sari Giering por la oportunidad de trabajar en el National Oceanography Center, donde estoy terminando mi Tesis. A pesar de la intensidad de esta recta final, me siento como en casa trabajando con su equipo. Me gustaría agradecerte la enorme ayuda que me estás proporcionando y ojalá todo el mundo se contagie de tu entusiasmo por la ciencia.

Y por supuesto gracias a todos mis amigos que habéis estado a lo largo de estos años. A David, por esos vinos en tu terraza sin los cuales no me habría matriculado en el segundo año. A Clara, Daniela y Rocío, por apoyarme y aguantar mis momentos de frustración. Con vosotras HOME siempre es casa. A Javier por todas las risas pero también por los

momentos de apoyo. A Laura, que has sido mi compañera de alegrías y felicidad pero estando siempre en los peores momentos dándome tu apoyo incondicional. A mis vecinos y buenos amigos Yaiza y Toni, porque siempre veis el lado bueno de las cosas. Y a mi mamá, que sin saber muy bien a que me dedico, siempre has estado ahí. Gracias a todos los que habéis estado en este camino.

Finalmente, no me olvido de ti Trufo, mi perrihijo. Sin ti tendría más estabilidad emocional y económica, pero me has enseñado que un simple perro de perrera puede ser la mejor compañía del mundo. Y como no, gracias a ti Airam por hacerme tan feliz, por tu apoyo y compresión durante todos estos años. Gracias por la familia que tenemos.

Abstract

Increasing atmospheric CO_2 levels and rising global temperatures have intensified research on the ocean's role in carbon store. Biological processes play a crucial role in the ocean carbon cycle, transferring carbon from the surface to deeper waters as organic matter through the biological carbon pump. However, the exact contribution of these processes to the carbon export remains poorly understood across much of the ocean. Marine zooplankton, a diverse group of protistan and metazoan consumers, are key components of pelagic food webs, linking primary producers to higher trophic levels and recycling nutrients. Their sensitivity to environmental changes makes them valuable sentinels for long-term monitoring and for understanding climate change impacts on marine ecosystems. Here, we compiled and analyzed five decades (1971–2021) of mesozooplankton biomass data to assess temporal variability in three productive areas of the Canary Current System: North, South and around the islands, and close to the Northwest African coastal upwelling system. Using a Generalized Additive Mixed Model, we examined biomass trends over time, accounting for spatial differences, seasonal cycles, and diel variations. Our analysis revealed a significant long-term decline in mesozooplankton biomass north of the Canary Islands over the 50-year time-series, in contrast to more stable trends in the South and island-associated regions. Additionally, we observed significant differences in biomass between daytime and nighttime periods and across the annual cycle.

Zooplankton biomass, abundance, and size spectra varied seasonally, with higher chlorophyll *a* concentrations and primary production during the Late Winter Bloom (LWB) compared to the stratified season (SS), particularly in upwelling-influenced area. Cluster analysis of abundance distribution grouped stations by season (LWB vs SS) and identified a distinct group in the upwelling influenced area. Size-spectra analysis showed that food web were controlled by top-down processes during the LWB, while strong bottom-up processes dominated the SS due to food-limited conditions. We also observed a significant

difference between day and nighttime size spectra due to diel vertical migrations.

To further investigate zooplankton and micronekton-mediated carbon flux, we examined respiratory and active fluxes, which remain poorly understood. We first assessed this gap by the thorough evaluation of euphausiids' respiration rates to improve carbon transport estimates using a Generalized Additive Model. Our results indicate that epipelagic oxygen concentration, chlorophyll *a*, and the interaction between epipelagic temperature and mesopelagic oxygen concentration significantly influenced euphausiids' respiration rates. We also found a strong correlation between respiration (R) and specific electron transport system (ETS) activity, with R/ETS ratios exceeding the commonly assumed conservative value of 0.5 for respiratory flux estimation.

Finally, we estimated total active carbon flux (zooplankton and micronekton) from the Mediterranean Sea to the Atlantic Ocean around the Iberian Peninsula. Zooplankton active flux was higher in the oligotrophic Mediterranean waters than in the Atlantic Ocean (77.2 ± 21.2 vs 14.8 ± 3.4 mg $C{\cdot}m^{-2}{\cdot}d^{-1}$, respectively), whereas micronekton active flux was greater in the Atlantic waters (15.1 ± 9.4 vs 7.9 ± 6.8 mg $C{\cdot}m^{-2}{\cdot}d^{-1}$). Crustaceans, particularly decapods, played a dominant role in active carbon transport, especially in northern Atlantic stations, highlighting their ecological importance in the biological carbon pump.

Resumen

El aumento de los niveles atmosféricos de CO_2 y el incremento de las temperaturas globales han intensificado la investigación sobre la capacidad del océano para almacenar carbono. Los procesos biológicos desempeñan un papel crucial en el ciclo del carbono oceánico, transfiriendo carbono desde la superficie hacia aguas más profundas en forma de materia orgánica a través de la bomba biológica de carbono. Sin embargo, la contribución exacta de estos procesos a la exportación de carbono sigue siendo poco conocida en gran parte del océano. El zooplancton marino, un grupo diverso de consumidores protistas y metazoos, es un componente clave de las redes tróficas pelágicas, ya que vincula a los productores primarios con niveles tróficos superiores y recicla nutrientes. Su sensibilidad a los cambios ambientales los convierte en un grupo clave para el monitoreo a largo plazo y para comprender los impactos del cambio climático en los ecosistemas marinos.

En este estudio, recopilamos y analizamos datos de biomasa de mesozooplancton durante cinco décadas (1971–2021) para evaluar su variabilidad temporal en tres áreas productivas del Sistema de la Corriente de Canarias: el norte, el sur y las aguas alrededor de las islas, cercanas al sistema de afloramiento costero del noroeste de África. Mediante un Modelo Aditivo Mixto Generalizado, examinamos las tendencias de biomasa a lo largo del tiempo, considerando diferencias espaciales, ciclos estacionales y variaciones diarias. Nuestro análisis reveló una disminución significativa de la biomasa de mesozooplancton en el norte de las Islas Canarias durante la serie temporal de 50 años, en contraste con tendencias más estables en el sur y en las regiones carcanas a las islas. Además, observamos diferencias significativas en la biomasa entre los períodos diurnos y nocturnos, así como a lo largo del ciclo anual.

La biomasa, abundancia y espectros de tamaño del zooplancton variaron estacionalmente, con concentraciones más altas de clorofila *a* y mayor producción primaria durante

la época productiva (LWB, por sus siglas en inglés *Late Winter Bloom*) en comparación con la época estratificada (SS, por sus siglas en inglés *Stratified Season*), especialmente en las áreas influenciadas por el afloramiento. El análisis de agrupamiento de la distribución de abundancia clasificó las estaciones en dos grupos principales según la temporada (LWB vs SS) y un grupo distinto en la región de afloramiento. El análisis de espectros de tamaño indicó que la red trófica estuvo controlada por procesos denominados *top-down* durante el LWB, mientras que en la SS predominó un fuerte control *bottom-up* debido a condiciones limitadas de alimento. También observamos diferencias significativas entre los espectros de tamaño diurnos y nocturnos debido a la migración vertical diaria.

Para comprender mejor el flujo de carbono mediado por zooplancton y micronekton, examinamos los flujos respiratorio y activo, que siguen siendo poco conocidos. Para abordar esta brecha, evaluamos en detalle las tasas de respiración de los eufausiáceos utilizando un Modelo Aditivo Generalizado con el fin de mejorar las estimaciones del transporte de carbono. Nuestros resultados indican que la concentración de oxígeno epipelágico, la clorofila *a* y la interacción entre la temperatura epipelágica y la concentración de oxígeno mesopelágico influyeron significativamente en las tasas de respiración de los eufausiáceos. Además, observamos una fuerte correlación entre la respiración (R) y la actividad específica del sistema de transporte de electrones (ETS), con valores de R/ETS superiores al conservador 0.5 utilizado comúnmente para estimar el flujo respiratorio.

Finalmente, estimamos el flujo total de carbono activo (zooplancton y micronecton) desde el mar Mediterráneo hasta el océano Atlántico en torno a la Península Ibérica. El flujo activo de zooplancton fue mayor en las aguas oligotróficas del Mediterráneo que en el océano Atlántico (77.2 ± 21.2 frente a 14.8 ± 3.4 mg $C{\cdot}m^{-2}{\cdot}d^{-1}$, respectivamente), mientras que el flujo activo de micronecton fue superior en el Atlántico (15.1 ± 9.4 frente a 7.9 ± 6.8 mg $C{\cdot}m^{-2}{\cdot}d^{-1}$). Los crustáceos, en particular los decápodos, desempeñaron un papel dominante en el transporte activo de carbono, especialmente en las estaciones del Atlántico norte, destacando su importancia ecológica en la bomba biológica de carbono.

Contents

Abstract 1

Resumen 3

List of figures 11

List of tables 20

Chapter 1 **25**

1. Introduction **25**

1.1. Motivation 33

1.2. Thesis outline 34

Chapter 2 **36**

2. A 50-year (1971-2021) mesozooplankton biomass data collection in the Canary Current System: Base line, gaps, trends, and future prospect **37**

2.1. Abstract 39

2.2. Introduction 40

2.3. Material and methods 43

2.3.1. *Mesozooplankton database sources and analysis* 43

2.3.2. *Environmental parameters* 45

2.3.3. *Modeling mesozooplankton biomass* 46

2.3.4. *Databases comparison* 47

2.4. Results 49

2.4.1. *Time-series biases* 49

2.4.2. *Environmental parameters* 49

2.4.3. *Mesozooplankton time-series results* 51

2.4.4. *Annual cycle of environmental parameters and mesozooplankton biomass* . . . 55
2.4.5. *Modeling mesozooplankton biomass* . . . 57
2.4.6. *Databases comparison* . . . 59
2.5. Discussion . . . 61
2.5.1. *Time-series biases* . . . 61
2.5.2. *Mesozooplankton time-series* . . . 62
2.5.3. *Annual cycle* . . . 64
2.5.4. *Modeling mesozooplankton biomass* . . . 65
2.5.5. *Databases comparison* . . . 66
2.6. Conclusions . . . 67
2.7. Acknowledgments . . . 68
2.8. Author contributions . . . 68
2.9. Data availability statement . . . 69
2.10. Supplementary material . . . 70

Chapter 3 **82**

3. Mesozooplankton Size Structure in the Canary Current System. **83**

3.1. Abstract . . . 85
3.2. Introduction . . . 86
3.3. Material and methods . . . 90
3.3.1. *Field sampling* . . . 90
3.3.2. *Image analysis* . . . 91
3.3.3. *Zooplankton biovolume, abundance and biomass* . . . 92
3.3.4. *Cluster analysis* . . . 92
3.3.5. *Zooplankton Normalized Biomass Size Spectra* . . . 93
3.3.6. *Data analyses* . . . 94

3.4. Results . . . 95
3.4.1. *Environmental and biotic patterns* . . . 95
3.4.2. *Zooplankton structure* . . . 101
3.4.3. *Normalized biomass size distribution characterization* . . . 103
3.5. Discussion . . . 107
3.5.1. *Spatial and temporal patterns in the C-ATZ* . . . 107
3.5.2. *Abundance and composition* . . . 108
3.5.3. *Normalized Biomass Size Spectra* . . . 109
3.6. Conclusions . . . 112
3.7. Acknowledgments . . . 112
3.8. Author contributions . . . 113
3.9. Supplementary material . . . 114

Chapter 4 **116**

4. Respiration rates and its relationship with ETS activity in Euphausiids: Implications for active flux estimations **117**

4.1. Abstract . . . 119
4.2. Introduction . . . 120
4.3. Material and methods . . . 122
4.3.1. *Sampling and on-board experiments* . . . 122
4.3.2. *Specific ETS activity and protein content* . . . 123
4.3.3. *Estimation of respiration rates and ETS activity in the epipelagic and mesopelagic layer* . . . 124
4.3.4. *Data analysis* . . . 125
4.4. Results . . . 126
4.5. Discussion . . . 136
4.6. Conclusions . . . 141

4.7. Acknowledgments . . . 141
4.8. Author contributions . . . 142
4.9. Supplementary material . . . 142

Chapter 5 **147**

5. Relative importance of active flux by zooplankton and micronekton varies around the Iberian Peninsula. **147**

5.1. Abstract . . . 149
5.2. Introduction . . . 150
5.3. Material and methods . . . 152
5.3.1. *Sampling and study area* . . . 152
5.3.2. *Hydrography* . . . 152
5.3.3. *Trap-derived passive flux* . . . 153
5.3.4. *Zooplankton sampling* . . . 153
5.3.5. *Micronekton sampling* . . . 154
5.3.6. *Migrant biomass estimation* . . . 155
5.3.7. *Active flux* . . . 156
5.3.8. *Sensitive analysis* . . . 157
5.3.9. *Statistics* . . . 157
5.4. Results . . . 158
5.4.1. *Hydrography conditions* . . . 158
5.4.2. *Trap-derived Particulate Organic Carbon (POC) Flux* . . . 159
5.4.3. *Zooplankton and Micronekton Biomass Vertical Distribution* . . . 159
5.4.4. *Zooplankton and Micronekton ETS profiles* . . . 162
5.4.5. *Respiratory and total active flux* . . . 162
5.4.6. *Migrant biomass* . . . 165
5.4.7. *Carbon budget for active and sinking fluxes* . . . 166

5.4.8. *Correlation between biological and environmental parameters* . . 167
5.5. Discussion 172
5.5.1. *Zooplankton and micronekton carbon flux* 172
5.5.2. *Relationship between Biomass and Environmental Variables* . . . 175
5.5.3. *Relationship between Total Active Flux and Environmental Conditions* 176
5.5.4. *Passive vs Active flux* 177
5.6. Conclusions 177
5.7. Acknowledgments 178
5.8. Author contributions 178
5.9. Supplementary material 180
5.9.1. *Study area* 180
5.9.2. *Electron transfer system activity* 180
5.9.3. *Active flux* 181
5.9.4. *Sensitivity analysis* 183
Conclusions 191
Appendix A. Institutional Acknowledgments 196
Appendix B. Resumen Castellano 198
References 243

List of Figures

1.1. Image illustrating the high diversity of zooplanktonic organisms. Photo Credit: Marine Biological Association. 28

1.2. Scheme of the Biological Carbon Pump. Figure modified from U.S. Joint Global Ocean Flux Study (U.S. JGOFS). 29

1.3. Conceptual diagram illustrating of an ecosystem's normalized biomass size spectrum (NBSS; solid purple line) expressed as log-log biomass size class against normalized biomass (i.e., total biomass in logarithmic size bin/width of size bin). The dashed lines represent underlying biomass domes (i.e., phytoplankton, zooplankton, and nekton). 31

2.1. Location of the sampled oceanographic stations from 1971 to 2021. Green dots stand for samples obtained North of the Canary Islands, orange dots for samples obtained South and around the islands, and purple dots for those samples in the Upwelling influenced area. Yellow arrow stands for reference points of each delimited area (see text), yellow line indicates the separation between areas according to proximity to the coast and position in relation to the islands, and black line stands for 200 m depth bathymetry. GC stands for Gran Canaria, and F for Fuerteventura. 44

2.2. Time-series of (A) monthly average sea surface temperature (°C) North (29°N 15° 30′ W), South (27°N 15° 30′ W) and in the Upwelling influenced area (27°N 14°W) since 1971 obtained from remote sensing. (B) Satellite data of chlorophyll *a* concentration (mg·m^{-3}), and (C) primary production (mg C·m^{-2}·d^{-1}) from 2002 to 2020, also using remote sensing data (see text for coordinates explanation). 50

2.3. Mesozooplankton biomass (mg C·m^{-2}) in the upper 200 m depth during day and nighttime, from 1971 to 2021 in (A) all the area, (B) North, (C) South (and around) the islands, and (D) in the Upwelling influenced area. The size of the box is determined by the upper and lower quartiles, and median is indicated as a horizontal black line inside the box. Black dots represent the outliers and red dots inside the box stand for mean values. Regression line for each period (i.e. day or night) are presenting according to the period color. 52

2.4. Mesozooplankton biomass (mg C·m^{-2}) in the upper 200 m depth during the Late Winter Bloom (LWB) and the Stratified Season (SS), from 1971 to 2021 in (A) all the area, (B) North, (C) South (and around) the islands, and (D) in the Upwelling influenced area, pooled day and nighttime values. The size of the box is determined by the upper and lower quartiles, and median is indicated as a horizontal black line inside the box. Black dots represent the outliers and red dots inside the box stand for mean values. Regression line for each season (i.e. LWB or SS) are presenting according to the period color. 53

2.5. Mesozooplankton biomass (mg C·m^{-2}·d^{-1}) longitudinal distribution in the upper 200 m depth from 1971 to 2021, during day and nighttime. Green dots stand for mesozooplankton biomass. 54

2.6. Annual cycle of (A) temperature (°C) since 1971, (B) chlorophyll *a* concentration (mg·m^{-3}), (C) primary production (mg C·m^{-2}·d^{-1}) since 2002, and (D) mesozooplankton biomass (mg C·m^{-2}), pooled day and nighttime values. Green squares represent the North, orange dots the South (and around), and purple triangles the Upwelling influenced area. Symbols stand for mean values and lines above and under the dots for standard error. Environmental variables were obtained by remote sensing (see text). 56

2.7. Mesozooplankton biomass (mg C·m^{-2}) in the upper 200 m depth during the Late Winter Bloom (LWB) and the Stratified Season (SS), from 1994 to 2021 in the (A) North of the Canary Current System (CSS), during day and nighttime, (B) Hawaii Ocean Time-series (HOTS), and (C) Bermuda Institute of Ocean Sciences Time-series (BATS), during day and nighttime. Data from HOTS was downloaded from `https://hahana.soest.hawaii.edu/hot/hot-dogs/mextraction.html`, and BATS data from `https://bats.bios.edu/bats-data/`. The size of the box is determined by the upper and lower quartiles, and median is indicated as a horizontal black line inside the box. Black dots represent the outliers and red dots inside the box stand for mean values. Regression line for each season (i.e. LWB or SS) are presenting according to the period color. 60

2.8. Relationship between biomass values from 0-100 m depth and biomass values from 0-200 m depth using data from the project COCA (see Hernández-León et al., 2019b) and 5 data points located south of the Canary Islands . 70

3.1. Location of sampling stations: yellow diamonds stand for stations sampled during the Stratified Season (October 2018), and in green squares during the Late Winter Bloom (March 2019). Asterisks stand for night-hauls stations and number above mark-stations indicates the station number. T stands for the number of the transect. 91

3.2. Vertical sections (0-200 m) of temperature (°C) (A, B), salinity (PSU) (C, D) and chlorophyll *a* concentration (mg·m^{-3}) (E, F) during the Stratified Season (left panels) and the Late Winter Bloom (right panels) in transect T1W and T1E (see Fig. 3.1). Numbers on the top stand for station numbers, and black lines onside the graph for CTD-sampled stations across the transect. 97

3.3. Vertical sections (0-200 m) of temperature (°C) (A, B, C, D), salinity (PSU) (E, F, G, H) and chlorophyll *a* concentration (mg·m^{-3}) (I, J, K, L) during the Stratified Season in the stations close to the African coast (see Fig. 3.1). Numbers on the top stand for station numbers, and black lines onside the graph for CTD-sampled stations across the transect. . . . 98

3.4. Vertical sections (0-200 m) of temperature (°C) (A, B, C, D), salinity (PSU) (E, F, G, H) and chlorophyll *a* concentration (mg·m^{-3}) (I, J, K, L) during the Late Winter Bloom in the stations close to the African coast (see Fig. 3.1). Numbers on the top stand for station numbers, and black lines onside the graph for CTD-sampled stations across the transect. . . . 99

3.5. Spatial distribution of the percentages of zooplankton size-fractionated biomass obtained as protein content during the Stratified Season (A) and the Late Winter Bloom (B). Bubble size represent total biomass (mg C·m^{-2}). Colors on the maps correspond to monthly-mean sea surface temperature during October (2018) for the Stratified Season and March (2019) for the Late Winter Bloom. Asterisks stand for night-hauls stations. 100

3.6. A) Assemblages of zooplankton structure according to the abundance and composition for each sampled season and area. First two numbers of the x-labels correspond to the sampling year, and the rest to the code of the station as in Fig. 3.1. B) Results of the non-metric multidimensional scaling (nMDS) of zooplankton communities. C and D) Zooplankton taxonomic composition of the key organisms. Pink diamonds stand for those stations performed close to the upwelling African coast, pink asterisks stand for those stations sampled during the Late Winter Bloom, green squares correspond to an outgroup, and green crosses to stations performed during the Stratified season. Bubble size stand for abundance values for each selected taxon (number·m^{-3}). 102

3.7. Mesozooplankton NBSS for the grouped stations according to Fig. 3.6A cluster: A) SS-group, B) LWB-group, and C) Upwelling-group. Color in each NBSS corresponds to day hauls, and black for night hauls. 105

3.8. Mesozooplankton biomass (%) in each bin size for the different grouped stations according to Fig. 3.6A cluster. A) Correspond to the LWB-group during day, B) to the LWB-group during night, C) to the SS-group during day, and D) to the SS-group during night. The Upwelling group was not included in the graph (see text). 106

4.1. Locations of sampling stations during the DESAFIO 1 cruise conducted in February 2023. The background colours depict the monthly average sea surface temperature (SST, °C). The coloured dots indicate the specific stations where experiments were carried out. 123

4.2. Vertical distribution of (a-b) temperature (°C), (c-d) oxygen (ml·L^{-1}), and (e-f) chlorophyll *a* (mg·m^{-3}) along the latitudinal (left panel) and longitudinal (right panel) transects sampled during the DESAFIO 1 cruise. Note the different y-axes for the chlorophyll *a* vertical profiles 129

4.3. (a) Respiration rates (μl O_2·mg prot^{-1}·h^{-1}), (b) protein normalized ETS activity (μl O_2·mg prot^{-1}·h^{-1}), and (c) R/ETS ratios of migrant euphausiids obtained from incubations conducted along the oceanographic stations in the Atlantic transect. Measurements were estimated at surface temperature (orange), for the epipelagic layer (green), and for the mesopelagic temperature (blue) at each station (see text). Vertical lines indicate the standard error. 131

4.4. Relationship between euphausiid respiration rates and specific (sp) ETS activity estimated for the a) epipelagic (0-200 m depth) and the b) mesopelagic layer (200-1000 m depth). See text for explanation. 132

4.5. Relationship between euphausiid body weight (as protein content) and (a) total respiration rates (μl O_2·ind^{-1}·h^{-1}) and (b) respiration rate (μl O_2·mg prot^{-1}·h^{-1}) in the epipelagic layer (0-200 m depth). 133

4.6. Pearson's correlation between temperature (°C) in the epipelagic layer and average (a) respiration (μl O_2·mg prot^{-1}·h^{-1}), (b) specific (sp) ETS activity (μl O_2·mg prot^{-1}·h^{-1}), and (c) the R/ETS ratio in the epipelagic and mesopelagic layers per station. Only significant correlations are indicated with a line and standard deviation. Colours and numbers represent the stations. 134

4.7. Pearson's correlation between oxygen (ml·l^{-1}) in the epipelagic (upper panel) and mesopelagic (lower panel) layers and average (a,d) respiration (μl O_2·mg prot^{-1}·h^{-1}), (b,e) specific (sp) ETS activity (μl O_2·mg prot^{-1}·h^{-1}), and (c,f) the R/ETS ratio in the epipelagic and mesopelagic layers per station. Only significant correlations are indicated with a line and standard deviation. Colours and numbers represent the stations. . . . 134

4.8. Upper panel: Pearson's correlation between chlorophyll *a* (mg·m^{-3}) in the epipelagic layer and average (a) respiration (μl O_2·mg prot^{-1}·h^{-1}), (b) specific (sp) ETS activity (μl O_2·mg prot^{-1}·h^{-1}), and (c) the R/ETS ratio in the epipelagic and mesopelagic layers per station. Lower panel: Pearson's correlation between net primary production (mg C·m^{-2}·d^{-1}) in the epipelagic layer and average (d) respiration (μl O_2·mg prot^{-1}·h^{-1}), (e) specific (sp) ETS activity (μl O_2·mg prot^{-1}·h^{-1}), and (f) the R/ETS ratio in the epipelagic and mesopelagic layers per station. Only significant correlations are indicated with a line and standard deviation. Colours and numbers represent the stations. 135

5.1. Vertical profiles of (A) temperature (°C), (B) salinity, (C) oxygen (ml·L^{-1}), and (D) chlorophyll *a* (mg·m^{-3}) at Z1 (red), Z2 (blue), Z3 (purple), Z4 (orange), and Z5 (green). Note the different y-axis scale for chlorophyll *a*. 160

5.2. Biomass (mg C·m^{-3}) vertical distribution (0-700 m depth) of (A) zooplankton, (B) micronekton (mesopelagic fish and decapods), (C) mesopelagic fish, and (D) decapods during day (empty dots) and night (black dots) at the different zones. Note different x-axis scale for each station. Black lines stand for the sensitive analysis error. 163

5.3. Specific ETS activity (μl O_2·mg C^{-1}·h^{-1}) vertical profiles of (A) total zooplankton, (B) copepods, (C) euphausiids, (D) chaetognaths, (E) micronekton (mesopelagic fish and decapods), (F) mesopelagic fish, and (D) decapods. Empty dots are daytime activity values, while black dots are nighttime specific ETS activity. Black lines stand for the sensitive analysis error. 164

5.4. Respiratory (in green), mortality (in purple), gut (in dark red), and excretion (in orange) fluxes (mg C·m^{-2}·d^{-1}) of (A) zooplankton, (B) mesopelagic fish, and (C) decapods. 166

5.5. (A) Study zones sampled during the CSIC-SUMMER cruise, with background colors representing sea surface temperature (SST, °C) in October 2020. Zone 1 (Z1) corresponds to the south of the Balearic Islands, Zone 2 (Z2) to the western Alborán Sea, Zone 3 (Z3) to the Gulf of Cadiz, Zone 4 (Z4) off Lisbon, and zone 5 (Z5) off Galicia. Bubble size indicates total active flux (zooplankton + micronekton), with blue for zooplankton, grey for fish, and pink for decapods. (B) Percentage contribution to the biological carbon pump by passive flux (light orange), zooplankton (blue), and micronekton (purple; fish + decapods). For Z5 and Z2, we do not have direct passive flux measurements, so we applied the average value from Z1, Z3 and Z4 (shaded orange). (C) Percentage distribution of migrant biomass among zooplankton, fish, and decapods. (D) Carbon fluxes (mg C·m^{-2}·d^{-1}). (E) Migrant biomass values (mg C·m^{-2}). 168

5.6. Results of the correlation analysis between the zooplankton, mesopelagic fish, and decapods biomass, migrant biomass (Mig_biomass), and active flux with the environmental variables. T stands for temperature, Sal for salinity, Oxy for Oxygen, ML for he Mixed Layer depth (50 m depth), Epi for the 50200 m depth, and Meso for the 200-700 m depth. White stars stand for the significant p-values and grey crosses the same variables. White stars stand for significant p-values and grey crosses the same variables. All p-values are $p<0.5$ and $R^2> 0.78$. 169

5.7. Results of the correlation analysis between (A) zooplankton, (B) mesopelagic fish, and (C) decapods biomass, migrant biomass (Mig_Biomass), and active flux. White stars stand for significant p-values and grey crosses the same variables.All p-values are $p<0.5$ and $R^2> 0.78$. 171

List of Tables

2.1. Spearman correlation coefficients and p-values between the environmental variables and zooplankton biomass North, South (and around), and in the Upwelling influenced area. "n" stands for the number of samples in each area, "SST" for Sea Surface Temperature, "Chl *a*" for chlorophyll *a* concentration, and "PP" for primary production. 51

2.2. Average mesozooplankton biomass (mg C·m^{-2}) and standard deviation ($\pm$ SD) in all the area studied, North, South (and around the islands), and in the Upwelling influenced area sampled during the Late Winter Bloom (LWB) and the Stratified Season (SS), during day time. "n" stands for the number of samples in each area/season/period. 57

2.3. Results obtained from the GAMM for the 50-year time-series. β_0 evaluates biomass differences in the South over the period. $\beta_{0,\,North}$ evaluates differences between the South (reference area) and the North, and $\beta_{0,\,Upwelling}$ differences between the South and the Upwelling influenced. $\beta_{0,\,Night}$ evaluates daily biomass differences. β_1 examine biomass tendencies over the time in the South. $\beta_{1,\,North}$ evaluates differences in tendencies between the South and the North, and $\beta_{1,\,Upwelling}$ differences in tendencies between the South and the Upwelling influenced. s(day) correspond to the smoother for annual variations. 58

4a. Data information compiled for the time-series analysis. "Project" column indicates if the data belongs to a specific project, unfilled if not belong to any specific project. LWB stands for Late Winter Bloom (from January to April), and SS for Stratified Season (from May to December). Data not published is indicated in "Reference" column. *Only the northern transect was considered for the database. 71

4b. Continued: Data information compiled for the time-series analysis. "Project" column indicates if the data belongs to a specific project, unfilled if not belong to any specific project. LWB stands for Late Winter Bloom (from January to April), and SS for Stratified Season (from May to December). Data not published is indicated in "Reference" column. *Only the northern transect was considered for the database. 72

5a. Information of zooplankton biomass data points per year, month, area, and period. 73

5b. Continued: Information of zooplankton biomass data points per year, month, area, and period. 74

5c. Continued: Information of zooplankton biomass data points per year, month, area, and period. 75

5d. Continued: Information of zooplankton biomass data points per year, month, area, and period. 76

5e. Continued: Information of zooplankton biomass data points per year, month, area, and period. 77

5f. Continued: Information of zooplankton biomass data points per year, month, area, and period. 78

5g. Continued: Information of zooplankton biomass data points per year, month, area, and period. 79

5h. Continued: Information of zooplankton biomass data points per year, month, area, and period. 80

3.1. Average temperature, salinity, chlorophyll *a*, primary production, and zooplankton biomass (± standard deviation) for the different transects (see text) sampled during the stratified season and the late winter bloom cruise in the upper 200 m depth. *No value available for station 10. 96

3.2. Taxa regarded as discriminators between the zooplankton community assemblages from the SIMPER analysis up to a 70%. 103

3.3. Results from the linear regressions of the Normalized Biomass Size Spectra analysis. n: number of data points. 104

3.4. ANOVA results for mesozooplankton biomass. SS stands for Stratified Season and LWB for Late Winter Bloom. 114

4.1. Euphausiid biomass (mg protein·ind^{-1}), respiration rates (μl O_2·mg prot^{-1}·h^{-1}), specific (sp) ETS activities (μl O_2·mg prot^{-1}·h^{-1}), and R/ETS ratios measured in the 0-50 m depth layer, estimated for the epipelagic (0-200 m depth) and mesopelagic (200-1000 m depth) layers. 130

4.2. Estimated coefficients for selected variables from the best-fitting Generalized Additive Model (GAM) for the response variables. 136

3a. Euphausiid biomass (mg protein·ind^{-1}), respiration rates (μl O_2·mg prot^{-1}·h^{-1}), specific (sp) ETS activities (μl O_2·mg prot^{-1}·h^{-1}), and R/ETS ratios measured in the 0-50 m depth layer, estimated for the epipelagic (0-200 m depth) and mesopelagic (200-1000 m depth) layers. 143

3b. Continued: Euphausiid biomass (mg protein·ind^{-1}), respiration rates (μl O_2·mg prot^{-1}·h^{-1}), specific (sp) ETS activities (μl O_2·mg prot^{-1}·h^{-1}), and R/ETS ratios measured in the 0-50 m depth layer, estimated for the epipelagic (0-200 m depth) and mesopelagic (200-1000 m depth) layers. . 144

4.4. Results of Pearson's correlation between temperature (°C), oxygen (ml·L^{-1}), chlorophyll a (measured as fluorescence, mg·m^{-3}), and net primary production (mg C·m^{-2}·d^{-1}) with the average respiration (µl O_2·mg $prot^{-1}$·h^{-1}), specific ETS activity (µl O_2·mg $prot^{-1}$·h^{-1}), and R/ETS ratios of euphausiids in the epipelagic and mesopelagic layers. 145

5.1. Net primary production (0-200 m depth), passive organic carbon (POC) flux measured at 150 m depth, zooplankton, mesopelagic fish, and decapods migrant biomass (± sensitive analysis error) and active flux (± sensitive analysis error) from epipelagic layer (0-200 m depth) to mesopelagic layer (200-700 m depth). Micronekton values were estimated using a capture efficiency of 20 ± 13%. 161

5.2. Number of CTD casts, MOCNESS and Mesopelagos trawls, and sediment traps per study zone used for the present investigation. 188

5.3. Conversion factors used to estimate zooplankton and micronekton biomass and active flux. * different coefficients for certain zooplankton groups as explained in text. 188

5.4. Comparison of trap-derived POC flux (mg C·m^{-2}·d^{-1}), zooplankton and micronekton migrant biomass (mg C·m^{-2}), respiratory flux (mg C·m^{-2}·d^{-1}), and active flux (mg C·m^{-2}·d^{-1}) values obtained during the CSIC-SUMMER cruise to other studies. CE stands for capture efficiency. 189

Chapter 1

Introduction

Introduction

Marine zooplankton comprise a phylogenetically and functionally diverse assemblage of protistan and metazoan consumers occuping multiple trophic levels in pelagic food webs (Fig. 1.1). These organisms span a wide size range and are categorized into three operational size classes: microzooplankton, mesozooplankton, and macrozooplankton. The microzooplankton size class ($<$200 μm) is dominated by unicellular protistan consumers but also includes smaller juvenile stages of metazoan zooplankton species (Paffenhöfer, 1998; Quevedo and Anadón, 2000). Mesozooplankton (0.2–20 mm) primarily consists of copepods, euphausiids, jellyfish, chaetognaths, amphipods, marine gastropods, polychaetes, and ostracods, alongside large protists such as pelagic foraminifera and radiolaria (Stoecker et al., 1996). Finally, the term macrozooplankton is commonly used for larger planktonic animals ($>$20 mm), such as large gelatinous zooplankton.

This taxonomic diversity is reflected in their ecological roles, which are shaped by their physiology, feeding strategies, and life cycles. Zooplankton play a key role in marine ecosystems as trophic links between primary producers and higher consumers, such as fish and decapods. By consuming prey populations and serving as food for predators, they influence biomass stocks across trophic levels (Vanni, 2002). Additionally, zooplankton regulate microbial communities by grazing on algae and bacteria while also supplying nutrients, such as nitrogen and phosphorus, back to phytoplankton (Sterner, 2009; Kalinowska et al., 2024). Through these processes, zooplankton mediate the transformation of particulate carbon and nutrients into dissolved pools, influencing marine biogeochemical cycles (Steinberg and Landry, 2017). Their short generation times and sensitivity to environmental cues make them valuable indicators of climate change impacts on marine ecosystems (Hay, 2009).

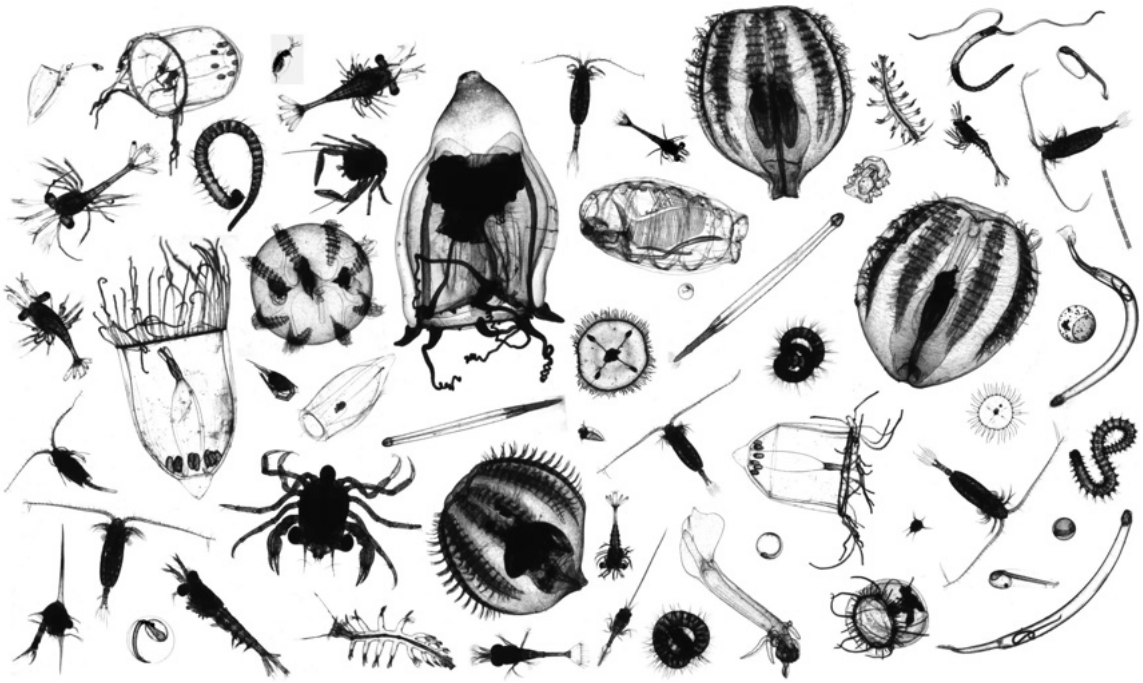

Figure 1.1. Image illustrating the high diversity of zooplanktonic organisms. Photo Credit: Marine Biological Association.

Despite their relatively small size, many zooplankton species undertake extensive ontogenetic and/or diel vertical migrations, often exceeding 200 m depth (Hays et al., 2001; Harris et al., 2014). These migrations contribute to biogeochemical cycling by transporting organic carbon to deeper waters via respiration (Longhurst et al., 1990), excretion (Steinberg et al., 2002), gut flux (Angel, 1989), and mortality (Zhang and Dam, 1997). As a result, zooplankton play a crucial role in the efficiency of the biological carbon pump, regulating carbon exchange between the atmosphere, the surface ocean, and the deep sea (Kwon et al., 2009; Parekh et al., 2006).

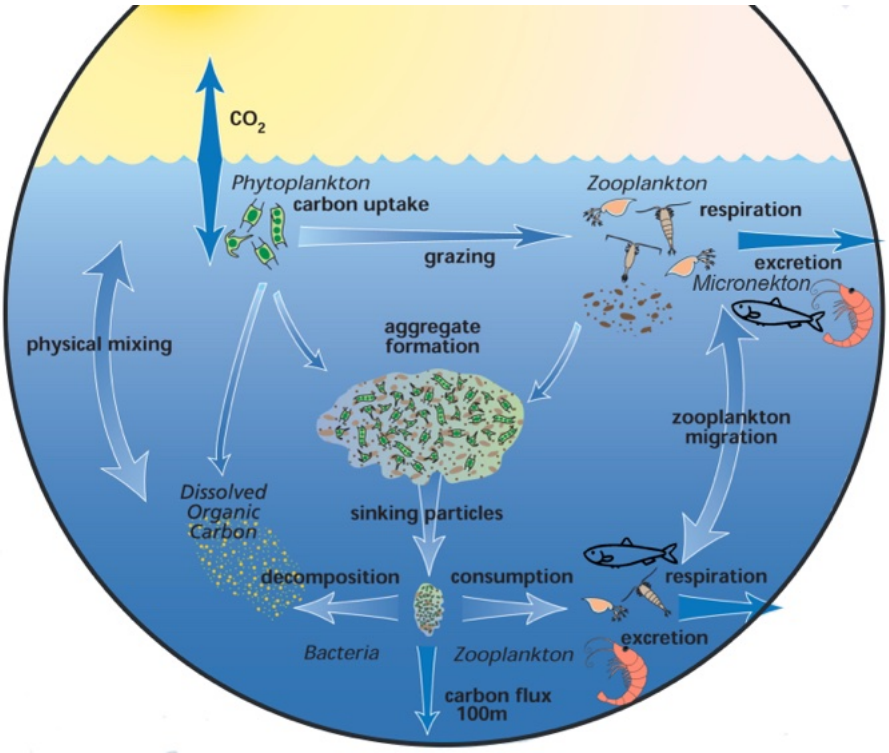

Figure 1.2. Scheme of the Biological Carbon Pump. Figure modified from U.S. Joint Global Ocean Flux Study (U.S. JGOFS).

The biological carbon pump (Fig. 1.2) describes the set of mechanisms driving the carbon flux from the euphotic to the meso- and bathypelagic layers through interactions between the physical, chemical, and biological components of the pelagic system (Longhurst and Harrison, 1989). One critical component of this pump is the active flux, referring to the transport of organic matter by vertically migrating meso- and bathypelagic zooplankton and micronekton (Longhurst and Harrison, 1988). These organisms perform diel vertical migrations, remaining at depth during daylight hours, moving upwards near the surface at night to feed, and returning to depth before dawn (Lampert, 1989; Steinberg et al., 2002; Bianchi et al., 2013). A key outcome of these up-and-down movements is the transport of organic matter to the deep sea (Romero-Romero et al., 2019), where it is remineralized and may remain sequestered for years to centuries (Nowicki et al., 2022; Pinti et al., 2023).

While active flux has been widely studied in zooplankton (Hernández-León et al., 2019b), empirical investigations of both zooplankton (0.2–20 mm) and micronekton (2–20 cm, including mesopelagic fish and decapods) remain limited. To date, only five studies have concurrently examined their active flux contributions: Hidaka et al. (2001) in the North Pacific, Ariza et al. (2015) and Hernández-León et al. (2019) in the North Atlantic, Kwong et al. (2020) in Southeast Australia, and Baker et al. (2025) in the Southern Ocean. Consequently, our knowledge on the relative importance of these two groups is limited, with significant gaps in understanding how their contributions to active flux vary across regions or environmental conditions.

To assess the contributions of zooplankton to the biological carbon pump, it is essential to evaluate their biomass, abundance, and size distribution, as these factors directly influence transfer efficiency and predator-prey dynamics. Body size is a primary determinant of energy flow, species diversity, and population structure (Peters and Wassenberg, 1983; Woodward et al., 2005). Marine size-structured food webs constrain prey-predator interactions (Li et al., 2018) and regulate biomass, physiology, and growth rates across trophic levels (Carpenter et al., 1987; Vanni and Findlay, 1990). A widely used method for characterizing zooplankton communities is the normalized biomass size spectrum (NBSS) (Fig. 1.3) (Martin et al., 2006; Sprules and Munawar, 1986). NBSS parameters provide insights into the ecological processes shaping zooplankton communities, including trophic interactions, environmental drivers, and energy flow (Sprules and Munawar, 1986). The slope of the NBSS, which relates biomass to body size, is a key metric: a slope steeper than -1 indicates dominance by smaller zooplankton, whereas a flatter slope suggests a more even biomass distribution across size classes (Zhou, 2006; Atkinson et al., 2021). The NBSS intercept reflects energy availability at the base of the food chain (Platt and Denman, 1978; Zhou, 2006).

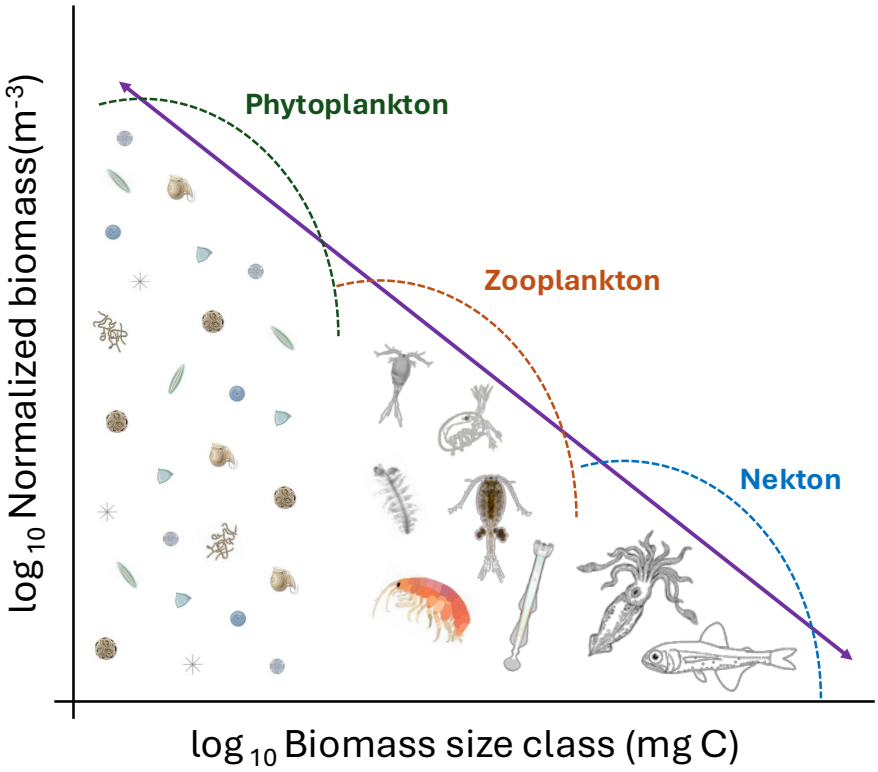

Figure 1.3. Conceptual diagram illustrating of an ecosystem's normalized biomass size spectrum (NBSS; solid purple line) expressed as log-log biomass size class against normalized biomass (i.e., total biomass in logarithmic size bin/width of size bin). The dashed lines represent underlying biomass domes (i.e., phytoplankton, zooplankton, and nekton).

Zooplankton are also key indicators of ecosystem health and global change, particularly given the dynamic nature of oceanic physical and chemical conditions. Understanding the spatiotemporal variability of zooplankton communities is essential for assessing ecosystem structure and function (Zhao et al., 2022) and predicting climate change impacts (Batchelder et al., 2013; Hays et al., 2005; Shi et al., 2020), which has already affected zooplankton biomass, abundance, composition, size structure, phenology, and distribution in different marine regions (Richardson, 2008; Mackas et al., 2012; Brun et al., 2019; Conroy et al., 2023; Huggett et al., 2023; Kodama et al., 2022). These shifts have cascading effects on biogeochemical cycles, diel vertical migrations, and the efficiency of carbon flux (Brun et al., 2019), as well as food-web structure and energy transfer (Ratnarajah et al., 2023). Long-term monitoring programs provide essential data on seasonal to

decadal variations in zooplankton communities at local, regional, and global scales (Pitois and Yebra, 2022). Time series analyses are particularly valuable for identifying trends in productivity-related processes, such as recruitment and food web interactions (Beaugrand and Reid, 2003; Brosset et al., 2016; Yebra et al., 2020). Given the increasing pressures on marine environments, expanding observational data on zooplankton is crucial for tracking ecosystem changes and informing conservation efforts (Parr et al., 2003).

In summary, zooplankton are central to marine food webs, biogeochemical cycles, and climate change research. However, knowledge gaps persist regarding their role in active flux and their response to environmental change. Addressing these uncertainties requires integrated approaches that combine biomass and size spectrum analyses with long-term monitoring to enhance our understanding of zooplankton contributions to oceanic carbon cycling and ecosystem dynamics.

1.1. Motivation

The overarching goal of this dissertation is to evaluate the zooplankton biomass, abundance, size structure, and carbon flux in different areas of the North Atlantic Ocean. While changes in zooplankton had been observed across the region, common or contrasting patterns across time-series stations remain underexplored (Pitois and Yebra, 2022). Due to the absence of a fixed monitoring station, we reviewed, gather, and curate all available mesozooplankton biomass data to analyse the variability over the last five decades (1971-2021) in three different productive areas of the Canary Current System, establishing a crucial baseline for future research. Additionally, this dissertation investigates the distribution, abundance, composition, and size spectra of zooplankton over the annual cycle in both open-ocean and upwelling-influenced regions.

Furthermore, this thesis presents the first evaluation of euphausiids' respiration rates using a Generalized Additive Model, providing more accurate estimations and deeper insights into carbon transport. It also contributes to the field by offering the sixth comprehensive study on total active flux, incorporating both zooplankton and micronekton, alongside assessments of passive flux.

1.2. Thesis outline

This thesis establishes a mesozooplankton biomass baseline over the last five decades (1971–2021) in three areas of the Canary Current System. It explores spatial, temporal, and diel patterns of mesozooplankton biomass, abundance, taxonomic composition, size spectra, and carbon flux across different regions of the Atlantic Ocean. The dissertation is structured into four main chapters, each addressing a specific aspect of the mesozooplankton community. Every chapter includes an introduction, a detailed explanation of data and methodology, and a thorough discussion of the results.

Chapter 2 establishes the mesozooplankton community biomass baseline over five decades (1971–2021) in three distinct areas of the Canary Current System across different productive seasons and light periods. This chapter, published in Progress in Oceanography, employs a Generalized Additive Mixed Model to analyze the spatial, temporal, and diel patterns of the mesozooplankton community. Further analyses of seasonal and spatial fluctuations in mesozooplankton size spectra, abundance, and biomass are presented in Chapter 3, published in Marine Environmental Research.

Different aspects of the active flux performed by the mesozooplankton community are discussed in Chapters 4 and 5. Chapter 4, published in Frontiers in Marine Science, evaluates the respiration rates of a key mesozooplankton group to provide accurate estimates of mesozooplankton active flux. Chapter 5, currently under review in Limnology and Oceanography, investigates the spatial variability of mesozooplankton and micronekton active flux. This chapter presents a comprehensive assessment of total active flux across different regions of the Atlantic Ocean and the Mediterranean Sea, offering novel insights into active flux dynamics. Finally, Chapter 6 provides a synthesis of the main findings and concluding remarks.

Chapter 2

A 50-year (1971-2021) mesozooplankton biomass data collection in the Canary Current System: Base line, gaps, trends, and future prospect

Progress in Oceanography, 12 June 2023.

https://doi.org/10.1016/j.pocean.2023.103073

María Couret[1,*], José M. Landeira[1], Ángelo Santana del Pino[2], and Santiago Hernández-León[1]

[1]Instituto de Oceanografía y Cambio Global, IOCAG, Universidad de Las Palmas de Gran Canaria, Unidad Asociada ULPGC-CSIC, Campus de Taliarte, 35214 Telde, Gran Canaria, Canary Islands, Spain.

[2]Departamento de Matemáticas, Universidad de Las Palmas de Gran Canaria, Canary Islands, Spain

2.1. Abstract

Mesozooplankton have been widely used as a bioindicator of marine ecosystems due to their key position in ocean food webs, rapid response to environmental changes, and ubiquity. Here, we show mesozooplankton biomass values in the Canary Current System from 1971 to 2021 in three different areas in relation to mesoscale activity: (1) scarcely affected by mesoscales structures (North of the Canary Islands), (2) affected by mesoscale activity and the presence of the islands (South and around the islands), and (3) close to the Northwest African coastal upwelling system (Upwelling influenced). A Generalized Additive Mixed Model (GAMM) was used to analyze the general mesozooplankton biomass trend throughout the studied period discriminating differences in biomass between the areas, annual cycle, and day-nighttime periods. The GAMM showed a significant negative biomass tendency North of the Canary Islands over the 50-year time-series compared to the South and around the islands, and significant differences between day and nighttime periods ($p<0.001$) and the annual cycle ($p<0.0001$). Linear regression analyses showed different tendencies depending on the area, season, and period. When comparing biomass data of the most oligotrophic zone (north of the islands) with other tropical-subtropical time-series stations in Hawaii (HOTS) and Bermuda (BATS), we obtained increasing biomass tendencies for both fixed time stations but decreasing tendency for our time-series.

Keywords: Time-series, Mesozooplankton biomass, Canary Current System, GAMM, Seasonality

2.2. Introduction

Zooplankton are the suitable sentinel through long-term monitoring due to their key role in almost all the marine food-web. They are responsible for multiple ecosystem services: from regulating fish recruitment via grazing on primary producers or feeding upon microzooplankton (Lomartire et al., 2021) to the transport of carbon downwards into the deep-sea (Hernández-León et al., 2020). Zooplankton mediate the export and sequestration of carbon through (1) consumption of large suspended particles decreasing their sinking rates (Svensen and Nejstgaard, 2003; Mayor et al., 2020), and through (2) diel vertical migrations (DVMs) enhancing active carbon transport efficiency. The outcome of these DVMs influence fish migration, food availability (Perissinotto and McQuaid, 1992), marine food webs trophic interactions (Sommer and Stibor, 2002; Trebilco et al., 2020), population dynamics, flux of energy (Winemiller and Polis, 1996), and recycling processes in the upper ocean (Legendre and Rivkin, 2005; Serranito et al., 2016).

Long-term series become the approach for understanding the natural variability of marine systems and detecting anthropogenic environmental changes (see Parr et al., 2003). Especially nowadays that climate change is a global threat for marine ecosystems, time-series are a valuable tool for tracing those changes. Although effects of climate change on ocean ecosystems are not fully understood, it is known that external variations of temperature or salinity might result in a cascade of indirect interactions and feedbacks through the food web with unpredictable consequences (Johnson et al., 2011; Marshall and Alvarez-Noriega, 2020). During the last decades, anthropogenic pressure over marine ecosystems led into a general tendency for developing plankton indicators to report on ecosystems status and trends (Serranito et al., 2016; Bedford et al., 2020), as plankton community changes are more likely to happen at a shorter time span compared to higher trophic levels (Hays et al., 2005; Serranito et al., 2016). Thus, under the currently climate change scenario, long-term monitoring has become a major concern in biological oceanography

providing crucial information of the habitat conditions, dynamics, and species status, as well as giving integral science support for ecosystem-based management of resources, activities, and services (Harvey et al., 2020). This not only enables the assessment of ecosystem services and the impacts of human activities, but also helps to forecast future trends (Kaufman et al., 2009; Bedford et al., 2020).

The Canary Current System (CCS) is located within the eastern boundary gyre of the North Atlantic Ocean, comprising oceanic oligotrophic waters and the upwelling system off Northwest Africa, showing high variability in physical, chemical, and biological properties (Barton et al., 1998). The CCS holds one of the most important Eastern Boundary Upwelling Systems (EBUS) largely characterized by their high productivity supporting industrial fishing activities (Barton et al., 1998; Schmidt et al., 2020; Fischer et al., 2020; Harvey et al., 2020). However, this area is distinct from other EBUS, such as California, Humboldt, and Benguela, because of the presence of the Canary Islands. The archipelago extends westward from near the African coast to the open ocean, acting as a barrier to the path of the Canary Current inducing an intense mesoscale activity (Barton et al., 2004; Hernández-León et al., 2007). Waters north of the islands are characterized by a sharp oligotrophy due to water column stratification during most of the year, with a sharp deep chlorophyll maximum (Hernández-León et al., 2007).During the winter season, the thermocline and the nutricline (80-100 m depth) are eroded due to surface cooling and convective water mixing (De León and Braun, 1973; Hernández-León et al., 2007; Cianca et al., 2007; Neuer et al., 2007). Then, nutrients are able to reach the euphotic zone, increasing primary production and chlorophyll *a* values (De León and Braun, 1973; Braun, 1980; Arístegui et al., 2001), allowing organisms to burst (Armengol et al., 2019), and promoting the so-called Late Winter Bloom (LWB, Menzel and Ryther, 1961). In spring, the seasonal thermocline is reestablished, restricting the injection of nutrients into the euphotic zone and limiting primary production (Schmoker et al., 2012). The southern area of the archipelago also follows this annual cycle but it holds cyclonic and anticyclonic eddies

shed by the islands and occasional upwelling filaments, enhancing zooplankton biomass (Doty and Oguri, 1956; Hernández-León et al., 2001, 2007).

Zooplankton time-series in different areas of the world showed plankton changes in composition, structure, abundance, biomass, species distribution, and phenology (Hoffmeyer, 2004; Fernández de Puelles et al., 2007; Chiba et al., 2009; Escribano et al., 2012; Steinberg et al., 2012; Bedford et al., 2020). Trends of zooplankton variations are directly related to sea surface temperature (Bedford et al., 2020), water column stratification, primary production (Steinberg et al., 2012), and bottom-up or top-down cascading trophic interactions (Escribano et al., 2012). Knowledge of all variables affecting zooplankton trends is an arduous task, involving the parameterization of both abiotic and biotic factors, interactions between the components of the food web, and the increasingly growing anthropogenic footprint on the oceans. A tentative mesozooplankton time-series in the CCS started in 2012 with the project called "Radial Profunda de Canarias" (RaProCan, Canary Islands Deep Transect, Vélez-Belchí et al., 2015), sampling during the productive season (known as Late Winter Bloom, LWB, from January to April) and the stratified season (SS, from May to December). However, there are no long-term mesozooplankton studies in the CCS. Hence, our aim is to provide the existing data of mesozooplankton biomass in order to establish the mesozooplankton community baseline of the last five decades (1971-2021) in three distinct areas of the CCS during the LWB and the SS, and day-nighttime periods. Spatial, temporal, and diel patterns of mesozooplankton time-series were analyzed using Generalized Additive Mixed Model (GAMM) and linear-regression analysis. Moreover, we compared our time-series to other long-term studies in the Pacific and Atlantic Oceans, such as the time-series stations off Hawaii (HOTS) and Bermuda (BATS). Finally, we explored different time periods in our database to see how biomass tendencies change according to the studied years.

2.3. Material and methods

2.3.1. *Mesozooplankton database sources and analysis*

All the biomass data used in this study is related to mesozooplankton (>200 μm) in the epipelagic layer (0-200 m). First, we compiled all biomass values from existing data published in scientific literature or provided by authors (see Table 4a). Then, we divided the studied area in three different zones according to their mesoscale activity: (1) "North" of the islands, (2) "South and around" the islands, and (3) "Upwelling influenced" area. The division was done according to the mesoscale activity of the area: North grouped those stations sampled north of the Canary Islands, thus oceanic waters not affected by the presence of the islands. South and around (therefore just South) comprised those stations affected by the presence of the islands, thus including those stations close to the islands as they are also influenced due to their proximity. Finally, the third group of stations was characterized because of the influence of the upwelling system (see Fig. 2.1). The limits between the South and the Upwelling area was selected following the results of Hernández-León et al. (2002a) observing a decrease in chlorophyll, primary production, and zooplankton biomass at 60-80 Km from the African coast. A total of 1967 biomass measurements performed in the three areas between 1971 and 2021 were compiled (Fig. 2.1, Table 5a). Biomass values obtained as protein content (Lowry et al., 1951) were transformed to dry weight using a ratio of 2.49 given by Hernández-León et al. (2019a) for tropical and subtropical waters, and converted to carbon units assuming a carbon content of 40% of dry weight (Dam and Peterson, 1993).

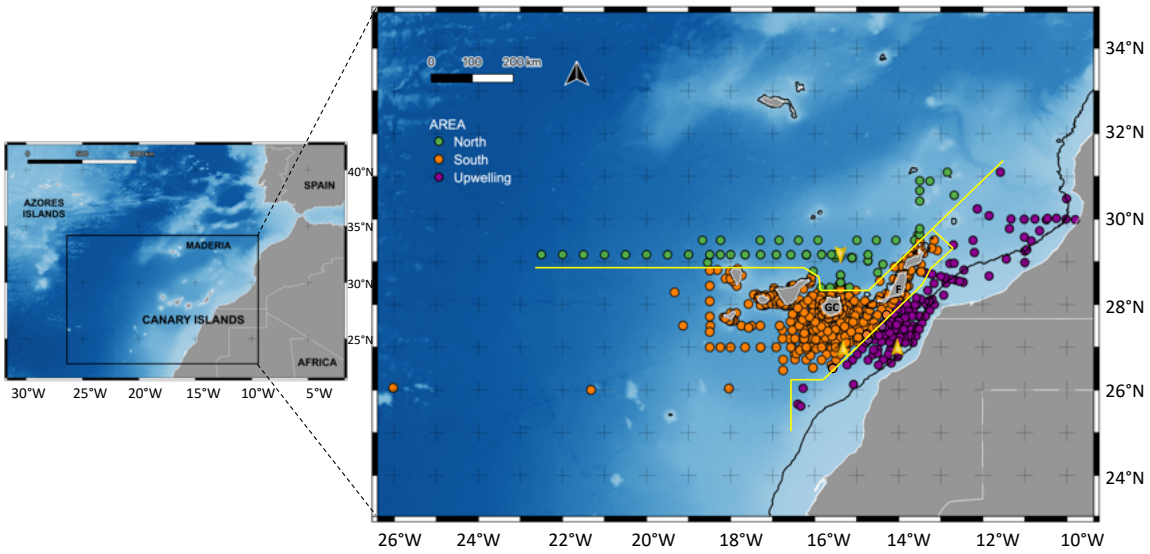

Figure 2.1. Location of the sampled oceanographic stations from 1971 to 2021. Green dots stand for samples obtained North of the Canary Islands, orange dots for samples obtained South and around the islands, and purple dots for those samples in the Upwelling influenced area. Yellow arrow stands for reference points of each delimited area (see text), yellow line indicates the separation between areas according to proximity to the coast and position in relation to the islands, and black line stands for 200 m depth bathymetry. GC stands for Gran Canaria, and F for Fuerteventura.

We obtained a relationship between biomass values from 0 to 100 m depth and biomass values from 0 to 200 m depth using data from the project COCA (see Hernández-León et al., 2019b) and 5 data points located south of the Canary Islands. The relationship was obtained by comparing data from 0 to 200 m depth with 0-100 m depth in the same station sampled every 20-40 m depth intervals using a Longhurst-Hardy Plankton Recorder (LHPR) net (see 2.8). For this comparison, we used day (n = 21) and night (n = 21) samples obtaining the following relationship:

$$\ln(\text{biomass}_{\,0-200\ m\ depth}) = 0.684 + 0.945\ \ln(\text{biomass}_{\,0-100\ m\ depth})$$

(R^2= 0.894, p<0.001, n =42)

Then, the biomass values from 100 m depth to the surface of our database were converted to 0-200 m biomass values and added to our database using the obtained regression (Fig. 2.8).

Mesozooplankton biomass distribution over the 50-years period was studied by averaging annual values in the different areas, distinguishing between day-nighttime periods, to account for changes due to DVM, and between the sampled seasons (i.e. LWB or SS) due to seasonality. Afterwards, least- square linear regressions were fitted for each period and season in the different areas. Annual cycles of mesozooplankton biomass were studied by obtaining the monthly average value in the different areas. Finally, longitudinal zooplankton biomass distribution from the open ocean to the African coast was studied.

2.3.2. *Environmental parameters*

For a better understanding of biomass fluctuations over the study period in the different areas, we studied the annual cycles and time-series of sea surface temperature (SST), chlorophyll *a* (Chl *a*), and primary production (PP) in three fixed points in each area. Environmental data was obtained for the following coordinates (see Fig. 2.1, yellow arrows): (1) North: 29°N 15° 30′ W - coordinates of the European Station for Time-series in the Ocean of the Canary Islands (ESTOC); (2) South: 27°N 15° 30′ W, and (3) Upwelling influenced: 27°N 14°W. Fixed coordinates were selected for the environmental parameters in order to reduce spatial biases in the analysis. Monthly average SST values were directly downloaded from the NOAA website (https://psl.noaa.gov/data/timeseries/) since 1971, using the NCEP/NCAR reanalysis monthly means dataset. Monthly Chl *a* average data was obtained from the Ocean Color web site (https://oceancolor.gsfc.nasa.gov/) using OCI algorithm and Aqua MODIS information (available period from 2002 to 2021). Monthly average PP since 2002 was downloaded from the Ocean Productivity website (http://sites.science.oregonstate.edu/ocean.productivity/) using the Vertical Generalized Production Model (VGPM) as the standard algorithm.

Annual cycles of SST, Chl *a*, and PP were studied by monthly averaging values since 1971 for SST, and since 2002 for PP and Chl *a*. For the time-series tendencies, each environmental data set was detrended to remove the seasonal effects from the time-series, setting a moving average of 12 months, and using an additive model since random fluctuations in the data were roughly constant in size over time (annual cycle). Least-square linear regression analyses to describe tendencies were then performed. Finally, we performed Spearman correlation analyses between monthly values of environmental variables and zooplankton biomass at each location. Normality was tested based on histogram analysis and the Lilliefors (Kolmogorov-Smirnov) test (Lilliefors, 1967). Homogeneity of variance across groups was tested using Levene's test (Levene, 1960).

2.3.3. *Modeling mesozooplankton biomass*

Due to year-gaps biases of our database, we studied mesozooplankton biomass shifts through the 50-years period by using a Generalized Additive Mixed Model (GAMM). First, we transformed biomass (BM) using a Box-Cox transformation to adjust model residual normality:

$$\text{TBM} = \frac{BM^{\lambda}-1}{\lambda}$$

being $\lambda = 0.25$.

For the GAMM we selected the southern area as a reference to test biomass variations, as it was the area with more information:

$$\text{TBM} = \beta_0 + \beta_{0,\,North}\,\text{I}_{North} + \beta_{0,\,Upwelling}\,\text{I}_{Upwelling} + \beta_{0,\,Night}\,\text{I}_{Night} + \beta_1 t + \text{s(day)} + b(\text{cruise}) + \varepsilon$$

where TBM stands for the biomass transformed by Box-Cox transformation.

The model evaluates biomass differences (β_0) and biomass tendencies over the period studied (β_1), considering the random effect *b*(cruise) due to the measurements being made

over time by different ships (cruises). "β_0" stands for biomass global mean value in the South. That means that each β_0 compare biomass differences between the area and the South. "$\beta_{0,\,North}$ " represents biomass mean difference between the North and the South, and "$\beta_{0,\,Upwelling}$" biomass mean difference between the Upwelling influenced area to the South, while the other variables were kept constant. The term "$\beta_{0,Night}$" stands for biomass differences between day and nighttime periods, while keeping the other variables constant. "β_1" evaluates tendencies over the 50-years, keeping the South as the reference area, rather than biomass differences over the time (*t*). "s(day)" is a spline modeling the biomass seasonal pattern. The term *b*(cruise) is a random variable modelling the random variation existing from one cruise to another.

Data for each cruise were measured over several successive days, introducing autocorrrelation between measurements. Also, data from the different cruises were unevenly spaced in time. Thus, it was not possible to use a global autoregressive structure, and so the model included a continuous time autorregresive temporal correlation structure of data in each cruise. This structure assumed that values quite close in time were highly correlated with each other, and this correlation dampened rapidly as time passes. Finally, as time course measurements were sensitive to autocorrelation problems, so we reduced it by implementing an autocorrelative parameter ("*b*(cruise)") in the model. We compared the Bayesian information criterion (BIC) considering or not autocorrelation, obtaining lower values for the model with autocorrelation.

2.3.4. *Databases comparison*

In order to compare with other published time-series, we extracted mesozooplankton biomass values from the North time-series, as the ESTOC is located in that area. For BATS, we downloaded the available database of zooplankton from April 1994 to February 2020 (https://bats.bios.edu/bats-data/). For the analysis of tenden-

cies in each productive period, we distinguished an annual cycle as for the CCS (i.e the LWB from January to April, and the SS from May to December) (Madin et al., 2001). For HOTS, we downloaded the available data from January 1994 to July 2021 (https://hahana.soest.hawaii.edu/hot/hot-dogs/mextraction.html). Unfortunately, data was not available to download for the years 2002, 2003 and 2004. To analyze seasonal patterns, first we distinguished between summer, as the period of higher total mesozooplankton standing stocks, and winter, according to Landry et al. (2001). Then, we estimated the average values and standard deviation for the different seasons and performed linear regressions to obtain tendencies for each season.

2.4. Results

2.4.1. *Time-series biases*

We reviewed, gather, and curate the available mesozooplankton biomass data between 1971 and 2021 with the objective to obtain the baseline for future studies in the area. However, our database had evident biases: (1) mesozooplankton measurements were not performed in a fixed station throughout the years, seasons, and periods, (2) the important gaps for some years, mainly in the North and Upwelling influenced area, (3) the unbalanced number of samples collected during the main seasons (LWB and SS) and periods (day and nighttime), and (4) the absence of taxonomic composition data.

The first bias was addressed by separating the data geographically in three different areas according to their mesoscale activity and analyzing environmental parameters separately in those areas. The second and third bias cannot be directly addressed but were considered in the GAMM by adding the smoother for biomass variations throughout the years, seasons, and periods. Finally, absence of taxonomic data prevents community composition analysis, hampering to explain shifts in biomass due to abundance changes over the annual cycle and through the years.

2.4.2. *Environmental parameters*

Linear regression analysis of the environmental time-series (Fig. 2.2) showed an increase of all the studied parameters in the three areas. SST (Fig. 2.2A) exhibited an increase of about 0.5ºC since 1971 in all the areas, the North area showing the highest increase. The lowest temperatures were found in the Upwelling influenced area and the highest in the South, as expected. Chl *a* (Fig. 2.2B) and PP (Fig. 2.2C) showed the highest values in the Upwelling influenced area, as also observed during the annual cycles. Chl *a*

tendency was slightly higher in the Upwelling influenced, while the highest PP tendency occurred in the South. Time-series of environmental data also showed an important inter-annual variability.

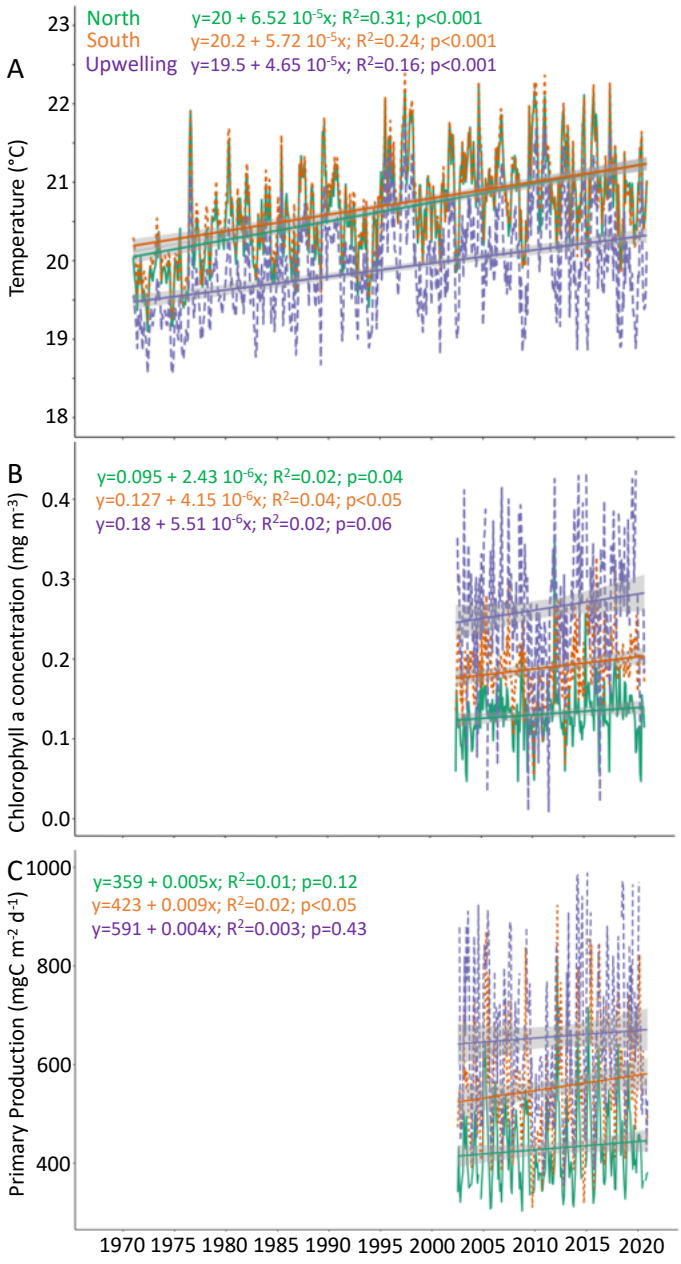

Figure 2.2. Time-series of (A) monthly average sea surface temperature (°C) North (29°N 15° 30′ W), South (27°N 15° 30′ W) and in the Upwelling influenced area (27°N 14°W) since 1971 obtained from remote sensing. (B) Satellite data of chlorophyll *a* concentration ($mg \cdot m^{-3}$), and (C) primary production ($mg\ C \cdot m^{-2} \cdot d^{-1}$) from 2002 to 2020, also using remote sensing data (see text for coordinates explanation).

Table 2.1. Spearman correlation coefficients and p-values between the environmental variables and zooplankton biomass North, South (and around), and in the Upwelling influenced area. "n" stands for the number of samples in each area, "SST" for Sea Surface Temperature, "Chl *a*" for chlorophyll *a* concentration, and "PP" for primary production.

Area	n	Environmental variable	Spearman correlation coefficient	p-value
North	278	SST	-0.31	<0.001
		Chl *a*	-0.23	0.001
		PP	-0.01	0.8
South and around	1516	SST	-0.29	<0.001
		Chl *a*	0.32	<0.001
		PP	0.33	<0.001
Upwelling influenced	173	SST	-0.09	0.3
		Chl *a*	-0.53	<0.001
		PP	-0.53	<0.001

Spearman correlation analysis showed a negative relationship between zooplankton biomass and SST in all areas, only not significant in the Upwelling area (Table 2.1). In that area and in the North, we obtained negative correlations between zooplankton biomass and Chl *a* and PP values, while in the South the correlations were significantly positives.

2.4.3. *Mesozooplankton time-series results*

Time-series linear regression analyses showed a significant general nighttime decreasing tendency of zooplankton biomass (Fig. 2.3A) but no significant tendency for the daytime period. However, different scenarios were observed according to the area. The North (Fig. 2.3B) showed a significant decreasing tendency during daytime, being not significant for the nighttime data over the 50-year time-series. The South (Fig. 2.3C) showed significant tendencies, increasing during daytime but decreasing during nighttime. In the Upwelling influenced area (Fig. 2.3D) we obtained decreasing tendencies over the years, independently of the period, but just significant during nighttime.

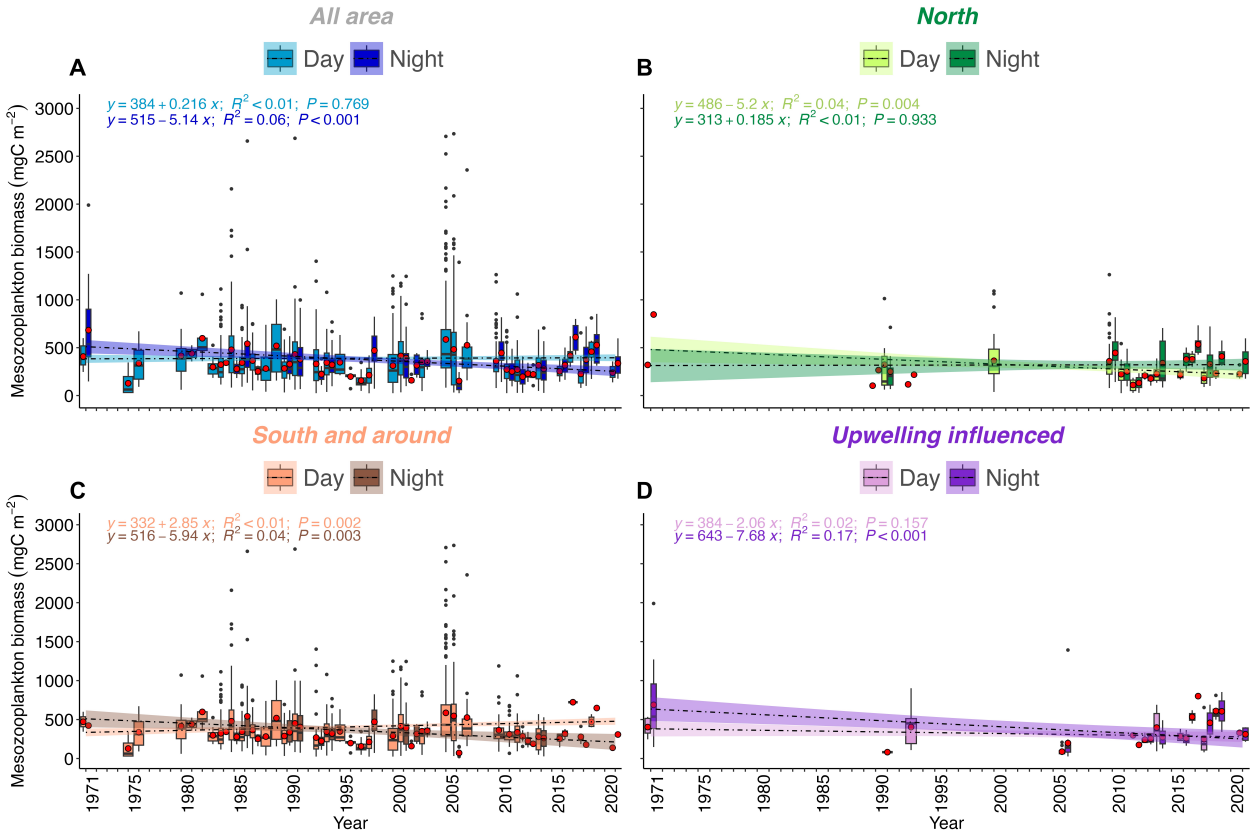

Figure 2.3. Mesozooplankton biomass (mg C·m^{-2}) in the upper 200 m depth during day and nighttime, from 1971 to 2021 in (A) all the area, (B) North, (C) South (and around) the islands, and (D) in the Upwelling influenced area. The size of the box is determined by the upper and lower quartiles, and median is indicated as a horizontal black line inside the box. Black dots represent the outliers and red dots inside the box stand for mean values. Regression line for each period (i.e. day or night) are presenting according to the period color.

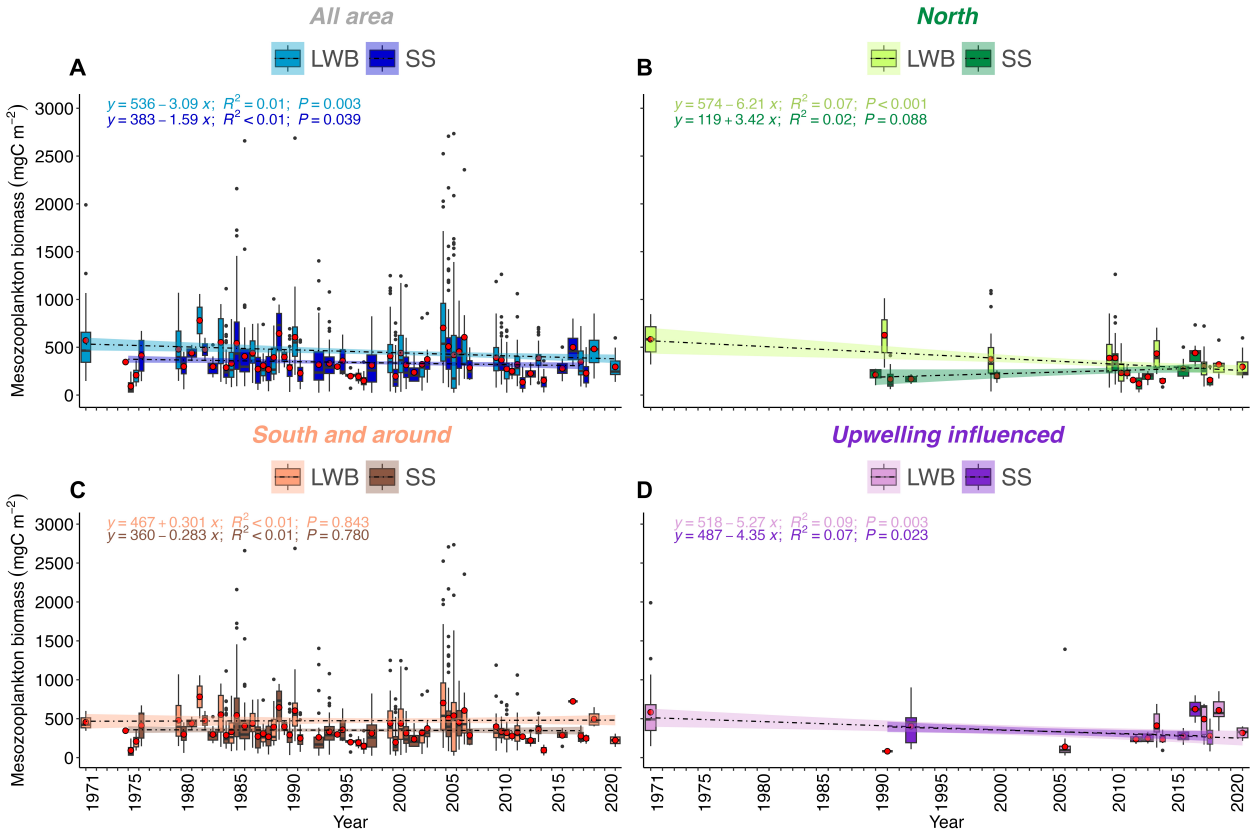

Figure 2.4. Mesozooplankton biomass (mg C·m^{-2}) in the upper 200 m depth during the Late Winter Bloom (LWB) and the Stratified Season (SS), from 1971 to 2021 in (A) all the area, (B) North, (C) South (and around) the islands, and (D) in the Upwelling influenced area, pooled day and nighttime values. The size of the box is determined by the upper and lower quartiles, and median is indicated as a horizontal black line inside the box. Black dots represent the outliers and red dots inside the box stand for mean values. Regression line for each season (i.e. LWB or SS) are presenting according to the period color.

When comparing biomass tendencies during different seasons over the 50-year period, we obtained significant biomass decreasing tendencies in all areas for both seasons (Fig. 2.4A). We also obtained a significant biomass decreasing tendency during the LWB in the North zone (Fig. 2.4B). No significant tendencies were observed in the South (Fig. 2.4C). For the Upwelling influenced area (Fig. 2.4D), both seasons also showed a significant biomass decreasing tendency.

Zooplankton showed a tendency of biomass increase towards the African coast (Fig. 2.5). Moreover, our results showed a biomass accumulation and increase south and around the islands, especially in Gran Canaria and Fuerteventura Islands (between $16.5°$N and $14°$W, location of the islands shown in Fig. 2.1).

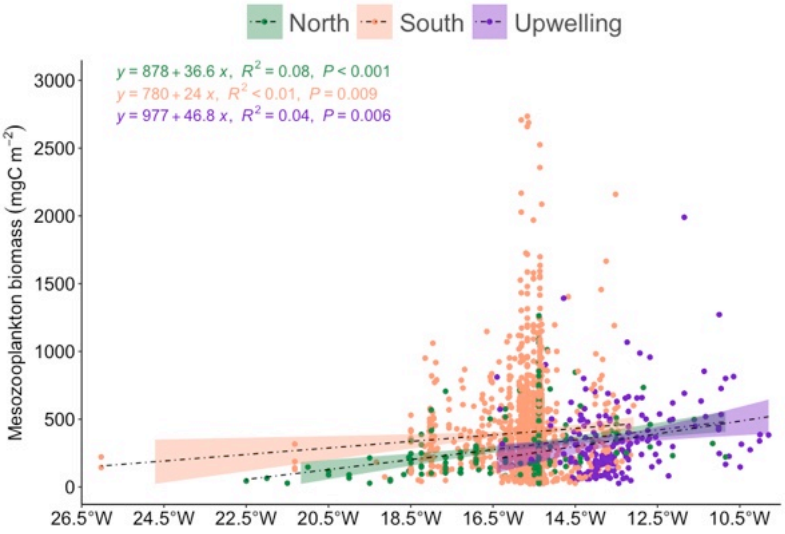

Figure 2.5. Mesozooplankton biomass (mg C·m^{-2}·d^{-1}) longitudinal distribution in the upper 200 m depth from 1971 to 2021, during day and nighttime. Green dots stand for mesozooplankton biomass.

2.4.4. *Annual cycle of environmental parameters and mesozooplankton biomass*

SST (Fig. 2.6A) displayed low temperatures during the LWB as expected, with the lowest values during March, and increasing during the SS. The lowest temperature for the different zones were found in the Upwelling influenced area throughout the annual cycle. In the latter area, Chl *a* (Fig. 2.6B) and PP (Fig. 2.6C) monthly average values were higher compared to the other areas, displaying a strong peak during August. For the North and South, the Chl *a* and PP maxima were found during February, right before the zooplankton biomass increase during March (see below).

Mesozooplankton biomass annual cycle (Fig. 2.6D) in the North and South displayed similar pattern throughout the year: a biomass increase during the LWB, then decreasing through the SS, and exhibiting a maximum during March. In the North, biomass showed higher values during March and June. On the other hand, in the Upwelling influenced area we found higher values during February, April, and August.

Zooplankton biomass values during the LWB and SS season are given in Table 2.2 jointly with the average values for all data, during daytime. As observed, average values during the LWB were about a 26% higher in the northern and southern areas compared to the stratified season.

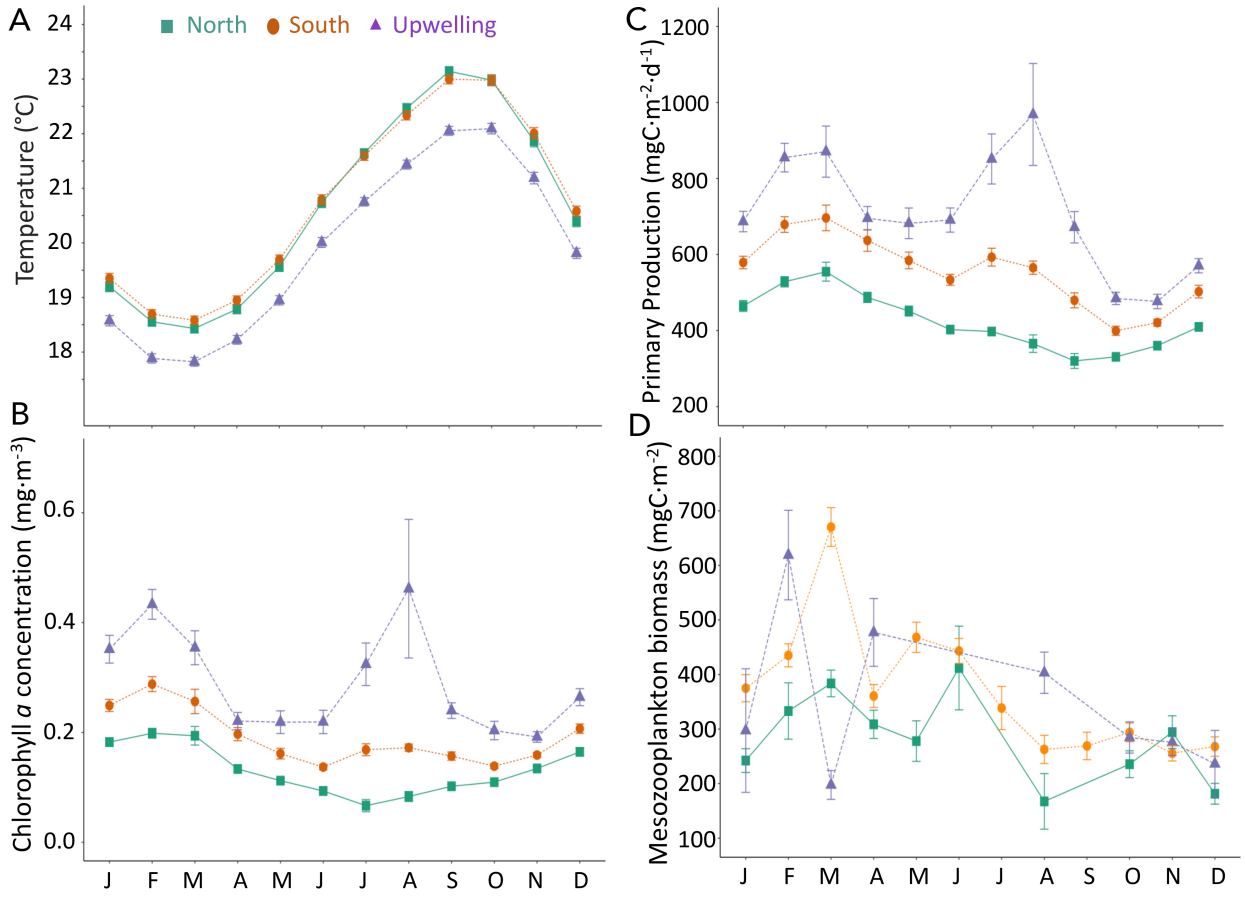

Figure 2.6. Annual cycle of (A) temperature (°C) since 1971, (B) chlorophyll *a* concentration (mg·m^{-3}), (C) primary production (mg C·m^{-2}·d^{-1}) since 2002, and (D) mesozooplankton biomass (mg C·m^{-2}), pooled day and nighttime values. Green squares represent the North, orange dots the South (and around), and purple triangles the Upwelling influenced area. Symbols stand for mean values and lines above and under the dots for standard error. Environmental variables were obtained by remote sensing (see text).

Table 2.2. Average mesozooplankton biomass (mg C·m^{-2}) and standard deviation ($\pm$ SD) in all the area studied, North, South (and around the islands), and in the Upwelling influenced area sampled during the Late Winter Bloom (LWB) and the Stratified Season (SS), during day time. "n" stands for the number of samples in each area/season/period.

Area	Season	Mesozooplankton biomass	n
All area	LWB	445.4 $\pm$ 353.8	709
	SS	343.0 $\pm$ 274.6	896
North	LWB	320.3 $\pm$ 200.4	115
	SS	239.9 $\pm$ 178.0	70
South and around	LWB	486.5 $\pm$ 377.5	543
	SS	352.3 $\pm$ 283.6	773
Upwelling influenced	LWB	289.8 $\pm$ 218.3	51
	SS	343.3 $\pm$ 193.0	53

2.4.5. *Modeling mesozooplankton biomass*

Due to our time-series biases mentioned above, we opted to use a GAMM that considered the information-gaps and could provide a more accurate statistic point of view for biomass differences between areas compared to the South (β_0) and tendencies (β_1) in the different areas through the 50-year study, seasons, and periods. Results from the model (Table 2.3) showed no significant biomass tendency in the South (β_1, p-value = 0.8) over the 50-year time-series. However, significant differences were found in the tendencies between the North and the South ($\beta_{1,\,North}$, p-value = 0.02), thus the North is undergoing a decrease of biomass ($\beta_{1,\,North}$ transformed biomass value tendency = -0.000081). No significant differences were found between the South and the Upwelling influenced tendencies ($\beta_{1,\,Upwelling}$, p-value = 0.61). The model found significant day/night differences ($\beta_{0,\,Night}$, p-value$<$0.0001), and biomass differences in the South through the 50-year studied ($\beta_{0,\,South}$, p-value$<$0.0001).

Table 2.3. Results obtained from the GAMM for the 50-year time-series. β_0 evaluates biomass differences in the South over the period. $\beta_{0,\,North}$ evaluates differences between the South (reference area) and the North, and $\beta_{0,\,Upwelling}$ differences between the South and the Upwelling influenced. $\beta_{0,\,Night}$ evaluates daily biomass differences. β_1 examine biomass tendencies over the time in the South. $\beta_{1,\,North}$ evaluates differences in tendencies between the South and the North, and $\beta_{1,\,Upwelling}$ differences in tendencies between the South and the Upwelling influenced. s(day) correspond to the smoother for annual variations.

Parameter	Transformed biomass values	±SD	p-value	edf
β_0	12.77	0.57	<0.0001	
$\beta_{0,North}$	1.51	1.07	0.16	
$\beta_{0,Upwelling}$	0.79	0. 93	0.39	
$\beta_{0,Night}$	0.90	0.23	<0.0001	
β_1	-0.000007	0	0.80	
$\beta_{1,North}$	-0.000081	0	0.02	
$\beta_{1,Upwelling}$	-0.000016	0	0.61	
s(day)			<0.0001	4.95

The model also showed a significant biomass annual variation (s(day) p-value$<$0.0001), increasing between January and March and decreasing through the rest of the year, as shown by the biomass annual cycles. The day/night variability found by the model in the linear regression tendencies, the seasonal changes in biomass obtained in the regression, and annual cycle were also supported by the model. However, environmental parameters were not considered in the model as the different way of obtaining the biological and environmental data introduced a source of variability larger than the amount of variability they could explain. This could be solved by obtaining the environmental and biological data at the same time.

2.4.6. *Databases comparison*

When comparing the same time frame of our North time-series (Fig. 2.7A) with those data of HOTS (Fig. 2.7B) and BATS (Fig. 2.7C), linear regression analysis showed a biomass decreasing tendency during both seasons in the North CCS time-series, whereas in the other time-series showed biomass increasing tendencies over the period studied. Our average values over the study period (299.95 $\pm$ 189.69 mg C·m^{-2}) were similar to those obtained in HOTS (325.77 $\pm$ 161.45 mg C·m^{-2}), but more than two-times lower than those recorded in BATS (749.25 $\pm$ 502.19 mg C·m^{-2}).

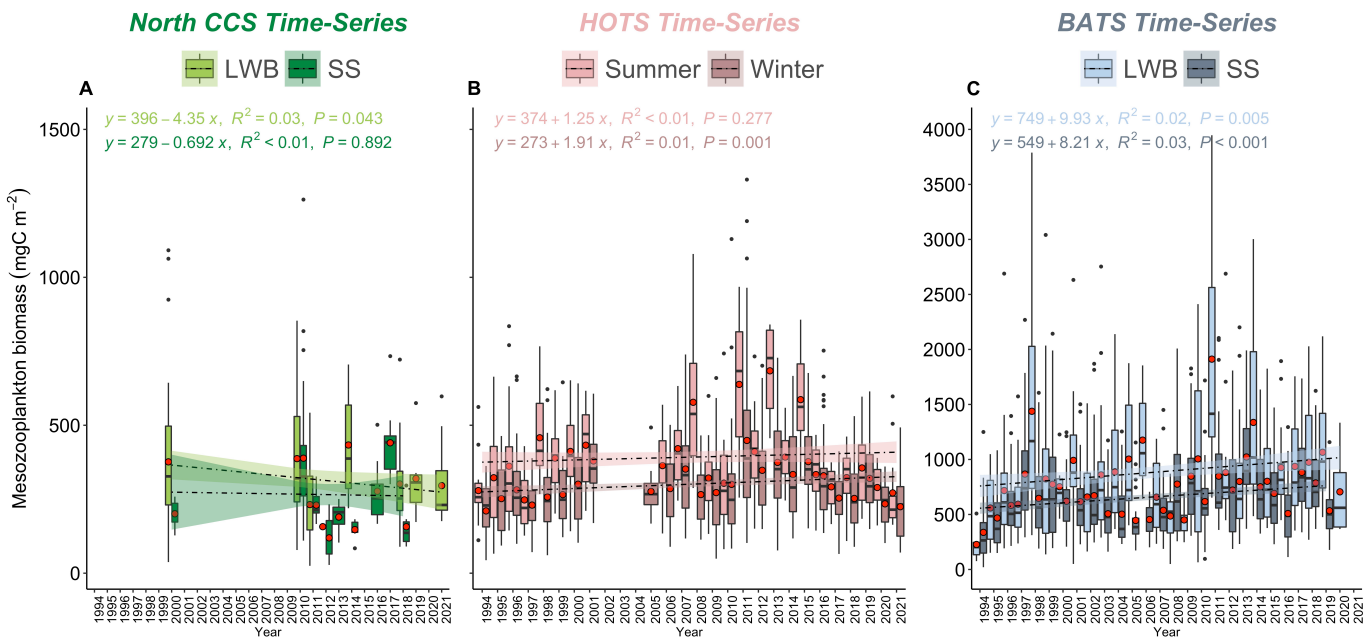

Figure 2.7. Mesozooplankton biomass (mg C·m^{-2}) in the upper 200 m depth during the Late Winter Bloom (LWB) and the Stratified Season (SS), from 1994 to 2021 in the (A) North of the Canary Current System (CSS), during day and nighttime, (B) Hawaii Ocean Time-series (HOTS), and (C) Bermuda Institute of Ocean Sciences Time-series (BATS), during day and nighttime. Data from HOTS was downloaded from https://hahana.soest.hawaii.edu/hot/hot-dogs/mextraction.html, and BATS data from https://bats.bios.edu/bats-data/. The size of the box is determined by the upper and lower quartiles, and median is indicated as a horizontal black line inside the box. Black dots represent the outliers and red dots inside the box stand for mean values. Regression line for each season (i.e. LWB or SS) are presenting according to the period color.

2.5. Discussion

Mesozooplankton biomass data over the last five decades (1971-2021) was compiled and examined in the CCS with the aim of providing a dataset for this subtropical region of the East Atlantic that lacks of a proper time-series station (Ratnarajah et al., 2023). GAMM model showed a significant decreasing tendency of mesozooplankton biomass over the 50-year period North of the islands, the most oligotrophic area. Tendencies were also obtained for a 30-year period in order to compare to other oceanic time-series in the ocean (HOT and BATS).

2.5.1. *Time-series biases*

Undeniably, the 50-year time-series showed some crucial biases complicating the interpretation of results, as mentioned above. Horizontal advection promotes a bias in sampling zooplankton communities, so hauls in the same geographical position also lacks sinopticity. Therefore, the division of the CCS in different areas makes our database somewhat feasible to become three time-series. Nevertheless, a fixed point could dismiss to a great extent the noise in the GAMM analysis, moreover in a highly variable area as the CCS. Further, the already well-known annual cycle of environmental parameters and zooplankton (Hernández-León et al., 2007), along with the lack of continuous data during the years and seasons, hampers the statistical analysis of the results. Also, a further major weakness of our database, which may account for much of the variation in zooplankton biomass is the lack of taxonomic information.

There is a growing recognition that knowledge of the community composition adds considerable interpretive value to any regional time-series (Mackas and Beaugrand, 2010). Standing zooplankton biomass production were used as a rough proxy for total annual productivity as it regulates material and energy flow through food webs, and therefore

the amount of food for higher trophic levels (Mackas and Beaugrand, 2010; Hébert et al., 2017). High ratios of new production to total community production results in zooplankton being dominated by large copepods with short, efficient and nutritionally-rich food webs, thus supporting larger food-webs. However, this top-down control might have a strong negative effect on standing stocks resulting in a zooplankton biomass decrease. This could be assessed only by taxonomic information (Kodama et al., 2022). Moreover, when the phytoplankton community depend on recycled nitrogen, the zooplankton is dominated by gelatinous zooplankton (salps, doliolids, ctenophores) and small crustaceans, supporting a far smaller biomass of higher trophic levels (see Richardson, 2008). Thus, zooplankton production is directly affected by the taxonomic and functional community structure (St-Gelais et al., 2023). Knowledge of the taxonomic composition could help to understand the natural variability of zooplankton.

2.5.2. *Mesozooplankton time-series*

Zooplankton is being notably affected by climate change, responding in terms of long-term shifts in their biomass and abundance, composition, size, phenology, and spatial distribution (Richardson, 2008; Mackas et al., 2012; Brun et al., 2019; Conroy et al., 2023; Huggett et al., 2023; Kodama et al., 2022). The outcomes lead to a still poorly understood renewal of the biogeochemical cycles, changes in daily vertical migrations which strongly influence the carbon flux (Brun et al., 2019), and shifts in the food-web size structure and transfer efficiency (Ratnarajah et al., 2023). Results from our database showed a general temporal decrease of zooplankton biomass over the 50-year period, contrasting with reported tendencies in other time-series carried out in other subtropical oceanic sites (Madin et al., 2001; Steinberg et al., 2012). Analysis of the causes of zooplankton shifts over the 50-year period in a such different area is a tough task, thus we opted for the analysis of each area separately.

We found a zooplankton biomass decreasing tendency during the daytime and during the LWB, and a negative Spearman correlation with the environmental variables in the northern area. This decrease during the LWB might be related to the temperature increase as warmer and more stratified waters are usually associated with lower biomass (Steinberg et al., 2012). Atmospheric patterns from 1950 to 2008 showed a rather clear change in the CCS (Alonso-Pérez et al., 2011). While the Azores High during winter displayed an oceanic pattern transporting oceanic winds from the Northern Atlantic Ocean, during the 21^{st} century the high pressure entered the African continent transporting winds from the Sahara Desert. This change in the wind pattern during winter could be enhancing ocean temperature in the CCS as observed for the area (Arístegui et al., 2009). Thus, a higher ocean stratification could be diminishing the erosion of the seasonal thermocline during winter as the effect of less convective mixing (Cianca et al., 2007). However, the available time-series of chlorophyll and primary production do not show this tendency. In any case, the latter time-series are still short ($\approx$ 20 years) and interannual variability could mask the real tendency. In fact, the zooplankton biomass time-series during the last 10 years showed a positive tendency (not shown) due to the low biomass during 2010 and large biomass during years 2017 and 2019, something also observed in the chlorophyll and PP data.

The upwelling affected area also showed a mesozooplankton biomass decreasing trend independently of the period or season. This decrease could be driven by atmospheric pattern described above but also wind forcing and other oceanic processes influencing the upwelling system. Global modeling studies projected consistent changes in the dominant subtropical atmospheric pressure systems that drive coastal upwelling in the EBUSs. In the CCS, climate models project a poleward displacement of the Azores High, resulting in stronger and weaker upwelling-favorable winds off the Iberian Peninsula and northwest Africa, respectively. Weakening upwelling intensity is especially prevalent during summer off northwest Africa, while the intensification in the northern CCS corresponds with more

frequent high-intensity upwelling events and an extension of the upwelling season (see references in Bograd et al., 2023). Marrero-Betancort et al. (2020) showed a decreasing trend of wind intensity from the 1960s to 2010 and increasing thereafter in CCS. This decreasing trend could explain, at least in part, the decrease in zooplankton biomass as the effect of the expected decrease in Ekman transport due to the decrease in wind intensity. However, how the EBUS will respond to anthropogenic climate change is still unknown and changes in the upwelling system is clearly outside of the scope of this study.

The spatial distribution of zooplankton biomass across the longitudinal gradient showed higher values near the African coast and south and around the islands. The island-mass effect was long ago described in the Canary Island waters (Hernández-León, 1988b, 1991; Hernández-León et al., 2001). These studies explained the higher zooplankton biomass around the islands as the effect of accumulation due to the physical disturbance of the current due to the presence of the islands. Zooplankton biomass is also transported by upwelling filaments generated in the upwelling system (Hernández-León et al., 2002b). This effect of mesoscale activity in the area promoted higher zooplankton biomass values near the African coast and around the islands, decreasing towards the central gyre waters (Fig. 2.5).

2.5.3. *Annual cycle*

The production cycle in the CCS is well documented (see Hernández-León et al., 2007): during most of the annual cycle the oceanic area is characterized by strong stratification but the thermocline is eroded during the LWB due to atmospheric cooling, promoting convective mixing, and allowing organisms to burst (Cianca et al., 2007; Neuer et al., 2007; Schmoker et al., 2012; Armengol et al., 2019). The enhanced PP allows zooplankton to grow increasing their biomass, and with a community characterized mainly by Copepoda, Hydrozoa, and Salpidae (Couret et al., 2023b). After the LWB, the thermocline is

reestablished, and zooplankton biomass decreased after depleting the available food. During the rest of the annual cycle, the zooplankton is dominated by smaller size fractions (Couret et al., 2023b). Results from the 50-year time-series, clearly show this annual cycle of environmental variables and zooplankton biomass, increasing during the LWB and decreasing through the SS. However, in the North we also observed a biomass increase during late spring (June). This maximum coincides with the maximum penetration of solar light in the area and it should be the subject of future research. In the upwelling area, zooplankton showed a higher biomass in August due to the higher intensity of the Trade Wind promoting Ekman transport and upwelling (Hernández-León et al., 2007). These areas are complex systems supporting a diversity of mid-trophic-level species key to the incorporation of primary productivity into ecosystem diversity (Bograd et al., 2023).

2.5.4. *Modeling mesozooplankton biomass*

GAMM results contribute statistically to the analysis of mesozooplankton biomass, becoming a powerful tool for data analysis since they incorporate non-parametric regressions, smoothing techniques, and generalized distributional modeling (Liu and Xiang, 2019). The model found a significant negative biomass tendency only in the North over the 50-year period, but no significant tendency was found in the Upwelling influenced area where the linear regression showed significant tendencies (except during daytime). This discrepancy should be related to the different approaches used. The GAMM incorporated more factors in the analysis such as the daily variance, differences between cruises or season to year gaps, which makes the analysis more robust than the linear regression analysis. The differences between the North and South tendencies could be directly related to the accumulation of zooplankton biomass south of the islands due to "island-mass effect" (Doty and Oguri, 1956). This term is related to the increase of plankton biomass associated with oceanic islands due to the disturbance of the oceanic flow, forming ed-

dies downstream, thus affecting the distribution of nutrients, Chl *a*, PP and fish larvae (Hernández-León et al., 2001). The model also found significant day/night differences due to DVM, and between seasons (LWB and SS), because of the different productivities found around the annual cycle.

2.5.5. *Databases comparison*

The latest published time-series in Hawaii (station ALOHA) showed mesozooplankton biomass increasing over 20 years (1994-2013) related to bottom-up food-web dynamics (Valencia et al., 2016). In Bermuda (BATS), Steinberg et al. (2012) also found an increase of zooplankton biomass from 1994 to 2011, also suggesting to be promoted by bottom-up control. Extending the time-series analysis to 2021 in those time-series stations, we still obtained a positive tendency for both time-series stations (Fig. 2.7). By contrast, the North CSS time-series showed a biomass decreasing trend for that period.

Finally, time-series are crucial to understand the dynamics of pelagic ecosystems but most observational series were carried out only for a few decades long, limiting our understanding of long-term zooplankton dynamics (Jonkers et al., 2022). Mackas and Beaugrand (2010) suggested a century or more for the zooplankton time-series to be optimal. However, present-day time-series are to a great extent shorter and zooplankton interannual variability promote shifts in the total standing stock (Mackas and Beaugrand, 2010), community dominance and size structure (Conroy et al., 2023), spatial distribution (Huggett et al., 2023), or environmental-related variations (see Ratnarajah et al., 2023). Long time-series are needed to account for consistent biomass shift over time. Our study supports the notion that zooplankton in the North CCS time-series is decreasing as warming increases in the area. This could be the effect of the shift in the Atlantic Multidecadal Oscillation (AMO) as our time-series started during the colder period in the 70´s and finished during the warmer phase during the present century (Alexander et al., 2014). Thus, the decreas-

ing trend could be the effect of natural variability (AMO), or it is a symptom of the global warming in the area and the expected increase of oceanic deserts as the expansion of the subtropical gyre system (Siemer et al., 2021). A larger series is thus needed as suggested by Mackas and Beaugrand (2010).

2.6. Conclusions

Our database gathers all available mesozooplankton biomass data in three different mesoscale activity areas of the CCS, showing biomass patterns over the 50-year period and the two characteristic productive seasons in these subtropical waters. The lack of time-series monitoring programs in the tropical-subtropical East Atlantic add value to our historical compilation of zooplankton biomass data, highlighting the need for long-term surveillance of mesozooplankton biomass. We suggest that the present database should be considered as a baseline before setting a future permanent time-series monitoring program in the CCS.

For that, we encourage to set fixed time-series stations according to the mesoscale area with a monthly sampling strategy, or at least during the less and most productive season in each area (i.e. during the LWB in the North and South, and during August in the Upwelling influenced area). Light period must also be considered when sampling, ideally during both day- and nighttime to account for diel vertical migrants variability. Finally, we consider that in situ hydrographic parameters (e.g. temperature, salinity, chlorophyll a) measured jointly with zooplankton biomass would give a more accurate idea of the relationship between the abiotic and biotic components of the environment. In spite of the biases of this baseline data, the results showed a zooplankton biomass decreasing trend in the oligotrophic zone suggesting an effect of the increasing warming observed in the Canary Current. Whether this trend is natural variability as the effect of the AMO or global warming will remain.

2.7. Acknowledgments

This study was funded by projects RaProCan from the Spanish Institute of Oceanography (IEO), DESAFÍO (PID2020-118118RB-I00) from the Spanish Ministry of Science and Innovation, and projects TRIATLAS (Grant Agreement 817578) and SUMMER (Grant Agreement 817806) from the European Union (EU) Horizon 2020 Research and Innovation Programme, and the EU Interreg projects of cooperation RESCOAST (MAC2/3.5b/314) and MACCLIMA (MAC2/3.5b/254) from the V-A MAC 2014-2020. María Couret was supported by a postgraduate grant (TESIS2022010116) co-financed by the Agencia Canaria de Investigación, Innovación y Sociedad de la Información de la Consejería de Universidades, Ciencia e Innovación y Cultura and by the Fondo Social Europeo Plus (FSE+) Programa Operativo Integrado de Canarias 2021-2027, Eje 3 Tema Prioritario 74 (85%). José Landeira was supported by the Beatriz Galindo individual grant BEAGAL 18/00172.

2.8. Author contributions

M.C. and S.H.L. conceptualised, conceived, and developed the work with input from J.M.L.; M.C. and S.H.L. contributed to data acquisition; M.C. and A.S.P. developed the model; M.C. analysed the data and created all figures; M.C. drafted the manuscript, and all authors contributed substantially to its improvement. All authors approved the final submitted manuscript.

2.9. Data availability statement

The raw data supporting the conclusions of this article are publicly available through PANGAEA platform: Couret et al. (2023a) https://doi.org/10.1594/PANGAEA.962439.

2.10. Supplementary material

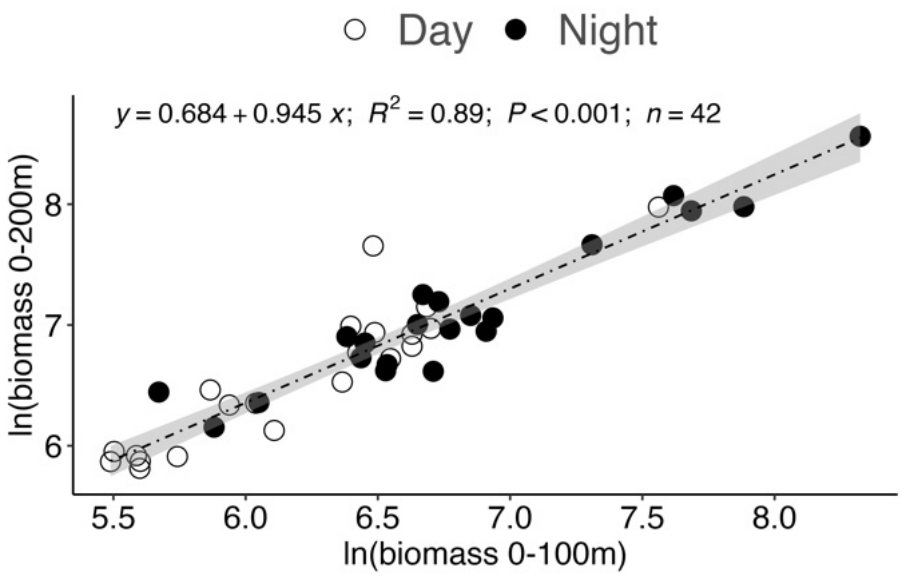

Figure 2.8. Relationship between biomass values from 0-100 m depth and biomass values from 0-200 m depth using data from the project COCA (see Hernández-León et al., 2019b) and 5 data points located south of the Canary Islands

Table 4a. Data information compiled for the time-series analysis. "Project" column indicates if the data belongs to a specific project, unfilled if not belong to any specific project. LWB stands for Late Winter Bloom (from January to April), and SS for Stratified Season (from May to December). Data not published is indicated in "Reference" column. *Only the northern transect was considered for the database.

Proyect	Reference	Year	Net depth (m)	Net type	Period	Zone	Season	Biomass units
Centre National Pour L'Exploitation Des Oceans (CNEXO)	Mediprod (1974)	1971	50	WP-2	Day and Night	North	LWB	$mgDW{\cdot}m^{-2}$
			200			Upwelling		
	Braun (1980)	1975-1976	200	WP-2	Day	South	LWB	$mgDW{\cdot}m^{-2}$
							SS	
	Real et al. (1981)	1976	200	WP-2	Day	South	SS	$mgDW{\cdot}m^{-3}$
	Santamaría et al. (1989)	1980	100	WP-2	Day	South	LWB	$mgDW{\cdot}m^{-3}$
							SS	
	Hernández-León (1988a)	1981-1982	200	WP-2	Day	South	LWB	$mgDW{\cdot}m^{-2}$
							SS	
	Fernández de Puelles and Braun (1996)	1983-1985	250	Juday Bogorov (50 cmx2)	Day and Night	South	LWB	$mgDW{\cdot}m^{-3}$
							SS	
Estudio de la Plataforma Sur (E.P.S.)	Hernández-León (1988b)	1984-1985	100	WP-2	Day and Night	South	LWB	$mgprot{\cdot}m^{-2}$
			200				SS	
	Hernández-León (1988c)	1986	100	WP-2	Day and Night	South	SS	
			200					
	Gómez (1991)	1986-1987	90	WP-2	Day	South	LWB	$mgprot{\cdot}m^{-2}$
							SS	
		1987-1988	25	WP-2	Day and Night	South	LWB	
							SS	
Taliarte	Unpublished	1988-1989	100	WP-2	Day	South	LWB	$mgprot{\cdot}m^{-2}$
							SS	
Canarias85	Hernández-León and Rodal (1987)	1985	50	WP-2	Day	South	SS	$mgprot{\cdot}m^{-3}$
			70					
			200					
Efecto de Masa de Isla en el Archipiélago Canario (E.M.I.A.C)	Almeida Peña (1996)	1989-1991	200	WP-2	Day and Night	North	LWB	$mgprot{\cdot}m^{-2}$
						South	SS	
"Coastal Transition Zone: Canary Islands" (Marine Science and Technology, MAST)		1991-1993	200	WP-2	Day and Night	North	SS	
				LHPR		South		
						Upwelling		

Table 4b. Continued: Data information compiled for the time-series analysis. "Project" column indicates if the data belongs to a specific project, unfilled if not belong to any specific project. LWB stands for Late Winter Bloom (from January to April), and SS for Stratified Season (from May to December). Data not published is indicated in "Reference" column. *Only the northern transect was considered for the database.

OIMAC (91/08 GAC)	Unpublished	1994	200	WP-2	Day and Night	South	SS	mgprot·m^{-2}
Fish Aggregation Devices (FADS)		1995-1996	100	WP-2	Day	South	LWB SS	mgDW·m^{-3}
Bocaina		1997	200	WP-2	Day	South	SS	mgDW·m^{-2}
FRENTES (C.I.C.Y.T. AMB95-0731)	Yebra et al. (2005)	1998	200	LHPR	Day and Night	South	SS	mgprot·m^{-2}
MESOPELAGIC (MAR97-1036)	Hernández-León et al. (2004)	2000	100	WP-2	Day	North South	LWB SS	mgDW·m^{-2}
PELAGIC (EU-CICYT 1FD97-1084)	Unpublished	2000-2003	90	WP-2	Day and Night	South	LWB SS	mgprot·m^{-2}
COCA I (REN2000 1471-CO2-O1-MAR)*	Hernández-León et al. (2019b)	2002	200	LHPR	Day and Night	South Upwelling	SS	mgprot·m^{-2}
COCA II (REN2000 1471-CO2-O1-MAR)*	Hernández-León et al. In prep	2003	200	LHPR	Day and Night	South Upwelling	LWB	
CONAFRICA (C.I.C.Y.T. CTM2004-02319)	Moyano et al. (2009)	2005-2007	90	WP-2	Day	South	LWB SS	mgprot·m^{-2}
	Unpublished	2006	200	LHPR	Day and Night	South Upwelling	LWB	
LUCIFER (CICYT CTM2008-03538)	Herrera et al. (2017)	2010-2011	200	WP-2	Day and Night	North South	LWB SS	mgDW·m^{-2}
CETOBAPH (CGL2009-13112)	Ariza et al. (2016)	2012	200	WP-2	Day and Night	North South	LWB	mgprot·m^{-2}
MIOCEAN (ULPGC-Master Internship data)	Unpublished	2019	200	WP-2	Day and Night	South	LWB	mgprot·m^{-2}
Radial Profunda de Canarias (RAPROCAN)	Couret et al. (2023b)	2012-ongoing	200	WP-2	Day and Night	North South Upwelling	LWB SS	mgprot·m^{-2}

Table 5a. Information of zooplankton biomass data points per year, month, area, and period.

Sampling	Month	Period	Zone	Number of biomass data points
1971	January	Night	Upwelling area	2
1971	January	Day	Upwelling area	1
1971	February	Night	North of the Islands	1
1971	February	Day	North of the Islands	1
1971	February	Night	South and around the Islands	1
1971	February	Day	South and around the Islands	2
1971	February	Night	Upwelling area	15
1971	February	Day	Upwelling area	9
1975	April	Day	South and around the Islands	1
1975	May	Day	South and around the Islands	1
1975	June	Day	South and around the Islands	1
1975	July	Day	South and around the Islands	1
1975	September	Day	South and around the Islands	1
1975	October	Day	South and around the Islands	1
1975	November	Day	South and around the Islands	1
1976	January	Day	South and around the Islands	1
1976	February	Day	South and around the Islands	1
1976	March	Day	South and around the Islands	1
1976	April	Day	South and around the Islands	1
1976	May	Day	South and around the Islands	1
1976	July	Day	South and around the Islands	6
1980	January	Day	South and around the Islands	6
1980	March	Day	South and around the Islands	6
1980	May	Day	South and around the Islands	3
1980	June	Day	South and around the Islands	3
1981	October	Day	South and around the Islands	1
1981	December	Day	South and around the Islands	1
1982	March	Day	South and around the Islands	1
1982	April	Day	South and around the Islands	1
1982	May	Day	South and around the Islands	1
1982	July	Day	South and around the Islands	1
1982	November	Day	South and around the Islands	1
1983	June	Day	South and around the Islands	1
1983	July	Day	South and around the Islands	1
1983	August	Day	South and around the Islands	1
1983	September	Day	South and around the Islands	1
1983	October	Day	South and around the Islands	2

Table 5b. Continued: Information of zooplankton biomass data points per year, month, area, and period.

1983	November	Day	South and around the Islands	3
1983	December	Day	South and around the Islands	2
1984	February	Day	South and around the Islands	1
1984	March	Day	South and around the Islands	3
1984	April	Night	South and around the Islands	1
1984	April	Day	South and around the Islands	7
1984	May	Day	South and around the Islands	10
1984	June	Day	South and around the Islands	9
1984	July	Day	South and around the Islands	9
1984	August	Day	South and around the Islands	9
1984	September	Day	South and around the Islands	9
1984	October	Day	South and around the Islands	9
1984	November	Day	South and around the Islands	1
1984	December	Day	South and around the Islands	21
1985	January	Day	South and around the Islands	10
1985	February	Day	South and around the Islands	12
1985	March	Day	South and around the Islands	9
1985	April	Day	South and around the Islands	9
1985	May	Day	South and around the Islands	9
1985	June	Day	South and around the Islands	51
1985	November	Night	South and around the Islands	2
1985	November	Day	South and around the Islands	25
1986	May	Night	South and around the Islands	25
1986	May	Day	South and around the Islands	43
1986	November	Day	South and around the Islands	6
1986	December	Day	South and around the Islands	6
1987	February	Day	South and around the Islands	9
1987	March	Day	South and around the Islands	7
1987	April	Day	South and around the Islands	2
1987	May	Day	South and around the Islands	7
1987	November	Day	South and around the Islands	4
1987	December	Night	South and around the Islands	3
1987	December	Day	South and around the Islands	5
1988	February	Day	South and around the Islands	5
1988	March	Day	South and around the Islands	5
1988	May	Day	South and around the Islands	5
1988	June	Day	South and around the Islands	6

Table 5c. Continued: Information of zooplankton biomass data points per year, month, area, and period.

1988	November	Day	South and around the Islands	7
1988	December	Day	South and around the Islands	1
1989	January	Day	South and around the Islands	2
1989	February	Day	South and around the Islands	2
1989	March	Day	South and around the Islands	4
1989	April	Day	South and around the Islands	2
1989	May	Day	South and around the Islands	8
1989	June	Day	South and around the Islands	2
1990	February	Day	South and around the Islands	5
1990	June	Night	North of the Islands	2
1990	June	Day	North of the Islands	1
1990	June	Night	South and around the Islands	13
1990	June	Day	South and around the Islands	31
1991	March	Night	North of the Islands	2
1991	March	Day	North of the Islands	2
1991	March	Night	South and around the Islands	22
1991	March	Day	South and around the Islands	27
1991	October	Night	North of the Islands	7
1991	October	Day	North of the Islands	5
1991	October	Night	South and around the Islands	23
1991	October	Day	South and around the Islands	24
1991	October	Day	Upwelling area	1
1993	August	Night	North of the Islands	1
1993	August	Day	North of the Islands	1
1993	August	Night	South and around the Islands	7
1993	August	Day	South and around the Islands	33
1993	August	Day	Upwelling area	31
1994	October	Night	South and around the Islands	13
1994	October	Day	South and around the Islands	11
1994	November	Night	South and around the Islands	15
1994	November	Day	South and around the Islands	12

Table 5d. Continued: Information of zooplankton biomass data points per year, month, area, and period.

1995	April	Day	South and around the Islands	1
1995	May	Day	South and around the Islands	1
1995	June	Day	South and around the Islands	1
1995	July	Day	South and around the Islands	1
1995	August	Day	South and around the Islands	1
1995	September	Day	South and around the Islands	1
1996	July	Day	South and around the Islands	1
1996	August	Day	South and around the Islands	1
1996	September	Day	South and around the Islands	1
1996	October	Day	South and around the Islands	1
1996	November	Day	South and around the Islands	1
1996	December	Day	South and around the Islands	1
1997	January	Day	South and around the Islands	1
1997	March	Day	South and around the Islands	1
1997	April	Day	South and around the Islands	1
1997	November	Day	South and around the Islands	14
1998	June	Night	South and around the Islands	3
1998	June	Day	South and around the Islands	6
1998	July	Night	South and around the Islands	2
1998	July	Day	South and around the Islands	2
2000	January	Day	North of the Islands	8
2000	January	Day	South and around the Islands	8
2000	February	Day	North of the Islands	15
2000	February	Day	South and around the Islands	18
2000	March	Day	North of the Islands	23
2000	March	Day	South and around the Islands	20
2000	April	Day	North of the Islands	4
2000	April	Day	South and around the Islands	6
2000	May	Day	North of the Islands	4
2000	May	Day	South and around the Islands	4
2000	July	Day	South and around the Islands	12
2000	August	Day	South and around the Islands	12
2000	September	Day	South and around the Islands	18

Table 5e. Continued: Information of zooplankton biomass data points per year, month, area, and period.

2000	October	Day	South and around the Islands	12
2000	November	Day	South and around the Islands	14
2000	December	Day	South and around the Islands	13
2001	January	Day	South and around the Islands	12
2001	February	Night	South and around the Islands	17
2001	February	Day	South and around the Islands	43
2001	April	Day	South and around the Islands	6
2001	May	Day	South and around the Islands	12
2001	June	Day	South and around the Islands	12
2002	September	Night	South and around the Islands	5
2002	September	Day	South and around the Islands	5
2003	January	Day	South and around the Islands	6
2003	May	Night	South and around the Islands	4
2003	May	Day	South and around the Islands	4
2005	January	Day	South and around the Islands	18
2005	February	Day	South and around the Islands	17
2005	March	Day	South and around the Islands	24
2005	April	Day	South and around the Islands	19
2005	May	Day	South and around the Islands	24
2005	June	Day	South and around the Islands	18
2005	July	Day	South and around the Islands	9
2005	August	Day	South and around the Islands	12
2005	October	Day	South and around the Islands	12
2005	November	Day	South and around the Islands	22
2005	December	Day	South and around the Islands	19
2006	January	Day	South and around the Islands	23
2006	February	Day	South and around the Islands	13
2006	March	Day	South and around the Islands	26
2006	March	Night	Upwelling area	18
2006	March	Day	Upwelling area	22
2006	April	Night	South and around the Islands	11
2006	April	Day	South and around the Islands	24
2006	April	Night	Upwelling area	1
2006	May	Day	South and around the Islands	14
2006	June	Day	South and around the Islands	15
2006	July	Day	South and around the Islands	4
2006	August	Day	South and around the Islands	4
2006	September	Day	South and around the Islands	3

Table 5f. Continued: Information of zooplankton biomass data points per year, month, area, and period.

2006	October	Day	South and around the Islands	1
2006	November	Day	South and around the Islands	3
2006	December	Day	South and around the Islands	4
2007	January	Day	South and around the Islands	1
2007	February	Day	South and around the Islands	4
2007	March	Day	South and around the Islands	3
2007	April	Day	South and around the Islands	4
2007	May	Day	South and around the Islands	3
2007	June	Day	South and around the Islands	1
2010	February	Night	North of the Islands	1
2010	February	Day	North of the Islands	2
2010	February	Day	South and around the Islands	2
2010	March	Night	North of the Islands	4
2010	March	Day	North of the Islands	9
2010	March	Day	South and around the Islands	9
2010	April	Night	North of the Islands	3
2010	April	Day	North of the Islands	5
2010	April	Day	South and around the Islands	6
2010	May	Night	North of the Islands	3
2010	May	Day	North of the Islands	5
2010	May	Day	South and around the Islands	5
2010	June	Night	North of the Islands	3
2010	June	Day	North of the Islands	6
2010	June	Day	South and around the Islands	6
2010	November	Night	North of the Islands	1
2010	November	Day	North of the Islands	2
2010	November	Day	South and around the Islands	2
2010	December	Night	North of the Islands	4
2010	December	Day	North of the Islands	8
2010	December	Day	South and around the Islands	8
2011	January	Night	North of the Islands	3
2011	January	Day	North of the Islands	8
2011	January	Day	South and around the Islands	8
2011	February	Night	North of the Islands	3
2011	February	Day	North of the Islands	6
2011	February	Day	South and around the Islands	10
2011	March	Night	North of the Islands	1
2011	March	Day	North of the Islands	3
2011	March	Day	South and around the Islands	9

Table 5g. Continued: Information of zooplankton biomass data points per year, month, area, and period.

2011	April	Night	North of the Islands	5
2011	April	Day	North of the Islands	10
2011	April	Day	South and around the Islands	8
2011	May	Night	North of the Islands	3
2011	May	Day	North of the Islands	6
2011	May	Day	South and around the Islands	6
2011	June	Night	North of the Islands	1
2011	June	Day	North of the Islands	2
2011	June	Day	South and around the Islands	2
2012	April	Day	North of the Islands	1
2012	April	Night	South and around the Islands	8
2012	April	Day	South and around the Islands	29
2012	December	Night	North of the Islands	12
2012	December	Day	North of the Islands	11
2012	December	Night	South and around the Islands	1
2012	December	Night	Upwelling area	1
2012	December	Day	Upwelling area	1
2013	October	Night	North of the Islands	3
2013	October	Day	North of the Islands	2
2013	October	Night	South and around the Islands	1
2013	October	Day	South and around the Islands	7
2013	October	Night	Upwelling area	5
2013	October	Day	Upwelling area	5
2014	April	Night	North of the Islands	2
2014	April	Day	North of the Islands	3
2014	April	Night	South and around the Islands	10
2014	April	Day	South and around the Islands	11
2014	April	Night	Upwelling area	5
2014	April	Day	Upwelling area	10
2014	October	Night	North of the Islands	3
2014	October	Day	North of the Islands	3
2014	October	Night	South and around the Islands	6
2014	October	Day	South and around the Islands	5
2014	October	Night	Upwelling area	4
2014	October	Day	Upwelling area	4
2016	November	Night	North of the Islands	3
2016	November	Day	North of the Islands	5

Table 5h. Continued: Information of zooplankton biomass data points per year, month, area, and period.

2016	November	Night	South and around the Islands	3
2016	November	Day	South and around the Islands	3
2016	November	Night	Upwelling area	3
2016	November	Day	Upwelling area	6
2017	October	Night	North of the Islands	4
2017	October	Day	North of the Islands	6
2017	October	Night	South and around the Islands	1
2017	October	Night	Upwelling area	1
2017	October	Day	Upwelling area	2
2018	April	Night	North of the Islands	5
2018	April	Day	North of the Islands	6
2018	April	Day	South and around the Islands	3
2018	April	Night	Upwelling area	2
2018	April	Day	Upwelling area	3
2018	October	Night	North of the Islands	3
2018	October	Day	North of the Islands	3
2018	October	Night	South and around the Islands	1
2018	October	Day	South and around the Islands	2
2018	October	Night	Upwelling area	5
2018	October	Day	Upwelling area	3
2019	February	Night	South and around the Islands	1
2019	February	Day	South and around the Islands	3
2019	March	Night	North of the Islands	3
2019	March	Day	North of the Islands	3
2019	March	Day	South and around the Islands	3
2019	March	Night	Upwelling area	3
2019	March	Day	Upwelling area	4
2021	March	Night	North of the Islands	7
2021	March	Day	North of the Islands	6
2021	March	Night	South and around the Islands	1
2021	March	Day	South and around the Islands	1
2021	March	Night	Upwelling area	4
2021	March	Day	Upwelling area	2

Chapter 3

Mesozooplankton Size Structure in the Canary Current System.

Marine Environmental Research, 4 April 2023.

https://doi.org/10.1016/j.marenvres.2023.105976

María Couret[1,*], José M. Landeira[1], Victor M. Tuset[1], Airam N. Sarmeinto-Lezcano[1], Pedro Vélez-Belchí[2], and Santiago Hernández-León[1]

[1]Instituto de Oceanografía y Cambio Global, IOCAG, Universidad de Las Palmas de Gran Canaria, Unidad Asociada ULPGC-CSIC, Campus de Taliarte, 35214 Telde, Gran Canaria, Canary Islands, Spain.

[2]Instituto Español de Oceanografia, CO Canarias, Santa Cruz de Tenerife, Spain

3.1. Abstract

Changes in plankton composition influences the dynamics of marine food webs and carbon sinking rates. Understanding the core structure and function of the plankton distribution is of paramount importance to know their role in trophic transfer and efficiency. Here, we studied the zooplankton distribution, abundance, composition, and size spectra for the characterization of the community under different oceanographic conditions in the Canaries-African Transition Zone (C-ATZ). This region is a transition zone between the coastal upwelling and the open ocean showing a high variability because of the physical, chemical, and biological changes between eutrophic and oligotrophic conditions through the annual cycle. During the late winter bloom (LWB), chlorophyll *a* and primary production were higher compared to that of the stratified season (SS), especially in the upwelling influenced area. Abundance distribution analysis clustered stations into two main groups according to the season (productive versus stratified season), and one group sampled in the upwelling influenced area. Size-spectra analysis showed steeper slopes during daytime in the SS, suggesting a less structured community and a higher trophic efficiency during the LWB due to the favorable oceanographic conditions. We also observed a significant difference between day and nighttime size spectra due to community change during diel vertical migration. Cladocera were the key taxa differentiating an Upwelling-group, from a LWB- and SS-group. These two latter groups were differentiated by Salpidae and Appendicularia mainly. Data obtained in this study suggested that abundance composition might be useful when describing community taxonomic changes, while size-spectra gives an idea of the ecosystem structure, predatory interactions with higher trophic levels and shifts in size structure.

Keywords: Mesozooplankton, size spectra, abundance distribution, community structure, Canaries-African Transition Zone

3.2. Introduction

The determination of zooplankton community characteristics such as the abundance, biovolume, and size spectra has a great importance in biogeochemical cycles, energy flow, and vertical particle flux (Buitenhuis et al., 2010; Kiørboe, 2013; Noji, 1991). Zooplankton is widely used as bioindicators for the identification of shifts in phenology (Mackas et al., 2012), physiological rates (Lenz et al., 2021), upwelling strength (Oksana and Viacheslav, 2012), atmospheric forcing (Hooff and Peterson, 2006), and latitudinal displacement of species (Berraho et al., 2015). It has a large influence on abundance and distribution of fishery resources, especially pelagic species (Shi et al., 2020).

Spatial and temporal changes in zooplankton community structure and distribution pattern are important for understanding the core structure and function of marine ecosystems (Zhao et al., 2022), and the potential impacts of climate change (Batchelder et al., 2013; Hays et al., 2005; Shi et al., 2020). In addition, body size is one of the primary determinants of energy flow, species diversity, and population crowding (Peters and Wassenberg, 1983; Woodward et al., 2005). Size shapes the community structure as marine foodwebs are size-structured, constraining prey-predator interactions and physiology (Li et al., 2018), and influences biomass and growth rates of populations in adjacent trophic levels (Carpenter et al., 1987; Vanni and Findlay, 1990). This parameter is used as a scaling factor and aggregation criterion to produce a macroscopic description of the pelagic ecosystems, with the objective of improving the predictive capacity of global models in anticipation of future responses of oceanic ecosystems to climate change (Stemmann and Boss, 2012). In this context, a method widely used for characterizing zooplankton is the normalized biomass size spectra (NBSS) (Martin et al., 2006; Sprules and Munawar, 1986). The most frequently employed model was that of (Platt and Denman, 1977, 1978), who introduced a theoretical concept considering the biomass flux as a continuous energy flow. Quantitative empirical analyses of planktonic structure are usually based on the parame-

ters generated by the straight line fitted to the size spectrum. The slope mirrors the overall trend in biomass distribution among various size classes, the linear fit (r^2) reflects the stability of community structure, and the NBSS intercept is related to the total abundance of the system (Martin et al., 2006), and to the level of primary production (Dai et al., 2016; García-Comas et al., 2014). The theory suggests that the NBSS slope of a pelagic steady-state community, where biomass is evenly distributed over logarithmic size classes, will be -1 (Sheldon et al., 1972). However, empirical studies have demonstrated that the NBSS slopes do not follow linearity in non-equilibrated highly dynamic ecosystems (García-Comas et al., 2014; Quinones et al., 2003). Several factors influence the NBSS slopes, highlighting sampling location and season (Krupica, 2006), sample processing method (e.g., Optical Plankton Counter or ZooScan) (Naito et al., 2019; Vandromme et al., 2012), productivity gradient (Kwong et al., 2022), nutrient stress (Atkinson et al., 2021; Wang et al., 2020), mesoscale structures (Chen et al., 2020; Jagadeesan et al., 2020), ecological processes (Zhou et al., 2014; Zhou, 2006), water depth gradient (Dai et al., 2016), oligotrophy (García-Comas et al., 2014), inter alia. Even NBSS slopes are highly sensible to environmental conditions and depend on many factors, they have been widely used as a metric of size structure (Zhou, 2006). Thus, the normalization of the biomass size spectrum allowed comparison across systems and was found to be a useful tool to assess simple first-order system dynamics (Heath, 1995). Even so, all studies recognize that plankton size distribution leads to general improvements in the description and dynamics of zooplankton and dead particle models in the mesopelagic layers (Stemmann and Boss, 2012). It might also be a more effective approach when comparing aquatic communities (Cottingham, 1999; Cózar et al., 2003), and useful to evaluate resource availability and selective predation on zooplankton (Braun et al., 2021).

The Canaries-African Transition Zone (C-ATZ) is part of the Canary Current System (CCS) and it is located within the eastern boundary gyre of the North Atlantic Ocean, also holding the upwelling system off Northwest Africa (NWA). This region is a transi-

tion zone between the coastal upwelling and the open ocean showing a high variability because of the physical, chemical, and biological changes between eutrophic and oligotrophic conditions (Barton et al., 1998; Hernández-León et al., 2007). Comparison of communities that are distant in latitude but connected by similar hydrological, chemical, and environmental conditions offers an opportunity to identify the influence of biogeography and environmental conditions on the types of organisms that inhabit them (Boucher, 1982). Upwelling areas are advantageous environments for this approach, with a small number of abundant species having similar importance in every region (Berraho et al., 2015). The NWA upwelling system is under a permanent upwelling regime characterized by coastal sea surface temperatures colder than the oceanic ones at the same latitude. North of 21°N, upwelling-favorable conditions occur from April to September, with a maximum in July, and less upwelling-favorable conditions from October to March, with a minimum in December to January (Gómez-Gesteira et al., 2008). Seasonal changes and upwelling strength also show a close link with the production of phytoplankton and zooplankton. In particular, zooplankton follows a strong annual cycle of biomass, productivity, and development sequence (Bertram et al., 2001). In the open ocean, primary production varies within the annual cycle, controlled by the nutrient enrichment during the so-called Late Winter Bloom (LWB). Organisms burst due to convective mixing during winter (Armengol et al., 2019; Neuer et al., 2007) eroding the thermocline (Cianca et al., 2007; Schmoker et al., 2012) and promoting a slight increase in nutrients in the euphotic zone. In spring, the seasonal thermocline is reestablished, remaining through the summer and autumn, restricting the injection of nutrients into the euphotic zone, and therefore limiting primary production (Schmoker et al., 2012).

The C-ATZ was mainly studied during different periods in relation to the effect of upwelling filaments and eddies (Barton et al., 1998) on phytoplankton (Arístegui et al., 2004), zooplankton HernandezLeon2002feeding, and fish and invertebrate larvae (Landeira et al., 2017; Rodrıguez et al., 1999). There were large differences in productivity

and plankton biomass between the oligo-, meso-, and eutrophic areas of the CCS during the annual cycle (Hernández-León et al., 2007), but no studies analyzed the spatial and temporal variability and seasonality in the region. Therefore, the aims of the present study were (i) to describe the seasonal effect (i.e., Late Winter Bloom, LWB versus Stratified Season, SS) in the zooplankton (i.e., species richness, abundance, and biomass) of two adjacent dynamic systems as the Canary Islands and the African platform, and (ii) to examine zooplankton responses using size spectra as a stational and spatial ecological indicator of their structure. Given the seasonal and spatial fluctuations zooplankton biomass occurring in the transition zone from the coast to the ocean (Hernández-León et al., 2002a,b; Yebra et al., 2005) we hypothesize that the NBSS slope in the C-ATZ should be steeper in oligotrophic areas and flatter in areas with high productivity, highly depending on the abundance of organisms.

3.3. Material and methods

3.3.1. *Field sampling*

Zooplankton was collected during two cruises conducted from 21^{st} to 29^{th} October in 2018 (SS) and from 28^{th} February to 9^{th} March in 2019 (LWB) on board the R.V. Ángeles Alvariño. Sailing took place from the northwest of La Palma Island (Canary Islands) to the Western Sahara coast (NWA) (Fig. 3.1). Mesozooplankton samples were collected during either day or night using a double WP-2 net (UNESCO, 1968) equipped with a 200 μm mesh size. Tows were performed from 200 meters depth to the surface with a vertical speed of 0.67 m·s^{-1}. One of the samples from the double net was directly fixed on board with 4% formalin-seawater for later taxonomic studies, and the second sample was used for measuring biomass from protein content. The latter sample was sieved and size fractionated into 200, 500, and 1000 μm, frozen in liquid nitrogen, and stored at -80°C until later analysis.

Vertical profiles of temperature, salinity, and chlorophyll *a* (Chl *a*) were obtained using a CTD (Seabird 911plus) mounted on a General Oceanic rosette sampler. The system was equipped with a chlorophyll fluorometer (FluoroWetlabECO AFLFL) calibrated using solid standard provided by the company. Temperature, salinity, oxygen, and Chl *a* sections were represented using Ocean Data View using the DIVA gridding procedure (Schlitzer, 2015). Sea surface temperature (SST) monthly average values were downloaded from the NASA Ocean Color web site for each cruise and then plotted on QGIS, and primary production was obtained for each station from the Ocean Productivity web site using the Vertical Generalized Production Model (VGPM) (Behrenfeld and Falkowski, 1997) as the standard algorithm. Stations were gathered in transects according to their location: north of the islands and west of the strait between Lanzarote and Fuerteventura was called T1W, northeast was T1E, and the rest of the stations were grouped into T2, T3, T4, T5, T6, and

T7 from north to south (Fig. 3.1).

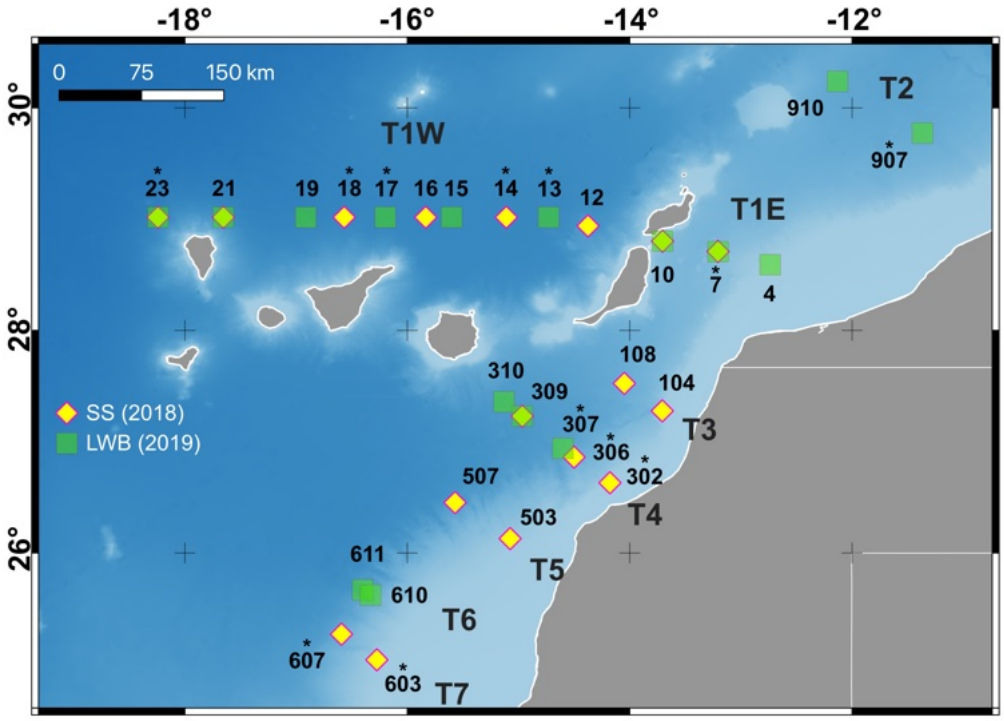

Figure 3.1. Location of sampling stations: yellow diamonds stand for stations sampled during the Stratified Season (October 2018), and in green squares during the Late Winter Bloom (March 2019). Asterisks stand for night-hauls stations and number above mark-stations indicates the station number. T stands for the number of the transect.

3.3.2. *Image analysis*

The taxonomic characterization of abundance and size distributions were performed using a representative subsample of the zooplankton community from the onboard fixed samples. In order to better represent all size classes, the subsample was divided into two categories using a 1000 μm mesh sieve and individually scanned. Thus, two images were obtained per station. Samples were imaged using an EPSON scan ver. 4990 at 2400 dpi, then processed in ZooProcess (Gorsky et al., 2010; Vandromme et al., 2012) and the resulting vignettes, along with a metadata file, were uploaded to EcoTaxa (`https://ecotaxa.obs-vlfr.fr/`; Picheral et al. (2017)) for machine-assisted identification, using a training set developed by the authors. Both training sets were validated up to a

95% for taxonomy classification.

3.3.3. *Zooplankton biovolume, abundance and biomass*

After vignette classification, we first transformed pixel size to length and then estimated image-based equivalent spherical diameter (ESD, mm). Then, we estimated biovolume (V, mm^3) assuming ellipsoidal shape. Ellipsoidal volume (mm^3) was calculated as:

$$V = \frac{4\Pi}{3} \times \frac{major\ axis}{2} \times \left(\frac{minor\ axis}{2}\right)^2$$

where major and minor axes (mm) of each object were provided by ZooProcess.

Abundances of each taxonomic zooplankton group were calculated as the number of organisms per station, and standardized to the number of organisms per cubic meter ($ind \cdot m^{-3}$). Biomass from the image analysis (dry mass, DM) was estimated following Maas et al. (2021), applying taxon-specific biovolume to DM conversion. Biomass was also estimated as protein content using bovine serum albumin (BSA) as the standard following the method given by Lowry et al. (1951) and modified by Rutter et al. (1968). Zooplankton protein content was converted to dry weight using the ratio of 2.49 given by Hernández-León et al. (2019a) for subtropical waters, and dry weight was converted into carbon units assuming carbon content as 40% of dry weight (Dam and Peterson, 1993).

3.3.4. *Cluster analysis*

Spatial and temporal variability of zooplankton abundances were analyzed by a hierarchical clustering and similarity profile routine (SIMPROF, $p<0.01$ and 999 permutations). The significant groups of the SIMPROF test were used as factors to test significant differences in temporal/spatial assemblages of the zooplankton using a one-way similarity analysis (ANOSIM). Data was transformed to log(x+1) to reduce the weighting of dominant

species, and similar matrices were clustered using Bray-Curtis method (Clarke and Warwick, 2001). A similarity percentages (SIMPER) test was then used to determine which taxon contributed most to characterize each group (Clarke and Gorley, 2006; Clarke and Warwick, 2001). After this, and using the same Bray-Curtis similarity matrix, a non-metric multidimensional scaling (nMDS) was performed. The groups were entered into the nMDS plot to visualize the spatial ordination of the groups of samples. Moreover, the nMDS plot was represented by superimposing bubbles of increasing size related to abundance values of key taxa detected in the SIMPER analysis. These multivariate analyses were carried out using PRIMER v7.0.20.

3.3.5. *Zooplankton Normalized Biomass Size Spectra*

Detrital particles, phytoplankton, organism parts, and those smaller than 200 μm maximum axis length were removed before the normalize biomass analysis. We created size-groups (i.e. bins) according to ESD measurements, grouping data into 30 size groups of 2 mm ranging from 0.98 mm to 91.24 mm. DM from the image analysis was estimated as explained above assuming the conversion factor of a Calanoida Copepoda when the taxonomic assignment did not fall into one of the pre-defined categories. DM was normalized to make the spectra independent of size group by dividing the biomass of each size group by the width (i.e., lower size limit) of the size group.

The NBSS were calculated following Platt and Denman (1977): the X-axis [$\log_2$ zooplankton biomass (mg C·ind^{-1})] was calculated by dividing zooplankton biomass (mg C·m^{-3}) by the abundance of each size class (ind·m^{-3}) and converting to $\log_2$; the Y-axis [$\log_2$ normalized biomass (ind·m^{-3})] was calculated by dividing the biomass (mg C·m^{-3}) in each size class by the interval of each size class [Δvolume (mm^{-3})] and converting to $\log_2$. A least-squares linear regression was fitted between the normalized biomass size spectrum (Dai et al., 2016; Quinones et al., 2003) and logarithm of the modal weight for

each size group to estimate the size structure of the community from station groups obtained by clustering (Chen et al., 2020). The extreme size ranges could be subject to error resulting in curvature of the log-linear relationship at either end of the spectrum. These inflection points at the extreme size ranges of each method were not included, as they could cause potential error in the calculation of the parameters of the spectrum (Marcolin et al., 2015; Martin et al., 2006). In addition, regressions were checked for outliers using the Bonferroni-adjusted p-value (<0.05) of studentized residuals and Cook's distance with the car package in R. When outliers were detected, regression parameters were newly estimated (Catherine et al., 2012). To identify the day-night influence within each group on the slopes of NBSS we performed an analysis of covariance (ANCOVA) using a post-hoc comparison of the slopes of fitted lines with the lsmeans package (Lenth and Lenth, 2018) in R. We also compared the variability between groups depending on time. In all cases, data were examined for normality using the Shapiro-Wilk test and homogeneity of variances by the Levene's test before analysis.

3.3.6. *Data analyses*

Seasonal and spatial differences in mesozooplankton biomass were tested using Kruskal-Wallis when variance homogeneity (Levene's test, Levene (1960)) or normal distribution (Shapiro-Wilk test) were not met with pairwise Wilcoxon test as post hoc test; and when the premises were not violated, an ANOVA was performed with the Tukey test as posterior test in R environment (Team, 2022a).

3.4. Results

3.4.1. *Environmental and biotic patterns*

Water column physical properties showed clear patterns at spatial and seasonal scale (Table 3.1, Fig. 3.2, Fig. 3.3, Fig. 3.4). During the SS we observed a marked stratification across all transects dismissing as we approached the African coast (Fig. 3.2A,C,E; Fig. 3.3). By contrast, during the LWB we observed a clear mixed layer in the first 150 m depth with lower water temperature and higher Chl *a* values, particularly in the transects close to the African coast (Fig. 3.2B,F; Fig. 3.4). Average values of temperature in the upper 200 m depth were about 1°C higher during the SS compared to the LWB. Seasonal and spatial differences in salinity were not prominent (difference of 0.1) (Table 3.1).

Integrated Chl *a* values were similar between both seasons, with larger differences in transect T1E. However, we found higher differences for primary production (PP) values, displaying higher values in transects inside the upwelling influenced area and showing the highest differences in oceanic water (T1) between both seasons (Table 3.1). The deep Chl *a* maximum was thicker and shallower during the LWB in oceanic waters (Fig. 3.2E,F), whereas in both cruises the signature of high Chl *a* concentration related to upwelled waters was noticeable off the African coast (Fig. 3.3I-L; Fig. 3.4G-I). Mesozooplankton biomass was higher during the LWB compared to the SS (Wilcoxon Test, W = 574, $p<0.001$), reaching maximum values close to the NWA coast and decreasing towards the open ocean (Table 3.1). In both seasons, we generally observed higher zooplankton biomass in night-sampled stations (Fig. 3.5). During the LWB, zooplankton biomass was two-fold higher in T1W and 2.5-fold higher along the transects in the upwelling influenced area. However, we obtained similar values for T1E during both seasons. Comparing the upwelling influenced transects in both seasons, biomass was on average two-times higher during the LWB (Table 3.1). Total biomass was dominated by large organisms (>1000

Table 3.1. Average temperature, salinity, chlorophyll *a*, primary production, and zooplankton biomass (± standard deviation) for the different transects (see text) sampled during the stratified season and the late winter bloom cruise in the upper 200 m depth. *No value available for station 10.

Season	Transect	Number of stations	Average temperature (°C)	Average salinity (PSU)	Integrated Chl a ($mg \cdot m^{-2}$)	Primary producion ($mg\ C \cdot m^{-2} \cdot d^{-1}$)	Zooplankton biomass ($mg\ C \cdot m^{-2}$)
Stratified season	T1W	6	19.25 ± 0.54	36.54 ± 0.12	0.16 ± 0.01	325.42 ± 19.11	157.11 ± 75.77
	T1E	2	18.25 ± 0.70	36.39 ± 0.04	0.25 ± 0.02	438.99*	353.80 ± 129.48
	T3	2	17.72 ± 1.31	36.21 ± 0.19	0.20 ± 0.04	675.29 ± 282.74	85.05 ± 7.54
	T4	3	17.52 ± 0.67	36.34 ± 0.09	0.28 ± 0.12	694.82 ± 448.86	294.07 ± 17.95
	T5	2	19.70 ± 0.14	36.64 ± 0.04	0.17 ± 0.01	398.28 ± 42.34	190.03 ± 17.33
	T7	2	18.85 ± 1.10	36.48 ± 0.16	0.19 ± 0.06	379.47 ± 2.40	409.43 ± 130.54
Late Winter Bloom	T1W	6	18.20 ± 0.31	36.63 ± 0.06	0.19 ± 0.03	532.77 ± 38.32	319.77 ± 139.74
	T1E	3	17.47 ± 0.36	36.50 ± 0.08	0.32 ± 0.03	758.55 ± 123.14	386.15 ± 180.25
	T2	2	17.05 ± 0.07	36.43 ± 0.01	0.24 ± 0.01	735.79 ± 46.76	675.75 ± 250.91
	T4	3	17.57 ± 0.45	36.51 ± 0.07	0.20 ± 0.05	796.06 ± 48.32	526.75 ± 114.14
	T6	2	17.51 ± 0.03	36.49 ± 0.01	0.18 ± 0.02	900.33 ± 78.37	691.39 ± 168.10

μm) during the SS (Fig. 3.5A; ANOVA, Tukey Test, $p<0.001$: Table 3.4), while during the LWB medium (500-1000 μm) and small (200-500 μm) organisms contributed most to the zooplankton biomass, but only the fraction >1000 μm significantly differed from the fraction 200-500 μm (ANOVA, Tukey Test, $p<0.05$: Table 3.4). We found larger biomass differences during the SS between the transects close to the upwelling system. T2 presented biomass values 2-fold lower than the other transects, with a higher contribution of medium and small-size organisms in contrast to the other stations where 70% of the biomass was due to large-size organisms.

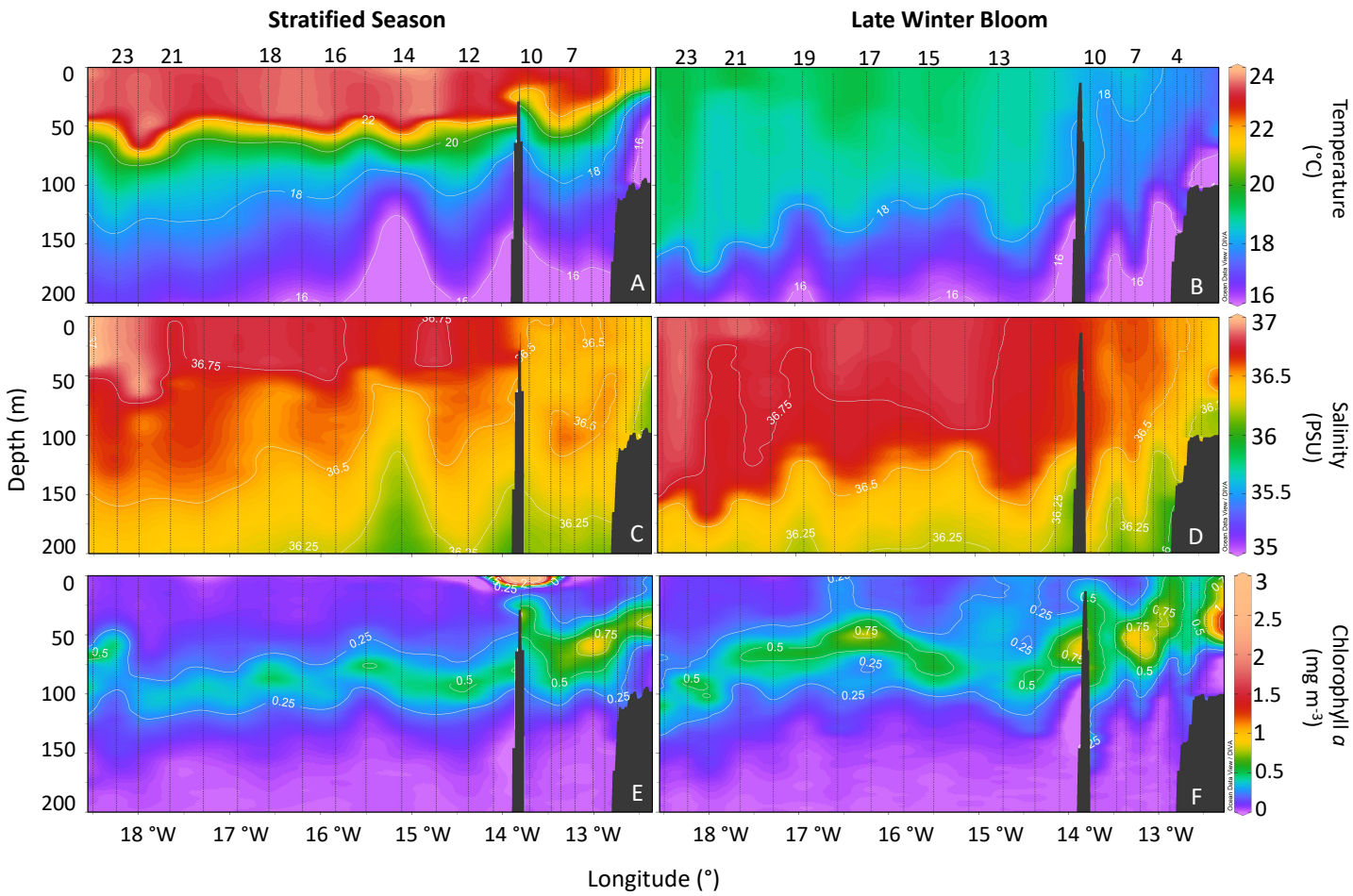

Figure 3.2. Vertical sections (0-200 m) of temperature (°C) (A, B), salinity (PSU) (C, D) and chlorophyll *a* concentration (mg·m^{-3}) (E, F) during the Stratified Season (left panels) and the Late Winter Bloom (right panels) in transect T1W and T1E (see Fig. 3.1). Numbers on the top stand for station numbers, and black lines onside the graph for CTD-sampled stations across the transect.

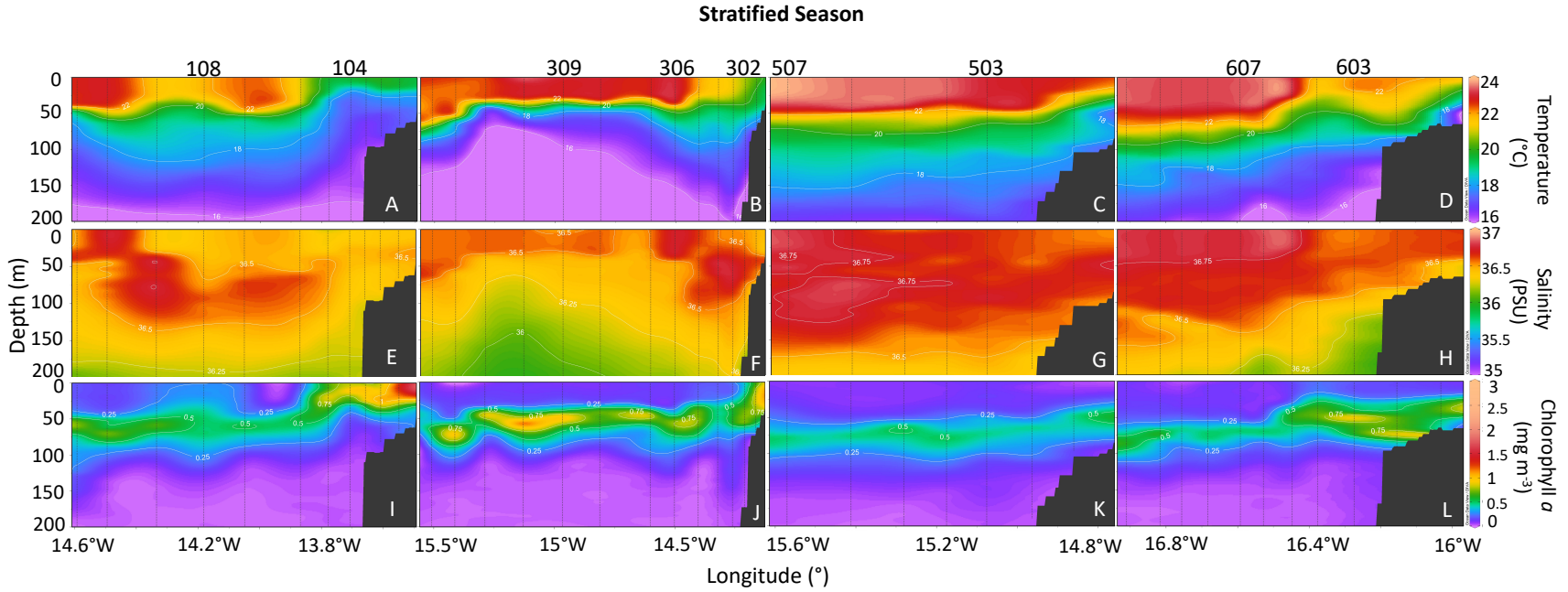

Figure 3.3. Vertical sections (0-200 m) of temperature (°C) (A, B, C, D), salinity (PSU) (E, F, G, H) and chlorophyll *a* concentration ($mg \cdot m^{-3}$) (I, J, K, L) during the Stratified Season in the stations close to the African coast (see Fig. 3.1). Numbers on the top stand for station numbers, and black lines onside the graph for CTD-sampled stations across the transect.

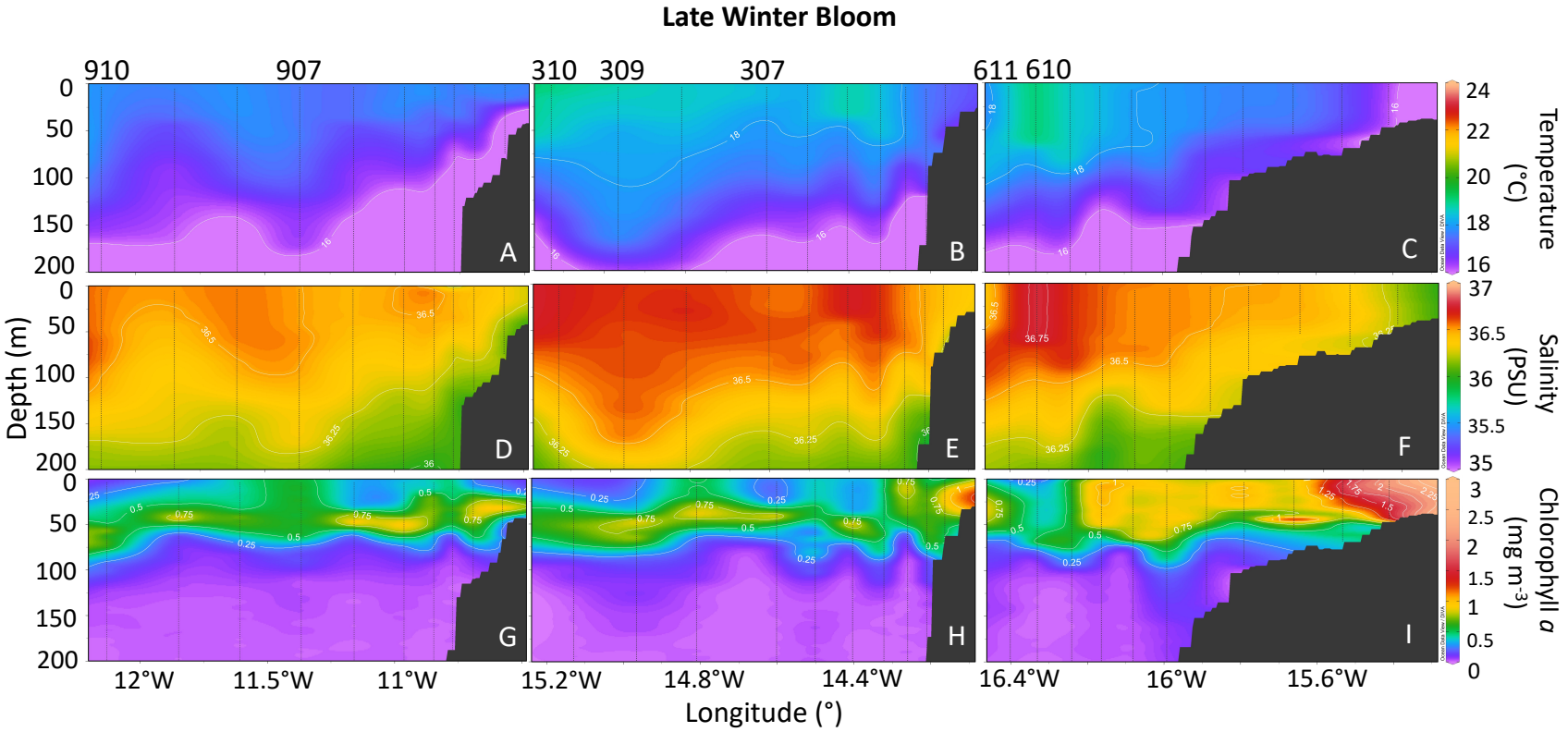

Figure 3.4. Vertical sections (0-200 m) of temperature (°C) (A, B, C, D), salinity (PSU) (E, F, G, H) and chlorophyll *a* concentration (mg·m^{-3}) (I, J, K, L) during the Late Winter Bloom in the stations close to the African coast (see Fig. 3.1). Numbers on the top stand for station numbers, and black lines onside the graph for CTD-sampled stations across the transect.

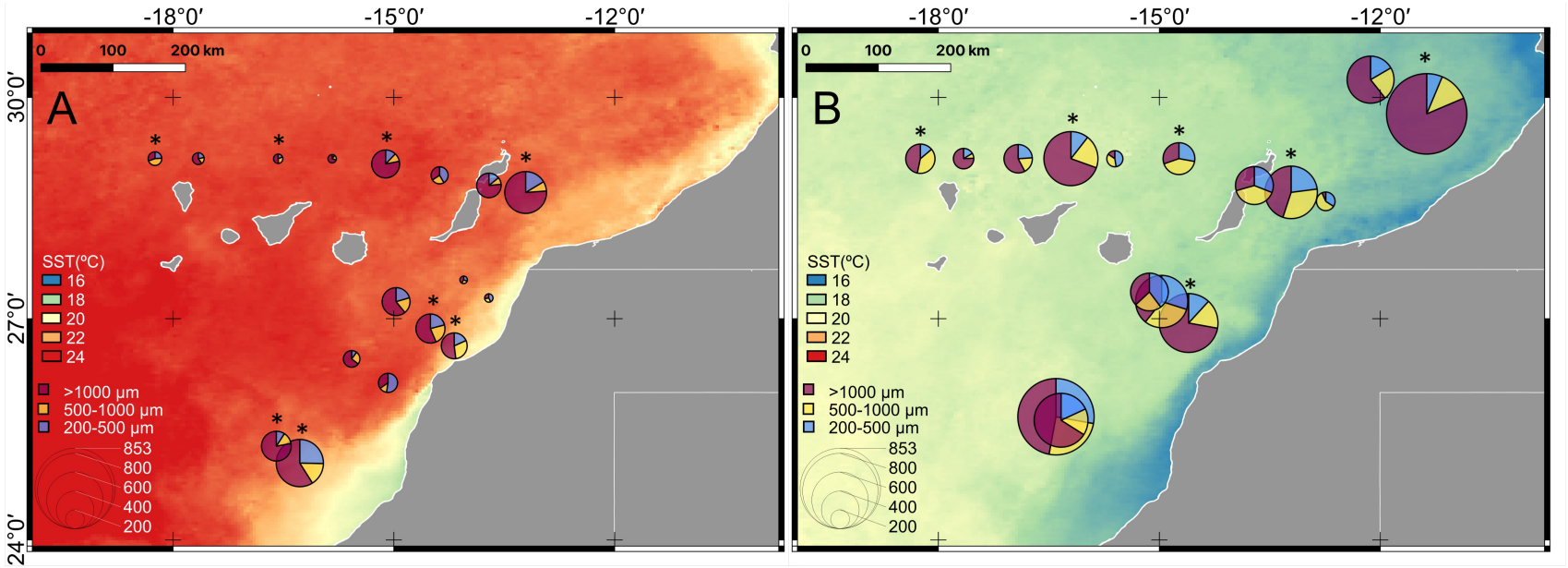

Figure 3.5. Spatial distribution of the percentages of zooplankton size-fractionated biomass obtained as protein content during the Stratified Season (A) and the Late Winter Bloom (B). Bubble size represent total biomass (mg C·m^{-2}). Colors on the maps correspond to monthly-mean sea surface temperature during October (2018) for the Stratified Season and March (2019) for the Late Winter Bloom. Asterisks stand for night-hauls stations.

3.4.2. *Zooplankton structure*

The SIMPROF test differentiated three main groups of stations ($p<0.001$) with a similarity of 80%: (1) the Upwelling-group composed by stations from the upwelling zone regardless of the season, (2) the LWB-group, and (3) the SS-group, with stations sampled according to the season. The station 603 sampled during the SS was not clustered in any of the three groups of stations. The ANOSIM tests (R-statistic = 0.779, $p<0.001$) also confirmed the significance of these gatherings (Fig. 3.6A), as well as the nMDS ordination (Fig. 3.6B). The SIMPER analysis showed the contribution of each taxonomic group (%) to the dissimilarity between the three groups (Upwelling, LWB, and SS, Table 3.2; 3.6C,D). Calanoida Copepoda were the taxon most contributing to the similarity in each group due to their high abundance, but they did not contribute to distinguish the SIMPROF groups. *Penilia* spp. and *Evadne* spp. accounted for the 27% of the dissimilarity to differentiate the Upwelling-group from the SS-group, whereas Salpidae and Appendicularia together contributed with the 14.5% of dissimilarity (Table 3.2). Cladocera and Appendicularia were also key taxa to discriminate the Upwelling-group from the LWB-group (almost 17% and 8.5% of dissimilarity, respectively), and Euphausiacea became important and accounting for almost 6% of the dissimilarity. Finally, the differences between the LWB- and SS-groups, were mostly driven by the Salpidae (13.9% of dissimilarity), followed by eggs (8.2%), Pteropoda and Heteropoda (6.7%), and other gastropod molluscs (6.5%).

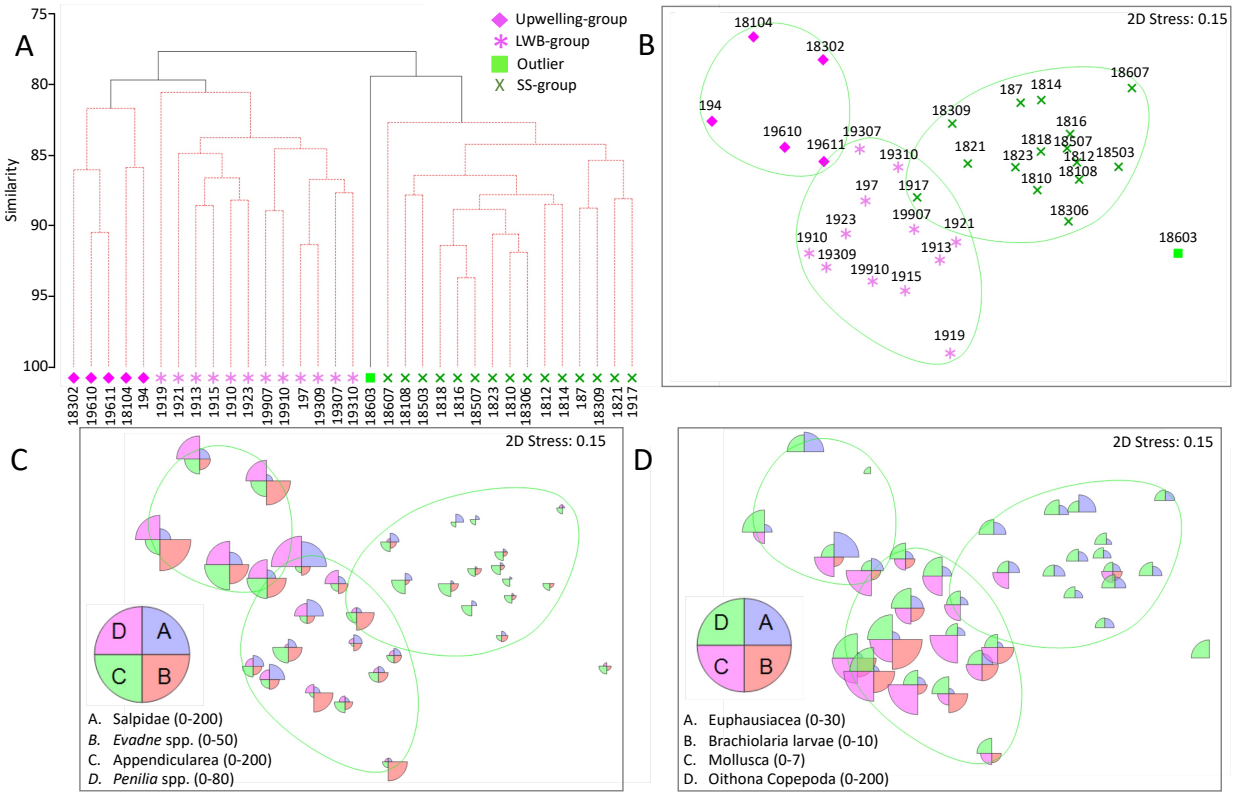

Figure 3.6. A) Assemblages of zooplankton structure according to the abundance and composition for each sampled season and area. First two numbers of the x-labels correspond to the sampling year, and the rest to the code of the station as in Fig. 3.1. B) Results of the non-metric multidimensional scaling (nMDS) of zooplankton communities. C and D) Zooplankton taxonomic composition of the key organisms. Pink diamonds stand for those stations performed close to the upwelling African coast, pink asterisks stand for those stations sampled during the Late Winter Bloom, green squares correspond to an outgroup, and green crosses to stations performed during the Stratified season. Bubble size stand for abundance values for each selected taxon (number·m^{-3}).

Table 3.2. Taxa regarded as discriminators between the zooplankton community assemblages from the SIMPER analysis up to a 70%.

	Upwelling-group vs SS-group		Upwelling-group vs LWB-group		LWB-group vs SS-group	
	Dissimilarity (%)	Contribution (%)	Dissimilarity (%)	Contribution (%)	Dissimilarity (%)	Contribution (%)
Penilia sp.	4.05	16.13	2.11	10.38	1.41	5.46
Evadne sp.	2.71	10.82	1.34	6.58	1.54	5.94
Salpidea	1.88	7.5	0.95	4.68	3.61	13.9
Appendicularia	1.75	6.99	1.73	8.52		
Corycaeidae copepoda	1.25	4.97	0.82	4.01		
Euphausiacea	1.17	4.67	1.22	5.98	1.28	4.94
Other Gastropoda	1.11	4.43			1.68	6.48
Echinodermata-larvae	1.03	4.11	0.92	4.53		
Polychaeta	1	3.98	0.76	3.74		
Egg	0.97	3.88	0.75	3.7	2.14	8.22
Pteropoda+Heteropoda	0.85	3.39	0.93	4.58	1.75	6.74
Brachiolaria			0.96	4.74	1.42	5.46
Oithona copepoda			0.95	4.67		
Siphonophorae			0.86	4.24		
Ostracoda					1.3	4.99
Foraminifera					1.15	4.43
Chaetognatha					1.02	3.91

3.4.3. *Normalized biomass size distribution characterization*

Overall NBSS slopes of mesozooplankton size spectra were fitted with a linear relationship, ranging from -0.45 to -1.73 (Fig. 3.7, Table 3.3). The elevations were remarkably constant in the SS-group (6.22 for day, and 6.48 for night), and variable in the LWB-group, ranging from 6.03 (day) to 7.06 (night). The Upwelling-group showed the lowest regression coefficient ($R^2 < 0.62$), with high errors in the estimation of linear parameters, a non-homogeneous distribution, and low number of samples (Fig. 3.7C; Table 3.3). Given that these biases can lead to misinterpretation of the ANCOVA analysis, we decided to not include it as a preventive measure. The overall NBSS slope for the SS-group on day (-0.97) was significantly different from those at night (-0.80; ANCOVA, F = 4.52, p = 0.036; Fig. 3.7A), indicating a higher proportion of large-sized zooplankton during the night, mainly Euphausiacea. While Chaetognatha were the main daytime organisms during the SS, Euphausiacea dominated the community at night (Fig. 3.8C,D). Although any diel variation was observed between the slopes for the LWB-group (ANCOVA, F = 0.02, p = 0.89), the large value of the intercept at night (7.056 ± 0.208) in relation to daytime

(6.03 ± 0.22) also showed a clear effect of DVM in the NBSS. The difference with the SS was the increased zooplankton biomass of smaller size fractions at night. This group was characterized by the large presence of Hydrozoa and Salpidae during the day and the night, with less Euphausiacea during the night compared to the SS-group. Comparing groups, the SS-group was characterized by a steeper NBSS slope (-0.969) than the LWB-group (-0.753; ANCOVA, F = 6.283, p = 0.014; Fig. 3.7B) for daytime, but both groups showed similar values (-0.802 and -0.743, respectively) during nighttime (ANCOVA, F = 0.763, p = 0.385). Biomass in each size bin (Fig. 3.8) showed similar taxa distribution for the smaller size bins, with high abundance of Copepoda such as Calanoida, *Oncaea* spp., and *Corycaeus* spp., Appendicularia, and Salpidae. As the bin increased, the taxa distribution shifted towards a community mainly dominated by Salpidae and Hydrozoa in the LWB-group, and by Chaetognatha and Euphausiacea in the SS-group.

Table 3.3. Results from the linear regressions of the Normalized Biomass Size Spectra analysis. n: number of data points.

Cluster	**Period**	**Intercept**		**Slope**		**R^2**	**n**	**Number of stations**
		Range	**Mean ± SD**	**Range**	**Mean ± SD**			
SS-group	Night	5.47 to 7.29	6.48 ± 0.17	-0.70 to -1.12	-0.80 ± 0.05	0.84	61	7
	Day	5.49 to 7.12	6.22 ± 0.18	-0.84 to -1.45	-0.97 ± 0.07	0.79	61	8
LWB-group	Night	6.62 to 7.93	7.06 ± 0.21	-0.61 to -0.95	-0.74 ± 0.05	0.84	44	5
	Day	5.38 to 7.16	6.03 ± 0.22	-0.73 to -1.67	-0.75 ± 0.06	0.79	51	7
UP-group	Night	6.5	6.50 ± 0.60	-0.84	-0.84 ± 0.25	0.62	9	1
	Day	5.74 to 7.53	6.55 ± 0.49	-0.49 to -1.73	-0.75 ± 0.18	0.47	23	4

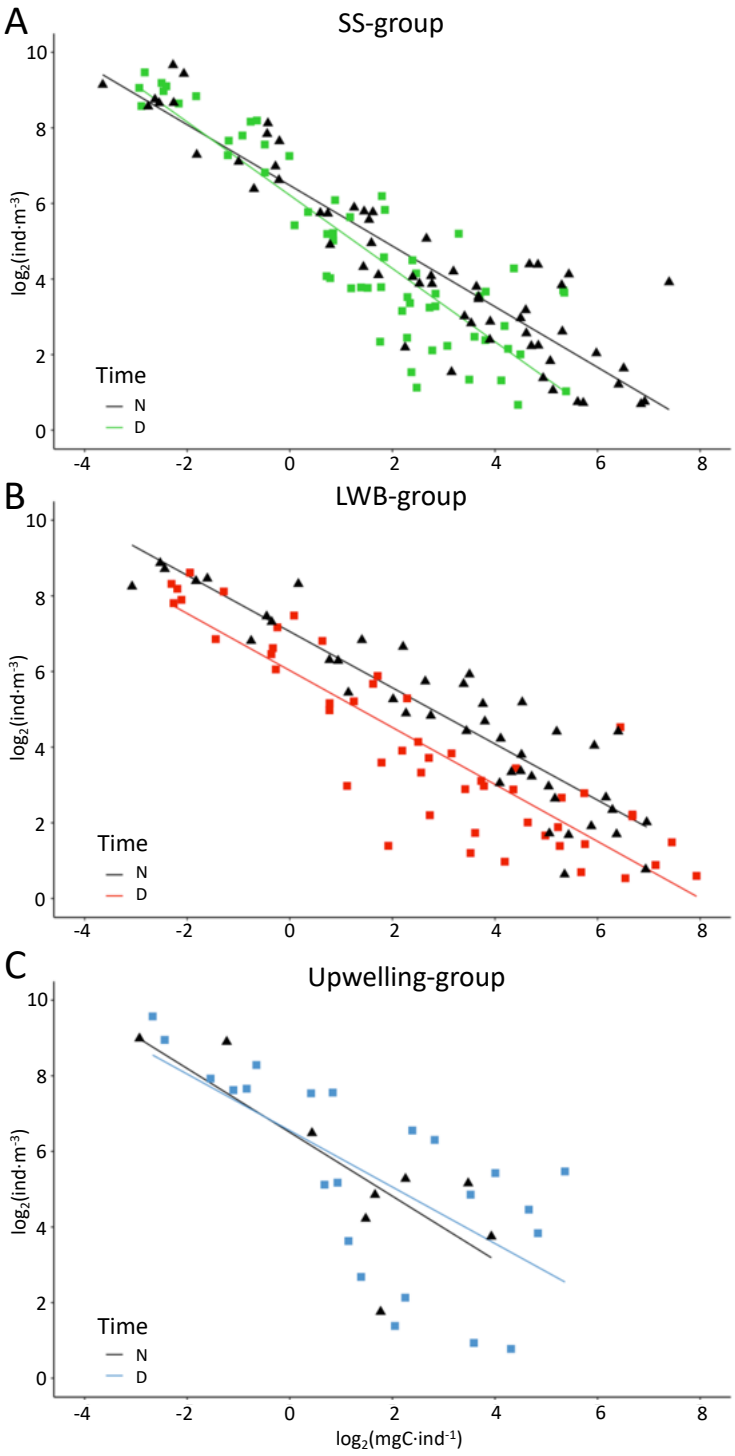

Figure 3.7. Mesozooplankton NBSS for the grouped stations according to Fig. 3.6A cluster: A) SS-group, B) LWB-group, and C) Upwelling-group. Color in each NBSS corresponds to day hauls, and black for night hauls.

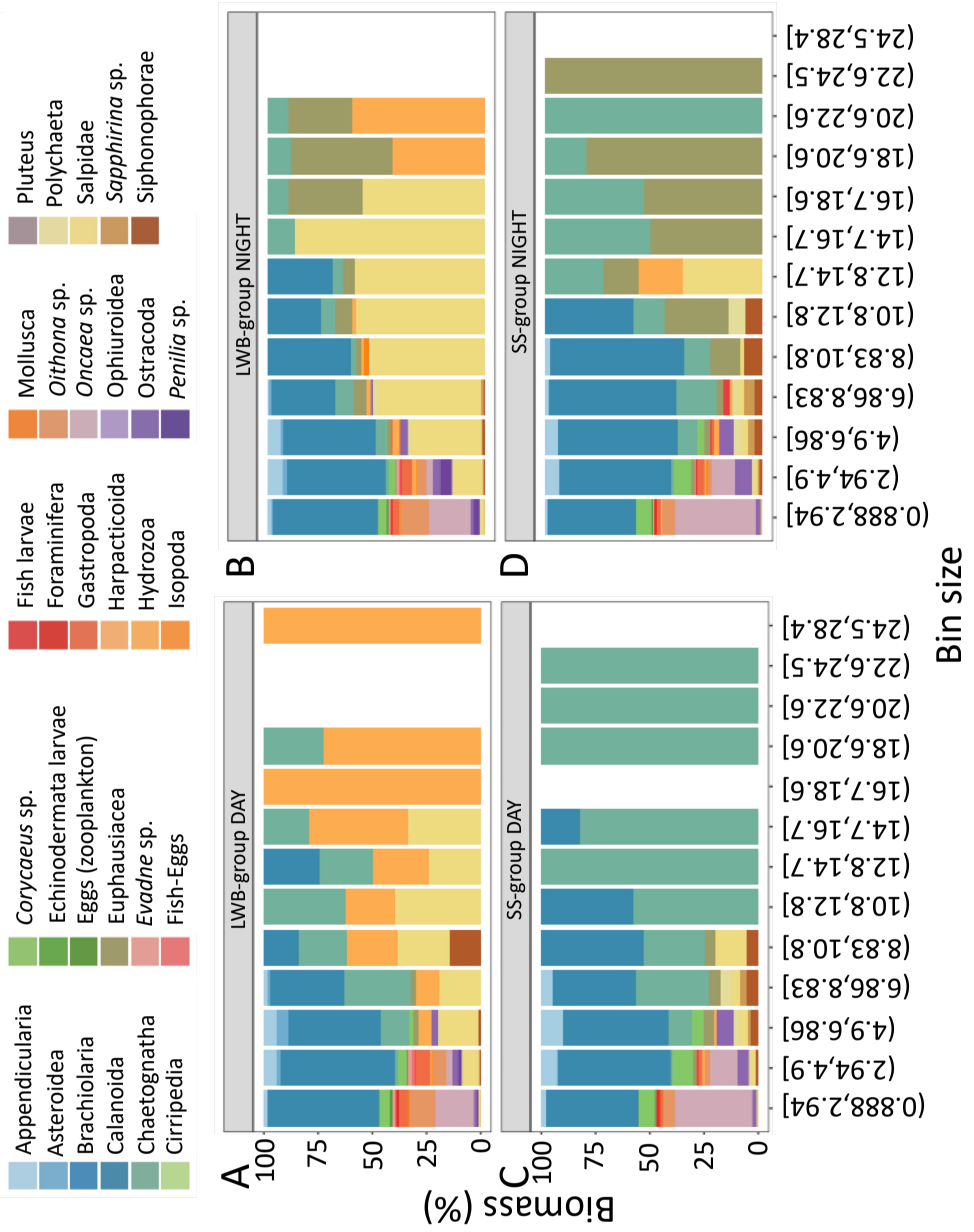

Figure 3.8. Mesozooplankton biomass (%) in each bin size for the different grouped stations according to Fig. 3.6A cluster. A) Correspond to the LWB-group during day, B) to the LWB-group during night, C) to the SS-group during day, and D) to the SS-group during night. The Upwelling group was not included in the graph (see text).

3.5. Discussion

3.5.1. *Spatial and temporal patterns in the C-ATZ*

Mesozooplankton biomass, abundance, and size distribution were spatially and temporarily determined in the C-ATZ. We detected clear environmental and community differences between the SS and LWB seasons, similar to those already reported before for this area (Braun, 1980; Hernández-León, 1988b; Hernández-León et al., 2007; Valdés and Déniz-González, 2015). We found a quite stratified water column with a sharp thermocline between 50 and 70 m depth, low integrated Chl *a*, and PP values during the SS, especially north of the Canary Islands. By contrast, water column properties during the LWB showed a wide mixed layer, and higher integrated Chl *a*, and PP values, as well as a shallower distribution of the deep Chl *a* maximum. Previous works in the C-ATZ studied the influence of the spatial and annual variability of the water column, mesoscale activity, and the upwelling and its filaments on plankton (see Hernández-León et al., 2007). We detected higher zooplankton biomass during the LWB enhanced by higher PP values, particularly noteworthy in the upwelling influenced area since the water intrusion pulses close to shore create large phytoplankton biomass events (Reyes-Mendoza et al., 2019). A relative high zooplankton biomass barely varied around the area between both the Cape Ghir and Cape Juby (T1E) due to a quasi-permanent upwelling filament off Cape Ghir and the intermittent filament off Cape Juby (Berraho et al., 2015). Finally, size fractionated mesozooplankton biomass showed a higher biomass of the larger size groups during the SS, as they have longer generation times than primary producers and therefore survive for longer periods. Also, a succession of small to medium and large Calanoida and gelatinous organisms from the upwelled waters to the ocean is normally the rule (Postel, 1990). These results suggest that the oceanographic conditions drive the mesozooplankton biomass, with clear environmental and ecological differences during the annual cycle in

the studied area.

3.5.2. *Abundance and composition*

Despite the wide variability of mesozooplankton biomass from the upwelling influenced area to offshore through the annual cycle, the common feature throughout the C-ATZ is the numerical dominance of Copepoda determined by the seasonality and the upwelling regime. Beside Copepoda, the organisms characterizing each season were Hydrozoa and Salpidae during the LWB, and Chaetognata and Euphausiacea during the SS. However, these organisms were not the key to cluster the stations into the three main groups. The difference between station groups was characterized by the abundance of seasonal organisms such as *Evadne* spp. and *Penilia* spp., as similarly reported by Hernández-León et al. (2007). Several studies in the area have demonstrated that Cladocera dominate along filaments of upwelled waters, as well as fish larvae (Hernández-León et al., 2007; Moyano et al., 2009). Cladocera burst in eutrophic areas (Liu et al., 2014), and constitute the main prey for fish, therefore their populations are affected by phytoplankton production and fish predation (Gliwicz et al., 2004). Moreover, the abundance of Salpidae helped to distinguish the intergroups variability. These organisms have a high grazing impact that can deplete the photic zone of phytoplankton and export huge quantities of organic matter to the deep sea (Dadon-Pilosof et al., 2019). Abundance might be used as an indicator of shifts in the community due to changes in the environmental conditions (e.g. temperature, chlorophyll, or water column stability) (Coyle et al., 2008). For instance, Copepoda differed between coastal and offshore waters, denoting a more structured assemblage with higher species diversity and evenness offshore (Berraho et al., 2015), with different species throughout the annual cycle (Corral, 1970). Moreover, weak upwelling conditions or even a strong seasonality in the Canary Current System entail low levels of productivity during the cold season close to North of Cape Beddouza (35°48′N).

It affects the zooplankton with low abundances and a high dominance of Copepoda. However, the zooplankton is less structured and balanced during the upwelling season (in summer), predominating few species but with high abundances (Berraho et al., 2015). The increase of water temperature and the decrease in food along the offshore have been considered as the main factors influencing the zooplankton body size, thus the NBSS slope, because of the size- dependent energy requirements needed to maintain basal metabolism (Brown et al., 2004; Ikeda, 1985; Zhou, 2006). Consequently, a size gradient from small to medium and large Calanoida and gelatinous organisms, such as Thaliacea and Siphonophorae, from the upwelled waters to the ocean is normally the rule (Postel, 1990) as observed here for the NBSS slopes. Nevertheless, this is the first report on the zooplankton assemblages in the C-ACTZ and the general patterns need to be corroborated and complemented with additional studies at local and regional scales.

3.5.3. *Normalized Biomass Size Spectra*

Size spectra obtained in this study showed a strong seasonal change in the zooplankton size structure and production off the C-ATZ in response to hydrological conditions, and a spatial separation between the upwelling area and the Canary Islands. Size-based normalized biomass/biovolume size spectra have been considered a tool of interest for plankton energy fluxes and the evaluation of the marine ecosystems structure (Dai et al., 2016; Platt and Denman, 1977; Quinones et al., 2003; Suthers et al., 2006). However, the way in which size diversity impacts the functioning of the ecosystem is an important but unclear question. The theory suggests that the NBSS slope in a stable marine ecosystems should be settled at approximately -1 (Sprules and Munawar, 1986). Even so, theoretical models and empirical studies still have some discrepancies, especially in strongly dynamic ecosystems where energy pulses through the system might unbalance the theoretical linearity of the system (Quinones et al., 2003; Sourisseau and Carlotti, 2006). Steeper slopes are gen-

erally related to a biomass decline with increasing size, thus lower transfer efficiency for higher trophic levels, to an increase of predation pressure on the smallest zooplankton (Brown et al., 2004; Noyon et al., 2022; Martin et al., 2006; Zhou, 2006), and to higher abundance of herbivorous zooplankton organisms, usually smaller in size compared to carnivorous species (Noyon et al., 2022). Moreover, some studies argued that this pattern could also occur due to the increase of juvenile organisms linked to an enhanced reproduction stimulated by food availability (García-Comas et al., 2014; Giering et al., 2019), whereas others authors link steeper slopes to oligotrophic and warmer waters where the conditions are more stable (Canales et al., 2016; Medellín-Mora et al., 2016; Sprules and Munawar, 1986). Our results showed steeper slopes for the SS-group, in agreement with oligotrophy conditions, higher water temperatures and water column stratification, previously reported by Hernández-León et al. (2007) and also obtained in this study. This outcome suggests an overall increase in predation pressure with size, and a loss of available energy to higher trophic levels during that season, thus a strong bottom-up control during the SS linked to food-limitation conditions.

On the other hand, the LWB-group showed more gradual slopes, with the highest intercepts, suggesting a wider size biomass distribution. During this season, the thermocline is eroded allowing nutrients to reach the euphotic zone enhancing primary and mesozooplankton production (Schmoker et al., 2012). The high productivity and lower water temperatures favored the abundance of different size spectra organisms flattening the LWB slopes and promoting higher trophic efficiency. This result was also obtained by García-Comas et al. (2014), showing also that food (Chl *a* concentration) overrides the influence of water temperature, being the trophic status the main factor influencing zooplankton size structure. In this sense, our results followed the theoretical models increasing the relative abundance of large organisms with increased energy availability. Schmoker and Hernández-León (2013) found that in the subtropical waters of the Canary Islands, microplankton are actively grazing on picoplankton and on heterotrophic prokaryotes, and

they are being, in turn, grazed by small mesozooplankton, highlighting the most likely top-down control of higher trophic levels on lower trophic levels existing in the planktonic food web. Moreover, increasing zooplankton size and taxonomic diversity enhances top-down control on phytoplankton (Ye et al., 2013). Thus, it seems that during the LWB the food webs are controlled by top-down processes.

Theoretically, less stable environments have higher secondary structuring processes and disturbances around the linear NBSS slope, lowering the r^2 value (Souza et al., 2020; Sprules and Barth, 2016). Low r^2 values denote that the community is unstructured or in a non-equilibrium state (Boudreau et al., 1991; Thiebaux and Dickie, 2011), while values close to 1 indicate communities close to steady-state equilibrium. The SS-group and the LWB-group showed similar r^2 values, ranging from 0.79 to 0.84 from day to night hauls, respectively (Table 3.3). This finding suggests a higher structured community than in the UP-group. In the latter group, size diversity instead of size spectrum could be a better approach for species diversity analysis and the understanding of an upwelling area. This parameter measures the continuous distribution of body size as the size deviation, which may represent an important functional diversity metric when determining the structure and functioning of a highly unstable aquatic ecosystem. Higher size diversity has higher efficiency of resource use; therefore, higher size diversity of zooplankton can increase zooplankton biomass, and the effect on trophic structure may have important management implications in aquatic ecosystems (Sun et al., 2021; Ye et al., 2013). The UP-group stations were characterized by the area they were sampled, not by the season, suggesting that zooplankton there display different properties than in oligotrophic areas. Patterns of zooplankton in the C-ATZ are scarce (see Hernández-León et al., 2007), and the taxonomic composition and distribution from the coast to the open ocean during the annual cycle remains still unknown.

Changes in zooplankton community size structure have the potential to alter the food web structure, thus the food quantity and quality for planktivorous fish (Lomartire et al.,

2021; Pitois et al., 2021). In this sense, the SS-group showed the strongest day-nighttime variability in the size structure spectra, meaning a strong shift of the community in a daily period. This phenomenon is commonly attributed to diel vertical migrations (DVM) where intermediate-sized specimens perform the largest DVM (Manríquez et al., 2012; Ohman and Romagnan, 2016; Rodriguez and Mullin, 1986). Consequences of changes in the size structure due to DVM are diverse indicating the state of the food web (Brierley, 2014). The C-ATZ is part of a wider system with different physical and biological features that provide large amounts of carbon that eventually is converted into fish biomass, supporting local pelagic fisheries. Therefore, planktonic size structure (Barnes et al., 2011; Woodworth-Jefcoats et al., 2013) need to be considered for the management and assessment of fishing resources addressing the size-dependent prey-predator relationships (Canales et al., 2016), and routinely monitoring.

3.6. Conclusions

In conclusion, our abundance results show the differences between the upwelling area and the transitional-open ocean area, while the size spectra show the shift in the control of the food webs trophic structure throughout the annual cycle. Our finding highlights the importance of taxonomic and size spectra studies in the C-ATZ for the evaluation of the ecosystem structure and prey-predator interaction with higher trophic levels.

3.7. Acknowledgments

The authors would like to thank Emilio Marañón for his useful comments on the manuscript. This study was partially funded by the Spanish Ministry project DESAFÍO (PID2020- 118118RB-100), TRIATLAS (Grant Agreement 817578), and SUMMER (Grant Agreement 817806). María Couret was supported by a postgraduate grant (TESIS2022010116)

co-financed by the Agencia Canaria de Investigación, Innovación y Sociedad de la Información de la Consejería de Universidades, Ciencia e Innovación y Cultura and by the Fondo Social Europeo Plus (FSE+) Programa Operativo Integrado de Canarias 2021-2027, Eje 3 Tema Prioritario 74 (85%). Airam Sarmiento-Lezcano was supported by a postgraduate grant from the Spanish Ministry of Science and Innovation (BES-2017-082540). José Landeira was supported by the Beatriz Galindo individual grant BEAGAL 18/00172.

3.8. Author contributions

M.C. contributed to the sampling onboard, laboratory analysis, and data processing. J.M.L. contributed to the abundance analyses. V.M.T. contributed to the size spectra analysis. A.S.L contributed to the data analysis and laboratory experiments. P.V.B. acted as the cruise leader. S.H.L. supervised this study and contributed to the editing of the manuscript. All authors contributed to article writing and discussion, approving the submitted version.

3.9. Supplementary material

Table 3.4. ANOVA results for mesozooplankton biomass. SS stands for Stratified Season and LWB for Late Winter Bloom.

Season	Variable	Df	Sum Sq	F value	p-value	Fraction Size (µm)	Diff	p-value
	Fraction	2	11.34	12.67	<0.001	200-500 to >1000	-0.97	<0.001
SS	Residuals	48	21.48			500-1000 to >1000	-1.03	<0.001
						500-1000 to 200-500	-0.06	0.963
	Fraction	2	4.18	4.07	<0.05	200-500 to >1000	-0.69	<0.05
LWB	Residuals	45	23.16			500-1000 to >1000	-0.53	0.103
						500-1000 to 200-500	0.16	0.802

Chapter 4

Respiration rates and its relationship with ETS activity in Euphausiids: Implications for active flux estimations

Frontiers in Marine Science, 3 October 2024.

https://doi:10.3389/fmars.2024.1469587

María Couret[1,*], Javier Díaz-Pérez[1], Airam N. Sarmiento-Lezcano[1], José María Landeira[1], Santiago Hernández-León[1]

[1]Instituto de Oceanografía y Cambio Global, IOCAG, Universidad de Las Palmas de Gran Canaria, Unidad Asociada ULPGC-CSIC, Campus de Taliarte, 35214 Telde, Gran Canaria, Canary Islands, Spain.

4.1. Abstract

Euphausiids, commonly known as krill, are crucial contributors to the ocean's active carbon pump, impacting carbon export and sequestration through their diel vertical migration. These organisms feed on organic matter in the epipelagic layer at night and release inorganic carbon in the mesopelagic layer during the day via respiration. Measuring respiration in the mesopelagic layer is challenging due to the difficulties in obtaining direct measurements, as well as the lack of comprehensive data, and reliance on conservative estimates. The measurement of the electron transfer system (ETS) activity is used as a proxy to assess respiration in the mesopelagic layer. However, accurate calibration of respiration rates and ETS activity is imperative through experimental measurements and empirical data. Here, we compared the respiration rates with their respective ETS activities of different species of euphausiids captured at night in the epipelagic layer of the Atlantic Ocean along a latitudinal (42-29°N, 25°W) and a longitudinal (25-13°W, 29°N) transect. Our results revealed a spatial trend in respiration rates, and consequently in ETS activities, with rates decreasing southward and increasing slightly towards the African upwelling region. The Generalized Additive Model (GAM) demonstrated that epipelagic oxygen concentration, chlorophyll *a*, and the interaction between epipelagic temperature and mesopelagic oxygen concentration significantly influenced euphausiids respiration rates. Furthermore, we observed a strong correlation between respiration and specific ETS activities, with R/ETS ratios exceeding the conservative value of 0.5, which is typically used to estimate respiratory flux.

Keywords: euphausiids, respiration rates, specific ETS activity, R/ETS ratio, vertical migration, active carbon pump

4.2. Introduction

Zooplankton migrant organisms, such as large copepods and euphausiids (Hernández-León et al., 2019), play a crucial role in the biological carbon pump by actively exporting carbon. This process is known as the active flux or migrant pump and refers to the active transport of organic matter by zooplankton and micronekton to the deepest areas of the ocean (Longhurst and Harrison, 1988). These organisms consume organic carbon at shallower depths and transport it to the mesopelagic layer through diel vertical migrations, where it is released through respiration (Longhurst et al., 1990), egestion (Angel, 1989), excretion (Steinberg et al., 2000), and mortality (Zhang and Dam, 1997). Zooplankton mortality, excretion, and feeding can be estimated from respiration rates (Ikeda and Motoda, 1978; Steinberg et al., 2000; Ariza et al., 2015). Therefore, respiration rates are of importance to assess the role of these organisms in exporting carbon to the mesopelagic layer.

Euphausiids are significant components of marine ecosystems, conducting vertical and horizontal migrations (Ens et al., 2023) that contribute to nutrient transfer and energy flux in the ocean. These organisms are found throughout the world's oceans, from coastal seas to the bathypelagic zone, with their distribution influenced by thermal characteristics and water masses (Letessier et al., 2011; Sutton and Beckley, 2022). Furthermore, they are a major contributor to global plankton community biomass (21%), trailing only behind copepods (47%), in terms of their total organic carbon (Longhurst, 1985). Euphausiids are pivotal in driving the biological pump, contributing significantly to the export and sequestration (sensu Lampitt et al., 2008) of atmospheric CO_2 into the deep ocean through fast-sinking faecal pellets (Cavan et al., 2019), respiration at depth (Stukel et al., 2023), and moulting (Kobari et al., 2010). Thus, they play a key role in the biological carbon pump and the cycle of essential nutrients in marine ecosystems.

Respiratory flux is estimated from the migrant biomass (night minus day biomass values in the epipelagic zone) and the respiration rates at the residence layer during daytime. These rates are determined by measuring migrant organisms captured during the night in the epipelagic zone and converting them to represent respiration at depth using empirical or published Q_{10} values (Le Borgne and Rodier, 1997). Alternatively, values from published equations relating respiration, body size, and temperature (Ikeda, 2013b), for euphausiids) are also used. Enzymatic activities related to cell respiration, such as the electron transfer system (ETS) activity, serve as an alternative proxy for estimating respiratory flux. This method offers advantages as samples can be frozen and stored until they are analysed. However, it requires the calibration of enzymatic proxies to physiological rates (Hernández-León et al., 2019b). The respiration to ETS (R/ETS) ratio in marine zooplankton reflects the scope of metabolic activity and typically ranges between 0.5 and 1 mainly depending on factors such as food availability and temperature (Hernández-León and Gómez, 1996).While conservative ratios of 0.5 are commonly used to assess the respiratory flux, Hernández-León et al. (2019b) observed a R/ETS value of 0.96 ± 0.29 for migrant copepods. This result suggests the need for a reassessment of this ratio to accurately evaluate respiratory fluxes and the carbon transported to the deep ocean by migrant organisms.

In this context, we performed respiration measurements on euphausiids captured at night in the epipelagic layer. We then analysed their specific ETS activity and correlated both sets of measurements to obtain the R/ETS ratio. The aim of the present study was to compare the in situ respiration rates with the specific ETS activities, aiming to derive accurate R/ETS ratios for euphausiids in a longitudinal and latitudinal transect in the North Atlantic Ocean.

4.3. Material and methods

4.3.1. *Sampling and on-board experiments*

The euphausiids used for experiments were collected during the "DisEntangling Seasonality of Active Flux In the Ocean" (DESAFIO I) cruise on board the R.V. "Sarmiento de Gamboa" during February 2023. The research vessel sailed from Vigo (Spain) to the Canary Islands (Spain), spanning from January 31^{st} to March 2^{nd}, 2023 (Fig. 4.1), sampling eleven oceanographic stations (thereafter ST). Vertical profiles of salinity, temperature, oxygen, conductivity, and fluorescence were obtained using a CTD (Seabird 911 plus) and a Seapoint fluorimeter mounted on a rosette sampler equipped with 12 l Niskin bottles.

Euphausiids were captured at night using a Bongo plankton net fitted with a 200 μm mesh and a non-filtering cod-end deployed in horizontal hauls between 0 and 50 m depth. From the plankton sample, euphausiids were sorted and those undamaged with active swimming behavior were selected for the experiments. One single euphausiid was introduced into each experimental bottle (0.5 L), which was filled with filtered (0.2 μm Whatman ® Polycap TC encapsulated filter) and oxygenated surface sea water. Oxygen consumption measurements were carried out using two 4-channel FireSting-O_2 meter, using 3 channels for the experimental organisms and one for the background respiration (without organism). Oxygen contactless sensors (Pyroscience, OXSP5) were attached to the experimental bottles for contactless oxygen read-out. Incubations were conducted placing the experimental bottles inside thermoregulated baths (15.5±0.5°C) in darkness. Total respiration rates (μl O_2·ind^{-1}·h^{-1}) were estimated as the regression slopes of oxygen concentration over time, subtracting background respiration. The first thirty minutes were discarded due to oxygen stabilization inside the bottles and the experiment ranged between 6.5 and 9 hours according to the oxygen concentration in the experimental bottles, that normally decreased from 100% to 85–90% of oxygen saturation. After the respiration

assays, euphausiids were picked and frozen in liquid nitrogen (-196 °C) for later analysis. In the laboratory, before the ETS analysis, euphausiids were classified to species level (or genus when further classification was not possible), photographed and digitized using a Nikon digital camera.

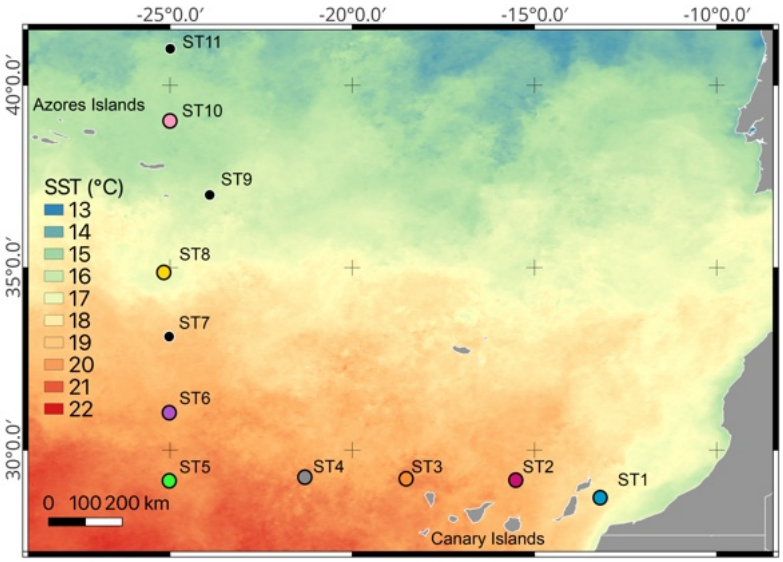

Figure 4.1. Locations of sampling stations during the DESAFIO 1 cruise conducted in February 2023. The background colours depict the monthly average sea surface temperature (SST, °C). The coloured dots indicate the specific stations where experiments were carried out.

4.3.2. *Specific ETS activity and protein content*

Electron transfer system (ETS) activity was measured following the method of (Packard, 1971) modified by Owens and King (1975); Kenner and Ahmed (1975); Gómez et al. (1996). Frozen samples were homogenized at the laboratory in a Teflon pestle at 0-4°C to avoid degradation of enzyme activity and proteins. Then, the homogenates were centrifuged at 4000 rpm at 4°C for 10 min. An aliquot was subsampled from the homogenate, incubated at 18°C in darkness using NADH, NADPH, succinate, and a tetrazolium salt (INT) as the artificial electron acceptor. After 20 min, the incubation was stopped with a quench solution. The ETS activity was estimated spectrophotometrically at 490 nm with

a turbidity baseline of 750 nm. In order to correct ETS activity for in situ temperature, we used the Arrhenius equation and an activation energy of 15 kcal mol^{-1} (King and Packard, 1975). Protein content was determined using the method of Lowry et al. (1951) modified by Rutter (1967), and using bovine serum albumin (BSA) as the standard. Finally, protein specific respiration rates (μl O_2·mg $prot^{-1}$·h^{-1}) were estimated to compared with the specific ETS activities (μl O_2·mg $prot^{-1}$·h^{-1}) and to estimate the R/ETS ratios.

4.3.3. *Estimation of respiration rates and ETS activity in the epipelagic and mesopelagic layer*

ETS activity of organisms incubated for respiration experiments and captured in the 0-50 m depth layer were converted to ETS activities in the epipelagic (0-200 m) and mesopelagic (200-1000 m) layers using the Arrhenius equation and the temperature of each layer. Respiration rates in the upper 50 m were directly measured, while rates for the epipelagic (0-200 m) and mesopelagic (200-1000 m) layers were estimated based on the measured rates from the 0-50 m depth using a Q_{10} value of 3 (Hernández-León et al., 2019b), which represents the factor by which the respiration rate increases for every 10°C rise in temperature, and the temperature (T) at each layer:

$$\text{Respiration rate}_{(0-200\ m\ depth)} = \text{Respiration rate}_{(0-50\ m\ depth)} \times 3^{\frac{T_{(0-200\ m\ depth)} - T_{(0-50\ m\ depth)}}{10}}$$

$$\text{Respiration rate}_{(200-1000\ m\ depth)} = \text{Respiration rate}_{(0-50\ m\ depth)} \times 3^{\frac{T_{(200-1000\ m\ depth)} - T_{(0-50\ m\ depth)}}{10}}$$

Both the Q_{10} value and the Arrhenius equation are used to describe the temperature dependence of biological and chemical processes, but they are applied differently based on the nature of the processes they describe and the assumptions behind each model. The Q_{10} value is commonly used in biological sciences to describe the temperature sensitivity of metabolic processes, including respiration, as it provides a simple and empirical measure of how these rates change with temperature (Mundim et al., 2020). In contrast, the Ar-

rhenius equation is based on the fundamental principles of chemical kinetics and provides insight into the energy barriers that must be overcome for electron transfer reactions to occur, making it directly related to the molecular and energetic properties of the enzymes and substrates involved (Owens and King, 1975).

4.3.4. *Data analysis*

The relationships between specific respiration rates and specific ETS activities, and the relationships between protein content and respiration rates were fitted using linear regression. Because of the general trend that metabolism is a power function of body weight, the values were log-transformed. Pearson's correlation was used to evaluate the relationship between euphausiids respiration rates, ETS activities, and R/ETS ratios against temperature, oxygen concentration, chlorophyll *a* values, and primary production. Differences in respiration rates between stations were tested using the analysis of the variance (one-way ANOVA). Respiration rates were transformed using a Box-Cox transformation to adjust normality. Normality was tested using the Shapiro-Wilk Test and homoscedasticity using the Bartlett test. Finally, a Generalized Additive Model (GAM) was applied to model the relationship between the response variable (respiration rates measured from euphausiids captured at night in the epipelagic layer) and predictors (individual protein content and environmental conditions in the epipelagic and mesopelagic layer). All analyses were performed in the programming language R (R Core Team, 2024). The map of the sampling region was created using the geographic information system QGIS (V.3.38.2) (QGIS Development Team, 2024).

4.4. Results

In the latitudinal transect, temperature values (Fig. 4.2a) increased from ST11 to ST5 in the epipelagic layer (0-200 m depth), while in the longitudinal transect (Fig. 4.2b) temperature was similar in all stations but slightly decreasing close to the African coast (i.e., ST1 and ST2). Oxygen vertical profiles (Fig. 4.2c) showed higher oxygen concentration in the epipelagic layer of the latitudinal transect, specially from ST11 to ST8. In the longitudinal transect (Fig. 4.2d), oxygen vertical profiles in the epipelagic layer showed an increase from the open ocean to the coast. On the other hand, mesopelagic oxygen concentration increased from the coast to the open ocean (from ST1 to ST6), reaching the highest values from ST11 to ST8. Vertical profiles of chlorophyll *a* (Chl *a*) in the upper 200 m layer showed higher values at the northern stations of the latitudinal transect (Fig. 4.2e) and at the stations close to the African coast (Fig. 4.2f).

Respiration rates measured in euphausiids captured in the first 0-50 m of the water column ranged from 19.65 ± 9.91 μl O_2·mg prot^{-1}·h^{-1} at ST10 to 4.64 ± 2.11 μl O_2·mg prot^{-1}·h^{-1} at ST3 (Table 4.1), displaying higher values at those stations where higher values of oxygen and Chl *a* were found (i.e. from ST10 to ST6). Respiration rates measured in the upper 50 m depth were similar to the rates estimated for the epipelagic layer (0-200 m depth) using the measured ETS and applying a Q_{10} value of 3 (Fig. 4.3a). In contrast, the estimated respiration rates for the mesopelagic layer (200-1000 m depth) were lower as expected (Fig. 4.3a, Table 4.1). Specific ETS activity, estimated using the Arrhenius equation as mentioned above (Fig. 4.3b), showed a similar pattern as the respiration rates, with higher values at ST10 decreasing along the latitudinal transect, and slightly increasing close to the African upwelling (ST1). R/ETS ratios in the upper 0-50 m depth ranged from 1.19 ± 0.49 at ST6 to 0.65 ± 0.12 at ST3 in the 0-50 m depth layer (Table 4.1, Fig. 4.3c), displaying similar values as the R/ETS obtained for the epipelagic layer (ranging from 1.18 ± 0.34 to 0.64 ± 0.12, respectively) and slightly higher than those obtained at depth

(ranging from 1.05 ± 0.3 to 0.56 ± 0.11, respectively) (Table 4.1). Estimated respiration for the epipelagic layer (0-200 m depth) showed a significant relationship with epipelagic specific ETS values (R^2 = 0.73, $p<0.001$, n = 66, see Fig. 4.4) and mesopelagic specific ETS values (R^2 = 0.76, $p<0.001$, n = 66). Total respiration rates (Fig. 4.5a) showed a positive relationship with body weight as protein content, while specific respiration rate (μl O_2·mg $prot^{-1}$·h^{-1}) significantly decreased with the increasing body weight as expected (Fig. 4.5b).

Pearson's correlation showed a significant negative correlation between the averaged epipelagic temperature and the respiration rates estimated for the epipelagic (r = -0.7, $p<0.05$) and for the mesopelagic layer (r = -0.77, $p<0.05$) (Fig. 4.6a, Supp. Table 3a). Moreover, specific ETS activity estimated for the mesopelagic layer also showed a significant negative correlation with the epipelagic temperature (r = -0.7, $p<0.05$) (Fig. 4.6b, Supp. Table 3a). However, no significant correlations were found between the epipelagic temperature and the epipelagic specific ETS activity nor the R/ETS ratios (Fig. 4.6bc, Supp. Table 4.4). On the other hand, a strong significant positive correlation was found between the epipelagic oxygen concentration (ml·L^{-1}) (Fig. 4.6 upper panel) and the estimated respiration rates (μl O_2·mg $prot^{-1}$·h^{-1}), both for the epipelagic (r = 0.95, $p<0.001$) and for the mesopelagic (r = 0.96, $p<0.001$) (Fig. 4.7a, Supp. Table 4.4) layers, as well as between the epipelagic oxygen concentration and the specific ETS activity, also for the epipelagic (r = 0.94, $p<0.001$) and for the mesopelagic (r = 0.96, $p<0.001$) (Fig. 4.7b, Supp. Table 4.4) layers. Likewise, mesopelagic oxygen concentration (Fig. 4.7 lower panel) also showed a strong significant positive correlation between the estimated respiration rates, both for the epipelagic (r = 0.78, $p<0.05$) and for the mesopelagic (r = 0.77, $p<0.05$) (Fig. 4.7d, Supp. Table 4.4) layer, and with the ETS activity for the epipelagic (r = 0.71, $p<0.05$) and mesopelagic (r = 0.72, $p<0.05$) (Fig. 4.7e, Supp. Table 4.4) layers. However, no significant correlations were found between the epipelagic and mesopelagic oxygen concentration and the R/ETS ratios (Fig. 4.7cf, Supp. Table 4.4). Finally, average

Chl *a* (Fig. 4.8 upper panel) and net primary production (Fig. 4.8 lower panel) obtained in the epipelagic layer did not show any correlation between the respiration rates, the ETS activities, nor the R/ETS ratios (Fig. 4.8cf, Table 4.4).

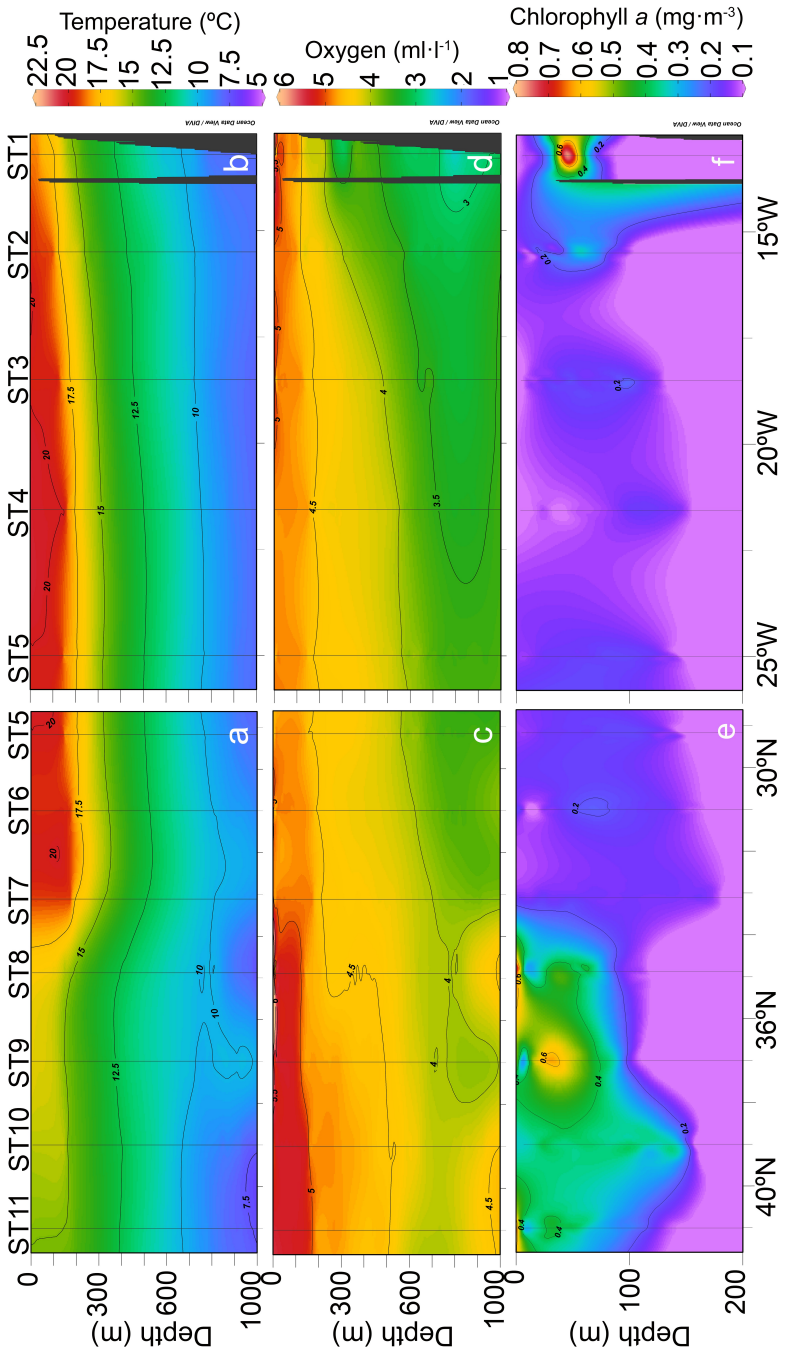

Figure 4.2. Vertical distribution of (a-b) temperature (°C), (c-d) oxygen (ml·L^{-1}), and (e-f) chlorophyll *a* (mg·m^{-3}) along the latitudinal (left panel) and longitudinal (right panel) transects sampled during the DESAFIO 1 cruise. Note the different y-axes for the chlorophyll *a* vertical profiles

Table 4.1. Euphausiid biomass (mg protein·ind^{-1}), respiration rates (μl O_2·mg prot^{-1}·h^{-1}), specific (sp) ETS activities (μl O_2·mg prot^{-1}·h^{-1}), and R/ETS ratios measured in the 0-50 m depth layer, estimated for the epipelagic (0-200 m depth) and mesopelagic (200-1000 m depth) layers.

Station	n	Body weight (mg protein·ind^{-1})	Respiration (μl O_2·mg prot^{-1}·h^{-1})			sp ETS activity (μl O_2·mg prot^{-1}·h^{-1})			R/ETS		
			0-50 m	0-200 m (Q_{10}=3)	200-1000 m (Q_{10}=3)	0-50 m	0-200 m	200-1000 m	0-50 m	0-200 m	200-1000 m
ST10	7	1.39±2.81	19.65±9.91	19.3±9.74	12.52±6.52	22.82±5.88	22.49±5.8	15.66±4.03	0.85±0.32	0.85±0.31	0.79±0.29
ST8	6	0.46±0.27	14.05±6.86	12.58±6.14	7.6±3.71	12.39±4.65	11.31±4.25	7.43±2.79	1.15±0.48	1.13±0.47	1.04±0.43
ST6	6	1.15±0.9	10.82±11.36	10.39±10.91	5.36±5.63	8.36±6.78	8.09±6.56	4.70±3.81	1.19±0.34	1.18±0.34	1.05±0.3
ST5	11	1.19±1.07	4.98±3.87	4.76±3.69	2.30±1.78	6.34±4.28	6.11±4.12	3.39±2.28	1.06±0.88	1.05±0.87	0.92±0.76
ST4	11	0.55±0.17	8.97±3.59	8.78±3.51	4.06±1.62	12.18±3.1	11.97±3.05	6.35±1.62	0.75±0.24	0.75±0.24	0.65±0.21
ST3	7	0.65±0.23	4.64±2.11	4.35±1.97	2.09±0.95	7.152.66	6.79±2.52	3.72±1.38	0.65±0.12	0.64±0.12	0.56±0.11
ST2	12	0.7±0.12	4.66±1.55	4.20±1.39	2.05±0.68	5.57±2.39	5.12±2.19	2.84±1.22	0.88±0.12	0.86±0.11	0.76±0.10
ST1	6	1.09±0.44	5.73±5.58	5.17±5.03	2.71±2.64	6.50±5.66	5.97±5.21	3.49±3.04	0.82±0.13	0.80±0.13	0.72±0.12

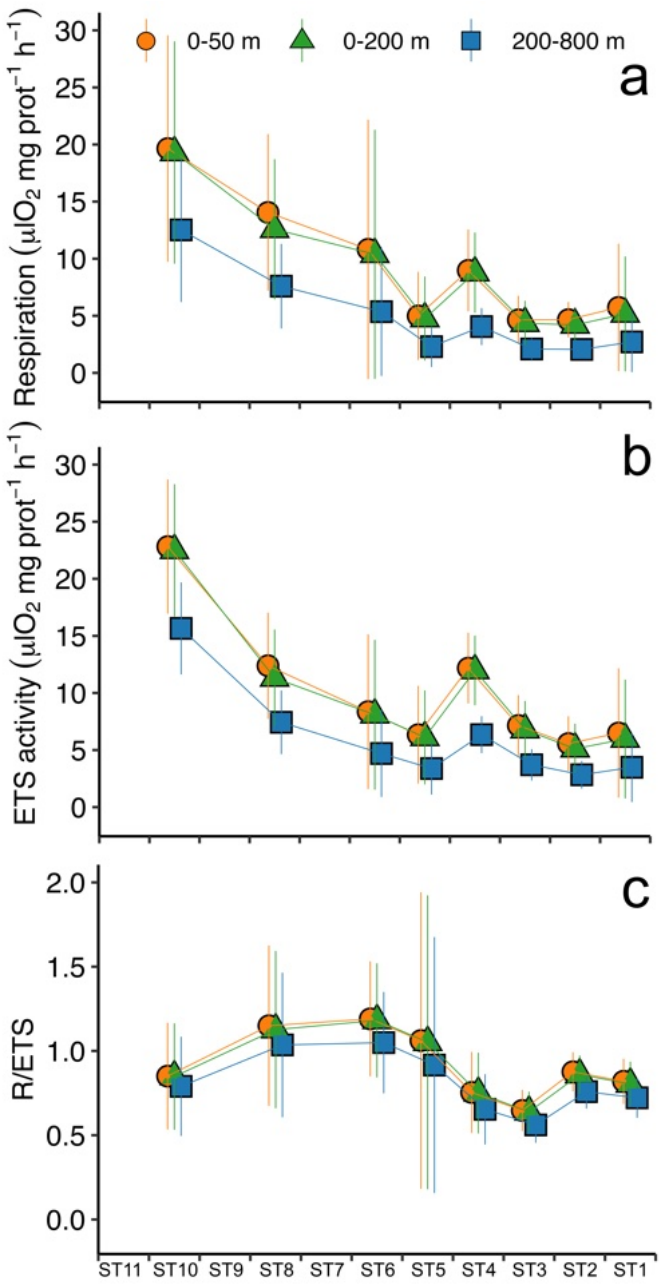

Figure 4.3. (a) Respiration rates (μl O_2·mg prot^{-1}·h^{-1}), (b) protein normalized ETS activity (μl O_2·mg prot^{-1}·h^{-1}), and (c) R/ETS ratios of migrant euphausiids obtained from incubations conducted along the oceanographic stations in the Atlantic transect. Measurements were estimated at surface temperature (orange), for the epipelagic layer (green), and for the mesopelagic temperature (blue) at each station (see text). Vertical lines indicate the standard error.

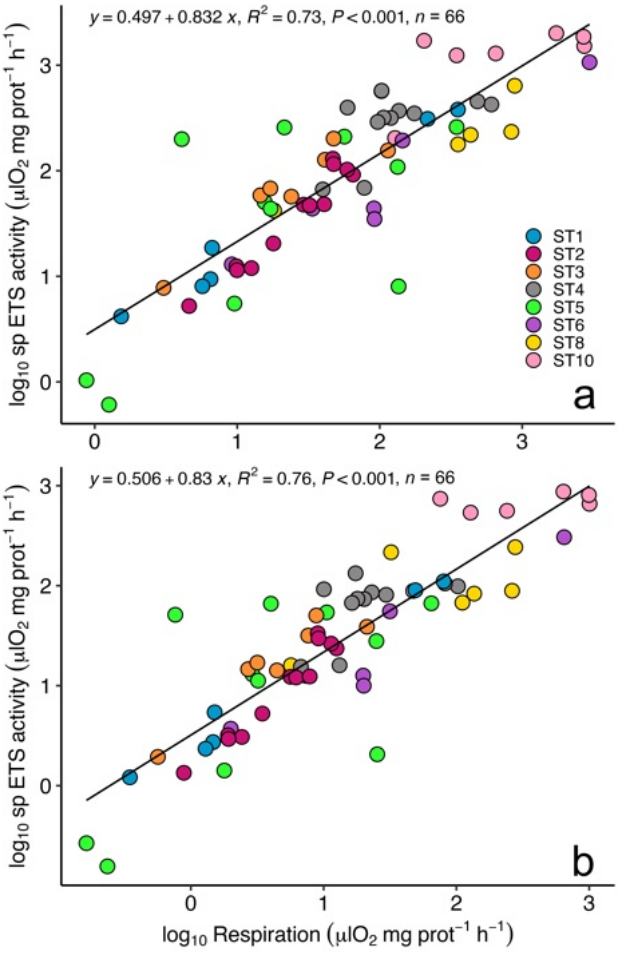

Figure 4.4. Relationship between euphausiid respiration rates and specific (sp) ETS activity estimated for the a) epipelagic (0-200 m depth) and the b) mesopelagic layer (200-1000 m depth). See text for explanation.

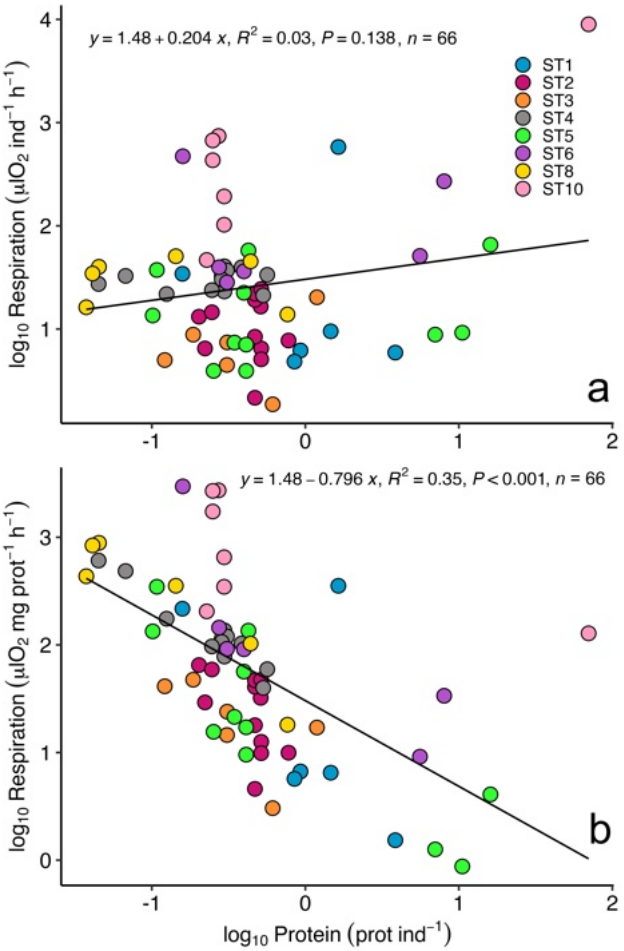

Figure 4.5. Relationship between euphausiid body weight (as protein content) and (a) total respiration rates (μl O_2·ind^{-1}·h^{-1}) and (b) respiration rate (μl O_2·mg prot^{-1}·h^{-1}) in the epipelagic layer (0-200 m depth).

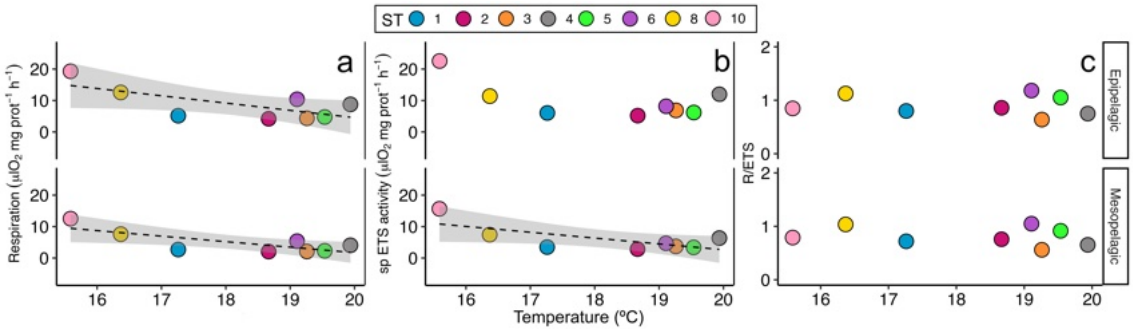

Figure 4.6. Pearson's correlation between temperature (°C) in the epipelagic layer and average (a) respiration (μl O_2·mg prot^{-1}·h^{-1}), (b) specific (sp) ETS activity (μl O_2·mg prot^{-1}·h^{-1}), and (c) the R/ETS ratio in the epipelagic and mesopelagic layers per station. Only significant correlations are indicated with a line and standard deviation. Colours and numbers represent the stations.

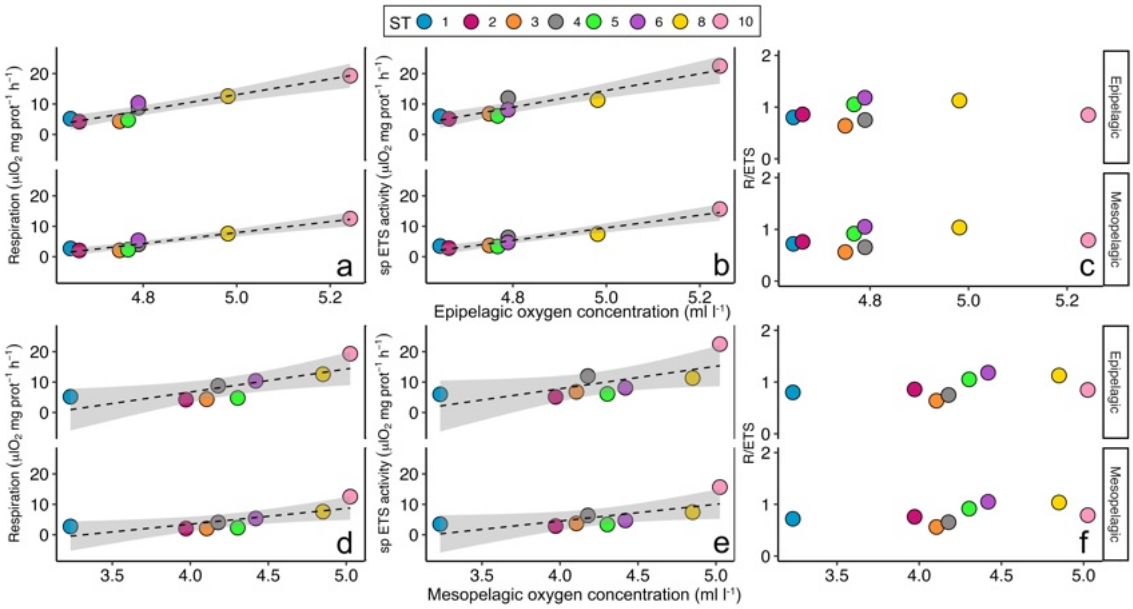

Figure 4.7. Pearson's correlation between oxygen (ml·l^{-1}) in the epipelagic (upper panel) and mesopelagic (lower panel) layers and average (a,d) respiration (μl O_2·mg prot^{-1}·h^{-1}), (b,e) specific (sp) ETS activity (μl O_2·mg prot^{-1}·h^{-1}), and (c,f) the R/ETS ratio in the epipelagic and mesopelagic layers per station. Only significant correlations are indicated with a line and standard deviation. Colours and numbers represent the stations.

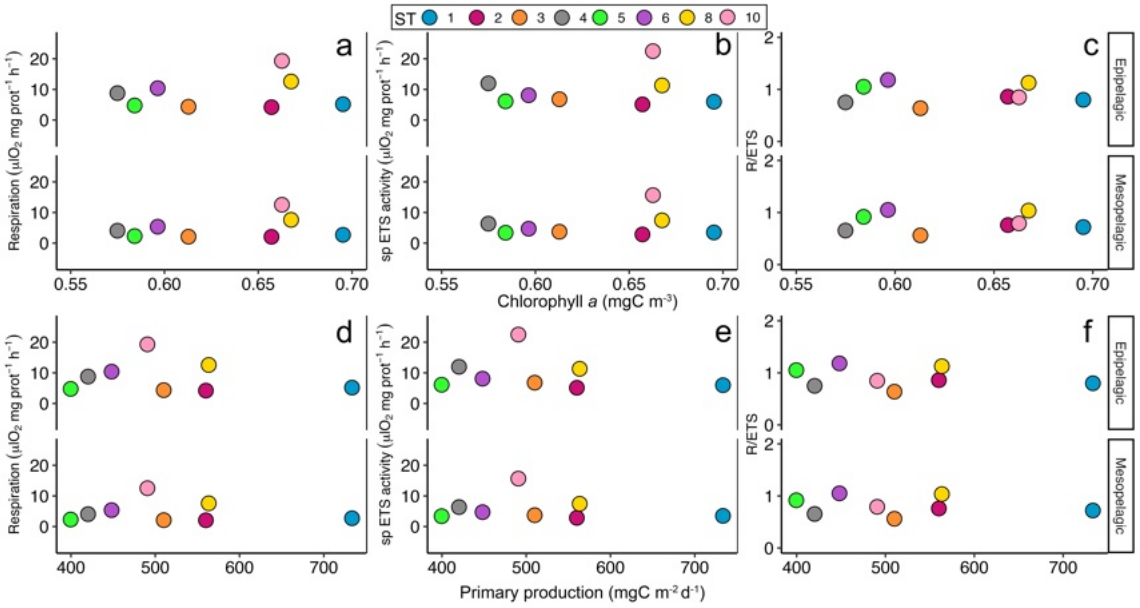

Figure 4.8. Upper panel: Pearson's correlation between chlorophyll *a* (mg·m^{-3}) in the epipelagic layer and average (a) respiration (μl O_2·mg prot^{-1}·h^{-1}), (b) specific (sp) ETS activity (μl O_2·mg prot^{-1}·h^{-1}), and (c) the R/ETS ratio in the epipelagic and mesopelagic layers per station. Lower panel: Pearson's correlation between net primary production (mg C·m^{-2}·d^{-1}) in the epipelagic layer and average (d) respiration (μl O_2·mg prot^{-1}·h^{-1}), (e) specific (sp) ETS activity (μl O_2·mg prot^{-1}·h^{-1}), and (f) the R/ETS ratio in the epipelagic and mesopelagic layers per station. Only significant correlations are indicated with a line and standard deviation. Colours and numbers represent the stations.

The ANOVA results showed significant differences between stations (F value = 6.55, $p<0.001$, df = 7), thus we modeled the variability of the respiration rates in the epipelagic layer between stations according to the environmental variables in the epipelagic and mesopelagic layers using a GAM, as mentioned above. Estimated coefficients from the best-fitting GAM based on different combinations of explanatory variables for the response variables are summarized in Table 4.2. The best-fitting GAM was selected using the Akaike information criterium (AIC, see Akaike, 1974). The optimal model included the effect of body weight, oxygen, and chlorophyll *a* in the epipelagic layer, and the interaction of temperature in the epipelagic layer and the oxygen concentration in the mesopelagic layer:

$$g(Y) = \text{Protein} + s(\text{Oxygen}_{Epipelagic\ Layer}) + s(\text{Chlorophyll}_{Epipelagic\ Layer}) + s(\text{Temperature}_{Epipelagic\ Layer} \times \text{Oxygen}_{Mesopelagic\ Layer})$$

where g() stands for the function of the response variable (Box-Cox transformed, here respiration rates) and s() denotes the smoother functions.

Table 4.2. Estimated coefficients for selected variables from the best-fitting Generalized Additive Model (GAM) for the response variables.

	Respiration rates (in μl O_2·mg prot^{-1}·h^{-1})	
	F value	p-value
Body weight	9.37	<0.01
s(Oxygen $_{Epipelagic\ Layer}$)	84.39	<0.001
s(Chlorophyll $_{Epipelagic\ Layer}$)	3.59	0.05
s(Temperature $_{Epipelagic\ Layer}$ × Oxygen $_{Mesopelagic\ Layer}$)	49.5	<0.001

4.5. Discussion

Euphausiid respiration rates, specific ETS activity, and R/ETS were estimated along a latitudinal and a longitudinal transect in the North Atlantic Ocean. To our knowledge, this is the first attempt to calibrate respiration rates and ETS activity through experimental measurements in euphausiids. We observed higher R/ETS ratios than the conservative value of 0.5 commonly used to assess the respiratory flux (Table 4.1) and found a close relationship between respiration rates and specific ETS activity (Fig. 4.4), with rates highly influenced by the oxygen concentration (Fig. 4.7).

Respiration rates in euphausiids are influenced by various environmental factors, such as temperature, body size, feeding rates, and the number of daylight hours (Clarke and

Morris, 1983). Significant variations were also observed among different species and seasons (Small and Hebard, 1967; Tremblay et al., 2014; Tarling, 2020). As previously reported by Ikeda (2013a), we also obtained an increase of total respiration rates with weight (Fig. 4.5a) and a decrease of specific respiration rate with the increasing of body weight (Fig. 4.5b), as body mass is one of the major determinants of zooplankton respiration rates (Hernández-León and Ikeda, 2005). Our results showed significant correlations between temperature (Fig. 4.6) and oxygen concentration (Fig. 4.7) with specific respiration rates and ETS activities. However, the correlations between chlorophyll *a* values and primary production with respiration rates, specific ETS activity, or R/ETS ratios were not statistically significant (Fig. 4.8), although the GAM results indicated that chlorophyll *a* significantly influences respiration rates (Table 4.2). This disagreement suggests that chlorophyll *a*, while not the primary driver, provides additional explanatory power in predicting euphausiid respiration rates (Chen and Smith, 2018). Indeed, the relationship between primary production and euphausiids' respiration rates, abundance, and species diversity is not straightforward (Tremblay et al., 2020). The GAM approach allows the detection of nonlinear relationships and the interactions between multiple environmental variables, thus revealing the indirect influence of chlorophyll *a* on euphausiid metabolism. In any case, our findings indicated that chlorophyll *a* does not directly influence respiration rates. Instead, other environmental factors such as temperature and oxygen concentration appear to have a more direct impact on respiration rates and specific ETS activity.

Temperature has different impacts on euphausiids respiration rates depending on the oxygen concentration (Tremblay et al., 2020). Moreover, oxygen in the mesopelagic layer also affects zooplankton by influencing their community structure, vertical distribution (Ekau et al., 2010), metabolic activity (Kiko and Hauss, 2019), feeding, and excretion rates (Robinson et al., 2010). Our findings, supported by the Generalized Additive Model (GAM) results (Table 4.2) and the Pearson's correlations (Fig. 4.6 and 4.7), indicated that temperature and oxygen concentration significantly influenced euphausiids respira-

tion rates. However, we observed a negative correlation between temperature and both euphausiid respiration rates and ETS activity, which contrasts with previous research on the effects of temperature on euphausiids metabolism (Iguchi and Ikeda, 2005; Kiko and Hauss, 2019). This discrepancy may be attributed to oxygen concentration having a greater impact on the metabolism of these organisms than temperature, as we obtained the highest respiration rates in areas with high mesopelagic oxygen concentration, lower epipelagic temperatures, and high chlorophyll *a* values (i.e., ST10 and ST8, Table 4.1). Similar results were previously reported by Kiko and Hauss (2019) in the Tropical Pacific, where theirs results indicated that oxygen is a key environmental variable that scales metabolic activity. However, research has focused on scenarios involving increasing temperatures and low oxygen concentrations, which could negatively impact hypoxia tolerance due to increased energy expenditures (Ekau et al., 2018). Yet, in this study, the higher respiration rates were observed in areas characterised by low temperature but high oxygen concentrations. Further research is needed to unravel the combined effects of temperature and oxygen concentrations on euphausiid physiological rates.

The influence of mesopelagic oxygen concentration on the euphausiids' respiration rates and enzymatic activity might be attributed to the diverse responses to varying oxygen levels. Some species exhibit a high degree of oxyconformity, decreasing their oxygen consumption rates as oxygen levels decline. Conversely, other species display strong oxyregulation, maintaining a consistent oxygen uptake irrespective of ambient oxygen levels (Herrera et al., 2019; Tremblay et al., 2020). Other individuals, at the limit of their aerobic scope (the difference between the routine and the maximum metabolic rate), reach a point where oxygen levels in the body fluids begin to decline and the capacity to adjust respiration becomes gradually limited (Pörtner, 2002). At this point, they reverted to anaerobic mode of mitochondrial metabolism caused by an excessive oxygen demand if reached the critical threshold temperature (Ollier et al., 2018; Tarling, 2020). The different adaptations of euphausiids to low dissolved oxygen concentrations affect the respiration

rates reflecting their ecophysiological plasticity (Werner, 2013) and are linked to the temperature they experience during the diel vertical migration (Tremblay et al., 2020). This leads to a vertical limitation of habitats for these diel vertical migrant organisms, shaping the different species' behavior, distribution and physiological processes (Tremblay et al., 2020). Under the actual global warming scenario of expanding and intensifying oxygen minimum zones (Stramma et al., 2008), and considering the key position of euphausiids in the trophic web dynamics (Lee et al., 2022), the physiological and behavioral adaptions, and strategies of these organisms to different levels of oxygen and temperatures should be further addressed.

The R/ETS ratio has been subject of debate since Packard et al. (1974). It appears that the R/ETS ratio in marine zooplankton is influenced by a combination of factors, including zooplankton size, temperature, metabolic activity, primary production, and the limitations of the measurement techniques used (Hernández-León and Gómez, 1996). However, the available database on R/ETS ratios remains relatively limited, which hampers the comprehensive study of the variables affecting respiration rates, thus the ETS activities and R/ETS ratios. High R/ETS ratios were associated with fed organisms exhibiting higher average respiration but lower ETS activity at the end of incubation, while lower R/ETS ratios are associated with low primary production scenarios (Hernández-León and Gómez, 1996). Despite these findings, the influence of oxygen concentration on R/ETS ratios in zooplankton was not previously studied. To explore the impact of environmental variables on the estimated epipelagic and mesopelagic R/ETS ratios, we applied the Generalized Additive Model (GAM) fitted for respiration rates. This approach was chosen due to the lack of significant correlations between temperature, oxygen concentration, chlorophyll a, or primary production values and the R/ETS ratios. While epipelagic oxygen and chlorophyll *a* significantly influenced ($p<0.05$ and $p<0.0001$, respectively) the epipelagic R/ETS ratios, both the epipelagic oxygen concentration ($p = 0.05$), chlorophyll *a* ($p<0.001$), and the interaction between epipelagic temperature and mesopelagic oxygen concentration ($p<0.05$)

influenced the mesopelagic R/ETS ratios. These results suggest a dependence between the respiration rates in the epipelagic layer during the nighttime (expected to be higher with increasing chlorophyll *a*) and the mesopelagic R/ETS during the daytime (due to increased metabolism at their residence depth), supporting the indirect influence of chlorophyll *a* on euphausiid metabolism.

Most studies quantifying the carbon transported to the deep ocean due to zooplankton and micronekton diel vertical migrations use a conservative R/ETS ratio of 0.5 (e.g. Ariza et al., 2015; Hernández-León et al., 2019; Hernández-León et al., 2019b; Sarmiento-Lezcano et al., 2022). However, it is known that R/ETS values are quite variable, usually ranging from 0.5 to 1.0, or even reaching ratios over 1 during periods of high primary production or nutrient-rich conditions (Hernández-León and Gómez, 1996). Using a single, fixed R/ETS ratio to estimate respiration from ETS measurements may lead to over- or underestimation of carbon flux, given that the ratio is not constant. In this context, we obtained a mean R/ETS value of 0.91 ± 0.19 (n = 66) in the epipelagic layer for different species of euphausiids (Table 3a), similarly to the R/ETS value of 0.96 ± 0.29 obtained by Hernández-León et al. (2019b) for migrant copepods. The estimated mean R/ETS ratio for the mesopelagic layer (Table 4.1) obtained in this study was 0.81 ± 0.18, indicating that respiration rates are higher compared to the conservative value of 0.5 commonly used. Consequently, a larger quantity of carbon is likely to be transported to the deep ocean due to migrant zooplankton and micronekton respiration at depth. The respiration of the mesopelagic organisms is a key controlling factor of carbon export to the deep ocean and plays a significant role in active carbon flux. Understanding the processes and mechanisms of mesopelagic respiration is crucial for accurately modelling and predicting the carbon cycle in the ocean.

4.6. Conclusions

In summary, we conducted respiration rate measurements on euphausiids captured in the epipelagic layer at night in areas with different environmental conditions. The resulting R/ETS ratios, both in the epipelagic and the mesopelagic layers, were higher than the conservative value of 0.5 typically used to assess active flux. We employed a GAM model to explore the relationship between the respiration rates obtained in the epipelagic layer at night and the environmental variables, revealing the influence of epipelagic oxygen concentration, chlorophyll *a*, and the interaction of epipelagic temperature and mesopelagic oxygen concentration on euphausiids respiration rates. However, further research is needed to evaluate the combined effects of the environmental variables on the respiration rates, as well as R/ETS ratios, in both the epipelagic and mesopelagic layer, and their influence on the biological carbon pump.

4.7. Acknowledgments

The authors wish to thank the crew and other scientists on board the R/V "Sarmiento de Gamboa" as well as the technicians of the "Unidad de Tecnología Marina" (UTM) for their support and help during the cruise. This work was supported by projects "DisEntangling Seasonality of Active Flux In the Ocean" (DESAFÍO, PID 2020- 118118RB-100) from the Spanish Ministry of Science and Innovation, and IMDEEP (ref: 2022CLISA15) from the Fundación CajaCanarias-La Caixa. María Couret was supported by a postgraduate grant (TESIS2022010116) co-financed by the Agencia Canaria de Investigación, Innovación y Sociedad de la Información de la Consejería de Universidades, Ciencia e Innovación y Cultura and by the Fondo Social Europeo Plus (FSE+) Programa Operativo Integrado de Canarias 2021-2027, Eje 3 Tema Prioritario 74 (85%). Airam Sarmiento-Lezcano was supported by a postdoctoral grant (IN606B-2024/018) from the "Agencia Gallega de In-

novación". Javier Díaz Pérez by a postgraduate grant (ULPGC2022-2) from Universidad de Las Palmas de Gran Canaria.

4.8. Author contributions

M.C. conceptualised, conceived, developed the experiments, analysed the data, and created all figures; J.D.P. taxonomically classified the organisms; A.S.L. analysed the data. M.C drafted the manuscript, and all authors contributed substantially to its improvement. All authors approved the final submitted manuscript.

4.9. Supplementary material

Table 3a. Euphausiid biomass (mg protein·ind^{-1}), respiration rates (μl O_2·mg prot^{-1}·h^{-1}), specific (sp) ETS activities (μl O_2·mg prot^{-1}·h^{-1}), and R/ETS ratios measured in the 0-50 m depth layer, estimated for the epipelagic (0-200 m depth) and mesopelagic (200-1000 m depth) layers.

Station	Species	Body weight (mg protein·ind^{-1})	Respiration (µl O_2·mg prot^{-1}·h^{-1})		**sp ETS activity (µl O_2·mg prot^{-1}·h^{-1})**			R/ETS		
			0-50 m	0-200 m (Q_{10}=3)	200-1000 m (Q_{10}=3)	0-50 m	0-200 m	200-1000 m	0-50 m	0-200 m	200-1000 m
ST10	*Euphausia krohnii*	0.57	31.60	31.05	20.14	24.42	24.07	16.75	1.29	1.29	1.20
ST10	*Euphausia krohnii*	0.55	31.44	30.90	20.04	26.68	26.30	18.31	1.18	1.17	1.09
ST10	*Euphausia krohnii*	0.55	25.96	25.51	16.55	27.59	27.19	18.93	0.94	0.94	0.87
ST10	*Euphausia hemigibba*	0.53	10.27	10.09	6.54	25.70	25.33	17.63	0.40	0.40	0.37
ST10	*Nematobrachion flexipes*	0.59	16.98	16.68	10.82	22.78	22.45	15.62	0.75	0.74	0.69
ST10	*Euphausia hemigibba*	0.59	12.90	12.68	8.22	22.37	22.05	15.35	0.58	0.58	0.54
ST10	*Thysanopoda obustifrons*	6.33	8.37	8.23	5.34	10.22	10.07	7.01	0.82	0.82	0.76
		1.39±2.18	**19.65±9.91**	**19.30±9.74**	**12.52±6.32**	**22.82±5.88**	**22.49±5.8**	**15.66±4.03**	**0.85±0.32**	**0.85±0.32**	**0.79±0.29**
ST8	*Euphausia krohnii*	0.26	21.30	19.06	11.51	18.10	16.53	10.86	1.18	1.15	1.06
ST8	*Euphausia americana*	0.89	3.93	3.52	2.13	5.55	5.07	3.33	0.71	0.69	0.64
ST8	*Euphausia americana*	0.24	15.63	13.98	8.45	11.37	10.39	6.82	1.37	1.35	1.24
ST8	*Euphausia americana*	0.70	8.36	7.48	4.52	17.21	15.71	10.33	0.49	0.48	0.44
ST8	*Euphausia americana*	0.25	20.80	18.62	11.24	11.70	10.69	7.02	1.78	1.74	1.60
ST8	*Euphausia sp.*	0.43	14.30	12.80	7.73	10.39	9.49	6.23	1.38	1.35	1.24
		0.46±0.27	**14.05±6.86**	**12.58±6.14**	**7.60±3.71**	**12.39±4.65**	**11.31±4.25**	**7.43±2.79**	**1.15±0.48**	**1.13±0.47**	**1.04±0.43**
ST6	*Euphausia krohnii*	2.47	4.80	4.61	2.38	5.33	5.16	3.00	0.90	0.89	0.79
ST6	*Euphausia krohnii*	0.45	33.56	32.22	16.63	21.34	20.65	12.00	1.57	1.56	1.39
ST6	*Euphausia americana*	0.67	7.39	7.09	3.66	5.35	5.17	3.01	1.38	1.37	1.22
ST6	*Euphausia krohnii*	2.11	2.73	2.62	1.35	3.15	3.04	1.77	0.87	0.86	0.76
ST6	*Euphausia krohnii*	0.60	7.42	7.12	3.68	4.83	4.68	2.72	1.53	1.52	1.35
ST6	*Euphausia krohnii*	0.57	9.04	8.68	4.48	10.17	9.84	5.72	0.89	0.88	0.78
		1.15±0.90	**10.82±11.36**	**10.39±10.91**	**5.36±5.63**	**8.36±6.78**	**8.09±6.56**	**4.70±3.81**	**1.19±0.34**	**1.18±0.34**	**1.05±0.30**
ST5	*Euphausia krohnii*	0.37	8.78	8.38	4.04	7.96	7.66	4.25	1.10	1.09	0.95
ST5	*Euphausia americana*	0.38	13.29	12.68	6.12	11.61	11.18	6.19	1.14	1.13	0.99
ST5	*Euphausia sp.*	0.67	6.04	5.77	2.78	10.60	10.21	5.66	0.57	0.56	0.49
ST5	*Euphausia krohnii*	0.69	8.84	8.43	4.07	2.57	2.47	1.37	3.45	3.41	2.97
ST5	*Euphausia krohnii*	3.34	1.93	1.84	0.89	10.35	9.97	5.52	0.19	0.18	0.16
ST5	*Euphausia americana*	2.33	1.16	1.11	0.53	0.84	0.81	0.45	1.39	1.37	1.20
ST5	*Euphausia americana*	2.78	0.99	0.94	0.46	1.05	1.02	0.56	0.94	0.93	0.81
ST5	*Euphausia americana*	0.55	3.45	3.30	1.59	5.70	5.49	3.04	0.61	0.60	0.52
ST5	*Euphausia krohnii*	0.63	3.97	3.79	1.83	11.57	11.14	6.17	0.34	0.34	0.30
ST5	*Euphausia hemigibba*	0.68	3.60	3.44	1.66	5.36	5.16	2.86	0.67	0.67	0.58
ST5	*Euphausia americana*	0.68	2.79	2.67	1.29	2.18	2.10	1.16	1.28	1.27	1.11
		1.19±1.07	**4.99±3.87**	**4.76±3.69**	**2.30±1.78**	**6.34±4.28**	**6.11±4.12**	**3.38±2.28**	**1.06±0.88**	**1.05±0.87**	**0.92±0.76**

Table 3b. Continued: Euphausiid biomass (mg protein·ind^{-1}), respiration rates (μl O_2·mg prot^{-1}·h^{-1}), specific (sp) ETS activities (μl O_2·mg prot^{-1}·h^{-1}), and R/ETS ratios measured in the 0-50 m depth layer, estimated for the epipelagic (0-200 m depth) and mesopelagic (200-1000 m depth) layers.

ST4	*Euphausia hemigibba*	0.59	8.64	8.46	3.91	13.26	13.04	6.91	0.65	0.65	0.56
ST4	*Euphausia krohnii*	0.76	5.07	4.96	2.29	6.30	6.19	3.28	0.80	0.80	0.70
ST4	*Euphausia krohnii*	0.59	6.78	6.63	3.06	6.39	6.29	3.33	1.06	1.06	0.92
ST4	*Euphausia krohnii*	0.60	8.17	7.99	3.69	12.40	12.19	6.46	0.66	0.66	0.57
ST4	*Euphausia krohnii*	0.58	7.76	7.59	3.51	12.44	12.23	6.48	0.62	0.62	0.54
ST4	*Euphausia hemigibba*	0.26	16.54	16.18	7.47	14.09	13.85	7.34	1.17	1.17	1.02
ST4	*Euphausia hemigibba*	0.54	7.44	7.28	3.36	11.93	11.73	6.22	0.62	0.62	0.54
ST4	*Euphausia krohnii*	0.66	7.65	7.49	3.46	16.04	15.77	8.36	0.48	0.47	0.41
ST4	*Euphausia krohnii*	0.78	6.03	5.89	2.72	13.67	13.44	7.13	0.44	0.44	0.38
ST4	*Euphausia krohnii*	0.31	15.00	14.67	6.78	14.50	14.25	7.56	1.03	1.03	0.90
ST4	*Euphausia krohnii*	0.40	9.63	9.42	4.35	12.94	12.72	6.75	0.74	0.74	0.65
		0.55±0.17	**8.97±3.59**	**8.78±3.51**	**4.06±1.62**	**12.18±3.10**	**11.97±3.05**	**6.35±1.62**	**0.75±0.24**	**0.75±0.24**	**0.65±0.21**
ST3	*Euphausia krohnii*	0.60	3.42	3.20	1.54	6.17	5.86	3.21	0.55	0.55	0.48
ST3	*Euphausia krohnii*	1.08	3.66	3.43	1.65	6.59	6.25	3.42	0.56	0.55	0.48
ST3	*Euphausia krohnii*	0.58	8.36	7.83	3.77	9.44	8.95	4.90	0.89	0.87	0.77
ST3	*Euphausia americana*	0.48	5.71	5.35	2.57	10.56	10.02	5.49	0.54	0.53	0.47
ST3	*Euphausia krohnii*	0.60	4.24	3.97	1.91	6.10	5.78	3.17	0.70	0.69	0.60
ST3	*Euphausia krohnii*	0.81	1.73	1.62	0.78	2.57	2.44	1.33	0.67	0.67	0.58
ST3	*Euphausia krohnii*	0.40	5.37	5.03	2.42	8.64	8.20	4.49	0.62	0.61	0.54
		0.65±0.23	**4.64±2.11**	**4.35±1.97**	**2.09±0.95**	**7.15±2.66**	**6.79±2.52**	**3.71±1.38**	**0.65±0.12**	**0.64±0.12**	**0.56±0.11**
ST2	*Euphausia americana*	0.75	3.33	3.00	1.47	3.20	2.94	1.63	1.04	1.02	0.90
ST2	*Euphausia americana*	0.72	2.15	1.94	0.95	2.23	2.05	1.14	0.96	0.95	0.83
ST2	*Euphausia americana*	0.75	3.00	2.70	1.32	3.26	2.99	1.66	0.92	0.90	0.80
ST2	*Euphausia americana*	0.52	4.81	4.33	2.12	5.83	5.36	2.97	0.82	0.81	0.71
ST2	*Euphausia krohnii*	0.72	3.89	3.50	1.71	4.04	3.71	2.06	0.96	0.94	0.83
ST2	*Euphausia americana*	0.90	3.01	2.71	1.33	3.13	2.88	1.60	0.96	0.94	0.83
ST2	*Euphausia krohnii*	0.75	5.02	4.52	2.21	5.80	5.33	2.95	0.87	0.85	0.75
ST2	*Euphausia krohnii*	0.72	5.56	5.00	2.45	5.86	5.38	2.98	0.95	0.93	0.82
ST2	*Euphausia krohnii*	0.72	5.90	5.32	2.60	9.02	8.28	4.59	0.65	0.64	0.57
ST2	*Euphausia americana*	0.50	6.80	6.13	3.00	7.76	7.12	3.95	0.88	0.86	0.76
ST2	*Euphausia krohnii*	0.54	6.53	5.88	2.88	8.13	7.47	4.14	0.80	0.79	0.69
ST2	*Euphausia krohnii*	0.75	5.93	5.35	2.61	8.57	7.87	4.36	0.69	0.68	0.60
		0.69±0.12	**4.66±1.55**	**4.20±1.39**	**2.05±0.68**	**5.57±2.39**	**5.12±2.19**	**2.83±1.22**	**0.88±0.12**	**0.86±0.11**	**0.76±0.10**
ST1	*Euphausia krohnii*	1.18	2.50	2.25	1.18	2.88	2.65	1.55	0.87	0.85	0.76
ST1	*Euphausia krohnii*	1.24	14.19	12.79	6.71	14.36	13.19	7.71	0.99	0.97	0.87
ST1	*Euphausia krohnii*	0.45	11.47	10.34	5.43	13.14	12.08	7.06	0.87	0.86	0.77
ST1	*Euphausia krohnii*	0.97	2.53	2.28	1.20	3.88	3.56	2.08	0.65	0.64	0.57
ST1	*Euphausia krohnii*	0.93	2.36	2.13	1.12	2.69	2.48	1.45	0.88	0.86	0.77
ST1	*Euphausia krohnii*	1.80	1.34	1.20	0.63	2.02	1.86	1.09	0.66	0.65	0.58
		1.09±0.44	5.73±5.58	**5.17±5.03**	**2.71±2.64**	**6.50±5.66**	**5.97±5.21**	**3.49±3.04**	**0.82±0.13**	**0.80±0.13**	**0.72±0.12**

Table 4.4. Results of Pearson's correlation between temperature (°C), oxygen (ml·L^{-1}), chlorophyll a (measured as fluorescence, mg·m^{-3}), and net primary production (mg C·m^{-2}·d^{-1}) with the average respiration (µl O_2·mg $prot^{-1}$·h^{-1}), specific ETS activity (µl O_2·mg $prot^{-1}$·h^{-1}), and R/ETS ratios of euphausiids in the epipelagic and mesopelagic layers.

Environmental data	Parameter	df	p-value	r
Temperature in the Epipelagic layer (Figure 6)	Respiration (Epipelagic layer)	6	<0.05	-0.7
	Respiration (Mesopelagic layer)	6	<0.05	-0.77
	sp ETS activity (Epipelagic layer)	6	0.09	-0.63
	sp ETS activity (Mesopelagic layer)	6	<0.05	-0.7
	R/ETS (Epipelagic layer)	6	0.75	-0.13
	R/ETS (Mesopelagic layer)	6	0.56	-0.24
Oxygen in the Epipelagic layer (Figure 7)	Respiration (Epipelagic layer)	6	<0.001	0.95
	Respiration (Mesopelagic layer)	6	<0.001	0.96
	sp ETS activity (Epipelagic layer)	6	<0.001	0.94
	sp ETS activity (Mesopelagic layer)	6	<0.001	0.96
	R/ETS (Epipelagic layer)	6	0.69	0.17
	R/ETS (Mesopelagic layer)	6	0.55	0.25
Oxygen in the Mesopelagic layer (Figure 7)	Respiration (Epipelagic layer)	6	<0.05	0.78
	Respiration (Mesopelagic layer)	6	<0.05	0.77
	sp ETS activity (Epipelagic layer)	6	<0.05	0.71
	sp ETS activity (Mesopelagic layer)	6	<0.05	0.72
	R/ETS (Epipelagic layer)	6	0.30	0.42
	R/ETS (Mesopelagic layer)	6	0.24	0.46
Chlorophyll a in the Epipelagic layer (Figure 8)	Respiration (Epipelagic layer)	6	0.63	0.20
	Respiration (Mesopelagic layer)	6	0.49	0.29
	sp ETS activity (Epipelagic layer)	6	0.74	0.14
	sp ETS activity (Mesopelagic layer)	6	0.58	0.23
	R/ETS (Epipelagic layer)	6	0.86	-0.08
	R/ETS (Mesopelagic layer)	6	0.98	0.01
Net primary production in the Epipelagic layer (Figure 8)	Respiration (Epipelagic layer)	6	0.68	-0.17
	Respiration (Mesopelagic layer)	6	0.79	-0.11
	sp ETS activity (Epipelagic layer)	6	0.60	-0.22
	sp ETS activity (Mesopelagic layer)	6	0.71	-0.16
	R/ETS (Epipelagic layer)	6	0.59	-0.23
	R/ETS (Mesopelagic layer)	6	0.68	-0.17

Chapter 5

Relative importance of active flux by zooplankton and micronekton varies around the Iberian Peninsula.

Limnology and Oceanography, Under Review

María Couret[1,*], Airam N. Sarmiento-Lezcano[1,2], José María Landeira[3], Sarah L.C. Giering[4], Will Major[4], M. Pilar Olivar[5], Javier Díaz-Pérez[1], Arturo Castellón[6], Santiago Hernández-León[1]

[1]Instituto de Oceanografía y Cambio Global, IOCAG, Universidad de Las Palmas de Gran Canaria, Unidad Asociada ULPGC-CSIC, Campus de Taliarte, 35214 Telde, Gran Canaria, Canary Islands, Spain.

[2]Centro Oceanográfico de A Coruña, Instituto Español de Oceanografía, IEO, 15080 A Coruña, Spain.

[3]Department of Biology, Norwegian University of Science and Technology, Trondhjem Biological Station NO-7491 Trondheim, Norway

[4]Ocean BioGeosciences, National Oceanography Centre, Southampton, European Way, Southampton, UK.

[5]Institut de Ciències del Mar (CSIC). Passeig Marítim 37-49, Barcelona 08003, Spain.

[6]Unidad de Tecnología Marina (CSIC). Passeig Marítim 37-49, Barcelona 08003, Spain.

5.1. Abstract

The biological pump is a set of processes transferring organic carbon from the surface to the deep ocean, playing a crucial role in the ocean's carbon cycle. Estimating the carbon transported to the deep ocean by the biological carbon pump is a challenge because of the complex and variable nature of the pathways involved, as well as the lack of comprehensive measurements. While zooplankton active flux has been addressed in different studies, supporting fluxes equivalent to 10-30% of the particle export, the role of micronekton in the active flux is scarcely known. Moreover, the capacity of both communities to export carbon is still poorly understood. Here, we show the results of both active (zooplankton and micronekton) and passive fluxes from the Mediterranean Sea to the Atlantic Ocean around the Iberian Peninsula. Water column physical properties differed between the Mediterranean and Atlantic Ocean zones, with chlorophyll *a* values two-times higher in the upwelling off Portugal. Particulate organic carbon fluxes were estimated using sediment traps, with values ranging from 4.24 ± 0.2 to 7.94 ± 3.9 mg C·m^{-2}·d^{-1}. Zooplankton active flux was higher in the Mediterranean Sea compared to the Atlantic Ocean (77.2 ± 21.2 and 14.8 ± 3.4 mg C·m^{-2}·d^{-1}, respectively), whereas micronekton active flux was larger in the Atlantic Ocean (15.1 ± 9.4 and 7.9 ± 6.8 mg C·m^{-2}·d^{-1}). This latter flux was mainly driven by decapods, especially in the northern Atlantic stations, showing the importance of these organisms in the active transport of carbon.

Keywords: Mesopelagic migrant pump, carbon flux, Mediterranean Sea, Atlantic Ocean, zooplankton, micronekton

5.2. Introduction

The biological carbon pump describes the set of mechanisms driving the carbon flux from the euphotic to the meso- and bathypelagic layers through interactions between the physical, chemical, and biological components of the pelagic system (Longhurst and Harrison, 1989). Organic carbon is transported downwards by three different mechanisms: (1) the sinking of organic matter through the water column, the so-called passive or gravitational flux (Carlson et al., 1994; Mestre et al., 2018), (2) the physical mixing of dissolved and particulate organic matter (Buesseler et al., 2007), and (3) the active flux, also known as migrant pump, referring to the active transport of organic matter by zooplankton and micronekton to the deepest areas of the ocean (Longhurst and Harrison, 1988). While passive flux has been extensively studied in the past (see Honjo et al. (2008); Guidi et al. (2015), research of active flux is scarce due to the complex sampling, distribution, and composition of these communities.

Active flux is driven by meso- and bathypelagic organisms performing diel vertical migrations. Diel vertical migrants show a high diversity and a wide size spectrum: they are primarily zooplankton (mainly large copepods and euphausiid, Hernández-León et al. (2019)), mesopelagic fishes (mainly myctophiids, Davison et al. (2013); Olivar et al. (2017)), large crustaceans (decapods and euphausiids, Ariza et al. (2016)), and cephalopods (Judkins and Vecchione, 2020). These organisms remain at depth during daylight hours, move upwards to near the surface at night to feed and return back to depth before dawn (Lampert, 1989; Steinberg et al., 2002; Bianchi et al., 2013). At depth, organic carbon is released via several processes such as respiration (Longhurst et al., 1990), excretion (Steinberg et al., 2002), gut flux (Angel, 1989), and mortality (Zhang and Dam, 1997). A key effect of these up-and-down movements is the transport of organic matter to the deep sea (Romero-Romero et al., 2019), where it is remineralized and may remain at depth for years, decades, or centuries (Nowicki et al., 2022; Pinti et al., 2023). Carbon

exported by diel vertical migrants can locally account for more than 80% of the total flux (passive plus active) (Stukel et al., 2018; Hernández-León et al., 2019b), and has been estimated to increase total flux by 14% (Archibald et al., 2019).

Most of the research into active flux has focussed on zooplankton (see Hernández-León et al. (2019b)), and - to our knowledge - only five studies have empirically investigated both zooplankton (0.2-20 mm) and micronekton (20-200 mm, such as mesopelagic fish and decapods) active flux concurrently: Hidaka et al. (2001) in the North Pacific, Ariza et al. (2015) and Hernández-León et al. (2019) both in the North Atlantic Ocean, Kwong et al. (2020) in Southeast Australia, and Baker et al. (2025) in the Southern Ocean. Consequently, our knowledge on the relative importance of these two groups is very limited, with significant gaps in understanding how their contributions to active flux vary across regions or environmental conditions. We here aim to cover this knowledge gap in the variability of the zooplankton and micronekton active flux across different productive regimes. To do so, we estimate the variability and efficiency of the total active and passive flux in contrasting environmental areas from the Mediterranean Sea to the Atlantic Ocean, around the Iberian Peninsula.

5.3. Material and methods

5.3.1. *Sampling and study area*

The study is part of the CSIC-SUMMER cruise carried out on board the RV "Sarmiento de Gamboa" around the Iberian Peninsula from September 28^{th} to October 25^{th}, 2020 (Olivar et al., 2022). Five zones were sampled repeatedly throughout the day and night: south of the Balearic Islands (Z1; 38.5°N, 2.5°E), western Alborán Sea (Z2; 36°N, 4°W), Gulf of Cádiz (Z3; 36°N, 8°W), off Lisbon (Z4; 38.1°N, 9.4°W), and off Galicia (Z5; 42°N, 9.5°W). Briefly, Z1 is oligotrophic yet a biodiversity hotspot, Z2 and Z3 are productive transition zones between the Atlantic and Mediterranean waters, Z4 and Z5 are upwelling zones (for detailed area descriptions see Supplementary Material SM1). We spent between 48 and 60 hours at each zone conducting repeated stations sampling zooplankton and micronekton for a minimum of two consecutive days during day- and nighttime. However, Z5 was limited to just one day and one night stations due to rough sea conditions (Supp. Table 5.2).

5.3.2. *Hydrography*

The vertical profiles of temperature, conductivity, and fluorescence were recorded from the surface to 1000 m depth using a SeaBird SBE 911plus CTD equipped with a Seabird-43 Dissolved Oxygen sensor and a Seapoint Fluorometer mounted on a rosette sampler equipped with 24 Niskin bottles of 12 L each. Fluorescence obtained in vertical profiles in the upper 200 m depth were converted to chlorophyll *a* (Chl *a*) according to (Yentsch and Menzel, 1963). The vertical profiles of temperature, salinity, and fluorescence were averaged every 1 dBar. Monthly average values (October 2020) of sea surface temperature (SST) were downloaded from the NASA's OceanColorWeb site with a spatial resolution

of 4x4 km and processed using the proto-algorithm from MODIS Ocean Team Computing Facility (MOTCF) based on satellite infrared retrievals of ocean temperature. Net primary production (NPP) was obtained from remote sensing data following Behrenfeld and Falkowski (1997) through the Ocean Productivity web site for the specific dates of the cruise and using the Vertical Generalized Production Model as the standard algorithm.

5.3.3. *Trap-derived passive flux*

Sediment trap-derived passive flux was measured at 150 m depth using a free-drifting multi-trap array with eight cylinders, as the model described by Knauer et al. (1979) and using the procedure described in Hernández-León et al. (2019). The trap was deployed during approximately 24 h with cylinders containing filtered seawater with a high salinity (~45 $g \cdot l^{-1}$ NaCl analytical reagent grade) to increase density. No poisons were added to retard bacterial decomposition. After recovering, samples were filtered onto pre-combusted (450°C for 12 h) 25 mm Whatman GF/F filters. Then, they were frozen at -20°C until analysis in a Carlo Erba CHNSO 1108 elemental analyzer (UNESCO, 1994).

5.3.4. *Zooplankton sampling*

Zooplankton samples were obtained using a MOCNESS-1 net with a 1 m^2 mouth opening area fitted with 200 μm mesh size (Wiebe et al., 1976). Oblique hauls were made from 700 m depth to the surface in eight strata: 700-600, 600-500, 500-400, 400-300, 300-200, 200-100, 100-50, 50-0 m, at about 1.5-2.5 knots (Supp. Table 5.2). Filtered volume was measured using an electronic flowmeter. After sampling, representative organisms - based on visual inspection of the most abundant species (mainly copepods, euphausiids, and chaetognaths) - were gently picked for enzymatic measurements, frozen in liquid nitrogen (-196°C) and preserved at -80°C. The rest of the sample was preserved in 4% buffered formalin and seawater. In the laboratory, a subsample was selected for taxo-

nomic analysis. Samples were digitized using an EPSON scan version 4990 at 2400 dpi, processed in ZooProcess (Gorsky et al., 2010; Vandromme et al., 2012), and uploaded to EcoTaxa (Picheral et al., 2017) to AI-supported manual classification. The body area (in pixel)-to-dry weight (DW) conversion was done using the equations provided by Lehette and Hernández-León (2009), assuming an uncertainty based on the standard error of the regression slope for general mesozooplankton (slope = 1.54 ± 0.03) and to carbon weight (CW) using a conversion factor for 0.40 ± 0.08 based on a literature review. Biomass estimates need to be corrected for potential net avoidance, which is commonly referred to as 'capture efficiency' (CE). For zooplankton, we assumed no net avoidance (Skjoldal et al., 2013). A sensitivity analysis for the conversion factors was carried out and is described in the Supplementary Material (SM4. Sensitivity analysis.).

5.3.5. *Micronekton sampling*

Details of the overall micronekton sampling operations during the cruise have been published by Olivar et al. (2022). Briefly, day and night samples were obtained using a Mesopelagos midwater trawl (Meillat, 2012) with a total length of 58 m and a graded mesh netting of 30 mm near the mouth and 4 mm in its lower part. At the end of the net, a VERDA multi-sampler (Castellón and Olivar, 2023) was fitted to enable stratified sampling (Supp. Table 5.2). The ship course was kept constant during the hauls, and ship speed was maintained at ca. 2 knots using the Speed Over Ground system provided by the onboard GPS. The volume of water filtered was calculated using the mean mouth area of 30 m^2 and the distance travelled during each haul, which was calculated by spherical trigonometry, from the latitude and longitude at the beginning and end of the hauls, using the haversine formula. On board, fish and decapods were sorted and identified. Wet weight was measured using a marine precision balance POLS S-182 P-15 (precision 2 g). Selected species of mesopelagic fishes and decapods (based on a visual assessment of the

most abundant types) were frozen in liquid nitrogen and stored at -80°C for later metabolic analysis. Biomass was estimated converting wet weight (WW) to DW using conversion factors of 0.18 ± 0.01 (Pakhomov et al., 2019) for decapods and 0.23 ± 0.04 (López-Pérez et al., 2020) for fishes, and then to CW using the above mentioned ratio. All micronekton CW estimates need to be corrected for potential net avoidance (CE). For the net we used for micronekton (Mesopelagos), there are - to our knowledge - no published data on CE. Hence, we assumed a CE of 20 ± 13% based on a literature review of other midwater trawls. The sensitivity analysis of these conversions, using a range of conversion factors, is described in Supplementary Material (SM4. Sensitivity analysis.).

5.3.6. *Migrant biomass estimation*

Zooplankton migrant biomass was calculated as the difference between the day and night integrated biomass in the upper 200 m. At Z4 and Z5, higher zooplankton biomass was found during daytime, which is common for upwelling and coastal transition zones due to mesoscale variability and high patchiness (Hernández-León et al., 2024). For these stations, we estimated zooplankton migrant biomass as the difference of biomass between day and night in the 200-700 m layer. Note that estimated migrant biomass using this 'deep-layer' (200-700 m depth) method is typically lower than the 'surface-layer' method (0-200 m depth) ('deep-layer' estimate as percentage of 'surface layer' estimate: 14%, 46% and 116% for Z1-Z3, respectively), thus our active flux estimates for Z4 and Z5 are hence likely underestimated.

5.3.7. *Active flux*

Zooplankton and micronekton active fluxes (AF) were estimated as the sum of the respiratory (RF), mortality (MF), gut flux (GF), and excretion (EF) (Eq. 1).

$$AF = RF + MF + GF + EF \qquad \text{(Eq. 1)}$$

Briefly, RF was estimated using electron transfer system (ETS) activity, measured following the method of Packard (1971) modified by Owens and King (1975), Kenner and Ahmed (1975), and Gómez et al. (1996). Respiration in carbon units was estimated applying a R/ETS ratio of 0.5 ± 0.1 (Hernández-León and Gómez, 1996; Hernández-León et al., 2019a; Couret et al., 2024) and a respiratory quotient of 0.97 ± 0.4 (Omori and Ikeda, 1984; Hernández-León and Ikeda, 2005). MF was estimated from growth assuming steady-state conditions (growth = mortality) in the mesopelagic zone, using the equation of Ikeda and Motoda (1978) relating respiration and growth and applying a conversion factor of 0.75 ± 0.19 for zooplankton (Omori and Ikeda, 1984) and 0.66 ± 0.17 for micronekton (Brett and Groves, 1979). EF was estimated using the values given by Steinberg et al. (2000), assuming that the excretion of dissolved organic carbon makes up 24 ± 26 % (range = 5-42%) of the total carbon metabolized. GF was estimated from respiration by assuming that zooplankton feeding is 2.5 ± 0.5 times respiration (Ikeda and Motoda, 1978), and migrant zooplankton egested 50% of the gut content at depth (Ariza et al., 2015). For micronektonic migrants, we assumed they egest an amount equivalent to the 40% of the respired carbon (Brett and Groves, 1979) and that they transport feces to the mesopelagic because of their density and the long gut passage time of large animals. Assuming that micronektonic migrants egest after the downward migration, the egestion should be double in relation to respiration during 24 h. Therefore, we used an egestion equivalent to 80 ± 16% of the respired carbon (Ariza et al., 2015). Detailed information is given in Supplementary Material (SM2-3).

5.3.8. *Sensitive analysis*

To account for the uncertainties and potential error propagation, we carried out a sensitive analysis for the biomass and metabolic rate estimates of both zooplankton and micronekton (mesopelagic fish and decapods) using the Monte Carlo method with a range of conversion factors (CF) (Supp. Table 5.3). Briefly, we incorporated uncertainties in measurements and conversion factors at each calculation step and conducted 100,000 simulations. The mean and standard deviation of these simulations were then calculated and presented as the final estimates. Detailed information is given in Supplementary Material (SM4).

5.3.9. *Statistics*

To assess the correlation between biomass, migrant biomass and active flux of zooplankton, decapods and fish with environmental parameters, we first calculated the average values of temperature, salinity, chlorophyll *a* concentration, and oxygen concentration for the regions in the approximate mixed layer (0-50 m), epipelagic (0-200 m) and mesopelagic (200-700 m) layers. We also included satellite-derived NPP and particulate organic flux (POC) flux measured by the sediment traps. The correlation between all parameters was calculated using R's cor function and visualized using the ComplexHeatmap package (Gu, 2022). We checked whether correlations are significant ($p<0.05$) using simple linear regression. Note that a discrepancy between a strong correlation and the lack of significance in the linear regression (or vice versa) could occur due to the small sample size ($n = 5$) and, in some cases, narrow range of parameter values. All regressions were visually checked, but care should be taken to not overinterpret individual results. All analyses were performed in the programming language R Team (2022b). The sampling map was generated using the geographic information system QGIS (V.3.22.3) QGIS (2021).

5.4. Results

5.4.1. *Hydrography conditions*

Vertical profiles of temperature (Fig. 5.1A) showed lower mean values at the northern Atlantic in the epi- (Z4 = 13.7°C and Z5 = 14.3°C) and mesopelagic (Z4 = 11.9°C and Z5 = 10.9°C) layer compared to the Mediterranean stations in the epi- (Z1 = 17.1°C and Z2 = 16.9°C) and mesopelagic layer (Z1 = 13.5°C and Z2 = 13.3°C). The Gulf of Cádiz showed similar epipelagic mean values as the Mediterranean stations (17.2°C), but lower mean temperature at depth (11.5°C). Salinity profiles (Fig. 5.1B) showed high mean values in the epipelagic at Z1 and Z2 (37.8 and 36.9, respectively), compared to the Atlantic stations, increasing at depth due to the high salinity of the Mediterranean Sea (38.5 for both). Salinity at Z3 decreased with depth, with a mean value of 36.3 in the epipelagic zone and 35.7 in the mesopelagic zone, likely influenced by the presence of less saline Atlantic waters. Z4 and Z5 exhibited a consistent salinity pattern within the first 400 m of depth, with mean values of 35.7 and 35.6, respectively. Beyond this depth, salinity increased slightly, reaching 36.3 at Z4 and 36.0 at Z5 by 800 m. Surface oxygen levels were similar across all stations, with values of 4.7, 5.0, 4.9, 5.1, and 5.2 ml·L^{-1} at Z1 through Z5, respectively (Fig. 5.1C). Higher oxygen concentrations were observed at depth at Z4 and Z5, coinciding with the layers of lowest temperature and salinity. At Z1 and Z3, an oxygen peak occurred at 50-75 m depth, corresponding to the onset of the thermocline and a decline in temperature.

Epipelagic Chl *a* values (Fig. 5.1D) were generally low, displaying maximum values of 0.6 mg·m^{-3} at Z1, 0.7 mg·m^{-3} at Z2, 0.4 mg·m^{-3} at Z3, and 0.7 mg·m^{-3} at Z5, with the exception of Z4 in the upwelling zone off Portugal, where surface Chl *a* concentrations reached a maximum of 2.6 mg·m^{-3}. Higher net primary production values occurred at the Atlantic stations (1006 ± 449 mg C·m^{-2}·d^{-1}) compared to the Mediterranean stations

(451 ± 141 mg C·m^{-2}·d^{-1}), showing the highest values in Z4 (Table 5.1).

5.4.2. *Trap-derived Particulate Organic Carbon (POC) Flux*

Due to strong currents at Z2 and rough sea conditions at Z5, it was not possible to measure trap-derived POC flux at these stations. Across the remaining stations, POC flux values were relatively consistent, ranging from 4.2 ± 0.2 mg C·m^{-2}·d^{-1} at Z3 to 7.9 ± 3.9 mg C·m^{-2}·d^{-1} at Z1 (Table 5.1). No significant relationship (assessed by linear regression) was found between POC flux, primary production, or active flux values (not shown).

5.4.3. *Zooplankton and Micronekton Biomass Vertical Distribution*

Vertical profiles of zooplankton biomass showed the expected patterns of higher biomass in the upper 100 m layer and decreasing with depth (Fig. 5.2A), except at Z2 where a biomass peak was observed in the mesopelagic layer between 400 and 500 m depth. At Z1-3, mean zooplankton biomass in the epipelagic layer was higher during nighttime, whereas at the northern Atlantic stations (Z4-5) daytime mean biomass was greater. Micronekton biomass vertical profiles revealed higher values in the upper 300 m during nighttime compared to deeper layers, where greater variability in biomass distribution between day and night was found (Fig. 5.2B). This pattern was consistent for both mesopelagic fish (Fig. 5.2C) and decapods (Fig. 5.2D).

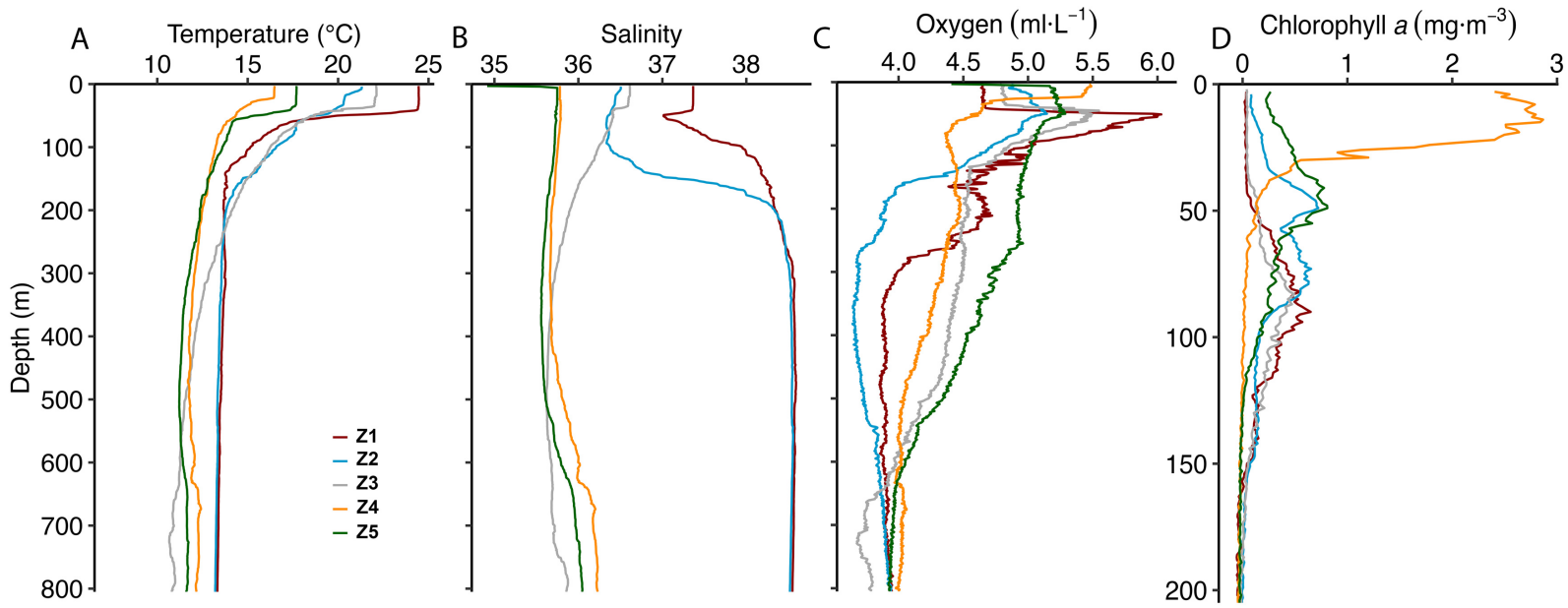

Figure 5.1. Vertical profiles of (A) temperature (°C), (B) salinity, (C) oxygen (ml·L^{-1}), and (D) chlorophyll *a* (mg·m^{-3}) at Z1 (red), Z2 (blue), Z3 (purple), Z4 (orange), and Z5 (green). Note the different y-axis scale for chlorophyll *a*.

Table 5.1. Net primary production (0-200 m depth), passive organic carbon (POC) flux measured at 150 m depth, zooplankton, mesopelagic fish, and decapods migrant biomass (± sensitive analysis error) and active flux (± sensitive analysis error) from epipelagic layer (0-200 m depth) to mesopelagic layer (200-700 m depth). Micronekton values were estimated using a capture efficiency of 20 ± 13%.

Zone	Net Primary Production	POC flux	Zooplankton		Mesopelagic fish		Decapods	
		Trap-estimated	Migrant biomass	Active flux	Migrant biomass	Active flux	Migrant biomass	Active flux
	(mg C·m^{-2}·d^{-1})	(mg C·m^{-2}·d^{-1})	(mg C·m^{-2})	(mg C·m^{-2}·d^{-1})	(mg C·m^{-2})	(mg C·m^{-2}·d^{-1})	(mg C·m^{-2})	(mg C·m^{-2}·d^{-1})
Z1	401	7.9±3.9	497±98	40.9±10.2	108±72	8.9±10.3	56±39	1.9±1.1
Z2	611		953±192	113.4±32.2	104±73	7.0±7.9	329±245	13.4±7.7
Z3	342	4.2±0.2	173±34	30.6±7.5	89±62	4.6±5.2	189±127	15.1±8.9
Z4	1324	5.5±0.6	174±34	12±2.5	98±66	4.3±4.9	450±302	42.1±24.1
Z5	688		29±6	1.8±0.3	6±4	0.3±0.3	338±231	22.6±13.2

5.4.4. *Zooplankton and Micronekton ETS profiles*

Zooplankton specific ETS activity profile represents the average specific ETS activity of the zooplankton community (Fig. 5.3A). Except for Z3, zooplankton specific ETS activities were higher in the upper 200 m depth during nighttime, gradually decreasing with depth. Copepods (Fig. 5.3B) and euphausiids (Fig. 5.3C) exhibited higher specific ETS activities, with more pronounced day-night and spatial variability compared to chaetognaths (Fig. 5.3D). Micronekton (mesopelagic fish and decapods average specific ETS activity) ETS values were not measured at all depths across the stations (Fig. 5.3E). Generally, micronekton specific ETS activity showed higher values at depth during the daytime, except at Z3.

5.4.5. *Respiratory and total active flux*

Zooplankton respiratory flux was almost 6-fold higher in the Mediterranean (26.9 ± 20.2 mg $C{\cdot}m^{-2}{\cdot}d^{-1}$) than in the Atlantic (4.6 ± 4.5 mg $C{\cdot}m^{-2}{\cdot}d^{-1}$) (Fig. 5.4). In contrast, total micronekton (mesopelagic fish and decapods) respiratory flux was lower in the Mediterranean by a factor of 2 compared to in the Atlantic (5.7 ± 2.5 and 10.8 ± 5.3 mg $C{\cdot}m^{-2}{\cdot}d^{-1}$, respectively). This difference was driven by changes in decapods migration: Like for zooplankton, mesopelagic fish respiratory fluxes were higher at Mediterranean stations (2.9 ± 2.8 mg $C{\cdot}m^{-2}{\cdot}d^{-1}$) compared to the Atlantic stations (1.1 ± 0.8 mg $C{\cdot}m^{-2}{\cdot}d^{-1}$), while decapods respiratory fluxes were higher by a factor of 3 at Atlantic stations (9.7 ± 6.6 mg $C{\cdot}m^{-2}{\cdot}d^{-1}$) compared to the Mediterranean stations (2.8 ± 1.7 mg $C{\cdot}m^{-2}{\cdot}d^{-1}$) (Fig. 5.4). Mortality, gut and excretion fluxes followed the same patterns as these are estimated based on respiration fluxes.

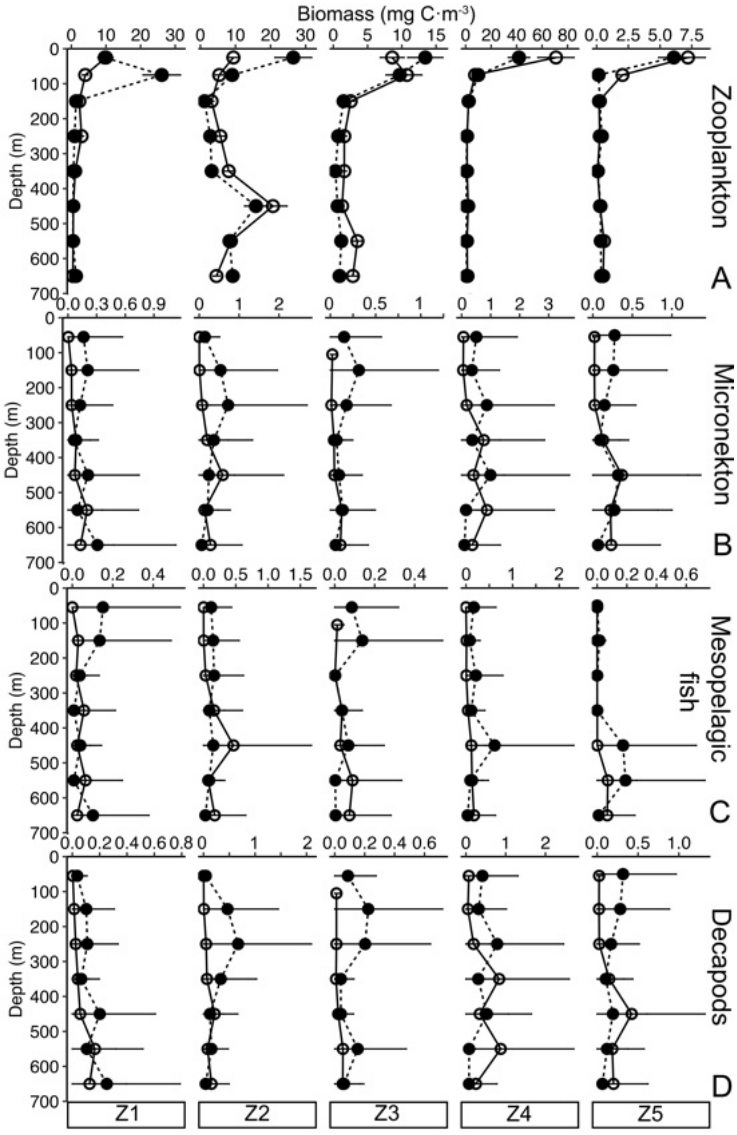

Figure 5.2. Biomass (mg C·m^{-3}) vertical distribution (0-700 m depth) of (A) zooplankton, (B) micronekton (mesopelagic fish and decapods), (C) mesopelagic fish, and (D) decapods during day (empty dots) and night (black dots) at the different zones. Note different x-axis scale for each station. Black lines stand for the sensitive analysis error.

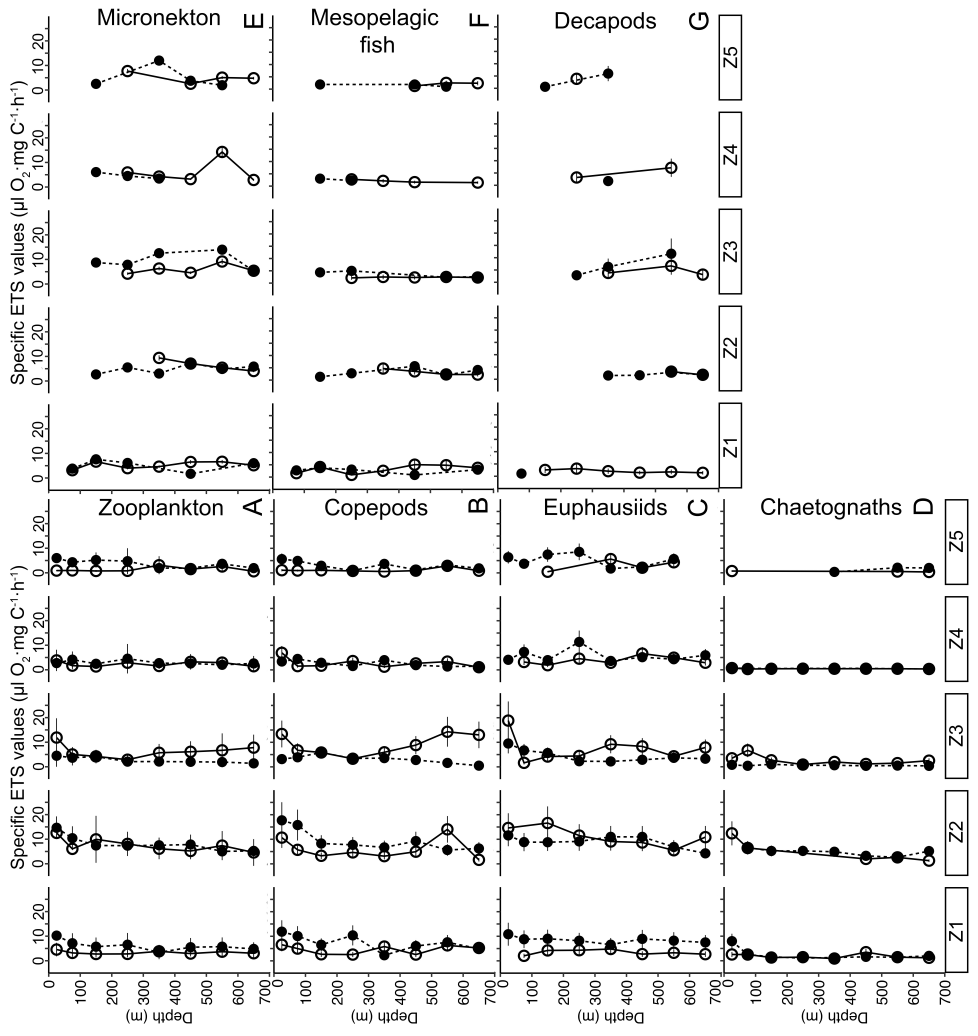

Figure 5.3. Specific ETS activity (μl O_2·mg C^{-1}·h^{-1}) vertical profiles of (A) total zooplankton, (B) copepods, (C) euphausiids, (D) chaetognaths, (E) micronekton (mesopelagic fish and decapods), (F) mesopelagic fish, and (D) decapods. Empty dots are daytime activity values, while black dots are nighttime specific ETS activity. Black lines stand for the sensitive analysis error.

5.4.6. *Migrant biomass*

Considerable variability in zooplankton migrant biomass was observed across zones, with higher values at the Mediterranean stations (497 and 953 mg C·m^{-2} at Z1 and Z2, respectively), accounting for 70% of the total migrant biomass, compared to Z3 (173 mg C·m^{-2}), Z4 (174 mg C·m^{-2}), and Z5 (29 mg C·m^{-2}) (Table 5.1, Fig. 5.5). In contrast, micronekton migrant biomass was higher in the Atlantic (Z3-5) compared to the Mediterranean (Z1-2) where migrant biomass exceeded 50% (Table 5.1, Fig. 5.5). Fish migrant biomass ranged from 6 at Z5 to 108 mg C·m^{-2} at Z1, while decapods biomass exhibited larger variability (ranging from 56 at Z1 to 450 mg C·m^{-2} at Z4) with an average biomass value 3-fold higher than mesopelagic fish migrants. At Z1, fish accounted for a larger proportion of migrant biomass than decapods, but the proportion of decapods increased progressively across the stations, reaching over 80% of the total migrant biomass at Z5 (Fig. 5.5).

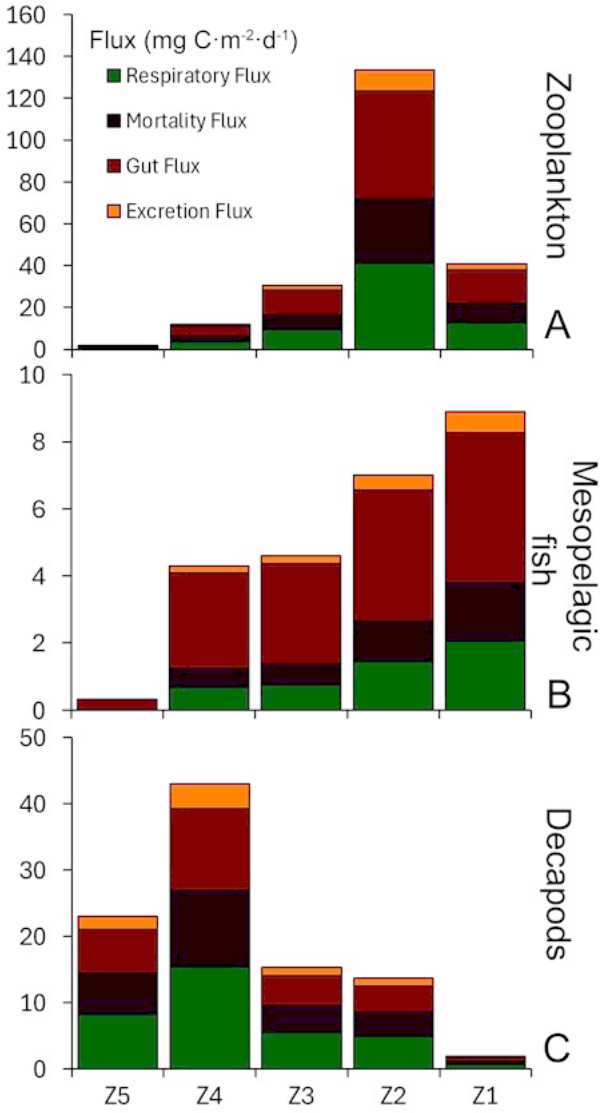

Figure 5.4. Respiratory (in green), mortality (in purple), gut (in dark red), and excretion (in orange) fluxes (mg C·m^{-2}·d^{-1}) of (A) zooplankton, (B) mesopelagic fish, and (C) decapods.

5.4.7. *Carbon budget for active and sinking fluxes*

Total active flux (zooplankton and micronekton) displayed the highest value at station Z2 (133.8 mg C·m^{-2}·d^{-1}) and the lowest at station Z5 (24.6 mg C·m^{-2}·d^{-1}), while the remaining stations exhibited similar values: Z1 = 51.7, Z3 = 50.2, and Z4 = 58.4 mg C·m^{-2}·d^{-1} (Table 5.1, Fig. 5.5). In the Mediterranean (Z1-2), micronekton active flux

contributed to the total flux by 13% at Z1 and 18% at Z2 to the carbon flux, while zooplankton active flux was the dominant contributor (Fig. 5.5). In contrast, at Z4 and Z5, zooplankton active flux accounted for only 7% and 19% of the total flux, respectively, playing a relatively minor role. Instead, micronekton activity drove the majority of the flux in these zones due to decapods flux. Notably, POC flux was substantially lower, contributing just 13%, 8%, and 9% of the total carbon flux at Z1, Z3, and Z4, respectively.

5.4.8. *Correlation between biological and environmental parameters*

Zooplankton migrant biomass was significantly correlated with salinity (positive) and oxygen (negative) in the mesopelagic layer (Fig. 5.6). Similarly, zooplankton active flux was negatively correlated with oxygen in the mesopelagic. Fish active flux exhibited significant positive correlations with temperature in the mesopelagic layer and salinity in the epipelagic layer but was negatively correlated with oxygen in the first 50 m depth. Decapods biomass was significantly positively correlated with NPP and Chl *a* in the upper 50 m depth, and migrant biomass negatively correlated with salinity and temperature in the upper 50 m depth. Additionally, decapods active flux was significantly positively correlated to NPP, Chl *a* in the upper 50 m depth, and Chl *a* in the epipelagic layer. Strikingly, the matrix correlation revealed that decapods exhibited an opposite pattern compared to zooplankton and mesopelagic fish, showing positive correlation with productivity(both NPP and Chl *a*) but a negative correlation to temperature and salinity. Finally, POC flux exhibited a negative correlation with oxygen in the mesopelagic layer.

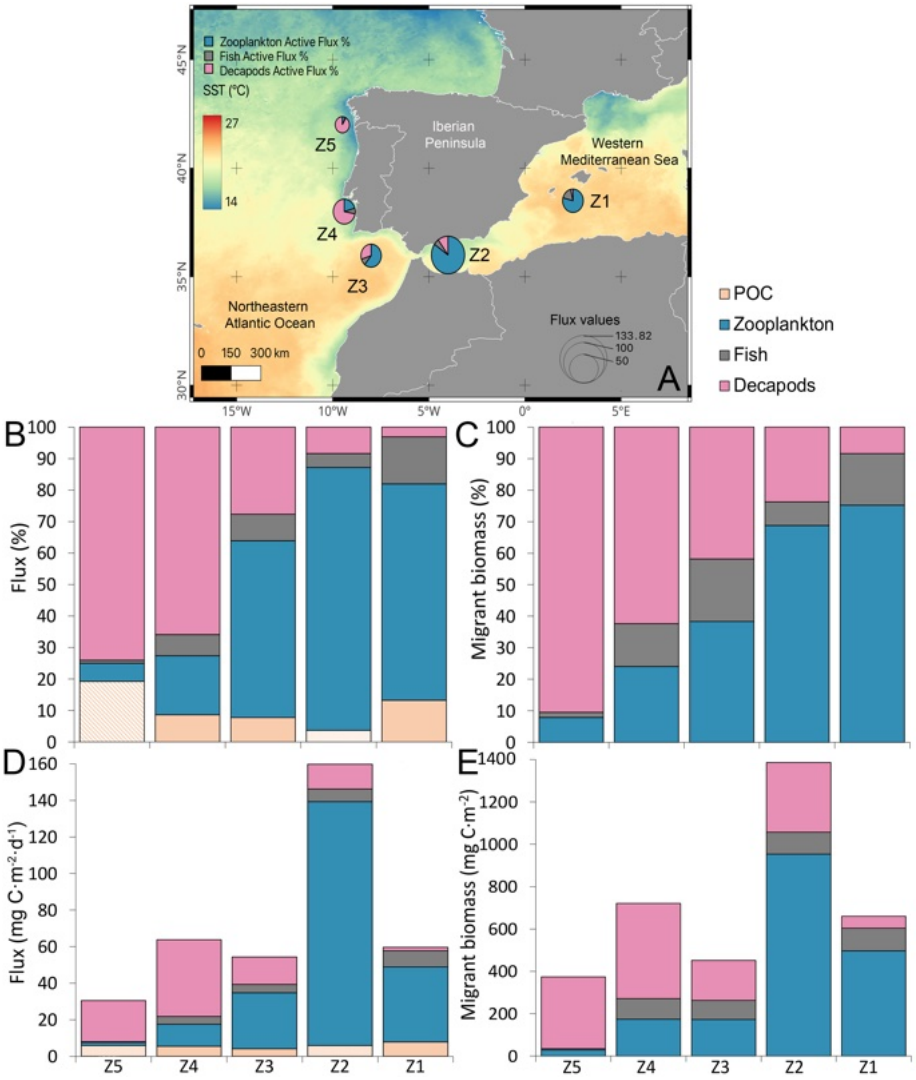

Figure 5.5. (A) Study zones sampled during the CSIC-SUMMER cruise, with background colors representing sea surface temperature (SST, °C) in October 2020. Zone 1 (Z1) corresponds to the south of the Balearic Islands, Zone 2 (Z2) to the western Alborán Sea, Zone 3 (Z3) to the Gulf of Cadiz, Zone 4 (Z4) off Lisbon, and zone 5 (Z5) off Galicia. Bubble size indicates total active flux (zooplankton + micronekton), with blue for zooplankton, grey for fish, and pink for decapods. (B) Percentage contribution to the biological carbon pump by passive flux (light orange), zooplankton (blue), and micronekton (purple; fish + decapods). For Z5 and Z2, we do not have direct passive flux measurements, so we applied the average value from Z1, Z3 and Z4 (shaded orange). (C) Percentage distribution of migrant biomass among zooplankton, fish, and decapods. (D) Carbon fluxes (mg $C{\cdot}m^{-2}{\cdot}d^{-1}$). (E) Migrant biomass values (mg $C{\cdot}m^{-2}$).

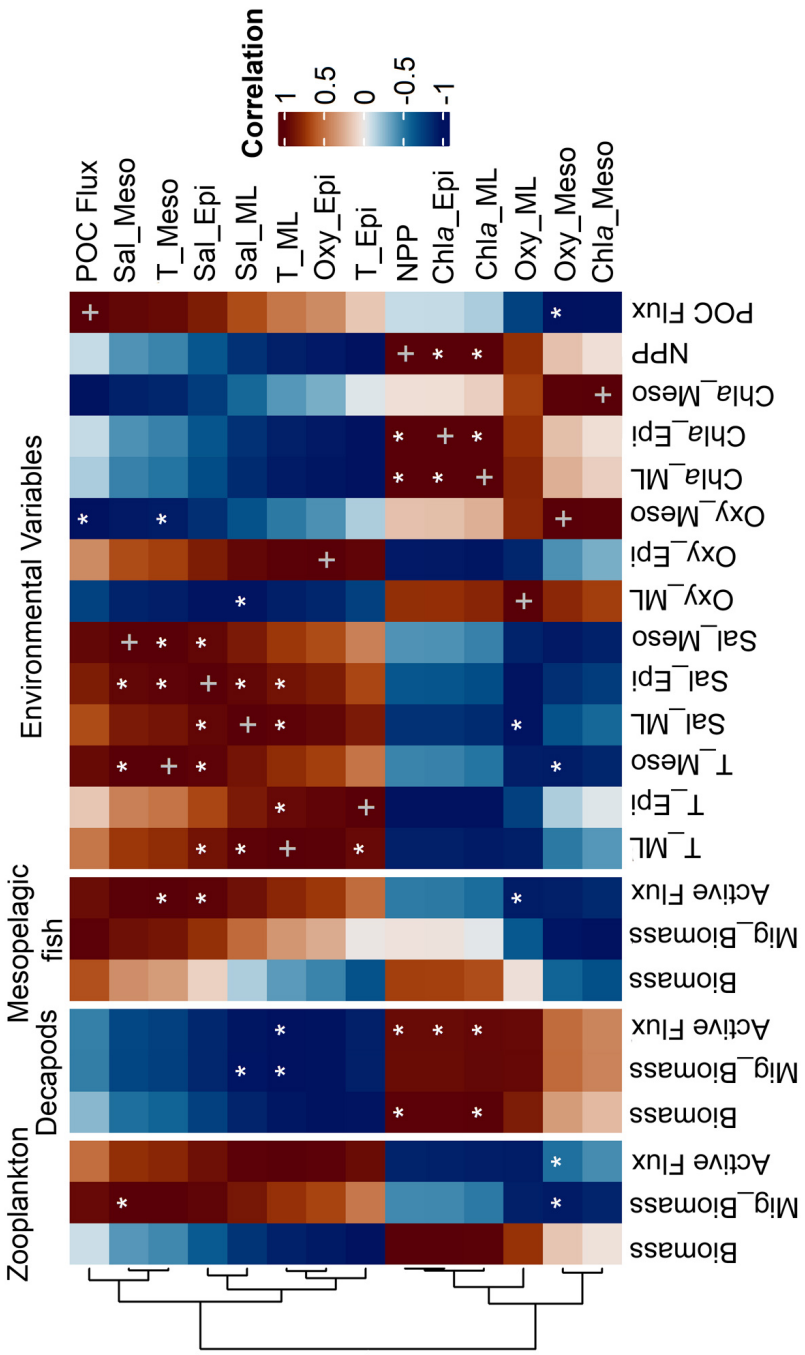

Figure 5.6. Results of the correlation analysis between the zooplankton, mesopelagic fish, and decapods biomass, migrant biomass (Mig_biomass), and active flux with the environmental variables. T stands for temperature, Sal for salinity, Oxy for Oxygen, ML for he Mixed Layer depth (50 m depth), Epi for the 50200 m depth, and Meso for the 200-700 m depth. White stars stand for the significant p-values and grey crosses the same variables. White stars stand for significant p-values and grey crosses the same variables. All p-values are $p<0.5$ and $R^2> 0.78$.

We only found a significant relationship between decapods and net primary production (R^2 = 0.845, $p<0.05$, n = 5), but no significant relationship between zooplankton nor fish and net primary production (not shown). Fish migrant biomass was the only variable that exhibited a significant positive relationship with biomass, while no significant relationship was observed between biomass and active flux in any of the other groups. Noteworthy here is that for both fish and decapods, total biomass and migrant biomass was positively correlated, whereas for zooplankton there appeared to be a negative correlation. Finally, in all three communities, migrant biomass was - as expected due to autocorrelation - significant positive correlation with active flux (Fig. 5.7).

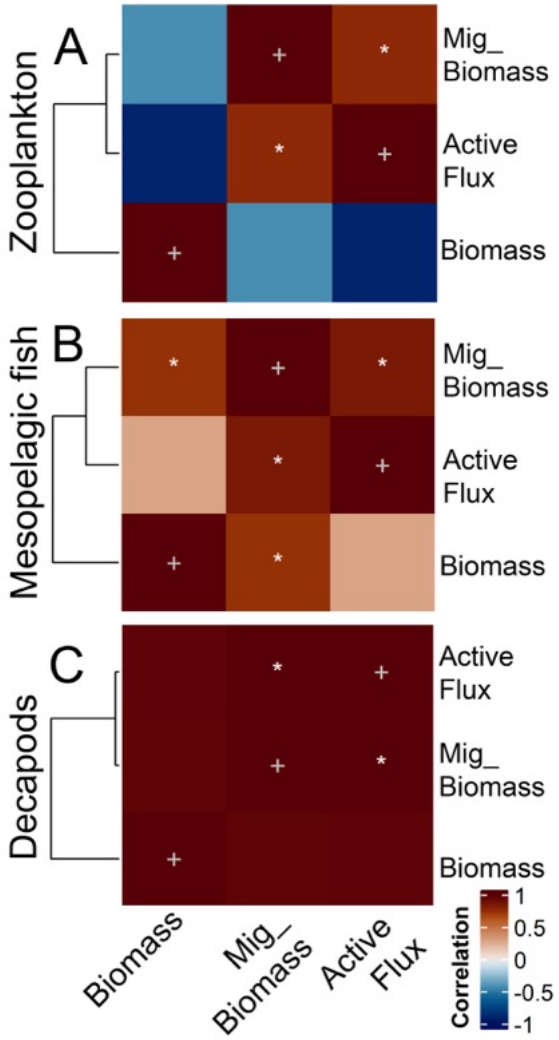

Figure 5.7. Results of the correlation analysis between (A) zooplankton, (B) mesopelagic fish, and (C) decapods biomass, migrant biomass (Mig_Biomass), and active flux. White stars stand for significant p-values and grey crosses the same variables.All p-values are $p<0.5$ and $R^2> 0.78$.

5.5. Discussion

This study quantifies the zooplankton and micronekton active and passive flux across different productive regimes in both the Mediterranean Sea and the Atlantic Ocean. To our knowledge, only one study quantified total active flux along a productivity gradient (Atlantic Ocean; Hernández-León et al. (2019)). Contrary to the previous study, we found that the total active flux did not vary consistently with the productivity of the area. Instead, total active flux depended on the composition of the migrating community, with varying contributions by zooplankton and micronekton. Strikingly, micronekton active flux was dominated by decapods, especially in the north Atlantic Ocean stations. Based on our understanding, no prior research has specifically addressed carbon active flux by micronekton in the Mediterranean Sea, and even data from the Atlantic Ocean remain scarce Stukel et al. (2018); Hernández-León et al. (2019). Furthermore, no studies have simultaneously examined active and passive flux in these two distinct regions (Supp. Table 5.4).

5.5.1. *Zooplankton and micronekton carbon flux*

The relative contribution of each group (zooplankton, decapods, and mesopelagic fish) to the carbon flux shifted from the Mediterranean Sea to the Atlantic Ocean. While zooplankton dominated the carbon flux in the Mediterranean Sea, micronekton -specifically decapods- played a particularly prominent role in the North Atlantic Ocean (Fig. 5.4).

While mesopelagic fish have recently become an intense subject of study (see Aksnes et al. (2023), our data highlights that the role of decapods in the active flux is substantial and may exceed active flux by both zooplankton and fishes. Despite decapod's high abundance in many parts of the world's oceans (Flock and Hopkins, 1992), their active flux has received little attention (Angel and Pugh, 2000; Schukat et al., 2013; Pakhomov

et al., 2019). Estimates of decapod active flux vary widely between studies with no clear agreement on the values. In the North Atlantic Ocean, previous estimates of decapod active flux varied by an order of magnitude (2 versus 12.1 mg C·m^{-2}·d^{-1}; (Angel and Pugh, 2000; Schukat et al., 2013)), while our estimates were up to 20 times higher (ranging from 15.1 to 42.1 mg C·m^{-2}·d^{-1}) compared to (Angel and Pugh, 2000). On the other hand, in the central North Pacific Subtropical Gyre, decapod active flux estimates were up to two orders of magnitude lower than those in our study (0.4 to 0.6 mg C·m^{-2}·d^{-1}; Pakhomov et al. (2019)). The large discrepancies between studies and regions, in addition to the limited availability of data, emphasize the urgent need to increase research efforts to better understand the contribution of decapods to the carbon flux.

We observed that decapods exhibited a strong -although no significant- positive correlation between active flux and biomass, suggesting that decapods biomass may offer insights into the ecological drivers of their active flux. Enhanced decapod biomass has been associated with oxygen minimum zones (Vereshchaka et al., 2016; Hernández-León et al., 2019), lower mesopelagic fish biomass (Ariza et al., 2015), and high productivity (Schukat et al., 2013; Hernández-León et al., 2019). The latter scenario may explain our findings, as decapod biomass (and active flux) were significantly influenced by NPP and Chl *a* (Fig. 5.5). Similarly, in the Costa Rica Dome (Stukel et al., 2018) and in the open-ocean upwelling of the Guinea Dome (Hernández-León et al., 2019), active transport by these pelagic micronektonic fauna was the dominant vertical transport mechanism in areas of high productivity. Although no direct explanation has been provided, it seems that the continuous fueling of primary production, the role of protists as an important intermediate trophic level in these upwelling systems, or both, in these areas of persistent productivity influence the contribution of the decapods to the biological pump. Despite the limited research on how environmental variables influence decapods distribution, high productivity appears to be a common factor driving increased decapods biomass.

In terms of both biomass and total active flux, the Alboran Sea (Z2) stands out in our

dataset. The relatively high zooplankton migrant biomass observed here, compared to other stations, may be linked to the influence of the anticyclonic gyre. This gyre enhances both migration from deeper waters and active flux by deepening the thermocline, which promotes the sinking of bacteria and phytoplankton due to inward motion (Arístegui et al., 1994, 1997), thereby providing a significant source of carbon (Yebra et al., 2005). Previous research on zooplankton active flux in that area reported a similar value of zooplankton migrant biomass to ours (993 and 953 mg C·m^{-2}, respectively), but a respiratory flux 2.4 times lower than ours (17.2 and 41.1 ± 5.4 mg C·m^{-2}·d^{-1}, respectively) (Yebra et al., 2018). Even though the values of migrant biomass were rather similar, the higher estimates in zooplankton respiratory flux in our study imply higher zooplankton active flux. The enhanced NPP obtained in this study compared to Yebra et al. (2018) (84 and 611 mg C·m^{-2}·d^{-1}, respectively) could explain the discrepancy in both respiration and active flux due to increased metabolic activity. This aligns with the expectation that productive areas, characterized by a large and consistent food supply, tend to exhibit higher carbon flux (Hernández-León et al., 2019). On the other hand, discrepancies in the respiratory fluxes might be related to variations in zooplankton body size (Hernández-León et al., 2024), as smaller organisms tend to exhibit higher respiration rates (Ikeda, 1985). Yebra et al. (2018) sampled the core of western anticyclonic gyre, that was found to host larger organisms compared to nearby areas (Valcárcel-Pérez et al., 2019). Thus, larger organisms at the core of the eddy likely exhibit lower respiration rates compared to those in surrounding areas, such as our sampling station.

The relatively low zooplankton migrant biomass values and active flux observed at the northern Atlantic stations could possibly be attributed to zooplankton biomass patchiness, which is a common pattern in upwelling zones (Barton et al., 1998). These sites (Z4 and Z5) also had higher zooplankton biomass at the surface during the day, contrary to expected diel vertical migration patterns. Mesoscale structures, such as eddies and upwelling filaments, promote large differences in phytoplankton and zooplankton populations over

short periods and distances in coastal transition zones (Hernández-León et al., 2024). In this context, we suggest that the higher zooplankton biomass found during daytime off Portugal and Galicia was related to important advection due to Ekman offshore transport in upwelling systems, which could induce large mesoscale variability.

5.5.2. *Relationship between Biomass and Environmental Variables*

While decapods biomass was influenced by the productivity of the area, zooplankton and mesopelagic fish biomass in the water column showed no significant relationship with any of the analyzed environmental variables (Fig. 5.6). This lack of correlation hampers the direct explanation for the distinct vertical profiles observed between the Mediterranean and the Atlantic Ocean. These results suggest that zooplankton and mesopelagic fish biomass vertical distribution in the water column should be also affected by other factors beyond the traditional environmental metrics of Chl *a*, NPP, temperature, salinity, and oxygen. Drivers may include nutrient stress impacting phytoplankton diversity (Tian et al., 2017), the depth of the deep chlorophyll maximum affecting the trophic coupling between phytoplankton and heterotrophic prokaryotic production (Marañón et al., 2021), as well as predation pressure and competition among zooplankton species (Gage and Tyler, 1991). Furthermore, shifts in the zooplankton feeding ecology -such as a transition from omnivorous to carnivorous or gelatinous filter-feeding zooplankton- could reduce food quality for fish, making it less nutritious (Heneghan et al., 2023).

Finally, it is worth mentioning that only fish biomass was significantly related to fish migrant biomass (Fig. 5.7). Thus, higher zooplankton and decapods biomass in the water column does not imply higher migratory biomass or higher fluxes as one might expect. These findings suggest that factors beyond biomass, such as species composition (Hays et al., 2001), behavior (Forward, 1988), trophic interactions (Pinti et al., 2019) or food supply, play a critical role in governing vertical migration and carbon transport. It becomes

increasingly evident that a comprehensive understanding of the influence of environmental conditions on biomass vertical distribution, requires looking beyond traditional metrics to uncover the mechanisms shaping biomass distribution.

5.5.3. *Relationship between Total Active Flux and Environmental Conditions*

We found no clear relationship between NPP and total active flux, with active flux estimates up to 10 times higher than previously reported under similar NPP (Ariza et al., 2015; Hernández-León et al., 2019). Instead, the total active flux varied depending on the composition of the migrating community, which -similarly to biomass- appeared to be influenced by different environmental variables. According to the correlation matrix, active flux by zooplankton and mesopelagic fish was -although no significant- negatively correlated to oxygen but positively correlated with temperature and salinity in the water column, while decapods active flux showed the inverse correlation matrix pattern (Fig. 5.6). Our loose interpretation of this pattern is that the active flux by these groups is on a broader scale influenced by water masses, with active flux by zooplankton and mesopelagic fish being, relatively, more prevalent in the warmer and saltier waters of the Mediterranean, whereas decapods dominate active flux in the colder fresher Atlantic waters.

Of particular interest is the significantly negative relationship between oxygen concentrations (in the mesopelagic) and zooplankton active flux. This relationship might be related with the influence of oxygen availability on the community structure, vertical distribution (Ekau et al., 2010), metabolic activity (Kiko and Hauss, 2019), as well as feeding and excretion rates (Robinson et al., 2010). However, care should be taken with zooplankton correlation as it is expected the avoidance of the mesopelagic zone if oxygen levels decline below approximately 20 μmol·O_2·kg^{-1} (Hauss et al., 2016). Thus, enhanced active flux by low oxygen up to a limit might be related to other factors such as food availability

while minimizing predation risk from larger predators that are less tolerant of low oxygen levels (Gilly et al., 2013).

5.5.4. *Passive vs Active flux*

Finally, our findings indicated that carbon flux was mainly driven by diel vertical migrants rather than by the passive flux (see 5.1, Fig. 5.4). Recent models suggested that active flux of carbon due to zooplankton diel vertical migration accounts for 10-18% of the passive flux (Aumont et al., 2018; Archibald et al., 2019; Nowicki et al., 2022) in areas of low productivity (Koppelmann and Weikert, 2007). In contrast, in high-productivity areas, carbon flux has been suggested to be primarily carried out by diel migrants, due to high biomass of low-turnover organisms such as zooplankton (Hernández-León et al., 2019). Thus, active flux is expected to be low on a global scale due to widespread oligotrophic conditions, as the transfer of organic carbon to the deep ocean should be enhanced along with net primary production (Davison et al., 2013; Hernández-León et al., 2020). However, our findings suggest that the relationship between the passive and active flux is not directly dependent on productivity.

5.6. Conclusions

This study examined different pathways of the biological carbon pump from the Mediterranean Sea to the Atlantic Ocean, revealing strong differences in the active flux between the two regions. We found no clear relationship between NPP and total active flux, instead active flux varied according to the composition of the migrating community. Zooplankton dominated the carbon flux in the Mediterranean Sea due to enhanced migrant biomass, and micronekton -especially decapods- played a particularly prominent role in the North Atlantic Ocean. While decapod active flux was influenced by the productivity of the area,

active flux by zooplankton and mesopelagic fish seemed to be related to the water masses. Finally, the relatively low contribution of passive flux compared to total active flux underscores the critical role of the mesopelagic-migrant pump in driving the biological carbon pump.

5.7. Acknowledgments

This work was supported by projects "Sustainable Management of Mesopelagic Resources" (SUMMER, H2020, Grant agreement No 817806), "DisEntangling Seasonality of Active Flux In the Ocean" (DESAFÍO, PID 2020- 118118RB-100), and IMDEEP (CajaCanarias-LaCaixa, ref. 2022CLISA15). María Couret was supported by a postgraduate grant (TESIS2022010116) co-financed by the Agencia Canaria de Investigación, Innovación y Sociedad de la Información de la Consejería de Universidades, Ciencia e Innovación y Cultura and by the Fondo Social Europeo Plus (FSE+) Programa Operativo Integrado de Canarias 2021-2027, Eje 3 Tema Prioritario 74 (85%). JDP by a postgraduate grant (ULPGC2022-2) from Universidad de Las Palmas de Gran Canaria. ASL by a postgraduate grant (IN606B-2024/018) from the "Agencia Gallega de Innovación". The authors wish to thank the crew and other scientists on board the R/V "Sarmiento de Gamboa" as well as the technicians of the "Unidad de Tecnología Marina" (UTM) for their support and help during the cruise.

5.8. Author contributions

M.C developed the work with input from A.S.L, J.M.L, S.L.C.G, M.P.O, and S.H.L; M.C, A.S.L, and J.D.P analysed the samples; M.C., A.S.L, J.M.L, M.P.O., and A.C contributed to data acquisition; M.C. analysed the data and created all figures; S.L.C.G and M.C develop the sensitive and correlation analysis; M.C. drafted the manuscript with spe-

cial input of S.L.C.G and S.H.L, and all authors contributed substantially to its improvement. All authors approved the final submitted manuscript.

5.9. Supplementary material

5.9.1. *Study area*

The south of the Mallorca channel (Balearic Islands, western Mediterranean, Z1) is characterised by the oligotrophy of its waters but considered as a hotspot of biological activity and biodiversity in the deep-sea (Massutí et al., 2021). In contrast, the Alborán Sea (Z2), unlike the general oligotrophy dominating most of the Mediterranean, holds two anticyclonic gyres of high biological productivity (Bárcena et al., 2004). This area together with the Gulf of Cádiz (Z3) is considered a transition zone between the Atlantic Ocean and the Mediterranean Sea, with water-mass exchange through the Strait of Gibraltar. This region couples the convergence of critical water masses regarding the Atlantic Meridional Overturning Circulation with a semi-permanent upwelling regime, itself connected to the larger dynamic cells off northwest Africa (Penaud et al., 2016). The area off Lisbon (Portugal, Z4) is characterised by a coastal upwelling, intensified during the summer when upwelled waters occupy the surface layers over the whole western shelf and part of the upper slope off Portugal (Fiuza, 1983). This scenario is also found in the Galician coast (Z5), showing upwelling favorable conditions during spring-summer (Villegas-Ríos et al., 2011).

5.9.2. *Electron transfer system activity*

Frozen samples were homogenized at the laboratory with a Teflon pestle in Tris-EDTA buffer at 0-4°C, to avoid degradation of enzyme activity and proteins. Then, the homogenates were centrifuged at 4000 rpm at 0°C for 10 min. An aliquot was subsampled from the homogenate and incubated, at 16°C for zooplankton and 18°C for micronekton, at darkness using NADH, NADPH, succinate, and a tetrazolium salt (INT) as the artificial

electron acceptor. After 20 min, the incubation was stopped with a quench solution. The ETS activity was estimated spectrophotometrically at 490 nm with a turbidity baseline of 750 nm. In order to correct ETS activity for in situ temperature (200-700 m layer, considered as the residence depth of migrants, Hays (2003), we used the Arrhenius equation and an activation energy of 15 kcal·mol^{-1} (King and Packard, 1975). Protein content was determined using the method of Lowry et al. (1951) modified by Rutter (1967), and using bovine serum albumin (BSA) as the standard. Zooplankton protein content was converted to dry weight (DW) using the ratio of 2.49 ± 1.73 recently given by Hernández-León et al. (2019a) for zooplankton in subtropical waters. ETS activity in micronekton was measured in the whole animal. Micronekton protein content was converted to DW using the ratio given by Bailey et al. (1995) of 2.21 ± 0.45 for mesopelagic fish, and 2.48 ± 1.09 for decapods.

5.9.3. *Active flux*

Zooplankton and micronekton active fluxes (AF) were estimated as the sum of the respiratory (RF), mortality (MF), gut flux (GF), and excretion (EF):

$$\text{AF} = \text{RF (Eq. S1-S3)} + \text{MF (Eq. S4ab)} + \text{GF (Eq. S5ab)} + \text{EF (Eq. S6)} \qquad \text{(Eq. 1)}$$

First, respiration at depth (R_{depth}) was determined using the average ETS activity and a quite conservative respiration to ETS (R/ETS) ratio of 0.5 ± 0.1, according to values ranging from 0.46 to 0.96 for zooplankton >1 mm (Hernández-León and Gómez, 1996), migrant copepods (Hernández-León et al., 2019a), euphausiids (Couret et al., 2024), and fish (Ikeda, 1989) (Eq. S1).

$$R_{depth} = ETS_{200-700\ m\ depth} \times (0.5 \pm 0.1) \qquad \text{(Eq. S1)}$$

Respiration (R) was converted into carbon units using a respiratory quotient (CO_2 respired/O_2 consumed) of 0.97 ± 0.4 (Omori and Ikeda, 1984) (Eq. S2).

$$R = R_{depth} \times (0.97 \pm 0.4) \qquad \text{(Eq. S2)}$$

RF was then estimated multiplying respiration by the migrant biomass (MB), assuming a mesopelagic residence time of 12 h (Ariza et al., 2015) (Eq. S3)

$$RF = R \times (MB \times 0.5) \qquad \text{(Eq. S3)}$$

Zooplankton mortality flux ($MF_{zooplankton}$) was estimated assuming steady-state conditions in the mesopelagic zone (growth= mortality), using the equation of Ikeda and Motoda (1978) that relates respiration and growth applying assimilation efficiencies of 30 and 70%, respectively (see review in Omori and Ikeda (1984)) (Eq. S4a).

$$MF_{zooplankton} = RF \times (0.75 \pm 0.19) \qquad \text{(Eq. S4a)}$$

For micronekton, mortality flux ($MF_{micronekton}$) was estimated from growth assuming steady state conditions and using the growth/metabolism ratio of 0.66 ± 0.17 (Brett and Groves, 1979) (Eq. S4b).

$$MF_{micronekton} = RF \times (0.66 \pm 0.17) \qquad \text{(Eq. S4b)}$$

Zooplankton gut flux ($GF_{zooplankton}$) was estimated assuming that feeding is 2.5 ± 0.5 times respiration (Ikeda and Motoda, 1978), and that migrant zooplankton egested 50% of the gut content at depth (Ariza et al., 2015) (Eq. S5a).

$$GF_{zooplankton} = RF \times (2.5 \pm 0.5 \times 0.5) \qquad \text{(Eq. S5a)}$$

For micronekton gut flux ($GF_{micronekton}$), we assumed that carnivorous organisms egest an amount equivalent to the 40% of the respired carbon (Brett and Groves, 1979), and they transport feces to the mesopelagic because of their density and the long gut passage time of large animals. Assuming that micronektonic migrants egest after the downward migration, the egestion should be double in relation to respiration during 24 h. Therefore, we used an egestion equivalent to 80 ± 16% of the respired carbon (Ariza et al., 2015) (Eq. S5b).

$$GF_{micronekton} = RF \times (0.8 \pm 0.16) \qquad \text{(Eq. S5b)}$$

EF was estimated using the values by Steinberg et al. (2000), who reported that excretion makes up 24 ± 26% of the respired plus excreted carbon (Eq. S6).

$$EF = RF \times (0.24 \pm 0.26) \qquad \text{(Eq. S6)}$$

5.9.4. *Sensitivity analysis*

To account for the uncertainties and potential error propagation, we carried out a sensitive analysis for the biomass and metabolic rate estimates of both zooplankton using the Monte Carlo method with a range of conversion factors (CF). Zooplankton carbon weight ($CW_{zooplankton}$) was estimated by converting the image area (in pixels) to DW (a_{DW} and b_{DW}) and then to carbon (CF_{CW}) (Eq. 2).

$$CW_{zooplankton} = (a_{DW} \times Area^{b_{DW}}) \pm \delta_{DW} \times CF_{CW} \pm \delta_{CW} \qquad \text{(Eq. 2)}$$

For the conversion of zooplankton area (in pixels) to DW (a_{DW} and b_{DW}), we used the equations provided in Table 1 by Lehette and Hernández-León (2009). We used the organism-specific regressions when possible (ostracods, chaetognaths, slaps, siphonophores, subtropical euphausiids, subtropical copepods, for which the number of observations was, respectively, n = 3551, 1678, 682, 159, 637, 52396). For the remaining organisms, we used the regression for general mesozooplankton (n = 6115). We assumed the error on these estimates based on the standard error of the regression slope for general mesozooplankton (slope = 1.54 ± 0.03). Hence, for the Monte Carlo simulation, we applied a random error of 2%. To convert DW to CW, we found several reported values for zooplankton: Banse (1996) suggested 0.4 based on two studies, Dam and Peterson (1993) assumed 0.4, and Andersen and Hessen (1991) measured 0.48 (range 0.40 - 0.57) based on measurements for 6 species. As most contemporary studies use the conversion factor 0.4, we also used this value as our mean but assumed a generous error (20%); hence we randomly sampled

from a distribution of 0.40 ± 0.08.

Micronekton carbon weight ($CW_{micronekton}$) was estimated by converting the total WW ($\sum$WW) (Eq. 3):

$$CW_{micronekton} = \sum WW \pm \delta WW \times CF_{DW} \pm \delta_{DW} \times CF_{CW} \pm \delta_{CW} \quad \text{(Eq. 3)}$$

The precision of the balance was 2 g, which we included in the Monte Carlo simulation (δWW = 2 g). For the conversion factor for WW to DW (CF_{DW}), we only found one study that provides a direct conversion of WW to DW for decapods (Pakhomov et al., 2019). These authors did not provide an uncertainty estimate for this conversion factor; however, the regression line was highly significant with an R^2 of 0.976. We hence assume a relatively low uncertainty (δ_{DW}) of 5%, and thus randomly sampled from a mean of 0.18 with a standard deviation of 0.01. For fish, López-Pérez et al. (2020) provide mean water content for 36 fish species from the subtropical Atlantic (0.77 ± 0.04; see their Table 3). We hence assumed a CF_{DW} of 0.23 ± 0.04 and randomly sampled from this distribution for our Monte Carlo simulation. For the conversion factor for DW to CW (CF_{CW}), we could not find any observations for micronekton, so we used the same distribution as explained above. Conversion factors used in this study are summarized in Supp. Table 5.3.

All CW estimates need to be corrected for potential net avoidance, which is commonly referred to as 'capture efficiency' (CE). A capture efficiency of 100% implies that all organisms in the water column were caught in the net. CE of 100% is commonly assumed for zooplankton collected, as the case here, with MOCNESS (Skjoldal et al., 2013). For the net we used for micronekton (Mesopelagos), there are - to our knowledge - no published data on CE. Reported values for CE of midwater trawls are 6-13% (Gj et al., 1984; May and Blaber, 1989), 14% (Koslow et al., 1997), 14-38% (Davison, 2011), and 33% (Pakhomov et al., 2019). Hence, we applied a mean of 20 ± 13% in the Monte Carlo simulation.

For the sensitivity analysis of zooplankton and micronekton metabolic rate estimates,

we employed the Monte Carlo method, integrating the conversion factors used for active flux conversions. Zooplankton ETS activity obtained as protein content was converted to DW using the ratio of 2.49 ± 1.73 given by Hernández-León et al. (2019a), hence assuming an error of 69%, and DW was converted to carbon as explained above. Micronekton protein content was converted to DW using the ratio given by Bailey et al. (1995) of 2.21 ± 0.45 for mesopelagic fish and 2.48 ± 1.09 for decapods, and DW was converted to carbon as explained above.

ETS in carbon units was converted to respiration using the ratio of 0.5 (Hernández-León and Gómez, 1996). The respiration to ETS (R/ETS) ratio in marine zooplankton reflects the scope of metabolic activity and typically ranges between 0.5 and 1 mainly depending on factors such as species, food availability and temperature (Hernández-León and Gómez, 1996; Hernández-León et al., 2019a; Couret et al., 2024). Hernández-León et al. (2019a) observed a R/ETS value of 0.96 ± 0.29 for migrant copepods and Couret et al. (2024) obtained a ratio of 0.81 ± 0.18 for euphausiids. To maintain a conservative approach, and generally all studies adopt a conversion factor of 0.5, we also used this value as our mean but assumed a generous error (20%); hence we randomly sampled from a distribution of 0.50 ± 0.10. Respiration was converted into carbon units using a respiratory quotient (CO_2 respired/O_2 consumed) of 0.97 (Omori and Ikeda, 1984). The respiratory quotient is a stoichiometric consequence of the elemental composition of the substrate being oxidized. These values span the range of 0.67 to 1.24 (0.955 ± 0.4), being the calculated value for protein is 0.97 (Hernández-León and Ikeda, 2005). Hence, for the Monte Carlo simulation we assumed a respiratory quotient ratio 0.97 ± 0.4. Respiration in carbon units at depth to respiration flux is estimated following Eq. S3, that is by multiplying respiration by the migrant biomass, assuming a mesopelagic residence time of 12 h (Ariza et al., 2015).

Mortality flux was estimated from the respiration flux using a factor of 0.75 (Omori and Ikeda, 1984) for zooplankton and 0.66 (Brett and Groves, 1979) for micronekton. Estima-

tion of zooplankton mortality rates in field populations is a challenging task that depends on multiple factors such as the swimming behaviour, and consequently in vulnerability to predators (Ohman, 2012), the developmental stage composition, and the environmental variables (Ohman, 2012). Thus, we assumed a conservative error of 25%; thus, values were sampled randomly from a distribution of 0.75 ± 0.19 and 0.66 ± 0.17, respectively.

Gut flux was estimated assuming that feeding is 2.5 times respiration (Ikeda and Motoda, 1978), and that migrant zooplankton egested 50% of the gut content at depth (Ariza et al., 2015). Feeding equation depends on digestion efficiency and gross growth efficiency which can differ to a great degree, not only among zooplankton species but also within a single species (see Table 3 of Ikeda and Motoda (1978). The latter authors chose values of 70% for digestion and 30% for gross growth as realistic values of zooplankton in the field, regardless of species and food habit. As this is the general equation used broadly to estimate gut flux from respiration, we used the value of 2.5 with a cautious assumption of a 20% error; thus, values were sampled randomly from a distribution of 2.5 ± 0.5. We assumed that migrant zooplankton egest 50% at depth following Ariza et al. (2015) estimations, as gut clearance only takes a few minutes in copepods (Dam and Peterson, 1988) and about 30-90 min in euphausiids (Gurney et al., 2002; Pakhomov and Froneman, 2004), while in fish, estimates range from 12 h to days (Baird et al., 1975). Following Ariza et al. (2015) estimations, and assuming a nocturnal distribution at roughly a 50 m depth and a mean downwards migration velocity of 5 cm·s^{-1} (Davison et al., 2013), organisms trespassing the base of the mixed layer (~150 m depth) should take about 30 min. This suggests that copepods will actively export relatively low amounts of fecal matter, while active swimmers like euphausiid gut flux will be partial. In any case, to be conservative, we assumed that zooplankton egested 50% at depth. Hence, for the Monte Carlo simulation, we applied a random error of 20% (assuming a normal distribution with a mean of 0.5 and a standard deviation of 0.1). For micronekton, gut flux was estimated assuming an egestion equivalent to 80% of the respired carbon (Ariza et al., 2015). Thus, we assumed

a normal distribution with a mean of 0.8 and a standard deviation of 0.16 (error of 20%).

Finally, excretion flux was estimated using the values by Steinberg et al. (2000), who reported that excretion makes up 24% of the respired plus excreted carbon. On average, excretion of dissolved organic carbon makes up 24% (range=5-42%) of the total carbon metabolized (excreted + respired) (Steinberg et al., 2000). Thus, we assumed a normal distribution of 24 ± 26%.

Table 5.2. Number of CTD casts, MOCNESS and Mesopelagos trawls, and sediment traps per study zone used for the present investigation.

Zone (Z)	CTD	MOCNESS 0-700 m Day 100 m-layers	MOCNESS 0-700 m Night 100 m-layers	Mesopelagos 0-200 m Day 100 m-layer	Mesopelagos 0-200 m Night 100 or 30 m-layers	Sediment traps
Z1 (Balears)	6	2	2	2	1	1
Z2 (Alboran)	5	2	2	1	3	0
Z3 (Cadiz)	7	3	2	2	2	1
Z4 (Lisboa)	4	2	2	2	2	1
Z5 (Galicia)	1	1	1	1	1	0

Table 5.3. Conversion factors used to estimate zooplankton and micronekton biomass and active flux. * different coefficients for certain zooplankton groups as explained in text.

Parameter	Factor		Zooplankton	Decapods	Fish
Biomass	CF_{DW}	WW-to-DW	-	0.18 ± 0.01	0.23 ± 0.04
	b_{DW}	area-to-DW	1.54* ± 0.03	-	-
	CF_{CW}	DW-to-CW	0.40 ± 0.08	0.40 ± 0.08	0.40 ± 0.08
	CE	Capture efficiency	1	0.20 ± 0.13	0.20 ± 0.13
Active flux	$CF_{Protein}$	Protein-to-DW	2.49 ± 1.73	2.48 ± 1.09	2.21 ± 0.45
	CF_{CW}	DW-to-CW	0.40 ± 0.08	0.40 ± 0.08	0.40 ± 0.08
	R/ETS	ETS-to-Respiration	0.5 ± 0.1	0.5 ± 0.1	0.5 ± 0.1
	RQ	Respiration-to-Respiration at depth (d^{-1}) using a Respiratory Quotient (RQ) of	0.97 ± 0.4	0.97 ± 0.4	0.97 ± 0.4
	Mortality Flux	Respiration flux-to-Mortality flux	0.75 ± 0.19	0.66 ± 0.17	0.66 ± 0.17
	Gut Flux	Respiration flux-to-Gut flux	2.5 ± 0.5 0.5 ± 0.1	0.88 ± 0.16	0.88 ± 0.16
	Excretion Flux	Respiration flux-to-Excretion flux	0.24 ± 0.26	0.24 ± 0.26	0.24 ± 0.26

Table 5.4. Comparison of trap-derived POC flux (mg C·m^{-2}·d^{-1}), zooplankton and micronekton migrant biomass (mg C·m^{-2}), respiratory flux (mg C·m^{-2}·d^{-1}), and active flux (mg C·m^{-2}·d^{-1}) values obtained during the CSIC-SUMMER cruise to other studies. CE stands for capture efficiency.

Source	Location	POC flux	Migrant biomass		Respiratory flux		Active flux		CE
			Zooplankton	Micronekton	Zooplankton	Micronekton	Zooplankton	Micronekton	
		(mg C·m^{-2}·d^{-1})	(mg C·m^{-2})		(mg C·m^{-2}·d^{-1})		(mg C·m^{-2}·d^{-1})		%
Hidaka et al. (2001)	Western equatorial North Pacific	54.8	281.1±214.3	402.6 ± 146.2	13.2 ± 8.3	22.5 ± 10.4	16.8 ± 9.6	23.8 ± 10.8	14
Ariza et al. (2015)	Atlantic Ocean (Canary Islands)	11.9 ± 5.8	266 ±127	201±61	3.4± 1.9	2.9± 1.0			14, 38 and 80
Hernández-León et al. (2019a)	Tropical and subtropical Atlantic Ocean	15.1 ± 6.4	771.6 ± 1007.6	300.9 ± 278.7	10.5 ± 14.5	2.9 ± 2.9	20.5 ± 27.6	7.8 ± 7.7	50
Kwong et al. (2020)	Centre frontal cold-core eddy (Southeast Australia)		214.1		9.4		16.1		
	Edge frontal cold-core eddy		90.6		4		8		
	Centre cold-core eddy		63.6	8	3.1	0.3	5.4	0.78	50
	Warm-core eddy		332.3	10.8-11.8	1.2	1.08-1.2	2.2	2.1-3.4	50
	Warm-core eddy		1421	53.8	48.6	5.5	88	13.5	50
Baker et al. (2025)	Southern Ocean	99.4 ± 17.2					17.8 ± 15.9	7.4 ± 2.3	
This Study	Mediterranean Sea	7.9 ± 3.9	725 ± 145	149 ± 107	26.9 ± 20.2	2.3 ± 1	77.2 ± 21.2	7.8 ± 6.8	20±13
	Atlantic Ocean (Iberian Peninsula)	4.9 ± 0.3	125 ± 25	195 ± 132	4.56 ± 4.5	4.3 ± 2.1	16.2 ± 3.4	14.8 ± 9.4	20±13

Conclusions

This thesis provides a comprehensive analysis of the spatio-temporal variability of mesozooplankton biomass, abundance, size spectra, and active flux in the North Atlantic Ocean. By compiling and analyzing five decades (1971–2021) of mesozooplankton biomass data, our key findings highlight:

- Significant decline in biomass in the oligotrophic zone north of the Canary Islands particularly during the Late Winter Bloom, likely linked to rising temperatures and increased stratification.
- Higher biomass was found near the African coast and around the islands, probably driven by upwelling and island-mass effects.
- Seasonal cycles revealed biomass peak during the Late Winter Bloom, except in upwelling regions, where maxima occurred in August due to intensified Trade Winds which enhance Ekman transport and upwelling.
- Findings highlighting the need for long-term monitoring at a fixed permanent time-series station to better understand seasonal and long term variability.

Distinct seasonal and spatial patterns were revealed by analyzing the annual variability of the mesozooplankton community across different contrasting areas:

- Zooplankton abundance distribution formed clusters based on seasonality and upwelling influence.
- Size-spectra analysis showed steeper slopes during daytime in the Stratified Season, indicating a less structured community, while the Late Winter Bloom exhibited higher trophic efficiency due to favorable conditions.
- Difference between day and nighttime in the size spectra could be attributed to com-

munity shifts associated with diel vertical migration.

- Taxonomic differences were notable, with Cladocera characterizing the Upwelling group and Salpidae and Appendicularia differentiated other seasonal groups.
- Outcomes showed the value of abundance composition for understanding taxonomic changes and size-spectra analysis for assessing ecosystem structure and predator-prey interactions.

Research on the biological carbon pump enabled us to identify key drives of euphausiids respiration. This chapter led to the following conclusions:

- Respiration rates and ETS activity followed a spatial trend, decreasing southward but increasing near the African upwelling region.
- Environmental factors such as epipelagic oxygen concentration, chlorophyll *a* levels, and interactions between epipelagic temperature and mesopelagic oxygen significantly influenced respiration rates.
- A strong correlation between respiration and ETS activity was observed, with R/ETS ratios exceeding the conservative threshold of 0.5.

Research of the contribution of the different pathways of the biological carbon pump in the twilight zone around the Iberian Peninsula revealed:

- Carbon flux was primarily driven by zooplankton and micronekton diel vertical migrants rather than by the passive flux.
- In the Mediterranean Sea, zooplankton dominated due to higher migrant biomass, whereas micronekton, particularly decapods, played a key role in the North Atlantic.
- Decapod active flux was influenced by productivity, while zooplankton and mesopelagic fish fluxes seemed to be linked to water masses.
- The relatively low contribution of passive flux highlights the crucial role of the

mesopelagic-migrant pump in carbon transport.

Appendix A. Institutional Acknowledgments

This thesis has been completed as part of María Couret Huertas work at IOCAG, in the doctoral program in Oceanography and Global Change. This study was supported by the “Sustainable Management of Mesopelagic Resources” (SUMMER, H2020, Grant agreement No 817806) project, the "Tropical and South Atlantic climate-based marine ecosystem prediction for sustainable management" (TRIATLAS, Grant Agreement 817578) project funded by the European Union, and the “DisEntangling Seasonality of Active Flux In the Ocean” (DESAFÍO, PID 2020- 118118RB-100) project funded by the Ministerio de Ciencia, Innovación y Universidades of the Spanish Government.

María Couret Huertas acknowledges the Agencia Canaria de Investigación, Innovación y Sociedad de la Información (ACIISI) grant program of “Apoyo al personal investigador en formación” TESIS2022010116. The research stay at the KOSMOS mesocosm experiment on ocean alkalinity enhancement conducted at the Marine Biological Station of the University of Bergen, Norway, was supported by the EU project Ocean Negative Emission Technologies (OceanNETs). The research stay at the Instituto Español de Oceanografía del CSIC, Centro Oceanográfico de Baleares was supported by the Agencia Canaria de Investigación, Innovación y Sociedad de la Información (ACIISI) grant for “Estancias Breves en España y en el Extranjero 2023” EST2023010021. The research stay at the Instituto Español de Oceanografía del CSIC, Centro Oceanográfico de A Coruña was supported by the Agencia Canaria de Investigación, Innovación y Sociedad de la Información (ACIISI) grant for “Estancias Breves en España y en el Extranjero 2024” EST2024010005.

Appendix B. Resumen Castellano

Objetivos

El objetivo principal de esta tesis es evaluar la biomasa, abundancia, estructura de tamaño y flujo de carbono del zooplancton en diferentes áreas del Océano Atlántico Norte. Diversos cambios han sido observados en las comunidades de zooplancton en diferentes localidades del Atlántico Norte, pero los patrones comunes o contrastantes de estos cambios no han sido evaluados correctamente debido a la ausencia de estaciones de mustreo fijas (Pitois and Yebra, 2022).

Por ello, hemos revisado, recopilado y curado todos los datos disponibles sobre la biomasa del mesozooplancton para analizar su variabilidad durante las últimas cinco décadas (1971-2021) en tres áreas productivas distintas del Sistema de la Corriente de Canarias, con el fin de establecer una línea base del mesozooplancton para futuros estudios.

Además, esta tesis explora la distribución, abundancia, composición y espectros de tamaño del zooplancton a lo largo del ciclo anual en diferentes áreas productivas: océano abierto y zona influenciada por el afloramiento.

Este estudio presenta la primera evaluación de las tasas de respiración de los eufausiáceos, utilizando un Modelo Aditivo Generalizado para estimarlas con precisión y comprender mejor el transporte de carbono. Además, esta tesis ha contribuido al campo de la investigación al proporcionar el sexto estudio enfocado en la estimación del flujo activo total, incorporando tanto el zooplancton como el micronekton, además del flujo pasivo.

Conclusiones

Esta tesis proporciona un análisis exhaustivo de la variabilidad espacio-temporal de la biomasa, abundancia, espectros de tamaño y flujo activo del mesozooplancton en el océano Atlántico Norte. A partir de la recopilación y análisis de cinco décadas (1971–2021) de datos de biomasa de mesozooplancton, se destacan los siguientes hallazgos clave:

- Un descenso significativo de la biomasa en la zona oligotrófica al norte de las Islas Canarias durante el Late Winter Bloom, probablemente asociado al aumento de temperaturas y a una mayor estratificación.
- Valores más elevados de biomasa cerca de la costa africana y alrededor de las islas, posiblemente impulsados por el afloramiento y el efecto de masa de isla al sur del archipiélago.
- Los ciclos estacionales mostraron un pico de biomasa durante el Late Winter Bloom, excepto en las regiones de afloramiento, donde los valores máximos se registraron en agosto debido a la intensificación de los vientos alisios, que favorecen el transporte de Ekman y el afloramiento.
- Los resultados subrayan la necesidad de un monitoreo a largo plazo en una estación de serie temporal fija para comprender mejor la variabilidad estacional y a largo plazo.

El análisis de la variabilidad anual de la comunidad de mesozooplancton en áreas diferentes reveló patrones espaciales y estacionales distintivos:

- La distribución de la abundancia de zooplancton formó grupos en función de la estacionalidad y la influencia del afloramiento.
- El análisis de los espectros de tamaño mostró pendientes más pronunciadas durante el día en la estación estratificada, lo que indica una comunidad menos estructurada,

mientras que el Late Winter Bloom presentó una mayor eficiencia trófica debido a condiciones oceanográficas favorables.

- Las diferencias entre los espectros de tamaño diurnos y nocturnos podrían atribuirse a cambios comunitarios asociados con la migración vertical diaria.
- Se observaron diferencias taxonómicas notables, siendo los Cladocera caracterizando el grupo de afloramiento, mientras que Salpidae y Appendicularia diferenciaban los grupos estacionales restantes.
- Estos resultados resaltan el valor de la composición de abundancia para comprender los cambios taxonómicos y el análisis de los espectros de tamaño para evaluar la estructura del ecosistema y las interacciones depredador-presa.

El estudio sobre la bomba biológica de carbono permitió identificar los principales factores que influyen en la respiración de los eufáusiaceos, llegando a las siguientes conclusiones:

- Las tasas de respiración y la actividad del sistema de transferencia de electrones (ETS) siguieron una tendencia espacial, disminuyendo hacia el sur pero aumentando en la región de afloramiento africana.
- Factores ambientales como la concentración de oxígeno epipelágico, los niveles de clorofila a y la interacción entre la temperatura epipelágica y la concentración de oxígeno mesopelágico influyeron significativamente en las tasas de respiración.
- Se observó una fuerte correlación entre la respiración y la actividad específica del ETS, con valores de R/ETS que superaron el umbral conservador de 0,5.

El análisis de las distintas vías de la bomba biológica de carbono en la zona mesopelágica alrededor de la Península Ibérica reveló que:

- El flujo de carbono fue impulsado principalmente por los migradores verticales di-

arios del zooplancton y el micronekton, en lugar del flujo pasivo.

- En el mar Mediterráneo, el zooplancton dominó debido a una mayor biomasa de migradores, mientras que en el Atlántico Norte el micronekton, en particular los decápodos, desempeñó un papel clave.
- El flujo activo de los decápodos estuvo influenciado por la productividad del área, mientras que los flujos activos del zooplancton y los peces mesopelágicos parecieron estar relacionados con las masas de agua.
- La baja contribución relativa del flujo pasivo, en comparación con el flujo activo total, subraya el papel crítico de la bomba migratoria mesopelágica en el transporte de carbono.

Bibliography

Akaike, H., 1974. A new look at the statistical model identification. IEEE Transactions on Automatic Control 19, 716–723. doi:10.1109/TAC.1974.1100705.

Aksnes, D.L., Løtvedt, A.S., Lindemann, C., Calleja, M.L., Morán, X.A.G., Kaarvedt, S., Thingstad, T.F., 2023. Effects of migrating mesopelagic fishes on the biological carbon pump. Marine Ecology Progress Series 717, 107–126.

Alexander, M.A., Kilbourne, K.H., Nye, J.A., 2014. Climate variability during warm and cold phases of the atlantic multidecadal oscillation (amo) 1871–2008. Journal of Marine Systems 133, 14–26.

Almeida Peña, C., 1996. Estudio de la biomasa y de la actividad de la enzima aspartato transcarbamilasa (ATC) en el mesozooplancton en diferentes áreas oceanográficas. Ph.D. thesis.

Alonso-Pérez, S., Cuevas, E., Querol, X., 2011. Objective identification of synoptic meteorological patterns favouring african dust intrusions into the marine boundary layer of the subtropical eastern north atlantic region. Meteorology and Atmospheric Physics 113, 109–124.

Andersen, T., Hessen, D.O., 1991. Carbon, nitrogen, and phosphorus content of freshwater zooplankton. Limnology and Oceanography 36, 807–814.

Angel, M.V., 1989. Vertical profiles of pelagic communities in the vicinity of the azores front and their implications to deep ocean ecology. Progress in Oceanography 22, 1–46. doi:10.1016/0079-6611(89)90009-8.

Angel, M.V., Pugh, P.R., 2000. Quantification of diel vertical migration by micronektonic

taxa in the northeast atlantic. Island, Ocean and Deep-Sea Biology , 161–179doi:10.1007/978-94-017-1982-7_16.

Archibald, K.M., Siegel, D.A., Doney, S.C., 2019. Modeling the impact of zooplankton diel vertical migration on the carbon export flux of the biological pump. Global Biogeochemical Cycles 33, 181–199. doi:10.1029/2018GB005983.

Arístegui, J., Barton, E.D., Álvarez-Salgado, X.A., Santos, A.M.P., Figueiras, F.G., Kifani, S., Hernández-León, S., Mason, E., Machú, E., Demarcq, H., 2009. Sub-regional ecosystem variability in the canary current upwelling. Progress in Oceanography 83, 33–48.

Arístegui, J., Hernández-León, S., Montero, M.F., Gómez, M., 2001. The seasonal planktonic cycle in coastal waters of the canary islands. Scientia Marina .

Arístegui, J., Sangrá, P., Hernández-León, S., Cantón, M., Hernández-Guerra, A., Kerling, J., 1994. Island-induced eddies in the canary islands. Deep Sea Research Part I: Oceanographic Research Papers 41, 1509–1525.

Arístegui, J., Tett, P., Hernández-Guerra, A., Basterretxea, G., Montero, M.F., Wild, K., Sangrá, P., Hernández-León, S., Canton, M., García-Braun, J., et al., 1997. The influence of island-generated eddies on chlorophyll distribution: a study of mesoscale variation around gran canaria. Deep Sea Research Part I: Oceanographic Research Papers 44, 71–96.

Ariza, A., Garijo, J., Landeira, J., Bordes, F., Hernández-León, S., 2015. Migrant biomass and respiratory carbon flux by zooplankton and micronekton in the subtropical northeast atlantic ocean (canary islands). Progress in Oceanography 134, 330–342.

Ariza, A., Landeira, J.M., Escánez, A., Wienerroither, R., de Soto, N.A., Røstad, A., Kaartvedt, S., Hernández-León, S., 2016. Vertical distribution, composition and mi-

gratory patterns of acoustic scattering layers in the canary islands. Journal of Marine Systems 157, 82–91. doi:10.1016/J.JMARSYS.2016.01.004.

Armengol, L., Calbet, A., Franchy, G., Rodríguez-Santos, A., Hernández-León, S., 2019. Planktonic food web structure and trophic transfer efficiency along a productivity gradient in the tropical and subtropical atlantic ocean. Scientific Reports 9, 1–19. doi:10.1038/s41598-019-38507-9.

Arístegui, J., Barton, E.D., Tett, P., Montero, M.F., García-Muñoz, M., Basterretxea, G., Cussatlegras, A.S., Ojeda, A., Armas, D.D., 2004. Variability in plankton community structure, metabolism, and vertical carbon fluxes along an upwelling filament (cape juby, nw africa). Progress in Oceanography 62, 95–113. doi:10.1016/j.pocean.2004.07.004.

Atkinson, A., Lilley, M.K., Hirst, A.G., McEvoy, A.J., Tarran, G.A., Widdicombe, C., Fileman, E.S., Woodward, E.M.S., Schmidt, K., Smyth, T.J., Somerfield, P.J., 2021. Increasing nutrient stress reduces the efficiency of energy transfer through planktonic size spectra. Limnology and Oceanography 66, 422–437. doi:10.1002/LNO.11613.

Aumont, O., Maury, O., Lefort, S., Bopp, L., 2018. Evaluating the potential impacts of the diurnal vertical migration by marine organisms on marine biogeochemistry. Global Biogeochemical Cycles 32, 1622–1643. doi:10.1029/2018GB005886.

Bailey, T.G., Youngbluth, M.J., Owen, G.P., 1995. Chemical composition and metabolic rates of gelatinous zooplankton from midwater and benthic boundary layer environments off cape hatteras, north carolina, usa. Marine Ecology Progress Series 122, 121–134. doi:10.3354/MEPS122121.

Baird, R., Thompson, N., Hopkins, T., Weiss, W., 1975. Chlorinated hydrocarbons in mesopelagic fishes of the eastern gulf of mexico. Bulletin of Marine Science 25, 473–481.

Baker, K., Halfter, S., Scoulding, B., Swadling, K.M., Richards, S.A., Bressac, M., Sutton, C., Boyd, P.W., 2025. Carbon injection potential of the mesopelagic-migrant pump in the southern ocean during summer. Frontiers in Marine Science 12, 1461723.

Banse, K., 1996. Zooplankton: pivotal role in the control of ocean production. Oceanographic Literature Review 5, 455.

Bárcena, M., Flores, J., Sierro, F., Pérez-Folgado, M., Fabres, J., Calafat, A., Canals, M., 2004. Planktonic response to main oceanographic changes in the alboran sea (western mediterranean) as documented in sediment traps and surface sediments. Marine Micropaleontology 53, 423–445.

Barnes, C., Irigoien, X., Oliveira, J.A.D., Maxwell, D., Jennings, S., 2011. Predicting marine phytoplankton community size structure from empirical relationships with remotely sensed variables. Journal of Plankton Research 33, 13–24. doi:10.1093/PLANKT/FBQ088.

Barton, E.D., Aristegui, J., Tett, P., Canton, M., García-Braun, J., Hernández-León, S., Nykjaer, L., Almeida, C., Almunia, J., Ballesteros, S., Basterretxea, G., Escanez, J., García-Weill, L., Hernández-Guerra, A., López-Laatzen, F., Molina, R., Montero, M.F., Navarro-Peréz, E., Rodríguez, J.M., Lenning, K.V., Vélez, H., Wild, K., 1998. The transition zone of the canary current upwelling region. Progress in Oceanography 41, 455–504. doi:10.1016/S0079-6611(98)00023-8.

Barton, E.D., Arístegui, J., Tett, P., Navarro-Pérez, E., 2004. Variability in the canary islands area of filament-eddy exchanges. Progress in Oceanography 62, 71–94. doi:10.1016/j.pocean.2004.07.003.

Batchelder, H.P., Daly, K.L., Davis, C.S., Ji, R., Ohman, M.D., Peterson, W.T., Runge, J.A., 2013. Climate impacts on zooplankton population dynamics in coastal marine ecosystems. Oceanography, 26, 34–51.

Beaugrand, G., Reid, P.C., 2003. Long-term changes in phytoplankton, zooplankton and salmon related to climate. Global Change Biology 9, 801–817.

Bedford, J., Ostle, C., Johns, D.G., Atkinson, A., Best, M., Bresnan, E., Machairopoulou, M., Graves, C.A., Devlin, M., Milligan, A., Pitois, S., Mellor, A., Tett, P., McQuatters-Gollop, A., 2020. Lifeform indicators reveal large-scale shifts in plankton across the north-west european shelf. Global Change Biology 26, 3482–3497. doi:10.1111/gcb.15066.

Behrenfeld, M.J., Falkowski, P.G., 1997. Photosynthetic rates derived from satellite-based chlorophyll concentration. Limnology and Oceanography 42, 1–20. doi:10.4319/lo.1997.42.1.0001.

Berraho, A., Somoue, L., Hernández-León, S., Valdés, L., 2015. Zooplankton in the canary current large marine ecosystem. in: Oceanographic and biological features in the canary current large marine ecosystem. Valdés, L. and Déniz-González, I. (eds). IOC-UNESCO, Paris. IOC Technical Series, No. 115, pp. 183-195. , 383 pp.

Bertram, D.F., Mackas, D.L., McKinnell, S.M., 2001. The seasonal cycle revisited: interannual variation and ecosystem consequences. Progress in Oceanography 49, 283–307. doi:10.1016/S0079-6611(01)00027-1.

Bianchi, D., Stock, C., Galbraith, E.D., Sarmiento, J.L., 2013. Diel vertical migration: Ecological controls and impacts on the biological pump in a one-dimensional ocean model. Global Biogeochemical Cycles 27, 478–491. doi:10.1002/gbc.20031.

Bograd, S.J., Jacox, M.G., Hazen, E.L., Lovecchio, E., Montes, I., Pozo Buil, M., Shannon, L.J., Sydeman, W.J., Rykaczewski, R.R., 2023. Climate change impacts on eastern boundary upwelling systems. Annual review of marine science 15, 303–328.

Boucher, J., 1982. Peuplement de copépodes des upwellings côtiers nord-ouest africains: I. composition faunistique et structure démographique. Oceanologica Acta 4, 49–62.

Boudreau, P.R., Dickie, L.M., Kerr, S.R., 1991. Body-size spectra of production and biomass as system-level indicators of ecological dynamics. Journal of Theoretical Biology 152, 329–339. doi:10.1016/S0022-5193(05)80198-5.

Braun, J.A.G., 1980. Estudios de producción en aguas de las islas canarias. i. hidrografía, nutrientes y producción primaria.: N. º 285. Boletín. Instituto Español de Oceanografía 5, 147–154.

Braun, L.M., Brucet, S., Mehner, T., 2021. Top-down and bottom-up effects on zooplankton size distribution in a deep stratified lake. Aquatic Ecology 55, 527–543. doi:10.1007/s10452-021-09843-8.

Brett, J.R., Groves, T.D.D., 1979. Physiological energetics. Fish Physiol. 8, 280–352.

Brierley, A.S., 2014. Diel vertical migration. Current biology : CB 24, R1074–R1076. URL: http://dx.doi.org/10.1016/j.cub.2014.08.054, doi:10.1016/j.cub.2014.08.054.

Brosset, P., Le Bourg, B., Costalago, D., Bănaru, D., Van Beveren, E., Bourdeix, J.H., Fromentin, J.M., Ménard, F., Saraux, C., 2016. Linking small pelagic dietary shifts with ecosystem changes in the gulf of lions. Marine Ecology Progress Series 554, 157–171.

Brown, J.H., Gillooly, J.F., Allen, A.P., Savage, V.M., West, G.B., 2004. Toward a metabolic theory of ecology. Ecology 85, 1771–1789.

Brun, P., Stamieszkin, K., Visser, A.W., Licandro, P., Payne, M.R., Kiørboe, T., 2019. Climate change has altered zooplankton-fuelled carbon export in the north atlantic. Nature Ecology and Evolution 3, 416–423. doi:10.1038/s41559-018-0780-3.

Buesseler, K.O., Antia, A.N., Chen, M., Fowler, S.W., Gardner, W.D., Gustafsson, O., Harada, K., Michaels, A.F., van der Loeff, M.R., Sarin, M., Steinberg, D.K., Trull, T.,

2007. An assessment of the use of sediment traps for estimating upper ocean particle fluxes. doi:10.1357/002224007781567621.

Buitenhuis, E.T., Rivkin, R.B., Séailley, S., Quéré, C.L., 2010. Biogeochemical fluxes through microzooplankton. Global Biogeochemical Cycles 24. doi:10.1029/2009GB003601.

Canales, M.T., Law, R., Blanchard, J.L., 2016. Shifts in plankton size spectra modulate growth and coexistence of anchovy and sardine in upwelling systems. Canadian Journal of Fisheries and Aquatic Sciences 73, 611–621. doi:10.1139/CJFAS-2015-0181/ASSET/IMAGES/CJFAS-2015-0181IEQ22.GIF.

Carlson, C.A., Ducklow, H.W., Michaels, A.F., 1994. Annual flux of dissolved organic carbon from the euphotic zone in the northwestern sargasso sea. Nature 371, 405–408. doi:10.1038/371405a0.

Carpenter, S.R., Kitchell, J.F., Hodgson, J.R., Cochran, P.A., Elser, J.J., Elser, M., Lodge, D., Kretchmer, D., He, X., von Ende, C.N., 1987. Regulation of lake primary productivity by food web structure. Ecology 68, 1863–1876.

Castellón, A., Olivar, M.P., 2023. Verda: A multisampler tool for mesopelagic nets. Journal of Marine Science and Engineering 11, 72.

Catherine, A., Escoffier, N., Belhocine, A., Nasri, A.B., Hamlaoui, S., Yéprémian, C., Bernard, C., Troussellier, M., 2012. On the use of the fluoroprobe®, a phytoplankton quantification method based on fluorescence excitation spectra for large-scale surveys of lakes and reservoirs. Water Research 46, 1771–1784. doi:10.1016/J.WATRES.2011.12.056.

Cavan, E.L., Belcher, A., Atkinson, A., Hill, S.L., Kawaguchi, S., McCormack, S., Meyer, B., Nicol, S., Ratnarajah, L., Schmidt, K., Steinberg, D.K., Tarling, G.A., Boyd, P.W.,

2019. The importance of antarctic krill in biogeochemical cycles. Nature Communications 2019 10:1 10, 1–13. doi:10.1038/s41467-019-12668-7.

Chen, B., Smith, S.L., 2018. Optimality-based approach for computationally efficient modeling of phytoplankton growth, chlorophyll-to-carbon, and nitrogen-to-carbon ratios. Ecological Modelling 385, 197–212. doi:10.1016/j.ecolmodel.2018.08.001.

Chen, Y., Lin, S., Wang, C., Yang, J., Sun, D., 2020. Response of size and trophic structure of zooplankton community to marine environmental conditions in the northern south china sea in winter. Journal of Plankton Research 42, 378–393. doi:10.1093/PLANKT/FBAA022.

Chiba, S., Sugisaki, H., Nonaka, M., Saino, T., 2009. Geographical shift of zooplankton communities and decadal dynamics of the kuroshio-oyashio currents in the western north pacific. Global Change Biology 15, 1846–1858. doi:10.1111/j.1365-2486.2009.01890.x.

Cianca, A., Helmke, P., Mouriño, B., Rueda, M.J., Llinás, O., Neuer, S., 2007. Decadal analysis of hydrography and in situ nutrient budgets in the western and eastern north atlantic subtropical gyre. Journal of Geophysical Research: Oceans 112, 7025. doi:10.1029/2006JC003788.

Clarke, A., Morris, D., 1983. Towards an energy budget for krill: the physiology and biochemistry of euphausia superba dana. Polar Biology 2, 69–86.

Clarke, K.R., Gorley, R.N., 2006. Primer v6: User manual/tutorial. PRIMER-E, Plymouth , 192.

Clarke, K.R., Warwick, R.M., 2001. Change in marine communities. An approach to statistical analysis and interpretation, 2, 1–68.

Conroy, J.A., Steinberg, D.K., Thomas, M.I., West, L.T., 2023. Seasonal and interannual

changes in a coastal antarctic zooplankton community. Marine Ecology Progress Series 706, 17–32. doi:10.3354/MEPS14256.

Corral, J., 1970. Contribución al conocimiento del plancton de canarias. Tesis Doctoral, Universidad de Madrid , 343 pp.

Cottingham, K.L., 1999. Nutrients and zooplankton as multiple stressors of phytoplankton communities: Evidence from size structure. Limnology and Oceanography 44, 810–827.

Couret, M., Díaz-Pérez, J., Sarmiento-Lezcano, A.N., Landeira, J.M., Hernández-León, S., 2024. Respiration rates and its relationship with ets activity in euphausiids: implications for active flux estimations. Frontiers in Marine Science 11, 1469587.

Couret, M., Landeira, J.M., del Pino, A.S., Hernández-León, S., 2023a. A 50-year (1971-2021) mesozooplankton biomass data base in the canary current system. doi:10.1594/PANGAEA.962439.

Couret, M., Landeira, J.M., Tuset, V.M., Sarmiento-Lezcano, A.N., Vélez-Belchí, P., Hernández-León, S., 2023b. Mesozooplankton size structure in the canary current system. Marine Environmental Research 188, 105976.

Coyle, K.O., Pinchuk, A.I., Eisner, L.B., Napp, J.M., 2008. Zooplankton species composition, abundance and biomass on the eastern bering sea shelf during summer: The potential role of water-column stability and nutrients in structuring the zooplankton community. Deep Sea Research Part II: Topical Studies in Oceanography 55, 1775–1791. doi:10.1016/J.DSR2.2008.04.029.

Cózar, A., García, C.M., Gálvez, J.A., 2003. Analysis of plankton size spectra irregularities in two subtropical shallow lakes (esteros del iberá, argentina). Canadian Journal of Fisheries and Aquatic Sciences 60, 411–420. doi:10.1139/F03-037.

Dadon-Pilosof, A., Lombard, F., Genin, A., Sutherland, K.R., Yahel, G., 2019. Prey

taxonomy rather than size determines salp diets. Limnology and Oceanography 64, 1996–2010.

Dai, L., Li, C., Yang, G., Sun, X., 2016. Zooplankton abundance, biovolume and size spectra at western boundary currents in the subtropical north pacific during winter 2012. Journal of Marine Systems 155, 73–83.

Dam, H.G., Peterson, W.T., 1988. The effect of temperature on the gut clearance rate constant of planktonic copepods. Journal of Experimental Marine Biology and Ecology 123, 1–14. doi:10.1016/0022-0981(88)90105-0.

Dam, H.G., Peterson, W.T., 1993. Seasonal contrasts in the diel vertical distribution, feeding behavior, and grazing impact of the copepod temora longicornis in long island sound. Journal of Marine Research 51, 561–594. doi:10.1357/0022240933223972.

Davison, P.C., 2011. The export of carbon mediated by mesopelagic fishes in the northeast pacific ocean. PhD Thesis, University of California, San Diego, CA. .

Davison, P.C., Checkley, D.M., Koslow, J.A., Barlow, J., 2013. Carbon export mediated by mesopelagic fishes in the northeast pacific ocean. Progress in Oceanography 116, 14–30. doi:10.1016/J.POCEAN.2013.05.013.

De León, A., Braun, J.G., 1973. Ciclo anual de la producción y su relación con los con los nutrientes en aguas de canarias. Boletín Instituto Español Oceanografía 167, 1–24.

Doty, M., Oguri, M., 1956. The island mass effect. Journal du Conseil / Conseil Permanent International pour l'Exploration de la Mer 22, 33–37.

Ekau, W., Auel, H., Hagen, W., Koppelmann, R., Wasmund, N., Bohata, K., Buchholz, F., Geist, S., Martin, B., Schukat, A., Verheye, H.M., Werner, T., 2018. Pelagic key species and mechanisms driving energy flows in the northern benguela upwelling ecosystem

and their feedback into biogeochemical cycles. Journal of Marine Systems 188, 49–62. doi:10.1016/j.jmarsys.2018.03.001.

Ekau, W., Auel, H., Portner, H.O., Gilbert, D., 2010. Impacts of hypoxia on the structure and processes in pelagic communities (zooplankton, macro-invertebrates and fish). Biogeosciences 7, 1669–1699. doi:10.5194/BG-7-1669-2010.

Ens, N.J., Er, J.F.D.W., Gauthier, S., 2023. Geographic variability in the seasonality of euphausiid diel vertical migrations among three locations in coastal british columbia, canada. ICES Journal of Marine Science 0, 1–12. doi:10.1093/ICESJMS/FSAD177.

Escribano, R., Hidalgo, P., Fuentes, M., Donoso, K., 2012. Zooplankton time series in the coastal zone off chile: Variation in upwelling and responses of the copepod community. Progress in Oceanography 97-100, 174–186. doi:10.1016/j.pocean.2011.11.006.

Fischer, G., Neuer, S., Ramondenc, S., Müller, T.J., Donner, B., Ruhland, G., Ratmeyer, V., Meinecke, G., Nowald, N., Klann, M., Wefer, G., 2020. Long-term changes of particle flux in the canary basin between 1991 and 2009 and comparison to sediment trap records off mauritania. Frontiers in Earth Science 8, 1–21. doi:10.3389/feart.2020.00280.

Fiuza, A.F., 1983. Upwelling patterns off portugal. In Coastal Upwelling Its Sediment Record: Part A: Responses of the Sedimentary Regime to Present Coastal Upwelling. Boston, MA: Springer US. 10 A, 85–98. doi:10.1007/978-1-4615-6651-9_5.

Flock, M.E., Hopkins, T.L., 1992. Species composition, vertical distribution, and food habits of the sergestid shrimp assemblage in the eastern gulf of mexico. Journal of Crustacean Biology 12, 210–223. doi:10.2307/1549076.

Forward, R., 1988. Diel vertical migration: zooplankton photobiology and behaviour.

Oceanogr. Mar. Biol. Annu. Rev 26, 1–393.

Gage, J.D., Tyler, P.A., 1991. Deep-sea biology: a natural history of organisms at the deep-sea floor. Cambridge University Press.

García-Comas, C., Chang, C.Y., Ye, L., Sastri, A.R., Lee, Y.C., Gong, G.C., hao Hsieh, C., 2014. Mesozooplankton size structure in response to environmental conditions in the east china sea: How much does size spectra theory fit empirical data of a dynamic coastal area? Progress in Oceanography 121, 141–157. doi:10.1016/J.POCEAN.2013.10.010.

Giering, S.L., Wells, S.R., Mayers, K.M., Schuster, H., Cornwell, L., Fileman, E.S., Atkinson, A., Cook, K.B., Preece, C., Mayor, D.J., 2019. Seasonal variation of zooplankton community structure and trophic position in the celtic sea: A stable isotope and biovolume spectrum approach. Progress in Oceanography 177, 101943. doi:10.1016/J.POCEAN.2018.03.012.

Gilly, W.F., Beman, J.M., Litvin, S.Y., Robison, B.H., 2013. Oceanographic and biological effects of shoaling of the oxygen minimum zone. Annual review of marine science 5, 393–420.

Gj, J., et al., 1984. Mesopelagic fish, a large potential resource in the arabian sea. Deep Sea Research Part A. Oceanographic Research Papers 31, 1019–1035.

Gliwicz, M.Z., Jawiński, A., Pawłowicz, M., 2004. Cladoceran densities, day-to-day variability in food selection by smelt, and the birth-rate-compensation hypothesis. Hydrobiologia 526, 171–186. doi:10.1023/B:HYDR.0000041605.72338.22.

Gómez, M., 1991. Biomasa y actividad metabólica del zooplancton en relación con un efecto de masa de isla en aguas de Gran Canaria. Ph.D. thesis.

Gómez, M., Torres, S., Hernández-León, S., 1996. Modification of the electron trans-

port system (ets) method for routine measurements of respiratory rates of zooplankton. South African Journal of Marine Science 17, 15–20.

Gorsky, G., Ohman, M.D., Picheral, M., Gasparini, S., Stemmann, L., Romagnan, J.B., Cawood, A., Pesant, S., García-Comas, C., Prejger, F., 2010. Digital zooplankton image analysis using the zooscan integrated system. Journal of Plankton Research 32, 285–303. doi:10.1093/PLANKT/FBP124.

Gu, Z., 2022. Complex heatmap visualization. Imeta 1, e43.

Guidi, L., Legendre, L., Reygondeau, G., Uitz, J., Stemmann, L., Henson, S.A., 2015. A new look at ocean carbon remineralization for estimating deepwater sequestration. Global Biogeochemical Cycles 29, 1044–1059. doi:10.1002/2014GB005063.

Gurney, L., Froneman, P., Pakhomov, E., McQuaid, C., 2002. Diel feeding patterns and daily ration estimates of three subantarctic euphausiids in the vicinity of the prince edward islands (southern ocean). Deep Sea Research Part II: Topical Studies in Oceanography 49, 3207–3227.

Gómez-Gesteira, M., Castro, M.D., Álvarez, I., Lorenzo, M.N., Gesteira, J.L., Crespo, A.J., 2008. Spatio-temporal upwelling trends along the canary upwelling system (1967–2006). Annals of the New York Academy of Sciences 1146, 320–337. doi:10.1196/ANNALS.1446.004.

Harris, B.P., Young, J.W., Revill, A.T., Taylor, M.D., 2014. Understanding diel-vertical feeding migrations in zooplankton using bulk carbon and nitrogen stable isotopes. Journal of plankton research 36, 1159–1163.

Harvey, C.J., Fisher, J.L., Samhouri, J.F., Williams, G.D., Francis, T.B., Jacobson, K.C., deReynier, Y.L., Hunsicker, M.E., Garfield, N., 2020. The importance of long-term ecological time series for integrated ecosystem assessment and ecosystem-based man-

agement. Progress in Oceanography 188, 102418. doi:10.1016/j.pocean.2020.102418.

Hauss, H., Christiansen, S., Schütte, F., Kiko, R., Edvam Lima, M., Rodrigues, E., Karstensen, J., Löscher, C.R., Körtzinger, A., Fiedler, B., 2016. Dead zone or oasis in the open ocean? zooplankton distribution and migration in low-oxygen modewater eddies. Biogeosciences 13, 1977–1989.

Hay, M.E., 2009. Marine chemical ecology: chemical signals and cues structure marine populations, communities, and ecosystems. Annual review of marine science 1, 193–212.

Hays, G., 2003. A review of adaptive significance and ecosystem consequenses of zooplankton diel vertical migrations. Hydrobiologia 503, 163–170.

Hays, G., Kennedy, H., Frost, B., 2001. Individual variability in diel vertical migration of a marine copepod: why some individuals remain at depth when others migrate. Limnology and Oceanography 46, 2050–2054.

Hays, G.C., Richardson, A.J., Robinson, C., 2005. Climate change and marine plankton. Trends in Ecology and Evolution 20, 337–344. doi:10.1016/j.tree.2005.03.004.

Heath, M.R., 1995. Size spectrum dynamics and the planktonic ecosystem of loch linnhe. ICES Journal of Marine Science 52, 627–642. doi:10.1016/1054-3139(95)80077-8.

Hébert, M.P., Beisner, B.E., Maranger, R., 2017. Linking zooplankton communities to ecosystem functioning: toward an effect-trait framework. Journal of Plankton Research 39, 3–12.

Heneghan, R.F., Everett, J.D., Blanchard, J.L., Sykes, P., Richardson, A.J., 2023. Climate-

driven zooplankton shifts cause large-scale declines in food quality for fish. Nature Climate Change 2023 13:5 13, 470–477. doi:10.1038/s41558-023-01630-7.

Hernández-León, S., 1988a. Algunas observaciones sobre la abundancia y estructura del mesozooplancton en aguas del archipiélago canario .

Hernández-León, S., 1988b. Annual cycle of mesozooplanktonic standing stock over an island shelf area in canary islands waters. Investigacion Pesquera (Spain) 52.

Hernández-León, S., 1988c. Gradients of mesozooplankton biomass and ets activity in the wind-shear area as evidence of an island mass effect in the canary island waters. Journal of Plankton Research 10, 1141–1154. doi:10.1093/plankt/10.6.1141.

Hernández-León, S., 1991. Accumulation of mesozooplankton in a wake area as a causative mechanism of the "island-mass effect". Marine Biology 109, 141–147.

Hernández-León, S., Almeida, C., Bécognée, P., Yebra, L., Arístegui, J., 2004. Zooplankton biomass and indices of grazing and metabolism during a late winter bloom in subtropical waters. Marine Biology 145, 1191–1200.

Hernández-León, S., Almeida, C., Gómez, M., Torres, S., Montero, I., Portillo-Hahnefeld, A., 2001. Zooplankton biomass and indices of feeding and metabolism in island-generated eddies around gran canaria. Journal of Marine Systems 30, 51–66. URL: https://doi.org/10.1016/S0924-7963(01)00037-9.

Hernández-León, S., Almeida, C., Portillo-Hahnefeld, A., Gómez, M., Rodriguez, J., Arístegui, J., 2002a. Zooplankton biomass and indices of feeding and metabolism in relation to an upwelling filament off northwest africa. Journal of Marine Research 60, 327–346.

Hernández-León, S., Calles, S., de Puelles, M.L.F., 2019a. The estimation of metabolism in the mesopelagic zone: disentangling deep-sea zooplankton respiration. Progress in oceanography 178, 102163.

Hernández-León, S., Gómez, M., Arístegui, J., 2007. Mesozooplankton in the canary current system: The coastal–ocean transition zone. Progress in Oceanography 74, 397–421.

Hernández-León, S., Gómez, M., Pagazaurtundua, M., Portillo-Hahnefeld, A., Montero, I., Almeida, C., 2002b. Vertical distribution of zooplankton in canary island waters: Implications for export flux. Deep-Sea Research Part I: Oceanographic Research Papers 48, 1071–1092. doi:10.1016/S0967-0637(00)00074-1.

Hernández-León, S., Ikeda, T., 2005. A global assessment of mesozooplankton respiration in the ocean. Journal of Plankton Research 27, 153–158.

Hernández-León, S., Putzeys, S., Almeida, C., Bécognée, P., Marrero-Díaz, A., Arístegui, J., Yebra, L., 2019b. Carbon export through zooplankton active flux in the canary current. Journal of Marine Systems 189, 12–21.

Hernández-León, S., Sarmiento-Lezcano, A., Couret, M., Armengol, L., Medina-Suárez, I., Fatira, E., Tuset, V., Limam, A., Sánchez Díez, A., Díaz-Pérez, J., et al., 2024. Seasonality of zooplankton active flux in subtropical waters. Limnology and Oceanography 69, 2564–2579.

Hernández-León, S., Gómez, M., 1996. Factors affecting the respiration/ets ratio in marine zooplankton. Journal of Plankton Research 18, 239–255.

Hernández-León, S., Koppelmann, R., Fraile-Nuez, E., Bode, A., Mompeán, C., Irigoien, X., Olivar, M.P., Echevarría, F., de Puelles, M.L.F., González-Gordillo, J.I., Cózar, A., Acuña, J.L., Agustí, S., Duarte, C.M., 2020. Large deep-sea zooplankton biomass mirrors primary production in the global ocean. Nature Communications 11, 11. doi:10.1038/s41467-020-19875-7.

Hernández-León, S., Olivar, M., de Puelles, M.F., Bode, A., Castellón, A., López-Pérez, C., Tuset, V.M., González-Gordillo, J., 2019. Zooplankton and micronekton active flux

across the tropical and subtropical atlantic ocean. Frontiers in Marine Science 6, 535. doi:10.3389/fmars.2019.00535.

Hernández-León, S., Rodal, D.M., 1987. Actividad del sistema de transporte de electrones y biomasa del mesozooplankton en aguas de las islas canarias. Boletín del Instituto Español de Oceanografía 4, 49–62.

Herrera, I., López-Cancio, J., Yebra, L., Hernández-Léon, S., 2017. The effect of a strong warm winter on subtropical zooplankton biomass and metabolism. Journal of Marine Research 75, 557–577. doi:10.1357/002224017822109523.

Herrera, I., Yebra, L., Antezana, T., Giraldo, A., Färber-Lorda, J., Hernández-León, S., 2019. Vertical variability of euphausia distinguenda metabolic rates during diel migration into the oxygen minimum zone of the eastern tropical pacific off mexico. Journal of Plankton Research 41, 165–176. doi:10.1093/plankt/fbz004.

Hidaka, K., Kawaguchi, K., Murakami, M., Takahashi, M., 2001. Downward transport of organic carbon by diel migratory micronekton in the western equatorial pacific: Its quantitative and qualitative importance. Deep-Sea Research Part I: Oceanographic Research Papers 48, 1923–1939. doi:10.1016/S0967-0637(01)00003-6.

Hoffmeyer, M.S., 2004. Decadal change in zooplankton seasonal succession in the bahía blanca estuary, argentina, following introduction of two zooplankton species. Journal of Plankton Research 26, 181–189. doi:10.1093/plankt/fbh023.

Honjo, S., Manganini, S.J., Krishfield, R.A., Francois, R., 2008. Particulate organic carbon fluxes to the ocean interior and factors controlling the biological pump: A synthesis of global sediment trap programs since 1983. Progress in Oceanography 76, 217–285. doi:10.1016/j.pocean.2007.11.003.

Hooff, R.C., Peterson, W.T., 2006. Copepod biodiversity as an indicator of changes in

ocean and climate conditions of the northern california current ecosystem. Limnology and Oceanography 51, 2607–2620. doi:10.4319/lo.2006.51.6.2607.

Huggett, J.A., Noyon, M., Carstensen, J., Walker, D.R., 2023. Patterns in the plankton – spatial distribution and long-term variability of copepods on the agulhas bank. Deep Sea Research Part II: Topical Studies in Oceanography 208, 105265. doi:10.1016/J.DSR2.2023.105265.

Iguchi, N., Ikeda, T., 2005. Effects of temperature on metabolism, growth and growth efficiency of thysanoessa longipes (crustacea: Euphausiacea) in the japan sea. Journal of Plankton Research 27, 1–10.

Ikeda, T., 1985. Metabolic rates of epipelagic marine zooplankton as a function of body mass and temperature. Marine Biology 85, 1–11. doi:10.1007/BF00396409.

Ikeda, T., 1989. Estimated respiration rate of myctophid fish from the enzyme activity of the electron-transport-system. Journal of the Oceanographical Society of Japan 45, 167–173.

Ikeda, T., 2013a. Metabolism and chemical composition of pelagic decapod shrimps: synthesis toward a global bathymetric model. Journal of oceanography 69, 671–686.

Ikeda, T., 2013b. Respiration and ammonia excretion of euphausiid crustaceans: synthesis toward a global-bathymetric model. Marine biology 160, 251–262.

Ikeda, T., Motoda, S., 1978. Estimated zooplankton production and their ammonia excretion in the kuroshio and adjacent seas. Fish. Bull. 76, 357–367.

Jagadeesan, L., Srinivas, T.N., Surendra, A., Kumar, G.S., Aswindev, M.P., Joseph, I., 2020. Copepods size structure in various phases of a cold-core eddy - normalised abundance size spectra (nass) approach. Continental Shelf Research 206, 104197. doi:10.1016/J.CSR.2020.104197.

Johnson, C.R., Banks, S.C., Barrett, N.S., Cazassus, F., Dunstan, P.K., Edgar, G.J., Frusher, S.D., Gardner, C., Haddon, M., Helidoniotis, F., Hill, K.L., Holbrook, N.J., Hosie, G.W., Last, P.R., Ling, S.D., Melbourne-Thomas, J., Miller, K., Pecl, G.T., Richardson, A.J., Ridgway, K.R., Rintoul, S.R., Ritz, D.A., Ross, D.J., Sanderson, J.C., Shepherd, S.A., Slotwinski, A., Swadling, K.M., Taw, N., 2011. Climate change cascades: Shifts in oceanography, species' ranges and subtidal marine community dynamics in eastern tasmania. Journal of Experimental Marine Biology and Ecology 400, 17–32. doi:10.1016/j.jembe.2011.02.032.

Jonkers, L., Meilland, J., Rillo, M.C., de Garidel-Thoron, T., Kitchener, J.A., Kucera, M., 2022. Linking zooplankton time series to the fossil record. ICES Journal of Marine Science 79, 917–924.

Judkins, H., Vecchione, M., 2020. Vertical distribution patterns of cephalopods in the northern gulf of mexico. Frontiers in Marine Science 7, 492167. doi:10.3389/FMARS.2020.00047/BIBTEX.

Kalinowska, K., Napiórkowska-Krzebietke, A., Bogacka-Kapusta, E., Stawecki, K., Traczuk, P., Ulikowski, D., 2024. Algae–zooplankton relationships during the year-round cyanobacterial blooms in a shallow lake. Hydrobiologia 851, 2025–2040.

Kaufman, L., Karrer, L., Peterson, C., 2009. Monitoring and evaluation. in: Mcleod, k., leslie, h. (eds.). ecosystem-based management for the oceans. Island Press, Washington, DC , 115–128.

Kenner, R.A., Ahmed, S.I., 1975. Measurements of electron transport activities in marine phytoplankton. Marine Biology 33, 119–127. doi:10.1007/BF00390716.

Kiko, R., Hauss, H., 2019. On the estimation of zooplankton-mediated active fluxes in oxygen minimum zone regions. Frontiers in Marine Science 6, 473486. doi:10.3389/FMARS.2019.00741/BIBTEX.

King, F.D., Packard, T.T., 1975. Respiration and the activity of the respiratory electron transport system in marine zooplankton. Limnology and Oceanography 20, 849–854. doi:10.4319/lo.1975.20.5.0849.

Kiørboe, T., 2013. Zooplankton body composition. Limnology and Oceanography 58, 1843–1850. doi:10.4319/LO.2013.58.5.1843.

Knauer, G.A., Martin, J.H., Bruland, K.W., 1979. Fluxes of particulate carbon, nitrogen, and phosphorus in the upper water column of the northeast pacific. Deep Sea Research Part A. Oceanographic Research Papers 26, 97–108. doi:10.1016/0198-0149(79)90089-X.

Kobari, T., Ueda, A., Nishibe, Y., 2010. Development and growth of ontogenetically migrating copepods during the spring phytoplankton bloom in the oyashio region. Deep Sea Research Part II: Topical Studies in Oceanography 57, 1715–1726. doi:10.1016/j.dsr2.2010.03.015.

Kodama, T., Igeta, Y., Iguchi, N., 2022. Long-term variation in mesozooplankton biomass caused by top-down effects: A case study in the coastal sea of japan. Geophysical Research Letters 49, e2022GL099037.

Koppelmann, R., Weikert, H., 2007. Spatial and temporal distribution patterns of deep-sea mesozooplankton in the eastern mediterranean – indications of a climatically induced shift? Marine Ecology 28, 259–275. doi:10.1111/J.1439-0485.2007.00154.X.

Koslow, J.A., Kloser, R.J., Williams, A., 1997. Pelagic biomass and community structure over the mid-continental slope off southeastern australia based upon acoustic and mid-water trawl sampling. Mar. Ecol. Prog. Ser. 146, 21–35.

Krupica, K., 2006. Evaluating size-based indices to monitor variation in scotian shelf zooplankton assemblages .

Kwon, E.Y., Primeau, F., Sarmiento, J.L., 2009. The impact of remineralization depth on the air–sea carbon balance. Nature Geoscience 2, 630–635.

Kwong, L.E., Henschke, N., Pakhomov, E.A., Everett, J.D., Suthers, I.M., 2020. Mesozooplankton and micronekton active carbon transport in contrasting eddies. Frontiers in Marine Science 6, 825.

Kwong, L.E., Ross, T., Lüskow, F., Florko, K.R., Pakhomov, E.A., 2022. Spatial, seasonal, and climatic variability in mesozooplankton size spectra along a coastal-to-open ocean transect in the subarctic northeast pacific. Progress in Oceanography 201, 102728. doi:10.1016/J.POCEAN.2021.102728.

Lampert, W., 1989. The adaptive significance of diel vertical migration of zooplankton. Functional Ecology 3, 21. doi:10.2307/2389671.

Lampitt, R.S., Achterberg, E.P., Anderson, T.R., Hughes, J.A., Iglesias-Rodriguez, M.D., Kelly-Gerreyn, B.A., Lucas, M., Popova, E.E., Sanders, R., Shepherd, J.G., Smythe-Wright, D., Yool, A., 2008. Ocean fertilization: A potential means of geoengineering? Philosophical Transactions of the Royal Society A: Mathematical, Physical and Engineering Sciences 366, 3919–3945. doi:10.1098/rsta.2008.0139.

Landeira, J.M., Brochier, T., Mason, E., Lozano-Soldevilla, F., Hernández-León, S., Barton, E.D., 2017. Transport pathways of decapod larvae under intense mesoscale activity in the canary-african coastal transition zone: implications for population connectivity. Scientia Marina 81, 299–315.

Landry, M.R., Al-Mutairi, H., Selph, K.E., Christensen, S., Nunnery, S., 2001. Seasonal patterns of mesozooplankton abundance and biomass at station aloha. Deep Sea Research Part II: Topical Studies in Oceanography 48, 2037–2061. doi:10.1016/S0967-0645(00)00172-7.

Le Borgne, R., Rodier, M., 1997. Net zooplankton and the biological pump: a comparison

between the oligotrophic and mesotrophic equatorial pacific. Deep Sea Research Part II: Topical Studies in Oceanography 44, 2003–2023.

Lee, H., Choi, J., Im, Y., Oh, W., Hwang, K., Lee, K., 2022. Spatial–temporal distribution of the euphausiid euphausia pacifica and fish schools in the coastal southwestern east sea. Water 2022, Vol. 14, Page 203 14, 203. doi:10.3390/W14020203.

Legendre, L., Rivkin, R.B., 2005. Integrating functional diversity, food web processes, and biogeochemical carbon fluxes into a conceptual approach for modeling the upper ocean in a high-co2 world. Journal of Geophysical Research C: Oceans 110, 1–17. doi:10.1029/2004JC002530.

Lehette, P., Hernández-León, S., 2009. Zooplankton biomass estimation from digitized images: a comparison between subtropical and antarctic organisms. Limnology and Oceanography: Methods 7, 304–308. doi:10.4319/lom.2009.7.304.

Lenth, R., Lenth, M.R., 2018. Package 'lsmeans'. The American Statistician 34, 216–221.

Lenz, P.H., Lieberman, B., Cieslak, M.C., Roncalli, V., Hartline, D.K., 2021. Transcriptomics and metatranscriptomics in zooplankton: Wave of the future? Journal of Plankton Research 43, 3–9. doi:10.1093/plankt/fbaa058.

Letessier, T.B., Falkenhaug, T., Debes, H., Bergstad, O.A., Brierley, A.S., 2011. Abundance patterns and species assemblages of euphausiids associated with the mid-atlantic ridge, north atlantic. Journal of Plankton Research 33, 1510–1525. doi:10.1093/PLANKT/FBR056.

Levene, H., 1960. Robust tests for equality of variances. In: I. Olkin, et al., Eds., Contributions to Probability and Statistics: Essays in Honor of Harold Hotelling, Stanford University Press, Palo Alto , 278–292.

Li, K., Ke, Z., Tan, Y., 2018. Zooplankton in the huangyan atoll, south china sea: A

comparison of community structure between the lagoon and seaward reef slope. Journal of Oceanology and Limnology 36, 1671–1680.

Lilliefors, H.W., 1967. On the kolmogorov-smirnov test for normality with mean and variance unknown. Journal of the American Statistical Association 62, 399–402. doi:10.1080/01621459.1967.10482916.

Liu, G., Liu, Z., Gu, B., Smoak, J.M., Zhang, Z., 2014. How important are trophic state, macrophyte and fish population effects on cladoceran community? a study in lake erhai. Hydrobiologia 736, 189–204. doi:10.1007/S10750-014-1906-5/TABLES/3.

Liu, L., Xiang, L., 2019. Missing covariate data in generalized linear mixed models with distribution-free random effects. Computational statistics & data analysis 134, 1–16.

Lomartire, S., Marques, J.C., Gonçalves, A.M., 2021. The key role of zooplankton in ecosystem services: A perspective of interaction between zooplankton and fish recruitment. Ecological Indicators 129. doi:10.1016/J.ECOLIND.2021.107867.

Longhurst, A., Harrison, W., 1989. The biological pump: profiles of plankton production and consumption in the upper ocean. Progress in Oceanography 22, 47–123.

Longhurst, A.R., 1985. Relationship between diversity and the vertical structure of the upper ocean. Deep Sea Research Part A. Oceanographic Research Papers 32, 1535–1570. doi:10.1016/0198-0149(85)90102-5.

Longhurst, A.R., Bedo, A.W., Harrison, W.G., Head, E.J., Sameoto, D.D., 1990. Vertical flux of respiratory carbon by oceanic diel migrant biota. Deep Sea Research Part A, Oceanographic Research Papers 37, 685–694. doi:10.1016/0198-0149(90)90098-G.

Longhurst, A.R., Harrison, G.W., 1988. Vertical nitrogen flux from the oceanic photic zone by diel migrant zooplankton and nekton. Deep Sea Research Part A, Oceanographic Research Papers 35, 881–889. doi:10.1016/0198-0149(88)90065-9.

López-Pérez, C., Olivar, M.P., Hulley, P.A., Tuset, V.M., 2020. Length–weight relationships of mesopelagic fishes from the equatorial and tropical atlantic waters: Influence of environment and body shape. Journal of Fish Biology 96, 1388–1398.

Lowry, O., Rosebrough, N., Farr, A., Randall, R., 1951. Protein measurement with the folin phenol reagent. The Journal of biological chemistry 193, 265–275.

Maas, A.E., Gossner, H., Smith, M.J., Blanco-Bercial, L., 2021. Use of optical imaging datasets to assess biogeochemical contributions of the mesozooplankton. Journal of Plankton Research 43, 475–491. doi:10.1093/PLANKT/FBAB037.

Mackas, D.L., Beaugrand, G., 2010. Comparisons of zooplankton time series. Journal of Marine Systems 79, 286–304.

Mackas, D.L., Greve, W., Edwards, M., Chiba, S., Tadokoro, K., Eloire, D., Mazzocchi, M.G., Batten, S., Richardson, A.J., Johnson, C., Head, E., Conversi, A., Peluso, T., 2012. Changing zooplankton seasonality in a changing ocean: Comparing time series of zooplankton phenology. Progress in Oceanography 97-100, 31–62. doi:10.1016/j.pocean.2011.11.005.

Madin, L.P., Horgan, E.F., Steinberg, D.K., 2001. Zooplankton at the bermuda atlantic time-series study (bats) station: diel, seasonal and interannual variation in biomass, 1994–1998. Deep Sea Research Part II: Topical Studies in Oceanography 48, 2063–2082. doi:10.1016/S0967-0645(00)00171-5.

Manríquez, K., Escribano, R., Riquelme-Bugueño, R., 2012. Spatial structure of the zooplankton community in the coastal upwelling system off central-southern chile in spring 2004 as assessed by automated image analysis. Progress in Oceanography 92-95, 121–133. doi:10.1016/j.pocean.2011.07.020.

Marañón, E., Van Wambeke, F., Uitz, J., Boss, E.S., Dimier, C., Dinasquet, J., Engel, A., Haëntjens, N., Pérez-Lorenzo, M., Taillandier, V., et al., 2021. Deep maxima of phy-

toplankton biomass, primary production and bacterial production in the mediterranean sea. Biogeosciences 18, 1749–1767.

Marcolin, C.R., Gaeta, S., Lopes, R.M., 2015. Seasonal and interannual variability of zooplankton vertical distribution and biomass size spectra off ubatuba, brazil. Journal of Plankton Research 37, 808–819. doi:10.1093/PLANKT/FBV035.

Marrero-Betancort, N., Marcello, J., Rodríguez Esparragón, D., Hernández-León, S., 2020. Wind variability in the canary current during the last 70 years. Ocean Science 16, 951–963.

Marshall, D.J., Alvarez-Noriega, M., 2020. Projecting marine developmental diversity and connectivity in future oceans. Philosophical Transactions of the Royal Society B: Biological Sciences 375, 20190450. doi:10.1098/rstb.2019.0450.

Martin, E.S., Harris, R.P., Irigoien, X., 2006. Latitudinal variation in plankton size spectra in the atlantic ocean. Deep-Sea Research Part II: Topical Studies in Oceanography 53, 1560–1572. doi:10.1016/J.DSR2.2006.05.006.

Massutí, E., Sánchez-Guillamón, O., Farriols, M.T., Palomino, D., Frank, A., Bárcenas, P., Rincón, B., Martínez-Carreño, N., Keller, S., López-Rodríguez, C., et al., 2021. Improving scientific knowledge of mallorca channel seamounts (western mediterranean) within the framework of natura 2000 network. Diversity 14, 4.

May, J., Blaber, S., 1989. Benthic and pelagic fish biomass of the upper continental slope off eastern tasmania. Marine Biology 101, 11–25.

Mayor, D.J., Gentleman, W.C., Anderson, T.R., 2020. Ocean carbon sequestration: Particle fragmentation by copepods as a significant unrecognised factor?: Explicitly representing the role of copepods in biogeochemical models may fundamentally improve understanding of future ocean carbon storage. BioEssays 42, 1–7. doi:10.1002/bies.202000149.

Medellín-Mora, J., Escribano, R., Schneider, W., 2016. Community response of zooplankton to oceanographic changes (2002-2012) in the central/southern upwelling system of chile. Progress in Oceanography 142, 17–29. doi:10.1016/j.pocean.2016.01.005.

Mediprod, G., 1974. Résultats de la campagne MEDIPROD: III:+ trois+: 13 juin-2 juillet 1972. Centre national pour l'exploitation des océans.

Meillat, M., 2012. Essais du chalut mésopélagos pour le programme mycto 3d-map de l? ird, à bord du marion dufresne. du 10 au 21 août 2012. Rapport de mission, Ifremer .

Menzel, D.W., Ryther, J.H., 1961. Nutrients limiting the production of phytoplankton in the sargasso sea, with special reference to iron. Deep Sea Research (1953) 7, 276–281. doi:10.1016/0146-6313(61)90045-4.

Mestre, M., Ruiz-González, C., Logares, R., Duarte, C.M., Gasol, J.M., Sala, M.M., 2018. Sinking particles promote vertical connectivity in the ocean microbiome. Proceedings of the National Academy of Sciences 115, E6799–E6807. doi:10.1073/pnas.1802470115.

Moyano, M., Rodríguez, J., Hernández-León, S., 2009. Larval fish abundance and distribution during the late winter bloom off gran canaria island, canary islands. Fisheries Oceanography 18, 51–61. doi:10.1111/J.1365-2419.2008.00496.X.

Mundim, K.C., Baraldi, S., Machado, H.G., Vieira, F.M., 2020. Temperature coefficient (q10) and its applications in biological systems: Beyond the arrhenius theory. Ecological Modelling 431, 109127. doi:10.1016/J.ECOLMODEL.2020.109127.

Naito, A., Abe, Y., Matsuno, K., Nishizawa, B., Kanna, N., Sugiyama, S., Yamaguchi, A., 2019. Surface zooplankton size and taxonomic composition in bowdoin fjord, northwestern greenland: A comparison of zooscan, opc and microscopic analyses. Polar Science 19, 120–129. doi:10.1016/J.POLAR.2019.01.001.

Neuer, S., Cianca, A., Helmke, P., Freudenthal, T., Davenport, R., Meggers, H., Knoll, M., Santana-Casiano, J.M., González-Davila, M., Rueda, M.J., Llinás, O., 2007. Biogeochemistry and hydrography in the eastern subtropical north atlantic gyre. results from the european time-series station estoc. Progress in Oceanography 72, 1–29. doi:10.1016/j.pocean.2006.08.001.

Noji, T.T., 1991. The influence of macrozooplankton on vertical particulate flux. http://dx.doi.org/10.1080/00364827.1991.10413459 76, 1–9. doi:10.1080/00364827.1991.10413459.

Nowicki, M., DeVries, T., Siegel, D.A., 2022. Quantifying the carbon export and sequestration pathways of the ocean's biological carbon pump. Global Biogeochemical Cycles 36, e2021GB007083. doi:10.1029/2021GB007083.

Noyon, M., Poulton, A.J., Asdar, S., Weitz, R., Giering, S.L., 2022. Mesozooplankton community distribution on the agulhas bank in autumn: Size structure and production. Deep Sea Research Part II: Topical Studies in Oceanography 195, 105015. doi:10.1016/J.DSR2.2021.105015.

Ohman, M.D., 2012. Estimation of mortality for stage-structured zooplankton populations: what is to be done? Journal of Marine Systems 93, 4–10.

Ohman, M.D., Romagnan, J.B., 2016. Nonlinear effects of body size and optical attenuation on diel vertical migration by zooplankton. Limnology and Oceanography 61, 765–770. doi:10.1002/LNO.10251.

Oksana, G., Viacheslav, V., 2012. Composition and structure of the zooplankton in coastal waters of mauritania in winter. Journal of Siberian Federal University. Biology 5, 136–150. doi:10.17516/1997-1389-0141.

Olivar, M.P., Castellón, A., Sabatés, A., Sarmiento-Lezcano, A., Emelianov, M., Bernal, A., Yang, Y., Proud, R., Brierley, A.S., 2022. Variation in mesopelagic fish community

composition and structure between mediterranean and atlantic waters around the iberian peninsula. Frontiers in Marine Science 9, 1028717. doi:10.3389/FMARS.2022.1028717/BIBTEX.

Olivar, M.P., Hulley, P.A., Castellón, A., Emelianov, M., López, C., Tuset, V.M., Contreras, T., Molí, B., 2017. Mesopelagic fishes across the tropical and equatorial atlantic: Biogeographical and vertical patterns. Progress in Oceanography 151, 116–137. doi:10.1016/J.POCEAN.2016.12.001.

Ollier, A., Chabot, D., Audet, C., Winkler, G., 2018. Metabolic rates and spontaneous swimming activity of two krill species (euphausiacea) under different temperature regimes in the st. lawrence estuary, canada. Journal of Crustacean Biology 38, 697–706. doi:10.1093/JCBIOL/RUY028.

Omori, M., Ikeda, T., 1984. Methods in marine zooplankton ecology. New York, NY: John Wiley and Sons 332.

Owens, T.G., King, F.D., 1975. The measurement of respiratory electron-transport-system activity in marine zooplankton. Marine Biology 30, 27–36. doi:10.1007/BF00393750.

Packard, T., 1971. The measurement of respiratory electron-transport activity in marine phytoplankton.

Packard, T., Harmon, D., Boucher, J., 1974. Respiratory electron transport activity in plankton from upwelled waters. Tethys 6, 213–222.

Paffenhöfer, G.A., 1998. Heterotrophic protozoa and small metazoa: feeding rates and prey-consumer interactions. Journal of Plankton research 20, 121–133.

Pakhomov, E., Froneman, P., 2004. Zooplankton dynamics in the eastern atlantic sector of the southern ocean during the austral summer 1997/1998—part 1: Community structure. Deep Sea Research Part II: Topical Studies in Oceanography 51, 2599–2616.

Pakhomov, E.A., Podeswa, Y., Hunt, B.P., Kwong, L.E., 2019. Vertical distribution and active carbon transport by pelagic decapods in the north pacific subtropical gyre. ICES Journal of Marine Science 76, 702–717.

Parekh, P., Follows, M.J., Dutkiewicz, S., Ito, T., 2006. Physical and biological regulation of the soft tissue carbon pump. Paleoceanography 21.

Parr, T.W., Sier, A.R., Battarbee, R.W., Mackay, A., Burgess, J., 2003. Detecting environmental change: science and society—perspectives on long-term research and monitoring in the 21st century. Science of The Total Environment 310, 1–8. doi:10.1016/S0048-9697(03)00257-2.

Penaud, A., Eynaud, F., Voelker, A.H.L., Turon, J.L., 2016. Palaeohydrological changes over the last 50 ky in the central gulf of cadiz: Complex forcing mechanisms mixing multi-scale processes. Biogeosciences 13, 5357–5377. doi:10.5194/BG-13-5357-2016.

Perissinotto, R., McQuaid, C.D., 1992. Land-based predator impact on vertically migrating zooplankton and micronekton advected to a southern ocean archipelago. Marine Ecology Progress Series 80, 15–27. doi:10.3354/MEPS080015.

Peters, R.H., Wassenberg, K., 1983. The effect of body size on animal abundance. Oecologia 60, 89–96.

Picheral, M., Colin, S., Irisson, J.O., 2017. Ecotaxa, a tool for the taxonomic classification of images .

Pinti, J., Devries, T., Norin, T., Serra-Pompei, C., Proud, R., Siegel, D.A., Kiørboe, T., Petrik, C.M., Andersen, K.H., Brierley, A.S., Visser, A.W., 2023. Model estimates of metazoans' contributions to the biological carbon pump. Biogeosciences 20, 997–1009. doi:10.5194/bg-20-997-2023.

Pinti, J., Kiørboe, T., Thygesen, U.H., Visser, A.W., 2019. Trophic interactions drive

the emergence of diel vertical migration patterns: a game-theoretic model of copepod communities. Proceedings of the Royal Society B 286, 20191645.

Pitois, S., Yebra, L., 2022. Contribution of marine zooplankton time series to the united nations decade of ocean science for sustainable development. ICES Journal of Marine Science 79, 722–726.

Pitois, S.G., Graves, C.A., Close, H., Lynam, C., Scott, J., Tilbury, J., van der Kooij, J., Culverhouse, P., 2021. A first approach to build and test the copepod mean size and total abundance (cmsta) ecological indicator using in-situ size measurements from the plankton imager (pi). Ecological Indicators 123, 107307. doi:10.1016/J.ECOLIND.2020.107307.

Platt, T., Denman, K., 1977. Organisation in the pelagic ecosystem. Helgoländer wissenschaftliche Meeresuntersuchungen 1977 30:1 30, 575–581. doi:10.1007/BF02207862.

Platt, T., Denman, K., 1978. The structure of pelagic marine ecosystems. Rapports et Proces Verbaux des Reunions .

Pörtner, H., 2002. Climate variations and the physiological basis of temperature dependent biogeography: systemic to molecular hierarchy of thermal tolerance in animals. Comparative Biochemistry and Physiology Part A: Molecular & Integrative Physiology 132, 739–761.

Postel, L., 1990. Die reaktion des mesozooplanktons, speziell der biomasse, aufkuÅnstennahen auftriebvor west afrika (doctoral dissertation, phd thesis, institutfuÅn r meereskunde, warnemünde: 127 pp). PhD Thesis, InstitutfuÅN r Meereskunde, Warnemünde , 127.

Fernández de Puelles, M., Braun, J., 1996. Micro and mesozooplankton in canarian waters (28°30′n 16°06′w). In:O. Llinás, J.A. González and M.J. Rueda (eds.) Oceanography

and Marine Resources in the Eastern Central Atlantic, pp 69-89. DGUI Gobierno de Canarias-Cabildo Insular de Gran Canaria .

Fernández de Puelles, M.L., Alemany, F., Jansá, J., 2007. Zooplankton time-series in the balearic sea (western mediterranean): variability during the decade 1994–2003. Progress in Oceanography 74, 329–354.

QGIS, 2021. Qgis geographic information system. QGIS Association .

Quevedo, M., Anadón, R., 2000. Spring microzooplankton composition, biomass and potential grazing in the central cantabrian coast (southern bay of biscay). Oceanologica Acta 23, 297–310.

Quinones, R.A., Platt, T., Rodríguez, J., 2003. Patterns of biomass-size spectra from oligotrophic waters of the northwest atlantic. Progress in Oceanography 57, 405–427. doi:10.1016/S0079-6611(03)00108-3.

Ratnarajah, L., Abu-Alhaija, R., Atkinson, A., Batten, S., Bax, N.J., Bernard, K.S., Canonico, G., Cornils, A., Everett, J.D., Grigoratou, M., Ishak, N.H.A., Johns, D., Lombard, F., Muxagata, E., Ostle, C., Pitois, S., Richardson, A.J., Schmidt, K., Stemmann, L., Swadling, K.M., Yang, G., Yebra, L., 2023. Monitoring and modelling marine zooplankton in a changing climate. Nature Communications 2023 14:1 14, 1–17. doi:10.1038/s41467-023-36241-5.

Real, F., de Armas Pérez, J.D., Braun, J.A.G., 1981. Distribución espacial de la clorofila a y del carbono orgánico particulado en aguas costeras superficiales de las islas canarias: N. º 292. Boletín. Instituto Español de Oceanografía 6, 107–116.

Reyes-Mendoza, O., Herrera-Silveira, J., Mariño-Tapia, I., Enriquez, C., Largier, J.L., 2019. Phytoplankton blooms associated with upwelling at cabo catoche. Continental Shelf Research 174, 118–131. doi:10.1016/j.csr.2018.12.015.

Richardson, A.J., 2008. In hot water: zooplankton and climate change. ICES Journal of Marine Science 65, 279–295.

Robinson, C., Steinberg, D.K., Anderson, T.R., Arístegui, J., Carlson, C.A., Frost, J.R., Ghiglione, J.F.O., Ndez-Leó, S.H., Jackson, G.A., Koppelmann, R., Guiner, B.Q., Ragueneau, O., Rassoulzadegan, F., Robison, B.H., Tamburini, C., Tanaka, T., Wishner, K.F., Zhang, J., 2010. Mesopelagic zone ecology and biogeochemistry – a synthesis doi:10.1016/j.dsr2.2010.02.018.

Rodrıguez, J., Hernández-León, S., Barton, E., 1999. Mesoscale distribution of fish larvae in relation to an upwelling filament off northwest africa. Deep Sea Research Part I: Oceanographic Research Papers 46, 1969–1984.

Rodriguez, J., Mullin, M.M., 1986. Diel and interannual variation of size distribution of oceanic zooplanktonic biomass. Ecology 67, 215–222. doi:10.2307/1938521.

Romero-Romero, S., Choy, C.A., Hannides, C.C., Popp, B.N., Drazen, J.C., 2019. Differences in the trophic ecology of micronekton driven by diel vertical migration. Limnology and oceanography 64, 1473–1483.

Rutter, W.J., 1967. "methods in developmental biology". in Methods in Developmental Biology, eds H. F. Wilt and N. K. Wessels (London: Academic Press) , 671–684.

Rutter, W.J., Kemp, J.D., Bradshaw, W.S., Clark, W.R., Ronzio, R.A., Sanders, T.G., 1968. Regulation of specific protein synthesis in cytodifferentiation. Journal of Cellular Physiology 72, 1–18. doi:10.1002/jcp.1040720403.

Santamaría, M., Braun, J.A.G., de Armas Pérez, J.D., Hardisson, F.R., Escánez, J., Villamandos, J.E., 1989. Estudio comparativo de las comunidades zooplanctónicas en san andrés y los cristianos (tenerife). Boletín. Instituto Español de Oceanografía 5, 57–70.

Sarmiento-Lezcano, A.N., Busquets-Vass, G., Rubio-Rodríguez, U., Olivar, M.P., Pena, M., Medina-Suárez, I., González-Rodríguez, E., Gómez-Gutiérrez, J., Robinson, C.J.,

Hernández-León, S., 2022. Active flux seasonality of the small dominant migratory crustaceans and mesopelagic fishes in the gulf of california during june and october. Progress in Oceanography 208, 102894.

Schlitzer, R., 2015. Data analysis and visualization with ocean data view. CMOS Bulletin SCMO 43, 9–13.

Schmidt, D.F., Amaya, D.J., Grise, K.M., Miller, A.J., 2020. Impacts of shifting subtropical highs on the california current and canary current systems. Geophysical Research Letters 47, 1–9. doi:10.1029/2020GL088996.

Schmoker, C., Arístegui, J., Hernández-León, S., 2012. Planktonic biomass variability during a late winter bloom in the subtropical waters off the canary islands. Journal of Marine Systems 95, 24–31. doi:10.1016/j.jmarsys.2012.01.008.

Schmoker, C., Hernández-León, S., 2013. Stratification effects on the plankton of the subtropical canary current. Progress in Oceanography 119, 24–31. doi:10.1016/J.POCEAN.2013.08.006.

Schukat, A., Bode, M., Auel, H., Carballo, R., Martin, B., Koppelmann, R., Hagen, W., 2013. Pelagic decapods in the northern benguela upwelling system: Distribution, ecophysiology and contribution to active carbon flux. Deep Sea Research Part I: Oceanographic Research Papers 75, 146–156. doi:10.1016/J.DSR.2013.02.003.

Serranito, B., Aubert, A., Stemmann, L., Rossi, N., Jamet, J., 2016. Proposition of indicators of anthropogenic pressure in the bay of toulon (mediterranean sea) based on zooplankton time-series. Continental Shelf Research 121, 3–12. doi:10.1016/j.csr.2016.01.016.

Sheldon, R.W., Prakash, A., Sutcliffe, W.H., 1972. The size distribution of particles in the ocean. Limnology and Oceanography 17, 327–340. doi:10.4319/LO.1972.17.3.0327.

Shi, Y., Wang, J., Zuo, T., Shan, X., Jin, X., Sun, J., Yuan, W., Pakhomov, E.A., 2020. Seasonal changes in zooplankton community structure and distribution pattern in the yellow sea, china. Frontiers in Marine Science 7, 391. doi:10.3389/FMARS.2020.00391/BIBTEX.

Siemer, J., Machín, F., González-Vega, A., Arrieta, J.M., Gutiérrez-Guerra, M., Pérez-Hernández, M.D., Vélez-Belchí, P., Hernández-Guerra, A., Fraile-Nuez, E., 2021. Recent trends in sst, chl-a, productivity and wind stress in upwelling and open ocean areas in the upper eastern north atlantic subtropical gyre. Journal of Geophysical Research: Oceans 126, e2021JC017268.

Skjoldal, H.R., Wiebe, P.H., Postel, L., Knutsen, T., Kaartvedt, S., Sameoto, D.D., 2013. Intercomparison of zooplankton (net) sampling systems: Results from the ices/globec sea-going workshop. Progress in Oceanography 108, 1–42. doi:10.1016/J.POCEAN.2012.10.006.

Small, L.F., Hebard, J.F., 1967. Respiration of a vertically migrating marine crustacean euphausia pacifica hansen1. Limnology and Oceanography 12, 272–280. doi:10.4319/lo.1967.12.2.0272.

Sommer, U., Stibor, H., 2002. Copepoda - cladocera - tunicata: The role of three major mesozooplankton groups in pelagic food webs. Ecological Research 17, 161–174. doi:10.1046/j.1440-1703.2002.00476.x.

Sourisseau, M., Carlotti, F., 2006. Spatial distribution of zooplankton size spectra on the french continental shelf of the bay of biscay during spring 2000 and 2001. J. Geophys. Res 111, 5–09. doi:10.1029/2005JC003063.

Souza, C.S.D., Conceicão, L.R.D., Freitas, T.S., Aboim, I.L., Schwamborn, R., Neumann-Leitão, S., Junior, P.D.O.M., 2020. Size spectra modeling of mesozooplankton over a tropical continental shelf. Journal of Coastal Research 36, 795–804. doi:10.2112/

JCOASTRES-D-19-00102.1.

Sprules, W.G., Barth, L.E., 2016. Surfing the biomass size spectrum: Some remarks on history, theory, and application. Canadian Journal of Fisheries and Aquatic Sciences 73, 477–495. doi:10.1139/CJFAS-2015-0115/ASSET/IMAGES/LARGE/CJFAS-2015-0115F14.JPEG.

Sprules, W.G., Munawar, M., 1986. Plankton size spectra in relation to ecosystem productivity, size, and perturbation. https://doi.org/10.1139/f86-222 43, 1789–1794. doi:10.1139/F86-222.

St-Gelais, N.F., del Giorgio, P.A., Beisner, B.E., 2023. Functional community structure modulates zooplankton production rates across boreal lakes. Freshwater Biology 68, 837–846.

Steinberg, D.K., Carlson, C.A., Bates, N.R., Goldthwait, S.A., Madin, L.P., Michaels, A.F., 2000. Zooplankton vertical migration and the active transport of dissolved organic and inorganic carbon in the sargasso sea. Deep Sea Research Part I: Oceanographic Research Papers 47, 137–158. doi:10.1016/S0967-0637(99)00052-7.

Steinberg, D.K., Goldthwait, S.A., Hansell, D.A., 2002. Zooplankton vertical migration and the active transport of dissolved organic and inorganic nitrogen in the sargasso sea. Deep-Sea Research Part I: Oceanographic Research Papers 49, 1445–1461. doi:10.1016/S0967-0637(02)00037-7.

Steinberg, D.K., Landry, M.R., 2017. Zooplankton and the ocean carbon cycle. Annual Review of Marine Science 9, 413–444. doi:10.1146/annurev-marine-010814-015924.

Steinberg, D.K., Lomas, M.W., Cope, J.S., 2012. Long-term increase in mesozooplankton biomass in the sargasso sea: Linkage to climate and implications for food web dynamics

and biogeochemical cycling. Global Biogeochemical Cycles 26, 1–16. doi:10.1029/2010GB004026.

Stemmann, L., Boss, E., 2012. Plankton and particle size and packaging: from determining optical properties to driving the biological pump. Annual Review of Marine Science 4, 263–290.

Sterner, R., 2009. Role of zooplankton in aquatic ecosystems, in: Encyclopedia of inland waters. Elsevier Inc., pp. 678–688.

Stoecker, D., Gustafson, D., Verity, P., 1996. Micro-and mesoprotozooplankton at 140* w in the equatorial pacific: heterotrophs and mixotrophs. Aquatic Microbial Ecology 10, 273–282.

Stramma, L., Johnson, G.C., Sprintall, J., Mohrholz, V., 2008. Expanding oxygen-minimum zones in the tropical oceans. Science 320, 655–658. doi:10.1126/science.1153847.

Stukel, M.R., Irving, J.P., Kelly, T.B., Ohman, M.D., Fender, C.K., Yingling, N., 2023. Carbon sequestration by multiple biological pump pathways in a coastal upwelling biome. Nature Communications 2023 14:1 14, 1–10. doi:10.1038/s41467-023-37771-8.

Stukel, M.R., Ohman, M.D., Kelly, T.B., Biard, T., 2018. The roles of suspension-feeding and flux-feeding zooplankton as gatekeepers of particle flux into the mesopelagic ocean in the northeast pacific. Frontiers in Marine Science 6, 1–16. doi:10.3389/fmars.2019.00397.

Sun, D., Chen, Y., Feng, Y., Liu, Z., Peng, X., Cai, Y., Yu, P., Wang, C., 2021. Seasonal variation in size diversity: Explaining the spatial mismatch between phytoplankton and mesozooplankton in fishing grounds of the east china sea. Ecological Indicators 131, 108201. doi:10.1016/J.ECOLIND.2021.108201.

Suthers, I.M., Taggart, C.T., Rissik, D., Baird, M.E., 2006. Day and night ichthyoplankton assemblages and zooplankton biomass size spectrum in a deep ocean island wake. Marine Ecology Progress Series 322, 225–238. doi:10.3354/MEPS322225.

Sutton, A.L., Beckley, L.E., 2022. Krill along the 110°e meridian: Oceanographic influences on assemblages in the eastern indian ocean. Deep Sea Research Part II: Topical Studies in Oceanography 202, 105133. doi:10.1016/J.DSR2.2022.105133.

Svensen, C., Nejstgaard, J.C., 2003. Is sedimentation of copepod faecal pellets determined by cyclopoids? evidence from enclosed ecosystems. Journal of Plankton Research 25, 917–926. doi:10.1093/plankt/25.8.917.

Tarling, G.A., 2020. Routine metabolism of antarctic krill (euphausia superba) in south georgia waters: absence of metabolic compensation at its range edge. Marine Biology 167, 1–15. doi:10.1007/S00227-020-03714-W/FIGURES/9.

Team, R.C., 2022a. R: A language and environment for statistical computing .

Team, R.C., 2022b. R: A language and environment for statistical computing, r foundation for statistical. Computing .

Thiebaux, M.L., Dickie, L.M., 2011. Structure of the body-size spectrum of the biomass in aquatic ecosystems: A consequence of allometry in predator–prey interactions. https://doi.org/10.1139/f93-148 50, 1308–1317. doi:10.1139/F93-148.

Tian, W., Zhang, H., Zhao, L., Zhang, F., Huang, H., 2017. Phytoplankton diversity effects on community biomass and stability along nutrient gradients in a eutrophic lake. International Journal of Environmental Research and Public Health 14, 95.

Trebilco, R., Melbourne-Thomas, J., Constable, A.J., 2020. The policy relevance of southern ocean food web structure: Implications of food web change for fisheries, conservation and carbon sequestration. Marine Policy 115, 103832. doi:10.1016/j.marpol.2020.103832.

Tremblay, N., Hünerlage, K., Werner, T., 2020. Hypoxia tolerance of ten euphausiid species in relation to vertical temperature and oxygen gradients. Frontiers in Physiology 11, 248. doi:10.3389/FPHYS.2020.00248.

Tremblay, N., Werner, T., Huenerlage, K., Buchholz, F., Abele, D., Meyer, B., Brey, T., 2014. Euphausiid respiration model revamped: Latitudinal and seasonal shaping effects on krill respiration rates. Ecological Modelling 291, 233–241. doi:10.1016/j.ecolmodel.2014.07.031.

UNESCO, 1968. Zooplankton sampling. Symposium on the Hydrodynamics of Zooplankton Sampling. Unesco. URL: https://unesdoc.unesco.org/ark:/48223/pf0000071517.

UNESCO, 1994. Protocols for the joint global ocean flux study (jgofs) core measurements. Manuals and Guides 29.

Valcárcel-Pérez, N., Yebra, L., Herrera, I., Mercado Carmona, J.M., Gómez-Jakobsen, F., Salles, S., 2019. Usefulness of semi-automatic image analysis for the assessment of zooplankton community structure in a highly dynamic area of the alboran sea (sw mediterranean) .

Valdés, L., Déniz-González, I., 2015. Oceanographic and biological features in the canary current large marine ecosystem. .

Valencia, B., Landry, M.R., Décima, M., Hannides, C.C., 2016. Environmental drivers of mesozooplankton biomass variability in the north pacific subtropical gyre. Journal of Geophysical Research: Biogeosciences 121, 3131–3143.

Vandromme, P., Lars, S., Garcìa-Comas, C., Berline, L., Sun, X., Gorsky, G., 2012. Assessing biases in computing size spectra of automatically classified zooplankton from imaging systems: A case study with the zooscan integrated system. Methods in Oceanography 1-2, 3–21. doi:10.1016/J.MIO.2012.06.001.

Vanni, M.J., 2002. Nutrient cycling by animals in freshwater ecosystems. Annual Review of Ecology and Systematics 33, 341–370.

Vanni, M.J., Findlay, D.L., 1990. Trophic cascades and phytoplankton community structure. Ecology 71, 921–937.

Vélez-Belchí, P., González-Carballo, M., Pérez-Hernández, M.D., Hernández-Guerra, A., 2015. Open ocean temperature and salinity trends in the canary current large marine ecosystem .

Vereshchaka, A., Abyzova, G., Lunina, A., Musaeva, E., Sutton, T., 2016. A novel approach reveals high zooplankton standing stock deep in the sea. Biogeosciences 13, 6261–6271. doi:10.5194/BG-13-6261-2016.

Villegas-Ríos, D., Álvarez-Salgado, X.A., Piedracoba, S., Rosón, G., Labarta, U., Fernández-Reiriz, M.J., 2011. Net ecosystem metabolism of a coastal embayment fertilised by upwelling and continental runoff. Continental Shelf Research 31, 400–413.

Wang, W., Sun, S., Sun, X., Zhang, G., Zhang, F., 2020. Spatial patterns of zooplankton size structure in relation to environmental factors in jiaozhou bay, south yellow sea. Marine Pollution Bulletin 150, 110698. doi:10.1016/J.MARPOLBUL.2019.110698.

Werner, T., 2013. rophic positioning, diel vertical migration and physiological constraints in euphausiid species of the namibian upwelling system .

Wiebe, P.H., Burt, K.H., Boyd, S.H., Morton, A.W., 1976. A multiple opening/closing net and environmental sensing system for sampling zooplankton .

Winemiller, K.O., Polis, G.A., 1996. Food Webs: What Can They Tell Us About the World?. Springer US. pp. 1–22. doi:10.1007/978-1-4615-7007-3_1.

Woodward, G., Ebenman, B., Emmerson, M., Montoya, J.M., Olesen, J.M., Valido, A.,

Warren, P.H., 2005. Body size in ecological networks. Trends in Ecology and Evolution 20, 402–409.

Woodworth-Jefcoats, P.A., Polovina, J.J., Dunne, J.P., Blanchard, J.L., 2013. Ecosystem size structure response to 21st century climate projection: large fish abundance decreases in the central n orth p acific and increases in the c alifornia c urrent. ,. Global Change Biology 19, 724–733.

Ye, L., Chang, C.Y., García-Comas, C., Gong, G.C., hao Hsieh, C., 2013. Increasing zooplankton size diversity enhances the strength of top-down control on phytoplankton through diet niche partitioning. Journal of Animal Ecology 82, 1052–1061. doi:10.1111/1365-2656.12067.

Yebra, L., Almeida, C., Hernández-León, S., 2005. Vertical distribution of zooplankton and active flux across an anticyclonic eddy in the canary island waters. Deep-Sea Research Part I: Oceanographic Research Papers 52, 69–83. doi:10.1016/j.dsr.2004.08.010.

Yebra, L., Espejo, E., Putzeys, S., Giráldez, A., Gómez-Jakobsen, F., León, P., Salles, S., Torres, P., Mercado, J.M., 2020. Zooplankton biomass depletion event reveals the importance of small pelagic fish top-down control in the western mediterranean coastal waters. Frontiers in Marine Science 7, 608690. doi:10.3389/FMARS.2020.608690/BIBTEX.

Yebra, L., Herrera, I., Mercado, J.M., Cortés, D., Gómez-Jakobsen, F., Alonso, A., Sánchez, A., Salles, S., Valcárcel-Pérez, N., 2018. Zooplankton production and carbon export flux in the western alboran sea gyre (sw mediterranean). Progress in Oceanography 167, 64–77. doi:10.1016/j.pocean.2018.07.009.

Yentsch, C.S., Menzel, D.W., 1963. A method for the determination of phytoplankton chlorophyll and phaeophytin by fluorescence. Deep Sea Research and Oceanographic

Abstracts 10, 221–231. doi:10.1016/0011-7471(63)90358-9.

Zhang, X., Dam, H.G., 1997. Downward export of carbon by diel migrant mesozooplankton in the central equatorial pacific. Deep Sea Research Part II: Topical Studies in Oceanography 44, 2191–2202. doi:10.1016/S0967-0645(97)00060-X.

Zhao, W., Dai, L., Chen, X., Wu, Y., Sun, Y., Zhu, L., 2022. Characteristics of zooplankton community structure and its relationship with environmental factors in the south yellow sea. Marine Pollution Bulletin 176, 113471. doi:10.1016/J.MARPOLBUL.2022.113471.

Zhou, L., Huang, L., Tan, Y., Lian, X., Li, K., 2014. Size-based analysis of a zooplankton community under the influence of the pearl river plume and coastal upwelling in the northeastern south china sea. http://dx.doi.org/10.1080/17451000.2014.904882 11, 168–179. doi:10.1080/17451000.2014.904882.

Zhou, M., 2006. What determines the slope of a plankton biomass spectrum? doi:10.1093/plankt/fbi119.